

Louisiana Tech University

**Louisiana Tech Digital Commons**

---

Doctoral Dissertations

Graduate School

---

Fall 11-2021

**Prevention of Organ-Specific Doxorubicin Induced Toxicity Using Physiologically-Based Pharmacokinetic Modeling and Therapeutic Drug Monitoring**

Hillary Husband

Follow this and additional works at: <https://digitalcommons.latech.edu/dissertations>

---

**PREVENTION OF ORGAN-SPECIFIC DOXORUBICIN  
INDUCED TOXICITY USING PHYSIOLOGICALLY-  
BASED PHARMACOKINETIC MODELING  
AND THERAPEUTIC DRUG  
MONITORING**

by

Hillary Renee Husband, B.S., M.S.

A Dissertation Presented in Partial Fulfillment  
of the Requirements for the Degree  
Doctor of Philosophy: Molecular Sciences and Nanotechnology

COLLEGE OF ENGINEERING AND SCIENCE  
LOUISIANA TECH UNIVERSITY

November 2021

LOUISIANA TECH UNIVERSITY

GRADUATE SCHOOL

September 16, 2021

Date of dissertation defense

We hereby recommend that the dissertation prepared by

**Hillary Renee Husband, B.S., M.S.**

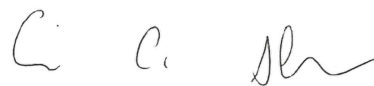
entitled **Prevention of Organ-Specific Doxorubicin Induced Toxicity Using**

**Physiologically-Based Pharmacokinetic Modeling and Therapeutic Drug**

**Monitoring**

be accepted in partial fulfillment of the requirements for the degree of

**Doctor of Philosophy in Molecular Sciences and Nanotechnology**



Eric A. Sherer

Supervisor of Dissertation Research



Gergana Nestorova

Head of Molecular Sciences and Nanotechnology

**Doctoral Committee Members:**

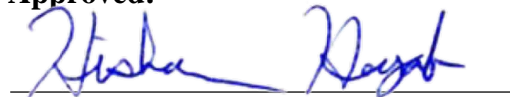
Mary Caldorera-Moore

Katie Evans

Songming Hou

Jamie Newman

**Approved:**



Hisham Hegab

Dean of Engineering & Science

**Approved:**



Ramu Ramachandran

Dean of the Graduate School

## ABSTRACT

Physiology-based pharmacokinetic models are mathematical models that characterize the behavior of a drug and have compartmental equations that are representative of specific tissues and physiological processes.[1, 2] Doxorubicin is an anthracycline antibiotic that is effective and widely used in anticancer therapy due to its potent cytotoxicity. Unfortunately, with that potency comes cardiotoxic side effects related to cumulative lifetime dose.[3] Specifically, the toxicity is related to the accumulation of the primary metabolite doxorubicinol (DOXol) in the heart.[4] Since the toxicity is organ-specific, the best way to characterize the behavior is through PBPK modeling.[2] Since PBPK models tend to be large systems of ODEs, several numerical methods were attempted for solving the model before a matrix-based approach was chosen.[5, 6] The eigenvalue/eigenvector solution was evaluated at three time points which were then included in a Composite Simpson's Rule numerical integration for the length of some time interval.[5, 7] The PBPK model, adapted from a pig model, was fit to mouse data and scaled to predict rat, rabbit, dog, pig, and human data sets using an allometric scaling equation on the blood:plasma partition coefficient  $B : P$ . [8, 9, 10]

Despite extensive investigation into dose adjustments for DOX, no covariates were consistently found to improve the efficacy and minimize toxicity except dosing schedule – infusion rate and duration.[11] The criterion for decreasing incidence of cardiotoxicity was maintaining a sub-toxic  $C_{max,heart,DOXol}$  in the heart while maximizing exposure, represented by area under the concentration-time-curve (AUC).

Thus, the original mouse data set was ideal since it included both DOX venous blood concentration and DOXol heart concentration.[12] The model was optimized at 10 time points between 1 minute and 72 hours with the goal of  $(AUC)$  maximization without exceeding  $C_{max,heart,DOXol}$ . Using these predictions, therapeutic drug monitoring could be executed by taking the plasma concentration samples during a patient's first DOX dose, PBPK model predictions could provide  $AUC$  and  $C_{max,heart,DOXol}$  data, which could then inform the infusion parameters for the next dose. Clinical thresholds for  $C_{max,vb}$  have been established for incidence of adverse effects, and in future work, perhaps a similar threshold for cardiotoxicity could also be established using tissue-specific measures.

## **APPROVAL FOR SCHOLARLY DISSEMINATION**

The author grants to the Prescott Memorial Library of Louisiana Tech University the right to reproduce, by appropriate methods, upon request, any or all portions of this Dissertation. It is understood that “proper request” consists of the agreement, on the part of the requesting party, that said reproduction is for his personal use and that subsequent reproduction will not occur without written approval of the author of this Dissertation. Further, any portions of the Dissertation used in books, papers, and other works must be appropriately referenced to this Dissertation.

Finally, the author of this Dissertation reserves the right to publish freely, in the literature, at any time, any or all portions of this Dissertation.

Author \_\_\_\_\_

Date \_\_\_\_\_

## **DEDICATION**

To my Mom and Dad – for showing me I could do anything to which I set my mind and for all they sacrificed for me to get to this point. I would not be the person I am without your unconditional love and support.

To my husband, John – for all the love and support you gave me and all you endured while I was in graduate school. Thank you for being my rock.

To all the wonderful medical professionals and staff at St. Jude Children’s Research Hospital who cared for me through three cancer diagnoses – mentally, emotionally, and physically.

To my grandfather, Paul Richard Danyluk. I know you would be so proud. I wish you were here to see me follow in your footsteps.

This work is the culmination of many hardships fought alongside the people listed here and many others. As much as this is my success, it is theirs. I love you all and am endlessly grateful.

## TABLE OF CONTENTS

ABSTRACT.....	iii
APPROVAL FOR SCHOLARLY DISSEMINATION .....	v
DEDICATION.....	vi
LIST OF TABLES.....	xiii
LIST OF FIGURES .....	xv
ACKNOWLEDGMENTS .....	xix
CHAPTER 1 DOXORUBICIN: PHYSIOLOGICAL OVERVIEW .....	1
1.1 Introduction.....	1
1.2 Mechanism of Action-Cytotoxicity .....	8
1.2.1 DNA Intercalation.....	9
1.2.2 Free Radical Generation and Oxidative Damage.....	10
1.3 DOX Metabolites .....	13
1.3.1 DOXol and Cardiotoxicity.....	16
1.4 Conclusion .....	20
1.5 Outline of Content in Each Chapter.....	21
CHAPTER 2 PHARMACOMETRICS OVERVIEW .....	23
2.1 Pharmacokinetic Versus Pharmacodynamic.....	23
2.2 Compartmental Body Models.....	25
2.2.1 Compartment Model Concept.....	25



2.2.2 Compartment Model Equations .....	27
2.3 Pharmacokinetics Concepts .....	30
2.3.1 Absorption.....	31
2.3.2 First-Order Kinetics .....	32
2.3.3 Zero-Order Kinetics .....	33
2.3.3.1 Flip-Flop Kinetics .....	34
2.3.4 Distribution .....	35
2.3.4.1 Membranes.....	37
2.3.4.2 Permeability .....	38
2.3.4.3 Transport Processes .....	42
2.3.4.4 Diffusion .....	42
2.3.4.5 Active Transport .....	43
2.3.4.6 Extent of Distribution .....	45
2.3.4.7 Binding.....	48
2.3.4.8 Binding Within Blood.....	49
2.3.4.9 Transporters and Binding in Tissues.....	50
2.3.4.10 Rate of Distribution to Tissues .....	52
2.3.5 Metabolism .....	53
2.3.6 Excretion .....	55
2.3.7 Summary of Pharmacokinetic Concepts .....	57
2.3.7.1 Absorption.....	57
2.3.7.2 Distribution .....	57
2.3.7.3 Metabolism .....	58

2.3.7.4 Excretion .....	58
2.3.7.5 Absorption and Disposition .....	58
2.4 Pharmacodynamics Concepts .....	59
2.4.1 Types of Pharmacodynamic Response .....	60
2.4.2 Assessment of Response .....	62
2.4.3 Graded Versus Quantal Response.....	63
2.4.4 Examples of Notable Pharmacodynamic Models .....	64
2.4.4.1 Direct Effect Models.....	64
2.4.4.1.1 The Levy Equation.....	64
2.4.4.1.2 $E_{max}$ Model .....	65
2.4.4.1.3 Biophase Model .....	66
2.4.4.1.4 Indirect Response Models.....	68
2.4.4.1.5 IDR Model I.....	68
2.4.4.1.6 IDR Model II.....	68
2.4.4.1.7 IDR Model III .....	68
2.4.4.1.8 IDR Model IV .....	68
2.5 Summary of Pharmacokinetics and Pharmacodynamics .....	69
2.6 Additional Considerations in PK/PD Modeling .....	72
2.6.1 Disease Modeling.....	72
2.6.1.1 Modeling Tumor Dynamics .....	73
2.6.1.2 Disease Progression .....	75
2.6.2 Clinical and Therapeutic Relevance .....	76
CHAPTER 3 PK/PD OF DOX AND DOXol.....	80

3.1 Current Models of DOX and DOXol.....	80
3.2 Inter-Patient and Inter-Dose Variability .....	83
3.3 PK Modeling Solutions to DOX Drawbacks .....	88
3.4 Investigating PBPK Models of DOX.....	91
3.5 Middle Ground - Minimal PBPK Modeling Approach .....	94
3.6 Conclusion .....	99
<b>CHAPTER 4 NUMERICAL METHODS FOR PBPK MODELING .....</b>	<b>101</b>
4.1 Traditional Numerical Methods .....	102
4.1.1 Euler’s Method.....	102
4.1.2 Runge-Kutta Methods.....	105
4.1.2.1 Stiffness.....	106
4.1.3 Adaptive-Step Runge-Kutta-Fehlberg .....	107
4.1.4 Summarizing Traditional Methods .....	111
4.2 Eigenvalue/Eigenvector Solution.....	112
4.2.1 Simple Homogeneous Example.....	113
4.2.2 Simple Non-Homogeneous Example.....	114
4.2.3 Numerical Integration Series of Eigenvalue/Eigenvector Solutions of Initial Value Problems .....	116
4.2.3.1 Adaptive Numerical Integration .....	119
4.3 Comparison of Methods.....	121
4.4 Compartmental Model Examples .....	122
4.4.1 Three-Compartment PK Model Example .....	122
4.4.2 Physiologically-Based Pharmacokinetic (PBPK) Example.....	125
4.5 Conclusion .....	127

CHAPTER 5 INTER-SPECIES SCALING .....	129
5.1 Allometry Concepts .....	129
5.2 Inter-Species Scaling of Doxorubicin.....	131
5.2.1 Determination of Model Parameters .....	132
5.2.2 Extrapolation to Humans .....	139
CHAPTER 6 CONCLUSIONS .....	154
6.1 Future Work .....	154
6.1.1 Therapeutic Drug Monitoring for DOX.....	154
6.1.1.1 Therapeutic Index .....	154
6.1.1.2 Therapeutic Drug Monitoring for DOX and DOXol .....	155
6.1.1.3 Use of PBPK Predictions for Therapeutic Dose Monitoring of DOX.....	162
6.1.2 Pharmacodynamic Studies.....	163
6.1.3 Application to Other Drugs.....	164
6.2 Conclusion .....	165
APPENDIX A EQUATIONS FROM DUBBELBOER MODEL.....	172
APPENDIX B FINAL MODEL EQUATIONS .....	177
APPENDIX C THREE COMPARTMENT MODEL EXAMPLE CODE.....	184
APPENDIX D FINAL MODEL CODE IN R .....	190
APPENDIX E MATRIX ODE SOLVER CODE.....	205
APPENDIX F MODEL FITS BY SPECIES .....	210
APPENDIX G CODE SETUP FOR PBPK PARAMETERS .....	218
APPENDIX H THERAPEUTIC OPTIMIZATION CODE.....	232
APPENDIX I ADDITIONAL ABBREVIATIONS .....	235

REFERENCES .....245

## LIST OF TABLES

<b>Table 1-1:</b> <i>List of Common Types of Cancer Treated with Doxorubicin from Prescribers' Digital Reference[49]</i> .....	7
<b>Table 1-2:</b> <i>Median Concentration of DOX and DOXol in Autopsy Tissue from 35 Human Patients in Stewart et al. Study; 35 Patients Received Cumulative Lifetime Dose of 30- 670 mg/m<sup>2</sup> with Last Dose from 1 - 931 Days (Source [62]).</i> .....	17
<b>Table 1-3:</b> <i>IC<sub>50</sub> for DOX and DOXol in Three Cancer Cell Lines from a Study by Olson et al.[66]</i> .....	20
<b>Table 3-1:</b> <i>Observed or Reported Half-Life Values for Sub-Clinical Species and Humans from Literature</i> .....	81
<b>Table 3-2:</b> <i>Observed or Reported AUC Values for Sub-Clinical Species and Humans from Literature</i> .....	81
<b>Table 3-3:</b> <i>Summary of Existing Models of Un-Encapsulated or “Free” DOX in Sub-Clinical Species and in Humans, as Reported from Literature</i> .....	83
<b>Table 3-4:</b> <i>Observed or Reported Clearance Values for sub-Clinical Species and Humans from Literature</i> .....	86
<b>Table 3-5:</b> <i>Observed or Reported Volumes of Distribution at Steady State of DOX for Sub-Clinical Species and Humans from Literature</i> .....	87
<b>Table 5-1:</b> <i>Calculated Maximum-Lifespan Potential and Brain Weight-Values Commonly used as Correction Factors for Inter-Species Scaling of Hepatically Eliminated Drugs like DOX in Several Laboratory Animals and to Humans (Source [161, 166, 167, 168, 169])</i> .....	132
<b>Table 5-2:</b> <i>Fraction of Body Weight of Each Sub-Compartment within the Kidney and the Liver Originally Determined in the Dubbelboer Pig Model and Used Throughout All Species in this Inter-Species Scaling (Source [8])</i> .....	134

<b>Table 5-3:</b> <i>Fraction of Total Body Weight for Each Respective Compartment for Each Species Used in Inter-Species Scaling of DOX. The Pig Parameters in Both Tables were Adapted from Dubbelboer.[145] Mouse, Rat, Dog, and Human Parameters were Adapted from The International Life Sciences Institute Resource.[173] The parameters for the Rabbit were Adapted from a Meta-Analyses Done by Davies.[174]</i> .....	135
<b>Table 5-4:</b> <i>Fraction of Total Cardiac Output for Each Respective Compartment for Each Species Used in Inter-Species Scaling Of DOX. The Pig Parameters in Both Tables were Adapted from Dubbelboer.[145] Mouse, Rat, Dog, And Human Parameters were Adapted from the International Life Sciences Institute Resource.[173] The Parameters for the Rabbit were Adapted from a Meta-Analyses Done by Davies.[174]</i> .....	136
<b>Table 5-5:</b> <i>Results of Sensitivity Analysis as Shown by Percent Change in the Objective Function Value (Inner Cells of Table) Given a Percent Change (Top Row in Table) in Parameter (Leftmost Column), Ranked from Most Change to Least Change</i> .....	138
<b>Table 5-6:</b> <i>The First Section Contains Parameter Values with Variability in Percent Coefficient of Variation Reported by Dubbelboer et al. [8] If No %CV is Reported, then the Parameter was Assumed or Taken From Literature by the Authors. The Second Section Contains Parameters that were Estimated for the New Model, Based on the Dubbelboer Model, Containing the Heart Compartment. These Parameters Remained Constant Across All the Data Sets Used in Scaling</i> .....	139
<b>Table 5-7:</b> <i>Final Parameter Values for CO, BW , and the Scaling Factors for Each of the Individual Data Sets</i> .....	150
<b>Table 5-8:</b> <i>Final Model Parameters for 5 Human Data Sets in Which Equation 5-4 Was Used to Scale B:P by Body Weight</i> .....	151
<b>Table 6-1:</b> <i>AUC and C<sub>max</sub> for the Predictions Generated by the PBPK Model</i> .....	160

## LIST OF FIGURES

<b>Figure 1-1:</b> Single-electron reduction-oxidation cycling of doxorubicin, taken from the review paper by Minotti et al.[15] .....	11
<b>Figure 1-2:</b> Main pathways of intracellular doxorubicin (DOX) biotransformation in mammalian cells, including catalytic enzymes involved in its metabolism. The downstream effects of the metabolites are also listed. (adapted from Edwardson et al. [52]).....	13
<b>Figure 1-3:</b> Molecular structure of doxorubicin .....	15
<b>Figure 2-1:</b> Schematic of a PK/PD workflow with feedback for the purpose of optimizing a dose regimen .....	24
<b>Figure 2-2:</b> Visualization of how the pharmacokinetic relationship of drug concentration versus time and the pharmacodynamic relationship of effect versus concentration come together to create an effect over time profile, adapted from Derendorf et al.[68] .....	25
<b>Figure 2-3:</b> Adapted from Ratain et al., examples of one-compartment (A), two-compartment (B), and three-compartment (C) concentration-time plot[70] .....	26
<b>Figure 2-4:</b> A way of combining the idea of material balance and the four pharmacokinetic processes (Absorption, Distribution, Excretion, and Metabolism) .....	31
<b>Figure 2-5:</b> Example of a one-compartment model with first-order absorption and also first-order elimination.....	33
<b>Figure 2-6:</b> Example of a one-compartment model with zero-order absorption and linear elimination .....	34
<b>Figure 2-7:</b> Schematic of the contributing factors of the net transport rate across membranes in the cell - the permeability of the membrane, the surface area of the cell, and the concentration difference inside and outside the cell .....	38
<b>Figure 2-8:</b> Simple two-compartment model, which implies that all drug in the body is contained in the plasma compartment (left) and the tissue compartment (right) with physiologic volumes of $V_p$ and $V_t$ , respectively .....	46



<b>Figure 2-9:</b> Disposition is a collective term that refers to the processes of distribution and elimination; elimination includes two of the ADME processes - metabolism and excretion.....	59
<b>Figure 2-10:</b> Illustration of the consideration of placebo response and baseline in addition to drug response when assessing the measured pharmacodynamic response of a drug .....	63
<b>Figure 2-11:</b> Simple schematic of the biophase model originally developed by Sheiner et al.[101], where $C_p$ represents the concentration in plasma compartment, $C_e$ represents the hypothetical effect compartment, and $k_{eo}$ is the first order distribution rate constant between compartments.....	67
<b>Figure 2-12:</b> Schematic of the inter-relation of pharmacokinetic and pharmacodynamic modeling (adapted from Zou et al.)([73]).....	70
<b>Figure 2-13:</b> Examples of the general shapes of the four basic functional forms that natural tumor growth models take - linear (A), exponential (B), logistic (C) and Gompertz (D) (adapted from Yin et al.)([114]).....	74
<b>Figure 2-14:</b> Simplified flow chart of the drug discovery process highlighting the contribution of PK and PD models at each phase of the process (adapted from Derendorf et al.([68]) .....	77
<b>Figure 3-1:</b> Example of a PBPK schematic, showing how each organ, represented as compartments, are connected by the circulatory system .....	92
<b>Figure 3-2:</b> PBPK schematic of doxorubicin from the “binding specific” pig model created by Dubbelboer et al. 2017; arterial blood is denoted by the red arrows and boxes, venous blood by blue arrows and boxes, non-metabolizing tissues are in green, and metabolizing tissues are in gold .....	95
<b>Figure 3-3:</b> Liver compartment schematic describing movement, metabolism, and excretion of DOX and DOXol in metabolizing tissues .....	96
<b>Figure 3-4:</b> Heart compartment schematic describing movement and metabolism of DOX and DOXol in metabolizing tissues .....	97
<b>Figure 3-5:</b> PBPK schematic of doxorubicin, adapted from the pig model created by Dubbelboer et al. 2017 to add a heart compartment as a metabolizing compartment; arterial blood is denoted by the red arrows and boxes, venous blood by blue arrows and boxes, non-metabolizing tissues are in green, and metabolizing tissues are in gold .....	98
<b>Figure 4-1:</b> A schematic of the general process of the matrix-based numerical method.....	117

<b>Figure 4-2:</b> Solutions to 2 x 2 example, solved with three different step-sizes and compared to the exact solution at each time point. The accuracy compared to the step-size here demonstrates the negligible loss of accuracy for larger step sizes using this method .....	118
<b>Figure 4-3:</b> A more detailed flow of the inputs and outputs of the matrix-based numerical method.....	122
<b>Figure 4-4:</b> A traditional representation of a three-compartment pharmacokinetic model described by Cascone et al.....	123
<b>Figure 4-5:</b> Plot of observed versus model predicted values for the human Remfentanil model, illustrating that the pbpkme method works at least as well as traditional numerical methods on classic compartmental pharmacokinetic models.....	124
<b>Figure 4-6:</b> Plot of observed versus model predicted values for the human Remfentanil model, illustrating that the pbpkme method works at least as well as traditional numerical methods on classic compartmental pharmacokinetic models.....	125
<b>Figure 4-7:</b> Predictions from the model solved with the matrix-based numerical method overlaid on the predictions generated by the digitized predictions from Dubbelboer et al.....	127
<b>Figure 5-1:</b> Flow chart of the process of developing the model structure and parameters, starting with Dubbelboer Model[8] and progressing to the mouse model that was used for inter-species scaling.[12] .....	142
<b>Figure 5-2:</b> Plot of cardiac output by body weight in kilograms of each study used for the allometric inter-species scaling .....	143
<b>Figure 5-3:</b> Heart DOXol concentration observations from van der Vijgh mouse data set with model predictions overlaid[12].....	144
<b>Figure 5-4:</b> Venous blood DOX concentration observations from four mouse data sets - A.) Asperen et al.[126], B.) Dai et al.[189], C.) Formelli et al.[33], and D.) van der Vijgh et al.[12] - with model predictions overlaid.....	144
<b>Figure 5-5:</b> Observed and predicted venous blood DOX concentration in rats after applying allometric scaling - A.) <i>with</i> MLP Correction Factor and B.) <i>without</i> MLP Correction Factor to the parameter $B : P$ (Data source: Rahman et al.[45]).....	147
<b>Figure 5-6:</b> Observed and predicted venous blood DOX concentration in rabbits after applying allometric scaling - A.) <i>with</i> MLP Correction Factor and B.) <i>without</i> MLP Correction Factor to the parameter $B : P$ (Data source: Johansen et al.[117]) .....	147

<b>Figure 5-7:</b> Observed and predicted venous blood DOX concentration in dogs after applying allometric scaling - A.) <i>with</i> MLP Correction Factor and B.) <i>without</i> MLP Correction Factor to the parameter $B : P$ (Data source: Oosterbaan et al.[192]).....	148
<b>Figure 5-8:</b> Observed and predicted venous blood DOX concentration in pigs after applying allometric scaling - A.) <i>with</i> MLP Correction Factor and B.) <i>without</i> MLP Correction Factor to the parameter $B : P$ (Data source: Dubbelboer et al.[8]).....	148
<b>Figure 5-9:</b> Observed and predicted venous blood DOX concentration in humans after applying allometric scaling - A.) <i>with</i> MLP Correction Factor and B.) <i>without</i> MLP Correction Factor to the parameter $B : P$ (Data source: Krarup et al.[45]).....	149
<b>Figure 5-10:</b> Plot of Blood:Plasma Partition Coefficient for each study used in the allometric interspecies scaling - the top plot shows the trend in the parameter with the Maximum Life-Span Potential (MLP) Correction Factor while the bottom plot shows the trend in the parameter without the correction factor.....	152
<b>Figure 6-1:</b> Schematic of the iterative process of the therapeutic dose monitoring approach outlined in this work for individualizing DOX therapy.....	160
<b>Figure 6-2:</b> Plot of venous blood $AUC$ values versus infusion duration at the maximum dose that does not exceed $C_{max,heart,DOXol}$ of $10^{-3}$ -the open circles represent the $AUC$ values, the closed dark green circle indicates the point at which the $AUC$ is highest; the solid line represents the infusion rate or maximum total dose for the corresponding infusion duration, with the blue closed circle indicating the dose at which the $AUC$ is highest; the vertical line highlights the optimal infusion duration at which $AUC$ is maximized while still remaining below $C_{max,heart,DOXol}$ .....	161
<b>Figure 6-3:</b> DOX venous blood concentration versus time plot in humans using the infusion parameters (infusion rate - $69.3 \mu\text{M}$ over 120 minutes) from the optimization shown in Table 6-1 and Figure 6-2 - $AUC$ for the infusion simulated out to 96 hours .....	161
<b>Figure 6-4:</b> DOXol heart concentration versus time plot in humans using the infusion parameters (infusion rate - $69.3 \mu\text{M}$ over 120 minutes) from the optimization shown in Table 6-1 and Figure 6-2 - $C_{max,heart,DOXol}$ is reached at 2827.25 minutes but does not exceed the threshold of $10^{-3}$ for the infusion simulated out to 96 hours.....	162

## **ACKNOWLEDGMENTS**

Special thanks to the Louisiana Board of Regents for the 2017 LBOR Fellowship that funded my time at Louisiana Tech.

## CHAPTER 1

### DOXORUBICIN: PHYSIOLOGICAL OVERVIEW

#### 1.1 Introduction

Doxorubicin (DOX) is an anthracycline antibiotic with antineoplastic activity which was approved by the FDA as a chemotherapy agent in 1974.[13] It was one of the first two anthracyclines isolated from *Streptomyces peucetius*, a type of actinobacteria, in the 1960's.[14, 15] It has since been one of the most commonly used drugs in cancer treatment. DOX is highly cytotoxic, making it an excellent anticancer drug but it is also known to cause extensive damage to healthy tissue.[16] It has been found to be efficacious in both adult and pediatric populations for a variety of cancer types, including solid tumors like small-cell lung cancer[17] and osteosarcoma[18], and blood cancers like non-Hodgkin lymphoma and leukemia.[19, 20] A list of common cancers treated with DOX is shown in Table 1-1. While this work will focus on the use of DOX in adults, it is worthwhile to mention that DOX has been a major player in pediatric oncology. The 5 year survival rate for pediatric cancers in general has increased from  $\approx 5\%$  in the 1960's to  $\approx 80\%$  in recent years, and anthracyclines like DOX are given in  $\approx 50\%$  of childhood cancer protocols.[14] It has been said that doxorubicin is the most effective anticancer drug to be developed, which is evidenced in its continued use today, 50 years after its discovery.[15] Over the years, with the development of more targeted therapies, it has

become relatively common in clinical practice to combine novel therapeutics with DOX rather than to replace DOX with the novel therapeutics.[21, 22, 23, 24, 25, 26] In addition to continuing to include DOX in current treatment protocols, different formulations of DOX have been utilized. These include encapsulation in liposomes and nanoparticles for enhanced and targeted drug delivery.[27, 28, 22, 23] DOX is not administered orally due to its low bioavailability in that formulation, unpredictable and generally poor permeability in the intestines.[29] The scope of this work will only consider “free”, or unencapsulated, doxorubicin, and the current models for DOX will be discussed in a following section.

Doxorubicin has a triphasic disposition, which means that it has three sequential half-lives.[30] Typically, a drug with triphasic disposition would be fit to a three compartment pharmacokinetic model, and such is the case for most models of DOX.[31, 17, 32] In some cases, the sampling frequency is too sparse to capture one of the half-life phases, and DOX is fit to a two-compartment model.[33] A more in depth analysis of current pharmacokinetic models of DOX will follow in a later section. For doxorubicin the first half-life is 5 - 10 minutes, the second half-life is 30-180 minutes, and the third is 24-36 hours.[30, 34] The terminal half-life of DOX is estimated to be between 30.8 hours to 48.4 hours; the terminal half life of DOXol is estimated to be between 27.8 hours and 66.2 hours[30, 17], with a detectable mean residence time (MRT) of 45.6 hours (range 26 hours - 83.1 hours).[35] When studied over a 48 hour sampling duration, the reported volume of distribution of DOX was  $572 \pm 215 \text{ L/m}^2$  to  $682 \pm 433 \text{ L/m}^2$  (Mean  $\pm$  Standard Deviation).[30, 17] Recall that volume of distribution is a surrogate proportionality constant to relate drug concentration in blood or plasma to the amount of drug in the

body.[36] The reported plasma clearance for DOX from the same studies was from  $492 \pm 155$  ml/min/m<sup>2</sup> to  $677 \pm 229$  ml/min/m<sup>2</sup>. [30, 17] A study that spanned over a 72 hour sampling duration fell within the estimated plasma clearance at  $598 \pm 142$  ml/min/m<sup>2</sup>. [30, 37] In terms of rates, the estimated rate of total clearance of DOX is broken down into three categories - renal clearance, hepatic clearance, and formation clearance. Formation clearance is the loss of parent drug due to conversion of the parent drug to a metabolite. The clearance rates for DOX are 30.7 L/hour for total clearance, 0.66 L/hour for renal clearance, 29.97 L/hour for hepatic clearance, and 0.39 L/hour for formation clearance to the primary metabolite DOXol. [11] DOX is also known to bind heavily to both tissues and plasma, with an estimated unbound fraction of about 15%. [11] Overall, DOX exhibits linear pharmacokinetics. [32]

A considerable obstacle in the clinical efficacy of DOX is its cardiotoxicity. [16] Myocardial lesions [4], congestive heart failure [18], and cardiomyopathy [38] are all common conditions resulting from DOX in patients. Both acute cardiotoxicity and cumulative dose contribute to the adverse effects, which often limits its use to induction therapy and short-term use under most protocols. The toxicity profile of DOX has led to substantial work in identifying equivalent drugs that maintain the therapeutic efficacy of DOX without the devastating side effects. Anthracyclines like epirubicin and idarubicin and a similar drug, mitoxantrone, have garnered some success in this search, but DOX remains the most utilized anthracycline. [39] A lifetime cumulative maximum of 550 mg/m<sup>2</sup> has been implemented to help curb morbidity in patients receiving DOX. [40, 19] A cumulative lifetime dose measurement is used for many drugs, as well as radiation, whose regimens include prolonged repeated dosing or exposure. Often times these

cumulative exposures are related to lifetime attributable risk (LAR), which can be used in risk-assessment analyses for the particular drug or toxin.[41] In cancer therapy, the risk of adverse damage by the drug and its total dose must outweigh the potential mortality of the patient. The level to which a lifetime cumulative maximum is set for a drug depends on the population of patients it is treating. For example, if doxorubicin was effective against athlete's foot, the risk of cardiotoxicity would far outweigh the benefit of relief from athlete's foot. However, the risk of cardiotoxicity does not outweigh the benefit of curbing a potentially fatal malignancy. The cumulative lifetime dose of doxorubicin was determined by relating the cumulative lifetime dose to the incidence of congestive heart failure in patients.[42] In a small study by Von Hoff et al., increased likelihood of doxorubicin-induced congestive heart failure (CHF) was found to be linked to increasing total dose. The incidence of patients developing CHF was 3% at 400 mg/m<sup>2</sup>, 7% at 550 mg/m<sup>2</sup>, and 18% at 700 mg/m<sup>2</sup>. Additionally, Von Hoff et al. found that the occurrence of CHF in these patients was significantly lower with a once per week dosing schedule than with a once per 3 weeks dosing schedule of doxorubicin administration.[43] One interesting observation from Table 1-1 is that the majority of the clinical dose regimens currently in use are the latter - once per 3 weeks dosing - which leads to a presumably higher risk for cardiotoxicity. One reason for this could be that the efficacy of DOX has been observed to be less with lower, more frequent doses of DOX. Some suggest that since the tumor growth phase is a relatively short window in the scope of the growth cycle of the cell. Tumor cells are most vulnerable to the cytotoxic effect of DOX during growth phase. Thus shorter, lower doses - even given frequently - are more likely to clear more quickly due to the first-order elimination of DOX and the drug effect is less likely



to coincide with the tumor's growth phase.[44] Unfortunately, the more effective dosing schedule does involve longer, less frequent infusions, but that schedule also correlates to higher incidence of CHF. Finally, the study by Von Hoff et al. revealed that as the age of the patient increased, the incidence of CHF likewise increased.[43, 42] Data from a large number of clinical trials compiled by Rahman et al. showed that approximately 25% of patients having a cumulative dose of 500 mg/m<sup>2</sup> experienced CHF. Additionally, some type of cardiotoxic event occurred in 50% of patients having a cumulative dose of 600 mg/m<sup>2</sup>, and nearly 100% of patients having a cumulative dose at or above 800 mg/m<sup>2</sup>. [45] Another meta-analysis of four clinical trials containing  $\approx$  1200 patients looked at the cumulative incidence of CHF in patients who received DOX. The study by Swain et al. found that an estimated 5% of patients at a cumulative dose of 400 mg/m<sup>2</sup> experienced CHF, 26% of patients experience CHF at 550 mg/m<sup>2</sup>, and 48% of patients experienced CHF at 700 mg/m<sup>2</sup>. [42] It is evident that while there is some variability in the percentage of patients who experience CHF following treatment with DOX, the trend is most certainly that the higher the cumulative dose, the higher the likelihood of adverse cardiovascular effects.

Considering all the historical data up until this point, it is widely accepted that 550 mg/m<sup>2</sup> is the maximum cumulative lifetime dose for DOX that is implemented in chemotherapy protocols. [14, 15, 3, 39, 46] It has been found that overall, approximately 2% of patients who receive a cumulative dose of DOX between 450 mg/m<sup>2</sup> and 550 mg/m<sup>2</sup> experience CHF. [39] The accepted maximum cumulative dose of 550 mg/m<sup>2</sup> is likely a compromise between increased percent risk per mg/m<sup>2</sup> of therapeutic exposure.

As shown in Table 1-1, DOX is more frequently used in combination therapy rather than as a single agent. The maximum tolerated dose (MTD) for a single dose of DOX is 10 mg/kg, which is a popular dose given in murine studies of DOX.[47] Acute toxicity is observed in humans at a 12 mg/kg at a single dose.[48] However, clinically, DOX is always given in cyclic repeated doses, which is also made clear by Table 1-1.[49] This consideration requires much lower doses than the MTD to be given per event. Typically, the highest clinical dose of DOX is 75 mg/m<sup>2</sup>, or 1.9 mg/kg, which is also the highest dose for repeated dosing shown in Table 1-1.[47]

Traditionally, the drugs used in combination regimens are given at or near their maximum tolerated doses (MTDs). While this is sometimes necessary due to virulent nature of cancer, it can introduce a higher risk of dose-related toxicity, which interferes with clinical success. Chemotherapy drugs given at doses close to their MTD are generally robust doses with high inter-patient variability in pharmacokinetic parameters, which could cause significant myeloablation in some patients.[23] Myeloablation refers to the administration of chemotherapy or radiation therapy that does not allow for hematologic recovery. In other words, myeloablation prevents the bone marrow from recovering from the cytotoxicity incurred from the therapy.[50] Support is needed to recover from myeloablation, including platelet or whole blood infusions, intravenous immunoglobulin (IVIG), or donor bone marrow or stem cells.[51] While myeloablation is desired in specific cases such as some bone marrow and stem cell transplants, in most cases it is avoided. Myeloablation compromises immune response and inhibits the effectiveness of accompanying chemotherapy or immunotherapy treatments.[23]

**Table 1-1:** List of Common Types of Cancer Treated with Doxorubicin from Prescribers' Digital Reference[49]

Typical Adult IV Dosing		
Indication	Single Agent	In Combination Therapy
Acute lymphoid leukemia (ALL)	60 to 75 mg/m <sup>2</sup> every 21 days	40 to 75 mg/m <sup>2</sup> every 21 to 28 days
Acute myeloid leukemia (AML)	60 to 75 mg/m <sup>2</sup> every 21 days	40 to 75 mg/m <sup>2</sup> every 21 to 28 days
Breast cancer	60 to 75 mg/m <sup>2</sup> every 21 days	40 to 75 mg/m <sup>2</sup> every 21 to 28 days
Endometrial sarcoma	N/A	45 mg/m <sup>2</sup> every 21 days for up to 7 cycles or until disease progression
Ewing's sarcoma	60 to 75 mg/m <sup>2</sup> every 21 days	40 to 75 mg/m <sup>2</sup> every 21 to 28 days
Gastric (stomach) cancer	60 to 75 mg/m <sup>2</sup> every 21 days	40 to 75 mg/m <sup>2</sup> every 21 to 28 days
Hodgkin lymphoma	N/A	25 mg/m <sup>2</sup> repeated every 7, 14, or 21 days in a 28 day cycle
Multiple Myeloma	N/A	9 mg/m <sup>2</sup> daily for 4 days, every 28 days for 3 to 4 cycles
Neuroblastoma	60 to 75 mg/m <sup>2</sup> every 21 days	40 to 75 mg/m <sup>2</sup> every 21 to 28 days
Non-Hodgkin lymphoma	N/A	50 mg/m <sup>2</sup> every 21 days for 3 to 8 cycles depending on response
Osteogenic sarcoma	30 to 45 mg/m <sup>2</sup> repeated for 2 or 3 days monthly	30 to 75 mg/m <sup>2</sup> repeated 2 or 3 days monthly
Ovarian cancer	60 to 75 mg/m <sup>2</sup> repeated every 21 days	40 to 75 mg/m <sup>2</sup> repeated every 21 to 28 days
Rhabdomyosarcoma	N/A	40 mg/m <sup>2</sup> daily for 2 days in a 52 day cycle, repeated based on staging at diagnosis
Small cell lung cancer	N/A	40 to 50 mg/m <sup>2</sup> every 3 to 4 weeks for 5 to 8 cycles
Soft tissue sarcomas (other)	N/A	15 mg/m <sup>2</sup> per day as a continuous IV infusion over 24 hours (CIV) for 4 days repeated every 21 days for 5 cycles
Thymoma	N/A	40 to 75 mg/m <sup>2</sup> every 21 to 28 days
Thyroid cancer	60 to 75 mg/m <sup>2</sup> every 21 days	40 to 75 mg/m <sup>2</sup> every 21 to 28 days
Transitional cell bladder cancer	60 to 75 mg/m <sup>2</sup> every 21 days	40 to 75 mg/m <sup>2</sup> every 21 to 28 days OR 30 mg/m <sup>2</sup> every 28 days for up to 3 cycles
Wilms tumor	60 to 75 mg/m <sup>2</sup> every 21 days	40 to 75 mg/m <sup>2</sup> every 21 to 28 days

Overall, there is a delicate balance between maximizing the cancer-killing effects of a chemotherapy regimen without causing counter-productive damage to healthy cells and systems. DOX has been and continues to be an integral component of countless chemotherapy regimens for over 50 years. Evaluating the balance of DOX-induced cardiotoxicity and life-saving therapeutic effect, from a quantitative perspective, adds great value to the existing knowledge.

## **1.2 Mechanism of Action-Cytotoxicity**

Although the exact mechanism for how DOX and other anthracyclines enter cells is not fully known, DOX is thought to enter the cell by passive diffusion through the plasma membrane.[52] There is also evidence to support that DOX may also enter the cell through carrier-mediated transport.[29] DOX then binds to proteasomes and breaches the nucleus through selective transport. Once inside the nucleus, DOX is in proximity to the DNA. Since DOX usually has a higher affinity for DNA than for the proteasome to which it is bound, it dissociates from the proteasome to bind to DNA. [52, 53] Once in the cells, DOX interacts directly with DNA, causing double-strand breaks in the DNA of rapidly dividing cells. Again, the complete mechanism is not fully understood[32, 54], despite years of use and study. However, there are two proposed and widely accepted mechanisms for the cytotoxic actions of DOX — (i) free radical generation and oxidative damage, (ii) DOX intercalation into DNA which inhibits topoisomerase II, possibly altering the chromatin structure.[55, 56] The following subsections will describe these two proposed mechanisms for the cytotoxicity of DOX in greater detail.

### 1.2.1 DNA Intercalation

DOX intercalates into DNA which causes a double-strand cleavage, allowing tyrosine remnants of topoisomerase II to form a covalent bond with the DNA. The intercalation effectively traps topoisomerase II, inhibiting proper DNA repair.[54, 15] DNA topoisomerases are large proteins that perform critical actions in DNA strand separation for transcription, replication, segregation, and genetic compaction into cells. Compaction poses a topological constraint in DNA replication, as the entire genome of a single cell, around 3 billion base pairs with an equivalent length of almost 2 meters, into a roughly 6  $\mu\text{m}$  diameter nucleus. Transcription and replication of genomes by copying each base by RNA and DNA polymerases requires DNA strand separation. This strand separation can create DNA super coiling in the flanking regions - regions adjacent to both the 3' and 5' ends of the DNA - where the two DNA strands are separated by polymerase-helicase complexes. Positive super-coiling occurs in front of the replication or transcription sites and negative super-coiling occurs behind it. Super coiling, if not checked by DNA topoisomerases, rapidly stalls replication and transcription and can cause abnormal DNA structures. In general, topoisomerases prevent super-helical tension and knotting in DNA compaction.

The human genome encodes for six topoisomerases. Broadly, there are two types of topoisomerases in humans, Type I and Type II, of which Type I is further subdivided into Type IA and Type IB.[53] Both types of topoisomerase can undo the detrimental super-coiling during DNA strand separation, but it has been shown that other topoisomerases will compensate for the absence of topoisomerase I. However, cells will die in the mitosis phase in the absence of topoisomerase II, since it is apparently vital for

chromosome segregation and condensation.[57] Only topoisomerase II can separate catenanes - interlinked duplex DNA circles. All cells require decatenation at the end of the replication phase to allow for the proper segregation of newly replicated chromosomes.[53] After the topoisomerase II-mediated DNA damage, growth arrest occurs at G1 and G2, which is followed by programmed cell death.[15]

This critical action performed by topoisomerase II makes it an excellent target for anti-cancer drugs. DOX is a DNA intercalator which acts in two ways to disturb topoisomerase depending on the concentration present. At low concentrations, DOX inhibits DNA religation by essentially poisoning topoisomerase II. At high concentrations, DOX prevents topoisomerase II from binding DNA, suppressing topoisomerase II.[53] To summarize, DOX is very effective in thwarting DNA unwinding and strand separation, which stops successful DNA replication and transcription.

Additionally, a recent study by Yang et al. discovered that DOX does enhance nucleosome turnover around gene promoters. Enhancement of nucleosome turnover is consistent with the observed action of DOX, as the enhancement of turnover continues to increase with time of exposure to DOX. This finding was realized by genetically defining a murine squamous cell carcinoma line before and after DOX treatment.[54]

### **1.2.2 Free Radical Generation and Oxidative Damage**

DOX has been found to induce the production of reactive oxygen species (ROS).[58] A semi-quinone is formed when a single electron is added to a quinone moiety in ring C of DOX. This semi-quinone quickly reduces to its parent compound, quinone, by reducing oxygen to ROS - hydrogen peroxide  $H_2O_2$ , for example. The semi-

quinone can also oxidize with the bond between daunosamine and ring A of DOX to form 7-deoxaglycone through reductive deglycosidation (Figure 1-1). Aglycones are notably soluble in lipids and intercalate into biological membranes in vulnerable tissues, forming ROS in close proximity to sensitive targets.[15]

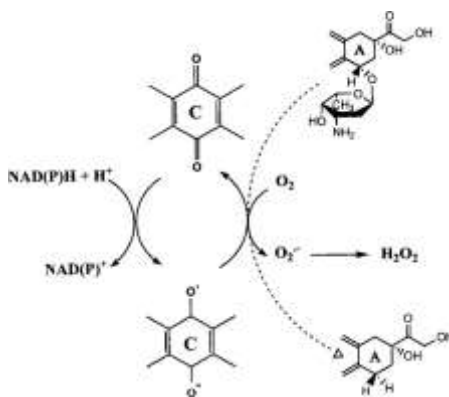


**Figure 1-1:** Single-electron reduction-oxidation cycling of doxorubicin, taken from the review paper by Minotti et al.[15]

DOX-induced ROS then initiate a number of signaling pathways that lead toward cell death by accelerating myofilament apoptosis, suppressing myofilament synthesis, altering cardiac energy metabolism, and causing ultrastructural changes to myocytes.

- (i) DOX-induced ROS activate the protein p53, a known tumor suppressor protein. p53 protein initiates apoptosis of myocytes through transcriptional p38 MAPK-dependent activation. MAPK (mitogen-activated protein kinases) is a target gene pathway often involved in p53-mediated apoptosis.[58, 59]
- (ii) Suppressing myocyte synthesis occurs through the down-regulation of cardiac progenitor cell (CPCs) regulatory transcription factor GATA-4. It is thought that sarcomere protein synthesis is inhibited by the DOX-induced down-regulation of GATA-4. GATA-4 is also critical for postnatal cardiomyocyte survival.[58]

- (iii) Adenosine triphosphate (ATP) is required for most vital processes in the body, but specific to the heart, ATP is required for the relaxation and contraction of the heart muscle. DOX diminishes cardiac energy reserves by lowering both phosphocreatine levels and ATP levels, destabilizing the ratio between the two. Adenosine monophosphate-activated protein kinase (AMPK) activates the catabolic pathway that leads to the production of ATP, and DOX reduces the level of AMPK expression, although the mechanisms underlying this inhibition are not clear.
- (iv) DOX simultaneously motivates calcium release and blocks sarcoplasmic reticulum reuptake of calcium. This interference notably disrupts calcium homeostasis, resulting in cytosolic calcium overload.[58] In an in-vitro study by Kim et al., calcium release from intracellular stores in rat cardiomyocytes was observed under treatment with different concentrations of DOX. The calcium release increased at 60 minutes after treatment with 1  $\mu\text{M}$  DOX and at 15 minutes after treatment with 5  $\mu\text{M}$  DOX.[60] This dose-dependence is consistent with the findings from the first proposed DOX mechanism of DNA intercalation.[53] The overload in calcium likely contributes to contractile dysfunction by activating calpain, a cysteine protease, and stimulating the release of cytochrome c, a proapoptotic factor. Calpains initiate protein turnover of structural and regulatory myofibrillar proteins through cleavage and release of large polypeptide fragments.[58]

The caveat, as with all antineoplastic agents, DOX can not differentiate between healthy cells and cancer cells.[16] The cytotoxic activity of DOX is a double-edged



sword. The properties of DOX that make it a potent and widely-used anticancer agent for over 50 years are the very same properties that limit its clinical use. DOX has a particularly devastating effect in cardiac muscle, which has been covered briefly in the discussion of proposed cytotoxic mechanisms of action above. The dose-dependence of the pharmacodynamic effects of DOX are elucidated in both of the generally accepted mechanisms of DOX, making it an interesting compound for study in dose optimization. The following sections will discuss how the major metabolite of DOX - doxorubicinol - plays a greater role in cardiac damage and a lesser role in therapeutic effect.

### 1.3 DOX Metabolites

DOX is considered a low- to moderate- clearance drug, with clearance values ranging from 42.8 to 68.1 liters per hour.[46] (Figure 1-2).

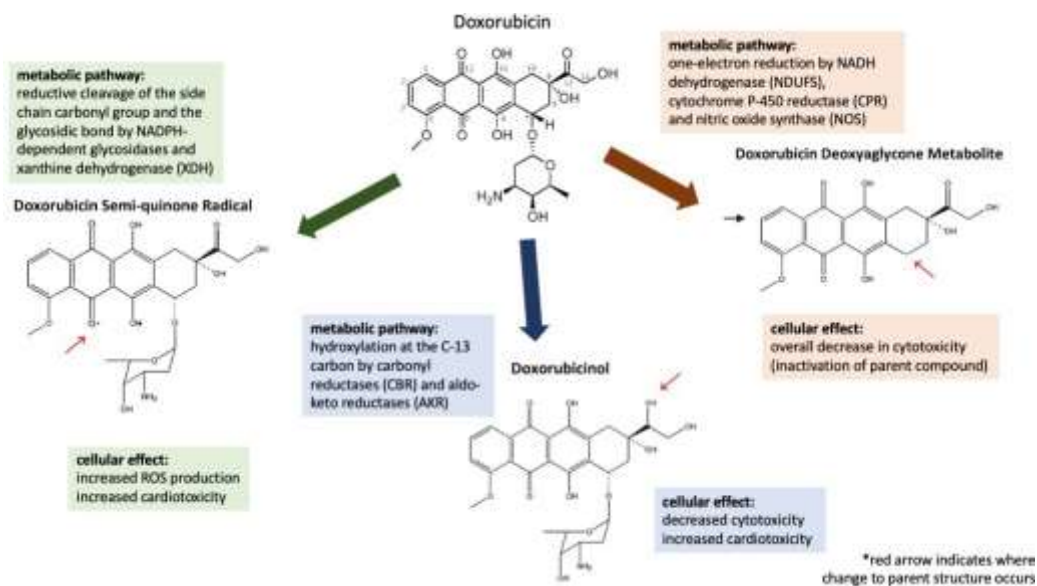


**Figure 1-2:** Main pathways of intracellular doxorubicin (DOX) biotransformation in mammalian cells, including catalytic enzymes involved in its metabolism. The downstream effects of the metabolites are also listed. (adapted from Edwardson et al. [52])

Within a week of administration, approximately 50% of the dose is eliminated through bile and 12% through urine. The fraction eliminated through bile consists of approximately 50% unchanged DOX, 23% DOXol, and the remaining 27% other metabolites. The fraction eliminated through urine is roughly 66% unchanged DOX and the remainder metabolites.[4] This is consistent with the clearance rates which were mentioned in the introduction and originally reported by Pippa et al. The clearance rate for DOX by hepatic clearance was  $\approx 97\%$  of the total clearance rate.[11] It has been estimated that approximately 50% of DOX clears from the body unchanged. The remaining half is converted into three DOX metabolites - doxorubicinol (DOXol), doxorubicin deoxyglycone metabolite (DDM), and doxorubicin semi-quinone radical (DSR) - through three unique metabolic pathways:

- (i) The secondary alcohol metabolite doxorubicinol (DOXol) is formed through hydroxylation at the C-13 carbon group. This hydroxylation is facilitated by carbonyl reducing enzymes, which are a heterogeneous group of cytosolic NADPH-dependent carbonyl reductases (CBR) and aldo-keto reductases (AKR).[52] Carbonyl reductases CBR1 and CBR3 are also known to contribute to the reduction of DOX to DOXol, but the extent to which each of these contributes is uncertain.[55] Accordingly, while both types of carbonyl reducing enzymes are involved, it has been shown that aldo-keto reductases are the primary enzymes involved in hydroxylation of DOX in the human heart.[52] Multiple studies have linked DOXol to cardiotoxicity.[52, 15, 4] Interestingly, since AKRs are fairly universal, the hydroxylation of DOX to DOXol occurs in all cell types.[52] This effect has been studied extensively in red blood cells, as well as liver and kidney

cells.[52, 61] Hydroxylation of DOX to DOXol is considered to be the major metabolic pathway and has been heavily investigated for decades.[52] Even still, the extent to which DOX metabolizes to DOXol is unclear (Figure 1-3).

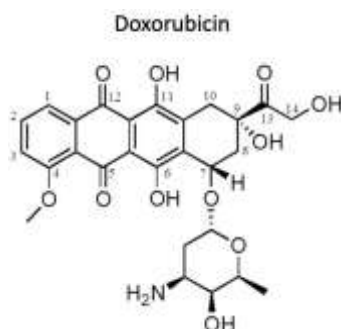


**Figure 1-3:** Molecular structure of doxorubicin

- (ii) The DOX deoxyglycone metabolite (DDM) is formed through the one electron reduction of DOX. The reduction is catalyzed by NADH dehydrogenase (NDUFS), cytochrome P-450 reductase (CPR), xanthine oxidase, and nitric oxide synthase (NOS), which leads to the transformation of the quinone moiety of DOX to a semiquinone radical. This semiquinone radical is stable only in anaerobic conditions, and when exposed to oxygen, it freely re-oxidizes to regenerate its parent compound, quinone. The re-oxidation of the semi-quinone radical to the quinone produce a superoxide anion ( $O_2^-$ ) and hydrogen peroxide ( $H_2O_2$ ) as byproducts, both of which are reactive oxygen species (ROS). These free radicals then cause protein aggregation, peroxidation of lipids within cellular membranes, and sometimes cell death. The oxidation-reduction cycling of DOX has been observed in the sarcoplasmic reticulum, mitochondria, and the cytoplasm.[52] In addition to the production of ROS, this redox cycling of DOX has been shown to produce aldehydes that escape the cell and contribute to DOX toxicity.[14, 52]

Interestingly, DOXol also goes through a similar redox cycle and thereby produces similar ROS byproducts and a DOXol deoxyglycone analog.[40]

- (iii) The last, and most poorly characterized metabolic pathway forms the doxorubicin semi-quinone radical (DSR). Perhaps it is least understood because it only accounts for  $\approx$ 1-2% of DOX metabolism. DSR formation occurs through reductive cleavage of the side-chain carbonyl group and the glycosidic bond, also producing hydroxyglycones and 7-deoxyglycones. It has been proposed that this reaction is catalyzed by an NADPH-dependent reductase- and hydrolase- type glycosidases and xanthine dehydrogenase (XDH). These glycosidases likely include the NADPH quinone oxidoreductases (NQO1) and NADPH-cytochrome P450 reductase (CPR).

These three DOX metabolic pathways vary in extent among different tissue types and conditions; however, in general, the secondary alcohol DOXol is the principal metabolite, with substantially lower percentages of the deoxyglycone metabolite and the semi-quinone radical. The remainder of this section will focus on the metabolite DOXol and its effects on cells.[52]

### **1.3.1 DOXol and Cardiotoxicity**

DOXol is thought to be the major metabolite and retains the therapeutic and cardiotoxic effect of the parent drug DOX.[52] The terminal half-life of DOXol is similar to that of DOX, around 60 hours.[34] It is common for antineoplastic drugs to be measurable in tissues for a prolonged time following administration and that toxicity is often related to drug concentration in the tissue.[62, 40] In a study done on tissue from autopsied human patients by Stewart et al., DOXol was the major metabolite species

found in all tissues.[40] A study conducted on a small cohort of breast cancer patients estimated the DOXol/DOX AUC ratio to be 0.26. Area under the concentration-time curve is a standard measure of drug exposure in pharmacokinetics and will be discussed more in following chapters.

Due to the known cardiotoxic effect of DOX, the potentially extended residence time in cardiac tissue is of most interest. This consideration coupled with the substantial presence of DOXol in cardiac tissue infer that DOXol likely contributes to the cardioxicity seen in patients receiving DOX.[40] Like DOX, DOXol binds significantly to plasma and tissues, with an unbound fraction of only 17%.[11]

Table 1-2 shows the median concentration in select tissues from the 35 autopsied patients. There is sizable variability in the range of values versus the median, which is likely due to a few factors - (i) the small sample size (n=35) with the caveat that not all tissues were able to be used for DOX measurement in all patients, (ii) the wide range in time from last DOX dose to moribund (1-931 days), and (iii) the large difference in cumulative lifetime dose (30-670 mg/m<sup>2</sup>).

**Table 1-2:** *Median Concentration of DOX and DOXol in Autopsy Tissue from 35 Human Patients in Stewart et al. Study; 35 Patients Received Cumulative Lifetime Dose of 30-670 mg/m<sup>2</sup> with Last Dose from 1 - 931 Days (Source [62])*

	Median DOX Concentration (ng/g)	Median DOXol Concentration (ng/g)
Heart	58 (0-1665)	92 (0-484)
Liver	115 (0-2030)	198 (0-674)
Kidney	53 (0-2773)	104 (0-896)

Each of these factors contribute to the variability in the DOX and DOXol measurements in tissues. The scarcity of available human autopsy tissue for such

observation along with ethical considerations are certainly obstacles, but the available data is nonetheless invaluable for comparison with subclinical studies. [40] As shown in Table 1-2, the liver and kidney both have higher concentrations per gram than the heart. Higher DOX and DOXol concentrations in the liver and kidney are also observed in animal species.[63, 64] However, the liver and kidney are not major sites of toxicity for patients receiving DOX, which leads to conjecture other factors differentiating DOX and DOXol behavior in tissues. One such conjecture is that liver and kidney tissues are rich in binding and inactivating substances due to their excretory and metabolic functionalities, which prevent DOX and DOXol from causing cellular damage in those tissues.[40] For example, reduced DOX toxicity is observed in the presence of glutathione - a common antioxidant found in the liver.[65]

In a study of isolated cardiac tissue from rabbits, DOXol was nearly 30 times more effectual at suppressing systolic cardiac function. A 90  $\mu\text{M}$  dose given at 50  $\mu\text{g}/\text{ml}$  decreased contractility, a measure of systolic function, by roughly 69% of the baseline measure. In contrast, a comparable dose of DOX, 350  $\mu\text{M}$  at 200  $\mu\text{g}/\text{ml}$ , only depressed contractility by about 11% of the baseline. The maximum dose of DOX at 700  $\mu\text{M}$  at 400 $\mu\text{g}/\text{ml}$  only decreased contractility by 29%. Myocardial resting stress, a measure of diastolic cardiac function, was also tested with both DOX and DOXol using the isolated rabbit cardiac tissue model. DOX also had a negligible effect on diastolic cardiac function even at 700  $\mu\text{M}$  dosing, while DOXol increased myocardial stress by approximately 395%. Therefore, DOXol suppressed both systolic and diastolic myocardial function more severely than DOX. Calcium pump activity, described as both  $\text{Ca}^{2+}$  stimulated ATPase sarcoplasmic reticulum activity and rate of calcium loading, was

also evaluated in both DOX and DOXol. DOX was not found to be a strong inhibitor of calcium pump activity, while DOXol nearly destroyed all calcium pump activity in the heart tissues.

This study highlights another interesting property of DOX and its metabolite DOXol - its extent of intracellular uptake. DOXol is known to have less intracellular uptake than DOX, and yet the major species residing in tissue has been shown over time to be DOXol.[66] The most reasonable explanation for this inequity is that the hydroxylation of DOX to DOXol is carried out primarily by aldo-keto reductases (AKR).[52] AKRs are abundantly present in most human tissues, so it is thought that during this observed prolonged residence time in the tissue, DOX metabolises to DOXol over time.

Disappointingly, the aggressive cell-destroying capabilities of DOXol does not translate to cancer cell destruction. A potency study was conducted in three different cancer cell lines using a metric called  $IC_{50}$ , which is the concentration of an inhibitor where 50% response is observed. In this case, the concentration of DOX or DOXol needed to inhibit the growth of colonies by 50% compared to the control group. As shown by the ratio of  $IC_{50DOXol} / IC_{50DOX}$  in Table 1-3, it takes 5 to 28 times as much DOXol to inhibit the same cancer cell lines as DOX. DOXol is therefore a much less effective anticancer agent in comparison to DOX. In fact, it has been estimated that DOXol is 75 times less effective than DOX while apparently contributing heavily to the cardiotoxicity associated with DOX.[15, 8] It is clear that factors beyond cumulative lifetime dose are at play in the marked cardiac damage caused by DOX. The profoundly greater cardiotoxic properties of DOXol and its conversion from DOX to DOXol in the

tissues. This finding has been applied clinically with the lifetime maximum dose cap applied to DOX and other anthracyclines.[52] This is one motivation for utilizing therapeutic dose monitoring in anticancer drugs. Maximizing cancer-killing effect generally means giving as much drug as can be reasonably tolerated. With the breadth of data available on popular drugs like DOX, it could be possible to have a more tailored approach in order to curb some of the devastating side effects.

**Table 1-3:** *IC<sub>50</sub> for DOX and DOXol in Three Cancer Cell Lines from a Study by Olson et al.[66]*

Cell line	Doxorubicin, <i>IC<sub>50</sub></i> in $\mu\text{M}$	Doxorubicinol, <i>IC<sub>50</sub></i> in $\mu\text{M}$	DMF, <i>IC<sub>50-ol/IC<sub>50-in</sub></sub></i>
PANC-1	$1.4 \pm 0.2$	$35.4 \pm 4.7$	25
PD PaCa	$1.6 \pm 0.2$	$44.5 \pm 0.5$	28
WD PaCa	$9.8 \pm 1.5$	$49.5 \pm 1.1$	5

#### 1.4 Conclusion

Doxorubicin is a chemotherapy agent which has particularly potent cytotoxic capabilities, and its three metabolites are thought to also be cytotoxic in varying intensities. DOXol is the major metabolite and plays the greatest role in cytotoxic activity.[33] In general, DOXol has a greater cardiotoxic effect and a lesser therapeutic effect than its parent drug. While DOXol accounts for the greater majority of DOX metabolites, it has a much lower intracellular uptake than DOX. Conversely, while DOXol has a lesser effect on cancer cells, it induces a higher toxicity in healthy cells, particularly cardiomyocytes. Cumulative lifetime dose certainly plays a role in DOX toxicity, and intracellular uptake occurs with both DOX and DOXol.[66] While DOXol has a lesser uptake, DOXol is typically found in greater amounts per gram in tissues. This



is likely due to the gradual conversion of DOX to DOXol in tissues by aldo-keto reductases which are present in most human tissues, abundantly so in cardiac tissue.[52] These paradoxes complicate the therapeutic dosing of DOX in cancer patients.

One way these challenges can be better understood is through the mathematical and statistical modeling using observed pre-clinical and clinical data.

## **1.5 Outline of Content in Each Chapter**

Chapter 1 has outlined the properties of the anthracycline Doxorubicin (DOX) as a potent chemotherapy agent and also a cardiotoxin. However, the primary metabolite Doxorubicinol (DOXol) has been found to be the main culprit for cardiotoxicity. The organ-specific toxicity of the metabolite DOXol in a specific tissue can be estimated using what is called a physiologically-based pharmacokinetic (PBPK) model.

The overview is intended to frame DOX/DOXol as a good candidate for pharmacokinetic modeling, specifically under the more physiologically based modeling methods that will be discussed in later sections.

Chapter 2 will continue with background information, introducing the concepts of pharmacokinetic modeling. The discussion of pharmacometrics will be agnostic to the specific drug, DOX, but the defining of terms and methodologies of this type of modeling is important for understanding the models in this work.

Chapter 3 will take the fundamentals from Chapter 2 and expand on existing pharmacokinetic models in DOX. However, a classic pharmacokinetic model cannot capture the specific organ concentrations, which is the interest of this work. Thus, the latter portion of Chapter 3 will introduce the more modern approach of physiologically-based pharmacokinetic (PBPK) modeling as it pertains to DOX. A whole-body PBPK

porcine model of DOX, adapted from literature, will be described in detail. The PBPK model is comprised of a system of 44 ordinary differential equations for which there is no exact solution, so numerical methods must be employed to solve the system.

Chapter 4 will walk through the process of testing different numerical methods on the system. The method needed to be both accurate and efficient, which for large systems of equations, can be a difficult balance in the programming language R. Once a suitable method was determined for solving the PBPK model in pigs, the model could be scaled across species - from sub-clinical species to humans. Sensitivity analysis and the optimization package 'optim' in R was used to fit the initial data set. This data set contained both DOXol heart tissue concentration and venous blood DOX concentration in mice. Allometric equations were tested on sensitive parameters one representative rat, rabbit, dog, pig, and human data set to determine the best relationship.

The final chapter discusses the potential application of the process of getting organ-level concentration predictions using a PBPK model and scaling it to humans. Therapeutic drug monitoring is used in many drugs similar to DOX in that they almost always have a narrow therapeutic index. Additional future work could include pharmacodynamic studies which relate pharmacodynamic response to some organ specific toxicity and the application of this process to other drugs.

## CHAPTER 2

### PHARMACOMETRICS OVERVIEW

#### 2.1 Pharmacokinetic Versus Pharmacodynamic

Pharmacometrics is a contemporary discipline that characterizes interactions between the drug and the patient using mathematical modeling of the physiology, pharmacology, and disease involved. The term “pharmacometrics” was coined by the Journal of Pharmacokinetics and Biopharmaceutics in 1982.[67] Pharmacometric modeling can be generalized as one input-response model that is divided into two pieces - pharmacokinetic and pharmacodynamic.[68] Pharmacokinetics is broadly described by Holford and Sheiner in 1982 as the “study of the movement into, through, and out of the body.” They went on to summarize the scope of pharmacokinetics as “the processes and rates of drug movement from the site of absorption into the blood, distribution into the tissues, and elimination by metabolism.”[69] In short, pharmacokinetics explains the input phase which characterizes the relationship of controllable drug inputs - dose amount, dosage form, frequency, and route of administration - and concentration over time.[68] Broadly, pharmacodynamics describes the effect of the drug once it reaches its site of action. Specifically, pharmacodynamics considers the factors affecting the relationship between the drug effect and the drug concentrations at the site of action. Pharmacodynamics and pharmacokinetics are critically enmeshed with each other, but they are two distinct components of a pharmacological profile. In short, pharmacokinetics

is how the body handles the drug and pharmacodynamics is how the drug affects the body.[69].

While they are considered separate sub-disciplines, they are more powerful when used together, as they each contain important information needed to capture observed relationships among dose, concentration, and effects over time, make predictions, and optimize dose regimens. For example, Figure 2.1 illustrates a simplified schematic of the input-response process for designing an optimum dose regimen. First, the pharmacokinetic phase explains how the drug input is related to the exposure - measured from concentration over time. Once the pharmacokinetic profile is obtained, the pharmacodynamic phase relates exposure to the effects on the body. The curved arrows give feedback at each step to adjust the dose regimen based on adverse or desired effect, which may require a change in concentration, and consequently, an adjustment in dose regimen, which affects the concentration. Using this model and trial-and-error adjustment can ultimately conclude in a mathematically optimized dose. The resultant PK/PD relationships are visualized in Figure 2-2. Pharmacologic effect can only be predicted and optimized with data from both the pharmacokinetic (concentration vs time) and the pharmacodynamic (effect vs concentration).[68]

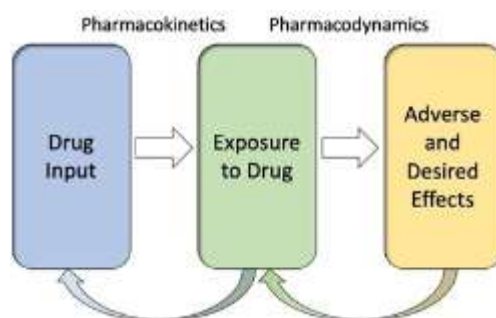


**Figure 2-1:** Schematic of a PK/PD workflow with feedback for the purpose of optimizing a dose regimen

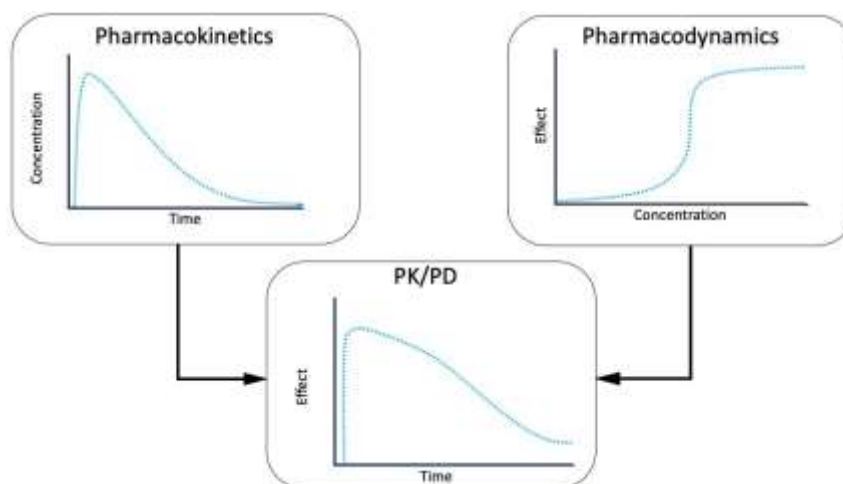


**Figure 2-2:** Visualization of how the pharmacokinetic relationship of drug concentration versus time and the pharmacodynamic relationship of effect versus concentration come together to create an effect over time profile, adapted from Derendorf et al.[68]

## 2.2 Compartmental Body Models

### 2.2.1 Compartment Model Concept

In pharmacokinetics and pharmacodynamic modeling, it is conventional to represent the body as a system of compartments. The simplest type of model is a one compartment model, which makes the assumption that the human body is one kinetically homogeneous compartment. It also assumes that any rates between compartments and the rate of elimination from the body are linear. In most cases, the anatomical analog for the single compartment in a one compartment model is the plasma or venous blood. However, the assumption cannot be made then that the one-compartment model is equivalent to the concentration of the drug in all the tissues and fluids in the body. Instead, modelers can interpret drug levels in other tissues and fluids in terms of rates of change. For example, a 25% decrease in the central compartment or plasma concentration corresponds to a 25% decrease in all other tissues and fluids in the body.[36]

One-compartment models are especially useful for drugs that distribute rapidly through the body, but often times drugs will not demonstrate a linear elimination from the body. In these cases, additional compartments are added to simulate the residence time of the drug in tissues and its eventual release back into the circulatory system before elimination.[36] Multi-compartment models tend to have a more defined distributive and post-distributive phase in their concentration versus time profiles as compared to the one-compartment model which appears to be more constant (Figure 2-3).[36, 70]

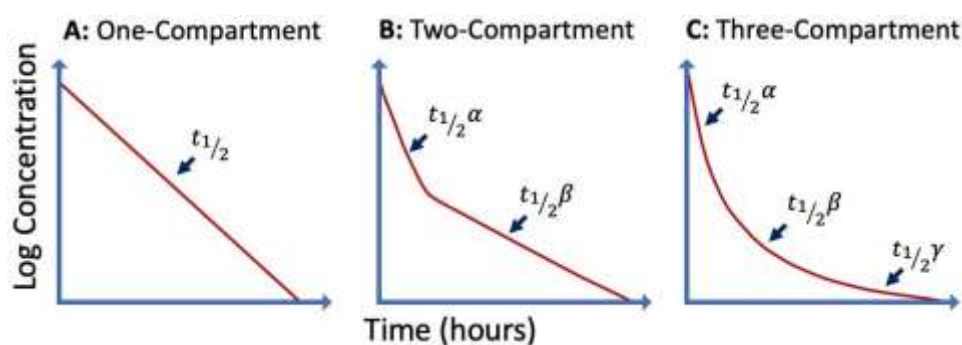


**Figure 2-3:** Adapted from Ratain et al., examples of one-compartment (A), two-compartment (B), and three-compartment (C) concentration-time plot[70]

The distributive phase characterizes the dosing of the drug and its initial dispersion to respective tissues and fluids in the body. The post-distributive phase includes the pseudo-equilibrium achieved as the drug is bound, metabolized, eliminated, transformed, etc. in the tissues and then released back into the circulation. The multiple compartments generally represent groups of organs, tissues, or fluids, which vary depending on the drug. In general, the organs, tissues, and fluids that decline more rapidly during the distributive phase than the post-distributive phase are included in what is called the central compartment. The peripheral compartments generally include more poorly perfused tissues in which drug concentrations will increase, reach steady state, and

slowly return to the venous blood. How these compartments are defined for a model is drug specific; therefore, the tissues and fluids included in the central compartment for one drug may be in a peripheral compartment for a different drug. For example, the brain is a highly perfused, or highly vascular, organ. However, in polar drugs which are unable to cross the blood-brain barrier, the brain would likely be included in the peripheral compartment; whereas, in lipid-soluble drugs that can cross the blood-brain barrier, the brain would likely be included in the central compartment.[68] It is important to note that although these compartments are mathematically representative of these tissues and fluids, compartments do not hold any true physiological reality.

The time courses of these drugs in terms of rates, particularly in the peripheral compartments, may not exactly correspond to any actual flow rates. The compartmental modeling approach allows for extremely complex systems to be modeled in a reasonable, simplified way. At best, these peripheral compartments are a conglomeration of physiological functional groups of tissues and fluids. The central compartment is generally what is compared or fit to observed data in order to make the descriptive and predictive models that are actually utilized. Peripheral compartments allow the modeler to simulate the complex time courses of drug levels throughout the body in an understandable and reasonably accurate manner.[36]

### **2.2.2 Compartment Model Equations**

Now that the concept of compartments has been introduced, these models can be discussed from a mathematical standpoint. From the perspective of an engineer, if the body represents a chemical plant, then the drug is the chemical moving through the various components in the chemical plant. The compartments can be thought of as the

components of the chemical plant – transforming, retaining, releasing – the chemical, or drug. A mass balance can be applied to the system, which is a physical application of the Law of Conservation of Mass. The mass entering the system must be equal to the mass leaving the system. This conservation of mass is true for drugs in the body - drug that enters the body is either stored, transformed, or eliminated from the system eventually. Each compartment is represented by an equation, which are then coupled into a system of equations. One can solve for as many unknowns as there are equations in the system; therefore, for example, there are three equations in a three compartment model, which allows the modeler to retrieve the unknown – concentration over time – for each compartment in the system.[71]

The equations for compartment models can be derived from ordinary differential equations, and the case of the one-compartment pharmacokinetic model is the simplest example to derive and discuss conceptually. Concentration time course for such a model is shown in Figure 2-3A. The following discussion will go through the considerations in the parameters and relationships in a simple one-compartment pharmacokinetic model.

Clearance (CL) is rarely measured directly in clinical practice, but rather it is calculated by one of the following equations using more measurable values:

$$CL = \frac{dose}{AUC}, \quad (\text{Eq. 2-1})$$

$$CL = \frac{R_{in}}{C_{ss}}, \quad (\text{Eq. 2-2})$$

where AUC, or area under the concentration-versus-time curve, is the drug exposure integrated over time,  $R_{in}$  is the infusion rate, and  $C_{ss}$  is the concentration at steady state.[70] Equation 2-1 is typically more convenient for bolus-type injections since the clearance is simply dose over exposure as measured by AUC. Equation 2-1 also shows



the practical relationship between dose and AUC - the lower the AUC for a given dose, the higher the clearance and conversely, the higher the AUC for a given dose, the lower the clearance. For continuous infusions, a steady state is achieved in the plasma, so Equation 2-2 is generally more convenient. The concentration at steady state ( $C_{ss}$ ) can be obtained from a single plasma measurement once the steady state is achieved. Then, clearance can be estimated by Equation 2-2 and the relationship observed. The higher the concentration at steady state given an infusion rate, the lower the clearance, and vice versa.

Clearance can also be considered a function of both distribution and elimination, as shown in the following model:

$$CL = V_{dist} \times k, \quad (\text{Eq. 2-3})$$

where  $V_{dist}$  is the volume of distribution and  $k$  is the elimination constant.  $V_{dist}$  is the volume of the compartment, or conceptually, the volume of liquid the dose is diluted, and  $k$  is inversely proportional to the half-life of the drug. Thus, a short half-life implies a large  $k$  value and therefore, a high clearance. A large  $V_{dist}$  implies a large volume to dilute the dose, and thus a low initial concentration. In general, a large  $k$  value and a large  $V_{dist}$  produce a high clearance rate and fairly low plasma concentrations.[36, 70, 72]

Now that some terms and relationships are defined, the simplest pharmacokinetic model follows,

$$C_p = \frac{dose}{V_{dist}} (e^{-kt}), \quad (\text{Eq. 2-4})$$

where  $C_p$  represents the concentration in the plasma, which is most commonly the central compartment. Equation 2-4 assumes that the injection occurs instantaneously and that the entire dose is also distributed evenly throughout the body instantaneously. Modifications

of the equation can be made for slower injections or infusions, where two equations would represent the model over different time intervals:

$$C_p = \frac{dose}{V_{dist} \times k \times T} (1 - e^{-kt}) \quad (\text{Eq. 2-5})$$

for the interval over which the drug is being administered, where  $k$  is still the elimination constant and  $T$  is the time interval over which the drug is administered. When the infusion ends, the kinetics play out as if an instantaneous bolus as in Equation 2-4 has occurred at the exact moment the infusion ends. There is an initial concentration of the existing concentration in the plasma, or  $C_p$ , at that time point. That equation for the concentration over time from the end of the infusion to the end of the time interval is as follows:

$$C_p = C_p \times T \times e^{-k(t-T)} \quad (\text{Eq. 2-6})$$

These equations explain how this one-compartment model operates under the assumption that the half-life, and thus  $k$ , will remain constant, and the instantaneous rate of change only depends on the current concentration. A one-compartment model is not often inadequate for more complex pharmacokinetic data, in such cases, the data is fit to a multi-compartment model. Which, as discussed in the Compartment Model Concept section, simply couples equations similar to Equations 2-4 and 2-5 into a system corresponding to the number of compartments needed to fit the data.

### 2.3 Pharmacokinetics Concepts

Pharmacokinetic modeling is often described as the characterization of the time courses of drug concentration through four major processes in the body (i) absorption, (ii) distribution, (iii) metabolism, and (iv) excretion, commonly referred to as ADME. More broadly, pharmacokinetics also considers the time course of the concentration relevant

metabolites of the parent drug and the development of suitable models to describe observations or predict outcomes.[70, 68]

One way to think of the four processes are in terms of what happens to the total dose. In Figure 2-4, the equivalence of the dose to the drug in four locations or processes in the body demonstrates the conservation of mass in a material balance. Figure 2-4 also shows that the ADME processes are sufficient to encompass any state a drug might be in transit through the body. The following subsections will discuss each of the ADME processes through the lens of pharmacokinetics. The following subsections will discuss each of the ADME processes through the lens of pharmacokinetics.



**Figure 2-4:** A way of combining the idea of material balance and the four pharmacokinetic processes (Absorption, Distribution, Excretion, and Metabolism)

### 2.3.1 Absorption

Absorption in pharmacokinetics is discussed in terms of systemic absorption and is defined as the course of action an unchanged drug undergoes from the site of administration to the site of measurement. For example, under this definition, we consider a drug that is given orally, decomposed by 50% in the gastrointestinal tract, and then metabolized completely in the liver. If the site of measurement is a vein in the arm, the unchanged drug never reaches the site of measurement. However, if the site of measurement is in the portal vein, 50% of the unchanged drug reaches the site of administration. Any loss of drug between the administration site and the measurement

site will contribute to a decrease in systemic absorption. There are many possible sites of loss, especially in orally administered drugs. In those cases, the drug must pass through the gastrointestinal tract and liver where drugs are often eliminated to some extent through metabolism or excretion. The loss, or elimination, of unchanged drug on this passage through the the gut, or any drug-eliminating organ, is referred to as the first-pass loss.[72] Drugs which have a high first-pass loss require higher doses when administered orally than when administered intravenously in order to reach the same therapeutic effect. Drugs, when given intravenously, are able to bypass the gastrointestinal tract and liver before reaching the circulation. However, absorption is not only applicable to orally administered drugs, but also to intramuscular, intrathecal, subcutaneous, or any other extravascular route of administration.[68] The term bioavailability more universally quantifies the extent of absorption as a fraction or percentage of the administered, unchanged drug that is absorbed intact and reaches the site of action following any route of administration.[72]

### **2.3.2 First-Order Kinetics**

The premise of first-order kinetics in terms of absorption following an extravascular dose is that the absorption of the drug is dependent on the concentration of the drug at that time.[73] In other words, the absorption rate is proportional to the amount remaining to be absorbed.[68] The most common approach to modeling absorption is to assume first order kinetics, which is illustrated in Figure 2-5, where  $A_1$  is the amount of drug at the administration site,  $A_2$  is the amount of drug in the body,  $CL$  is the clearance,  $V_{dist}$  represents the volume of distribution,  $dose$  is the amount of drug administered,  $k_a$  is the absorption rate, and  $F$  represents the bioavailability.

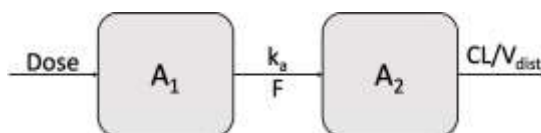


**Figure 2-5:** Example of a one-compartment model with first-order absorption and also first-order elimination

The model equations follow:

$$\frac{dA_1}{dt} = -k_a * A_1 \quad (\text{Eq. 2-7})$$

$$\frac{dA_2}{dt} = k_a * A_1 - \left(\frac{CL}{V_{dist}}\right) * A_2 \quad (\text{Eq. 2-8})$$

$$C_p = \frac{A_2}{V_{dist}} \quad (\text{Eq. 2-9})$$

The initial conditions for Equations 2-7 and 2-8 are:

$$A_1 = dose * F \quad (\text{Eq. 2.10})$$

$$A_2 = 0 \quad (\text{Eq. 2.11})$$

again, where *dose* is the amount of drug administered and *F* is the bioavailability. The concentration in the central compartment ( $C_p$ ), or the circulation, can be obtained by solving Equations 2-7 and 2-8 with initial conditions, Equations 2-10 and 2-11. The equation for the solution is as follows:[73]

$$C_p = \frac{F*k_a*Dose}{V_{dist}*(k_a - \frac{CL}{V_{dist}})} * \left( e - \frac{CL}{V_{dist}} * t - e^{-k_a*t} \right) \quad (\text{Eq. 2-12})$$

### 2.3.3 Zero-Order Kinetics

In the case where a drug is absorbed at an approximately constant rate, the absorption kinetics are said to be zero-order.[68] In other words, a constant amount (i.e. milligrams, moles, etc) of drug is absorbed per unit time. This is in contrast to first-order absorption kinetics in the aspect that the absorption is not dependent on the concentration at that time. An example of zero-order absorption and linear elimination in a one compartment model is shown in Figure 2-6,

where  $R_0$  is the zero-order input (i.e. intravenous injection or infusion),  $A_2$  is the amount of drug in the body,  $CL$  is the clearance, and  $V_{dist}$  is the volume of distribution. The model equation follows:

$$\frac{dA_2}{dt} = R_0 - \left(\frac{CL}{V_{dist}}\right) * A_2 \quad (\text{Eq. 2-13})$$

where again,  $C_p = A_2/V_{dist}$ , as noted in Equation 2-9. By solving Equation 2-13, the concentration of the drug in the central compartment  $C_p$  can be expressed as: [73]

$$C_p = \frac{R_0}{CL} * \left(1 - e^{-\frac{CL}{V_{dist}} - t}\right) \quad (\text{Eq. 2-14})$$



**Figure 2-6:** Example of a one-compartment model with zero-order absorption and linear elimination

The initial conditions for Equations 2-13 and 2-14 are:

$$R_0 = \text{dose} \quad (\text{Eq. 2-15})$$

$$A_2 = 0 \quad (\text{Eq. 2-16})$$

where *dose* is the amount of drug administered. The concentration in the central compartment ( $C_p$ ) can be obtained by solving Equations 2-13 and 2-14 with initial conditions, Equations 2-15 and 2-16.

### 2.3.3.1 Flip-Flop Kinetics

Particularly with orally administered drugs, frequent dosing can limit the effectiveness of a drug by lowering the likelihood that the patient will adhere to the dosing schedule. This problem is often referred to as patient compliance, and it is a major consideration in the drug delivery process. Sustained- and controlled- release formulations are ideal for drugs which require frequent doses due to its half-life, bioavailability, or other physiological property.[73]

However, in these cases, absorption is rate-limiting. That is to say, the absorption process is much slower than the elimination process. The peak concentration tends to occur later and is lower than in cases of first- and zero- order kinetics. At peak concentration, the rate of elimination increases and equals the rate of absorption. However, the absorption rate is so slow that there is still a substantial amount of drug yet to be absorbed well past the time of peak concentration. In this post-distributive phase, the plasma concentration is declining, since the elimination rate is still faster than the absorption rate, but the difference between the two rates is small. Thus, the rate of elimination is approximately equal to the rate of absorption. Eventually, there is no more drug left to be absorbed and the drug is eliminated from the body. This behavior can be deceptive, as it can appear that the elimination phase is very slow - when in fact it is the absorption that is slow.[68] Failing to recognize flip-flop kinetics when modeling orally administered drugs can lead to an incorrect characterization of the absorption process and an ill-specified model. Therefore, when possible, intravenous data is utilized to estimate the pharmacokinetic parameters associated with absorption.

#### **2.3.4 Distribution**

Distribution defines the process of reversible transfer of drug between the site of administration and peripheral tissues.[68] In terms of compartment models, peripheral tissues are the peripheral compartments in which, during the distributive phase, drug concentrations increase, reach steady state, and slowly return to the central compartment. Under these terms, the central compartment is the circulation.[36] The rate of transfer from the circulation is not necessarily the same rate of transfer back into the circulation. A good example of the difference in these rates is the enterohepatic cycle. Drug is secreted in the bile, stored in the gallbladder, and then released into the small intestine, where some of it is reabsorbed into the circulation.[68]

A term mentioned briefly but not well defined in Section 2.3.1 on Absorption was the  $V_{dist}$  or volume of distribution in the equations discussing clearance and absorption kinetics. The volume of distribution is not a literal volume of liquid, but rather a surrogate proportionality

constant to relate drug concentration in blood or plasma to the amount of drug in the body.[72, 36] Formally, it may be more appropriate to call it the *apparent* volume of distribution. If we were to consider the *actual* distribution volume of a drug, it would be a fraction of total body water.[36] For the average adult human, total body water (TBW) accounts for 50-70% of the body weight.[74] TBW is broadly subdivided into extracellular fluid and intracellular fluid. Intracellular fluids make up for approximately 62.5% of TBW and includes fluid contained within cells. Extracellular fluids make up the remaining 32.5% and includes plasma and interstitial fluid. These categories of account for approximately one-fifth and four-fifths of total extracellular fluids, respectively. Transcellular fluid, that is, fluids such as ocular, cerebrospinal, and gastrointestinal fluids that are contained in organs, are generally not included in calculations. It is also important to note that the blood volume is divided between both intra- and extracellular fluids. Intracellular fluids exist inside the blood cells and extracellular fluids are the blood plasma.[75] These values are estimates, as fluids in the body are always in flux between different compartments of the body due to regulative mechanisms that maintain appropriate concentrations throughout.[74]

Apparent volume of distribution varies by drug based on that specific drug's physicochemical properties. For instance, drugs that are more extensively bound to plasma proteins have apparent volumes of distribution that might be smaller than their actual volumes of distribution. Conversely, drugs that are more extensively bound to extravascular tissues have apparent volumes of distribution that might be much larger than their actual volumes of distribution. Apparent volumes of distribution in humans can range from as small as  $0.04L/kg$  to greater than  $20L/kg$  among different drugs, some values of which exceed total body size when taken literally.[36, 68, 72] Now that the distinction between apparent and actual volumes of distribution has been made, the term volume of distribution will interchangeably refer to the *apparent* volume of distribution hereafter.



#### 2.3.4.1 Membranes

To best explain drug distribution, it is important to discuss the role and function of membranes. Drug transport, a key component in drug distribution, is defined as the processes and transport systems that facilitate the movement through membranes. The purpose of the cell membrane is to maintain homeostasis inside and outside of the cell body. Extracellular fluid is high in chloride ions and sodium, and low in potassium, phosphates, and protein. Conversely, intracellular fluid is high in potassium, phosphates, and protein, and low in chloride ions and sodium. The balance of these substances is required for healthy functioning of the body's systems.

A lipid bilayer makes up the majority of the cellular membrane with many proteins either partially or fully penetrating the lipid. Although some more lipophilic substances will be able to pass directly through the lipid bilayer, many of these proteins which penetrate the membrane completely can function as transport proteins. There are two general types of these transport proteins - channel proteins and carrier proteins. Channel proteins have aqueous spaces throughout and can allow water and certain ions and molecules to move through freely. Carrier proteins bind with molecules or ions, and the resultant conformational changes in the protein molecule allow the substance to pass from one side of the membrane to the other. Both channel proteins and carrier proteins are selective in which ions and molecules are allowed to pass through them and by proxy, the membrane.[76] These two types of proteins are important for describing the transport processes of drugs across membranes. Channel proteins are key players in diffusion and carrier proteins are key players in both diffusion and active transport. Diffusion and active transport will be expounded upon in the Transport Processes section. A few terms and relationships should be briefly defined before discussing the properties of cellular membranes. Hydrophilic and hydrophobic are terms that refer to properties of substances that are attracted to or repelled by water, respectively. Likewise, lipophilic and lipophobic are

terms that refer to properties of substances that are attracted to or repelled by lipids, respectively. A substance that is soluble in water and poorly soluble in non-polar lipids could be described as both hydrophilic and lipophobic. Conversely, a substance that is soluble in non-polar lipids but not soluble in water could be described as hydrophobic and lipophilic. In other words, the pairs of terms are interchangeable. One way to quantify the lipophilicity of a substance is to measure its partitioning between n-octanol, which is an organic solvent whose properties mimic tissue membranes, and water. Substances with higher partition coefficients have higher lipophilicity and vice versa.[68]

#### 2.3.4.2 Permeability

Permeability is defined as the measure of a drug's ability to cross a membrane. A drug is considered highly permeable if it can pass through a membrane quickly and less permeable if it cannot. Quantitatively, permeability is expressed as ease of penetration of membrane in terms of velocity (distance per time). This unit comes from the concept of the net rate of transport of drug across a membrane as shown in Figure 2-7.



**Figure 2-7:** Schematic of the contributing factors of the net transport rate across membranes in the cell - the permeability of the membrane, the surface area of the cell, and the concentration difference inside and outside the cell

If we consider a simple example of two compartments ( $C_1$  and  $C_2$ ) separated by a membrane, the three components of net rate of transport are the concentration difference, the surface area ( $SA$ ) of the membrane, and the permeability of the substance ( $P$ ). Since

net rate of transport is measured in units of volume per time, the surface area of the membrane is in units of area, and the concentration difference between either side of the membrane is unit-less, then the permeability is in units distance per time or velocity. The concentration difference is treated like a scalar for the net rate of transport; when the concentration difference is zero, the system is at equilibrium and there is no net exchange between the two compartments and the equation in Figure 2-7 goes to zero.[68] Just like in chemical equilibrium, a net change of zero does not mean there is no movement between the compartments  $C_1$  and  $C_2$ , just that the movement is equal in both directions. The surface area of the membrane has a notable effect on the net rate of transport. Based on the illustrated equation in Figure 2-7, doubling the surface area effectively doubles the net rate of drug transport. Keep in mind that the permeability is a property of the drug and remains constant.

Size, lipophilicity, and degree of ionization (charge) are the three molecular properties that most affect the passage of a drug across a given membrane. Cell membranes tend to be inflexible which prevents drug molecules of a certain size or steric conformation to pass through the membrane. For instance, some membranes do not allow for water-soluble molecules to pass through, so they must take the paracellular pathway and slip through the tight channels between cells.[68] Molecular size is an obvious limitation for transport and has an underlying effect on all other molecular properties related to transport processes. Since the majority of the cell's membrane is made up of the lipid bilayer it is not surprising that a drug's lipophilicity is another major constraint on membrane permeability.[76] Typically, the lower the lipophilicity, the less its permeability and vice versa. However, molecular size does have an overarching effect on

the permeability. It will not matter how lipophilic the drug is if it is too large to easily pass through the membrane. For instance, for permeability across skin, if the molecular weight of a compound is doubled with the same lipophilicity, the permeability decreases almost 300-fold. An common example of the interaction of size and lipophilicity in terms of permeability is the movement of drugs to and from the central nervous system (CNS) via the blood-brain barrier (BBB).[68] The blood-brain barrier is formed by the brain endothelium and creates a diffusional restriction in order to protects the particularly sensitive spinal cord and brain from unwanted substances circulating in the blood. The barrier property of the BBB also controls the influx and efflux of substances needed by and excreted from the brain and rigidly controls the ion homeostasis which is vital for neuronal signaling throughout the body.[77] The blood-brain barrier is composed of tight junctions between the endothelial capillary cells which prevent paracellular transport and glial processes surrounding these capillaries which are highly resistant to polar substances. To recap, the more polar the drug, the more hydrophilic and the more lipophobic.[68]

The third major player in drug permeability across membranes is its charge or degree of ionization. While there are many ways the interaction between a given drug and a given membrane could be affected by charge, that effect is generally significant. As described before, molecular size, lipophilicity, and now charge, are connected in their effect on the drug's permeability. The larger and more hydrophilic a molecule it is, the slower its permeability, with only a few exceptions. If the molecule is charged, the permeability of the molecule is even slower. However, some drugs are only charged at

certain pH values, or a physiological pH. This makes the degree of ionization important for understanding the permeability of a drug.[68]

These pH dependencies are often purposeful in drug delivery systems to transport a drug to a target site. Anti-cancer agents are particularly good candidates for pH dependent drug delivery systems. Anti-cancer therapy aims to treat a specific target with cytotoxic agents without harming tissues along the route to the target. Additionally, issues with circulation stability and tumor-targeting can be solved by encapsulating or coating drugs within other compounds can change the surface charge of the drug and allow it to pass through or pass by certain membranes. It can also allow drugs to reach the target without being metabolized or released until it reaches a location in the body with a certain pH.[78]

Most drugs are weak acids or bases and exist in an equilibrium between ionized and un-ionized states. The pH partition hypothesis is a common theory that was derived from the observation that higher total concentration of a drug is generally found on the side of a membrane where the pH favors a greater degree of ionization for that drug. The pH partition hypothesis states that only non-polar, un-ionized drugs can pass through the membrane. It also states that at equilibrium, the concentrations of un-ionized species are equal on both sides of the membrane. Finally, it states that at equilibrium, although the concentration of un-ionized species are the same, the total concentration can still be wildly different depending on the degree of ionization of the drug at the local pH. Most of the observed evidence for the pH partition hypothesis comes from studies specific to anatomical locations where there is a high variation of pH (renal excretion studies, gastrointestinal absorption studies, etc.) The hypothesis fails to explain all observations,

so using it as a general rule can lead to inaccurate assumptions, especially in anatomical locations where there is less variation in pH.[68]

#### 2.3.4.3 Transport Processes

The transport of drugs across cell membranes falls into one of two categories: diffusion or active transport. Diffusion describes the random movement of individual molecules of a substance either through intermolecular spaces in a membrane or through carrier protein. The key difference between the two is that diffusion occurs along the concentration gradient and active transport occurs against the concentration gradient. A concentration gradient is simply a physical area over which the concentration of a substance differs. Substances will diffuse from a high concentration to a low concentration until it reaches a state of equilibrium.[76, 68]

#### 2.3.4.4 Diffusion

The first of the two processes, diffusion, is driven by the propensity of molecules to move down the concentration gradient. Diffusion is a phenomenon that occurs naturally, so no work is expended by the system. The movement of molecules across membranes is resultant of kinetic energy and is therefore passive. Diffusion always goes down the concentration gradient and therefore never occurs in the direction from low concentration to high concentration.[68] Diffusion across cell membranes takes place by either simple diffusion or facilitated diffusion. Simple diffusion can occur across cell membranes by two pathways: transcellularly and paracellular. Transcellular transport describes the passage of a lipophilic drug through the lipoidal membrane of the cells and is the most common drug transport route. Paracellular transport accounts for the transport of drugs between cells, through the paracellular pathway, when they are too polar to cross the lipoidal cell membrane.[68, 76] The term simple diffusion indicates that the kinetic movement of the ions or molecules passing through the membrane do so without

interacting with carrier proteins. Conversely, facilitated diffusion does require the interaction of a carrier protein in order to cross the cell membrane. The molecules or ions passing through the membrane chemically bind to the carrier protein which shuttles them across.[76] Hence, facilitated diffusion is often referred to as carrier-mediated diffusion. This process is still passive, however, since the carrier proteins that are carrying the molecules or ions of interest still move **down** a concentration gradient. No work is expended by the system since the movement across the membrane is resultant of kinetic energy.[68]

#### 2.3.4.5 Active Transport

The second type of process, active transport, requires work to be exerted by the system since the molecules or ions crossing the cellular membrane are going *against* the concentration gradient. In active transport, the drug moves from an area of low concentration to an area of high concentration. Recall that diffusion, which is passive, occurs when a drug moves from an area of high concentration to low concentration. This property is the fundamental difference between the two types of transport. Some common substances that are actively transported are sodium ions, iron ions, potassium ions, calcium ions, chloride ions, urate ions, and select sugars and amino acids. Active transport is subdivided again into two categories - primary active transport and secondary active transport, depending on the source of energy used to transport. Primary active transport describes cases when the breakdown of adenosine triphosphate (ATP) or some other high-energy phosphate compound is the source of energy for the transport. Secondary active transport describes cases where the energy for transport is derived from stored energy created during primary active transport. This energy is stored in the form of

ionic substances between the two sides of the cell membrane. Both primary and secondary active transport utilize carrier proteins. Recall that carrier proteins are also used in facilitated diffusion, but in active transport, the carrier protein functions differently. In active transport, the carrier protein is able to contribute energy to the transported molecule or ion to move it against the concentration or electrochemical gradient.[76]

One example of primary active transport is the sodium-potassium pump, which is vital for controlling cell volume. As mentioned in the previous section on Membranes (Section 2.3.4), extracellular fluid is high in sodium and low in potassium, while intracellular fluid is low in sodium and high in potassium. The sodium-potassium ( $Na^+ - K^+$ ) pump is responsible for maintaining the sodium and potassium concentration differences and also establishing a negative electrical voltage inside the cell. The ( $Na^+ - K^+$ ) pumps sodium ions outward from low concentration intracellularly to high concentration extracellularly through the cellular membrane.

Simultaneously it pumps potassium ions inward from low concentration extracellularly to high concentration intracellularly. Note that both potassium and sodium ions in this case are moving *against* their respective concentration gradient. [76]

There are two general types of secondary active transport - counter-transport and co-transport. Each of these will be explained with an example for clarity. Counter-transport refers to secondary active transport in the direction opposite of the primary ion. The sodium-calcium counter-transport occurs in nearly all cell membranes, where sodium ions are transported into the cells and calcium ions are transported out of the cells. In this case, since both ions are bound to the same carrier protein. Note here, the sodium ion is



moving *down* its concentration gradient. The transport uses stored energy from the sodium electrochemical gradient by allowing the sodium ions to flow along their gradient in exchange for the calcium ions entering.

Co-transport mechanisms are used for glucose and several amino acids, since they tend to be transported into cells against large concentration gradients. In the sodium-glucose co-transport, the transport protein has two binding sites on its exterior side, one for sodium and one for glucose. Similar to the sodium-calcium counter-transport mechanism, the energy is derived by allowing sodium to flow along its electrochemical gradient. A unique characteristic of this transport carrier protein is that a conformational change will occur in the protein only when both glucose and the sodium ion are bound at their exterior binding sites. This conformation change then happens automatically and allows both the sodium ion and glucose to pass into the cell.[76]

#### 2.3.4.6 Extent of Distribution

There are two factors that affect the concentration of drug in the plasma, or central compartment, after the drug has been successfully distributed throughout the body. The first is the dose administered, and the second is referred to as the extent of distribution. The extent of distribution is dependent on the apparent volume of distribution.[68] The apparent volume of distribution ( $V_{dist}$ ) which was discussed earlier in this section and refers to a proportionality constant which relates drug concentration in the plasma to the amount of drug in the rest of the body.[36] Here, it can be defined mathematically as the amount of drug in the body at equilibrium ( $A$ ) divided by the plasma drug concentration ( $C$ ):

$$V_{dist} = \frac{\text{Amount of Drug in Body at Equilibrium}}{\text{Plasma Drug Concentration}} = \frac{A}{C} \quad (\text{Eq. 2-17})$$

Knowing the volume of distribution ( $V_{dist}$ ) and the plasma volume ( $V_p$ ) allows for the estimation of the fraction of drug in the body that is within the plasma:

$$\text{Fraction of drug in body within plasma} = \frac{V_p}{V_{dist}} \quad (\text{Eq. 2-18})$$

If Equation 2-18 represents the fraction *within* the plasma, then Equation 2-9 (following) provides the fraction *outside* the plasma, or in the rest of the body:

$$\text{Fraction of drug outside the plasma} = \frac{V_{dist} - V_p}{V_{dist}} \quad (\text{Eq. 2-19})$$

In general, the larger the apparent volume of distribution, the smaller the fraction in plasma. Figure 2-8 may clarify why the apparent volume of distribution differs for different drugs.

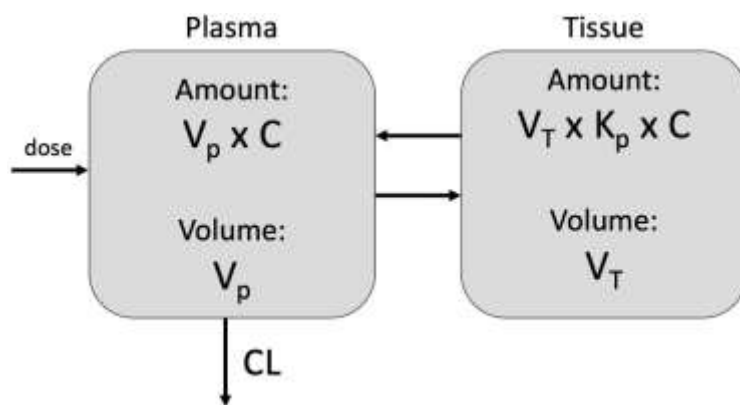


**Figure 2-8:** Simple two-compartment model, which implies that all drug in the body is contained in the plasma compartment (left) and the tissue compartment (right) with physiologic volumes of  $V_p$  and  $V_t$ , respectively

At equilibrium, the amount of drug,  $A$ , in each compartment is expressed in terms of the plasma concentration,  $C$ , the physiologic volumes of the two compartments,  $V_p$  and  $V_t$ , and the tissue-to-plasma partition coefficient ratio, denoted as  $K_p$ , by the following equation:

$$A = V_p \times C + V_t \times K_p \times C \quad (\text{Eq. 2-20})$$

where the first term on the right-hand side of the equation represents the amount of drug in the plasma and the second term represents the amount of drug in the tissue.[68] Conceptually, this equation reads:

$$\text{Amount in body} = \text{Amount in Plasma} + \text{Amount in Tissue} \quad (\text{Eq. 2-21})$$

where the first term on the right-hand side of the equation represents the amount of drug in the plasma and the second term represents the amount of drug in the tissue.[68]

Conceptually, this equation reads:

$$V_{dist} \times C = V_p \times C + V_t \times K_p \times C, \quad (\text{Eq. 2-22})$$

And dividing by  $C$ , we get

$$V_{dist} = V_p + V_t \times K_p \quad (\text{Eq. 2-23})$$

From Equation 2-23, we interpret the product term  $V_t \times K_p$  as the apparent volume of distribution for that tissue, when viewed from measurement of drug in the plasma. Following that logic, any number of compartments could be added on to complete the mass balance of drug amount in the body, with each compartment having its own physiologic volume and tissue-to-plasma partition coefficient  $K_p$ . Adding  $n$  compartments to Equation 2-23 would look like the following:

$$V_{dist} = V_p + V_{t,1} \times K_{p,1} + V_{t,2} \times K_{p,2} + \dots + K_{p,n} \times V_{t,n} \quad (\text{Eq. 2-24})$$

Values of  $K_p$  can be large for some tissues and small for others, which clarifies why the sum of the apparent volume of distribution terms (see Equation 2-23) could sum to a value much larger than the actual body volume.[72, 68] Consider the adipose tissue, which makes up about 20% of total body volume.[79] If a  $K_p$  value of adipose tissue for

this drug is 5 or greater, the adipose tissue alone has already equalled or exceeded the literal total body volume.

#### 2.3.4.7 *Binding*

The capacity of a drug to bind to blood components, plasma proteins, and tissues is a major factor in the distribution of a drug throughout the body. Total plasma concentration measurements include both bound and unbound drug.[68] However, an important distinction to make about interpreting total drug concentration is that only unbound drug can diffuse through membranes and exert a pharmacological effect.[72] Drugs that cannot pass through the cell membrane cannot reach the sites of activity, storage, or metabolism.[68] However, drugs that are bound to plasma proteins become too large to pass through the cell membrane, which means that the concentration of unbound drug drives drug transport, not the total concentration.[36, 68, 72] The ratio of unbound drug to total drug is referred to as the fraction unbound. The fraction unbound is also defined mathematically as,

$$F_u = \frac{C_u}{C} \quad (\text{Eq. 2-25})$$

where  $C_u$  is the concentration of unbound drug in the plasma and  $C$  is the total plasma concentration. For most drugs, the fraction unbound is constant throughout the infusion, so it matters very little whether total drug concentration or unbound drug concentration is measured. However, in some conditions, the fraction unbound will change. For instance, if the binding sites reach saturation or are altered in some way. Binding can be altered by another drug competing for the same binding protein. Patient characteristics including renal or hepatic impairment, recent surgery, or pregnancy, can alter the binding and

therefore, the fraction unbound. In these cases, measurement of the unbound concentration is necessary.[68]

There can be a wide variation in the volume of distribution for a specific drug between patients.[72, 80, 68] Some reasons for this phenomenon that will be discussed include (i) binding within blood, and (ii) binding in tissues. The following paragraphs will discuss how binding in each location affects the variation among patients, even for the same drug.

#### 2.3.4.8 Binding Within Blood

Drugs can bind to many different types of blood components, including plasma proteins and blood cells. This binding can cause the concentrations in plasma ( $C$ ), whole blood ( $C_{wb}$ ), and the unbound concentration in plasma water, ( $C_u$ ) to be widely different.[72] Plasma contains proteins that bind to drugs and its concentration is comprised of bound and unbound drug. Serum concentration is usually close to identical to that of the plasma concentration. Although the protein composition of serum is slightly different than that of plasma, they mainly differ in method of measurement. Plasma concentration is measured by adding an anticoagulant to whole blood and precipitating out the blood cells. The concentration in the supernatant fluid, plasma, is then measured. Serum concentration is measured by centrifuging whole blood after it has already clotted and removing cells and material that forms any clots. Usually the clots are primarily fibrin, and the binding of most drugs to fibrin or fibrinogen is negligible. The concentration of the remaining serum is then measured. Whole blood refers to the aggregate of red blood cells, white blood cells, platelets, and assorted plasma proteins. Typically, an anticoagulant is added and the drug is extracted into an organic phase after

denaturing the plasma proteins. The blood drug concentration represents the average over the whole sample, since concentrations in individual components or cell fractions can be varied. The technique for measuring blood drug concentration is more involved, so plasma concentration is the most typical measurement used due to ease of analysis. A major goal in measuring drug concentration is to relate it to therapeutic response and toxicity, and often times, while perhaps the simplest method, it is not the best representation. Nonetheless, plasma concentration remains the most reported in pharmaceutical literature.[68]

#### 2.3.4.9 Transporters and Binding in Tissues

The tissue-to-plasma equilibrium constant,  $K_p$ , value mentioned in the introduction to this section defines the ratio between drug concentration in tissues to drug concentration in the blood or plasma.[79] When discussing the relationship between  $K_p$  and the apparent volume of distribution, it was stated that  $K_p$  could be large or small depending on the properties of the tissue it represented. The main property that determines the  $K_p$  value for a certain tissue is the extent to which a drug tends to bind to that tissue. This process along with uptake and efflux transporters affect the determination of the  $K_p$  value for a specific tissue.[68]

Binding to tissue occurs when, although a drug may have a great affinity for binding to plasma proteins, it has a greater affinity for binding to tissue components. However, the binding of a drug to tissue components cannot be as readily measured as the binding of drug to plasma. This is because the integrity of the tissue's structure must be disrupted in order to directly measure the drug in tissues. However, tissue binding can be inferred from plasma measurements using the following mass balance: [68]

$$V_{dist} \times C = V_p \times C + V_{TW} \times C_{TW} \quad (\text{Eq. 2-26})$$

where  $V_{TW}$  is the aqueous volume outside the plasma where the drug is distributed and  $C_{TW}$  is the corresponding drug concentration outside of plasma. Conceptually, Equation 2.26 is interpreted as:

$$\text{Amount in Body} = \text{Amount in Plasma} + \text{Amount Outside of Plasma}$$

Drug *outside of plasma* is assumed to be drug *in tissue*. By dividing Equation 2-26 by  $C$ , which is the drug concentration in the plasma,

$$V_{dist} = V_p + V_{TW} \times \frac{C_{TW}}{C} \quad (\text{Eq. 2-27})$$

Just as Equation 2.25 describes the fraction unbound in plasma, the fraction unbound in tissues  $F_{u,TW}$  is related by:

$$F_{u,TW} = \frac{C_{u,t}}{C_{TW}} \quad (\text{Eq. 2-28})$$

where again,  $C_{u,t}$  is the drug concentration unbound in tissue and  $C_{TW}$  is the drug concentration outside of the plasma.

Since distribution equilibrium is reached when the unbound drug concentration in plasma  $C_u$  and the unbound drug concentration in tissues,  $C_{u,t}$  are equal, we get the equality:

$$\frac{C_{TW}}{C} = \frac{F_u}{F_{u,t}}, \quad (\text{Eq. 2-29})$$

which we can then substitute into Equation 2-28 to get:

$$V = V_p + V_{TW} \times \frac{F_u}{F_{u,t}} \quad (\text{Eq. 2-30})$$

The relationship in Equation 2-30 demonstrates that when  $F_u$  increases, the volume of distribution increases, but when  $F_{u,t}$  increases, the volume of distribution decreases.

#### 2.3.4.10 Rate of Distribution to Tissues

Upon administration of a drug - intravenous, oral, or otherwise - the systemic absorption and distribution to tissues takes some amount of time. Tissue distribution takes place to varying extents at different rates depending on the drug and the respective tissue.[68] The extent of the drug's partitioning into adipose tissues, the drug's ability to cross membranes, and the drug's likelihood to bind with blood or tissues are all factors that determine the distribution pattern of a drug. The ability of the drug to be delivered into the tissue by the blood is also a determining factor. Extravasation is a term used to describe drug uptake into tissues from the blood. Extravasation will move toward equilibrium between the blood and the tissue. The rate-limiting factors for distribution can be one of two processes - perfusion or permeability. Rate-limitation by perfusion is a delivery limitation, and rate-limitation by permeability is a limitation in membrane passage. Perfusion rate limitation tends to occur when the tissue membranes give virtually no barrier to entry for the drug. As expected, this type of rate-limitation is more likely to occur with small, highly lipophilic molecules that pass through the lipid bilayer readily. Most drugs, excluding macromolecules, can also move easily through more loosely-knit membranes such as capillary walls of muscle tissue. However, as the resistance to drug transport across the cell membrane increases, the source of rate limitation shifts from perfusion rate limited to permeability rate limitation. In this case, the problem is not the delivery of the drug to the tissue or the removal of the drug from the tissue, but the passage across the cell membrane.



### 2.3.5 Metabolism

Before discussing metabolism, another important concept in pharmacokinetics, elimination, should be mentioned. Elimination is the irreversible loss of drug from the site of measurement. Elimination of drugs from the body occurs through a number of pathways - through biliary excretion, urinary excretion or bio-transformation to other substances, but in pharmacometrics, is generalized into two processes - metabolism and excretion.[36, 68]

Metabolism is likely the most straight forward definition in terms of the four pharmacokinetic processes. Metabolism here maintains a traditional definition of the conversion of one chemical species to another. In most cases, the resulting metabolites are converted irreversibly and are considered part of the total elimination of the parent drug from the body. In notably fewer cases, the metabolite conversion is reversible and is converted back to the parent drug. This process is called metabolic interconversion. In these cases, metabolism is only considered a route of elimination to the degree in which that metabolite is eliminated and thus, unable to convert back to the parent drug.[68] Elimination of parent drug is sometimes called formation clearance of the metabolite.[11]

In most cases, metabolism will inactivate the drug, but some metabolites are pharmacologically active. Some metabolites are even more pharmacologically active than the parent drug. In some cases, a pharmacologically weak, or even inactive, drug with a may be administered for the purpose of the metabolite exacting the therapeutic effect on the target. These types of compounds are referred to as prodrugs.[81] Prodrugs are inactive compounds that are converted to active species in the body. Soft drugs are the antithesis to prodrugs in that they are pharmacologically active compounds that are

quickly metabolized after systemic absorption to minimize adverse effect on the body. The pharmacologic profiles of metabolites produced can vary. Some may have profiles similar to the parent drug, while others may behave completely differently or even produce adverse effects. Thus, the pharmacokinetics of any metabolites produced by a drug warrant therapeutic concern. When observing the body's response to a drug, the time course of all active substances in the body must be considered.[68]

Oxidation, reduction, hydrolysis, isomerization and conjugation are the most common metabolic reactions.[68, 81] The reaction pathway that occurs has the primary goal of making the compound easier to excrete from the body. The enzymes involved in perpetuating these reactions are found in most tissues in the body but are notably more concentrated in the liver.[81] It follows that while metabolism occurs in many tissues in the body, the primary site of metabolism is the liver.[81, 82]

Some capacity limitation exists for most drugs, which is caused by the limited number of enzyme sites. However, at the therapeutic concentration, which is what is actually given in practice, only a small percentage of the enzyme sites are occupied. In these cases, the metabolism rate of the drug is directly proportional to the concentration of drug in the body. In other words, its metabolism follows first-order kinetics.[81] Many of these capacity-limited reactions are described by the following Michaelis-Menten equation:

$$-\frac{dC}{dt} = \frac{V_{max} \times C}{K_m + C} \quad (\text{Eq. 2-31})$$

where  $-\frac{dC}{dt}$  describes the rate of decline of drug concentration at time  $t$ ,  $K_m$  is the Michaelis constant, and  $V_{max}$  is the theoretical maximum rate of the process. The Michaelis constant  $K_m$  for a drug can be obtained by determining  $C$  when  $\frac{dC}{dt} =$

$\frac{1}{2} V_{max}$ . [83] It is easily seen that  $K_m$  is in fact equivalent to the drug concentration at which the rate of the metabolism is one-half of  $V_{max}$ . There are special cases of the Michaelis-Menten equation - (i) where the Michaelis constant  $K_m$  is much larger than the drug concentration  $C$  and (ii) where the drug concentration  $C$  is much larger than the Michaelis constant  $K_m$ . In the first case, Equation 2.31 is reduced to:

$$\frac{dC}{dt} = \frac{V_{max}}{K_m} \times C \quad (\text{Eq. 2-32})$$

Equation 2-32 takes the form of first-order elimination kinetics – which would make the rate constant  $\frac{V_{max}}{K_m}$ . [36] Drug elimination is often observed to have first-order kinetics, so it follows that the majority of drugs have therapeutic concentrations that are much smaller than the Michaelis constant  $K_m$ . This observation consistent with the relatively low percentage of enzyme sites that are occupied by drugs and metabolites at therapeutic concentrations. [68] The second, less common case of Michaelis-Menten kinetics results when  $K_m$  is much larger than the drug concentration. In this second case, Equation 2.31 is reduced to:

$$-\frac{dC}{dt} = V_{max} \quad (\text{Eq. 2-33})$$

Under this condition, the rate does not depend on the drug concentration such that the constant rate is equal to  $V_{max}$ . [36] The other special case of the Michaelis-Menten equation follows zero-order kinetics since the rate is independent on the drug concentration. [36, 68]

### 2.3.6 Excretion

Excretion is the second elimination process - defined as the irreversible loss of the *unchanged* drug from the body. [68] The primary difference between elimination by

metabolism and elimination by excretion is that the drug is actually removed unchanged rather than removed by bio-transformation.[68]

The kidneys are the primary organs that excrete water-soluble compounds. The liver plays a smaller role than the kidneys in terms of excretion. Excretion through bile occurs to the extent that the drug is not reabsorbed by the GI tract in the enterohepatic cycle. Certain drugs and their metabolites are extensively excreted in bile. The drugs that undergo biliary excretion require active transport against a concentration gradient across the biliary epithelium. Another obstacle to biliary excretion occurs when plasma concentrations are high.[84] A transport maximum may be reached when more transporters are occupied, especially in the presence of substances with similar physiological properties.[76] Drugs that are most likely to be excreted by the liver through bile include drugs with a molecular weight greater than 300 grams/mole, having both polar and lipophilic groups. Smaller molecules are not readily excreted in bile. Although the liver is the lesser component in excretion, its indirect effect through metabolism is notable. Hepatic metabolism will often convert drugs to more water soluble compounds, thus allowing the kidneys to clear the drug through urine.[84]

The glomerulus is a filtration component in the kidney that is comprised of a complex bundle of capillaries lined with a delicate mesh of endothelial proteins.[85] About 20% of the plasma that reaches the glomerulus in the kidney is filtered through the glomerular endothelium. Most water and electrolytes are reabsorbed into circulation. However, polar compounds, including most drug metabolites are generally unable to diffuse through the renal tubules to be reabsorbed. These polar, water-soluble compounds are then excreted by the kidneys.

The governing concepts of membrane clearance that were discussed in the earlier section on absorption hold true for renal excretion.[84] Recalling the concept of fraction unbound, only unbound drug is contained in plasma reaching the glomerulus. Drug that is bound to plasma proteins are too large to diffuse through the pores of the glomerular endothelium and remain in circulation.[68, 76]. Along the lines of membrane clearance and absorption, we recall that the degree of ionization also plays a role in the passage of drugs across membranes. The pH of the solute a compound is in determines the ionization state of a weak acid or base, which includes most drugs.[78] Drugs that are weak acids or weak bases exist at some equilibrium between their ionized and un-ionized states. Urine pH varies widely, from 4.5 to 8. Lower urine pH, or more acidic urine, increases re-absorption of drugs that are weak acids and decreases the re-absorption of drugs that are weak bases. More acidic urine will also decrease the excretion of drugs that are weak acids and increase the excretion of drugs that are weak bases. The inverse is true for urine with a higher, more basic pH. With a few exceptions, the contribution to excretion of sweat, saliva, and respiration is relatively small.[84]

### **2.3.7 Summary of Pharmacokinetic Concepts**

#### **2.3.7.1 Absorption**

The absorption of a drug in pharmacokinetics is defined as the process by which an unchanged drug moves from the site of administration to the site of measurement.[68] Common routes or sites of administration include oral, intramuscular, intravenous, and subcutaneous. The most common site of measurement is an arm vein.[72, 73]

#### **2.3.7.2 Distribution**

The distribution of a drug in pharmacokinetics is defined as the process of reversible transfer of drug from one location to another in the body.[68] Drug moves to and from the site of

measurement and the peripheral tissues. The distribution process is observed at the site of measurement, usually the plasma.[68]

#### 2.3.7.3 Metabolism

The metabolism of a drug in pharmacokinetics is defined as the conversion of one chemical species to another chemical species.[83, 81] Metabolism is one of the two elimination processes. However, unlike excretion, metabolism can sometimes be reversible. In drugs where metabolism is reversible, the extent of elimination of the drug is only to the degree of which the metabolite is eliminated and unable to return to the original drug.[68]

#### 2.3.7.4 Excretion

The excretion of a drug in pharmacokinetics is defined as the irreversible removal of an unchanged drug from the body.[68] Excretion is the second of two elimination processes. The main organs that participate in the excretory process are the liver and the kidney, but a marginal amount of excretion is carried out through sweat and exhalation.[72, 36] However, renal filtration accounts for the majority of drug excretion.[84]

#### 2.3.7.5 Absorption and Disposition

The elimination of a drug from the body is linked on a physiologic and anatomic basis to both systemic absorption and distribution. Disposition is a term used to encompass the distribution and elimination of a drug from the body. An overarching term for this pair of processes is needed since it is often difficult to distinguish whether a decline in the plasma concentration of a drug is due to distribution or elimination. Another way to describe disposition is all kinetic processes successive to systemic absorption. From the previous two Subsections 2.3.5 and 2.3.6, it is important to emphasize that elimination consists of both metabolism and excretion. Figure 2-9 illustrates how the processes overlap using a simple two-compartment example.[68] Thus, the ADME process can be described as absorption (A) and disposition,

where disposition includes distribution (D) and the elimination processes metabolism (M) and excretion (E).

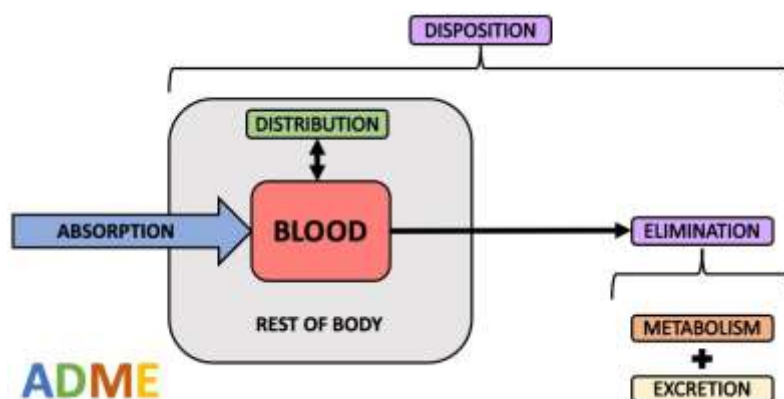


**Figure 2-9:** Disposition is a collective term that refers to the processes of distribution and elimination; elimination includes two of the ADME processes metabolism and excretion

## 2.4 Pharmacodynamics Concepts

Since the focus of this work is primarily pharmacokinetic modeling without the pharmacodynamic component, this section will outline important terms and goals in pharmacodynamic modeling. It should not be left without mention, but for the scope of the work, a general overview with some examples should be adequate background.

The relationship between the systemic exposure of a drug and the body's response to that exposure defines the pharmacokinetics of the drug. Drugs interact with different organs and tissues within the body to produce a therapeutic effect. In order to achieve the therapeutic effect, there must be an adequate exposure at the target site. The target site is the location in the body that the drug is expected to "treat".[68] For instance, in anti-cancer therapy, the drug's target site is the tumor.[86] However, in many cases, the administration site is far from the target site within the body. Another example of this could be an anti-psychotic drug, administered orally, then absorbed into circulation in the

gut, and delivered across the blood-brain-barrier to the brain.[77] Further, the target site may not be a plausible site of measurement (i.e. the brain, a tumor in the pancreas), so measurements of concentration in systemic circulation is often the surrogate site of measurement. These measurements are under the assumption that some fractional or scalar amount of the drug is at the target site. The assumption in classical pharmacodynamics is that any response caused by the administration of the drug is solely due to the parent drug, not its metabolites. Metabolites should of course be kept in mind, but the collective effect of the drug is measured as one lump effect unless otherwise specified.[68, 36]

#### **2.4.1 Types of Pharmacodynamic Response**

The term *response* is used to embrace a wide range of measurements depending on the purpose of the drug. Thus, responses can be classified in a number of different ways. Arguably the most important classification from a clinical standpoint is if the response is desired or harmful. However, this distinction may not always be straightforward.[68] For instance, the anticoagulant warfarin decreases clotting which can lead to a desired response - decreased likelihood of an embolism - or a harmful response - internal hemorrhage.[87] Broadly, pharmacodynamic responses fall into three categories - (i) clinical responses, (ii) surrogate endpoints, and (iii) biomarkers. The following paragraphs will discuss each class of pharmacodynamic response. Clinical responses (i) can be either objective or subjective. An objective clinical response could be measures like increase in survival time or decreased number of vomiting episodes, while a subjective clinical response could be “quality of life” or a sense of nausea. While these are useful, even some objective clinical responses can take years to manifest and thus,



tend to show great variability. These objective clinical responses often do not allow for intervention or guiding therapy.

For that reason, surrogate endpoints (ii) are useful to get simple, immediate measurements to guide therapy or verify that the treatment is actually having an effect. Surrogate endpoints are simple measurements that are not necessarily a direct response to the drug but correlate to the clinical effect.[68] Anti-hypertensive drugs are a good example of this concept. The clinical response to prolonged hypertension may be increased incidence of stroke, but it would take many years and a large population to gather the incidence of strokes to see if the drug actually decreases the risk. Instead, taking blood pressure measurements can serve as surrogate endpoints since it has been proven that lower blood pressure over time decreases the incidence of strokes.[88] Blood pressure measurements are on the causal pathway to the clinical response, so they are an excellent example of a surrogate endpoint.

Biomarkers (iii) make up the third and final category of pharmacodynamic responses. Generally, biomarkers are measurable effects produced by the drug. However, in practice, biomarkers are chosen that have some diagnostic or prognostic relevance.[68] For instance, blood glucose levels are good biomarkers for drugs like metformin and insulin that treat diabetes and insulin resistance.[89] Other biomarkers are used to monitor general adverse effects from the drug like liver function tests, kidney function tests, and white blood cell counts. These biomarkers are broadly referred to as safety biomarkers.[68]

In reality, drugs produce more than just one effect, so a biomarker need not be related to the actual clinical effect. It could be said, then, that all pharmacodynamic

responses are biomarkers unless that have either been accepted as clinical response or have been shown through scrupulous evaluation to predict therapeutic outcome and thus accepted as a surrogate endpoint. The biomarkers that are most likely to be accepted as a surrogate endpoint are those which are on the causal pathway between drug action and clinical response. In other words, these biomarkers measure an effect which has been shown to affect some disease state or clinical outcome.[68]

#### **2.4.2 Assessment of Response**

With the exception of endogenous compounds such as insulin, cortisol, and thyroxin, drugs are not naturally occurring in the human body. Thus, in most cases, there is no baseline amount of drug concentration in the body to take into account. However, in pharmacodynamic response, there does exist a baseline measurement. The blood pressure, glucose level, white blood cell count, and bilirubin levels from a particular patient while not on the drug serve as the baseline measurement, while the same measurements from a particular patient while on the drug serve to characterize the drug effect on the patient.[68] Baseline can be a difficult variable to identify due to the rhythmic or cyclic physiologic changes that the body goes through daily, weekly, monthly, or even hourly.[68, 76] For example, circadian rhythm has been shown to effect baseline cortisol levels.[90] The menstruation cycle in females certainly affect baseline hormone levels depending on the time of the month.[91]

For many drugs, there is also a placebo effect that factors into assessing the pharmacodynamic response. Placebo effect occurs when a patient receives what appears to be a certain drug treatment, while it is actually an inactive compound. What follows is a psychosocial phenomenon where the desired outcomes of the treatment actually come

from the patient's anticipation of the outcome rather than the actual drug treatment. There is evidence that taking a placebo effects activates neurotransmitters in dopaminergic, opioidergic, and vasopressinergic pathways in the brain which may mimic the desired effect, as if the patient received the active compound instead of a placebo. The effect of the active compound is not present, but there could be subtle improvements or changes that should be accounted for in the placebo arm of a study.[92] This is especially true when any of the endpoints are subjective or patient-reported. Therefore, several components must be considered when assessing the pharmacodynamic response to a drug, as illustrated in Figure 2-10.[68]

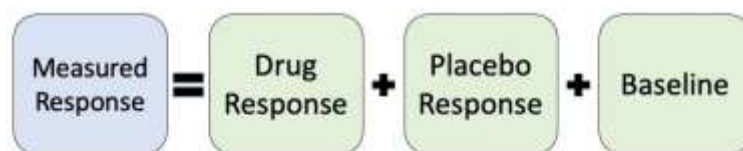


**Figure 2-10:** Illustration of the consideration of placebo response and baseline in addition to drug response when assessing the measured pharmacodynamic response of a drug

### 2.4.3 Graded Versus Quantal Response

Pharmacodynamic responses can be either graded or quantal. The magnitude of graded responses can be scaled or graded on a continuous spectrum within an individual, sometimes related to plasma or tissue concentration. Quantal responses, also referred to as all-or-nothing responses, do not occur on a continuous basis but discretely. It occurs, or it does not occur.[68]

When the measurable pharmacodynamic response is graded, concentration versus time and effect versus time data for each individual is combined to relate concentration versus effect. When a gradient of concentrations are investigated, a continuous

concentration-versus-effect profile can be achieved. Graded dose-response models are useful in determining whether the inter-individual variation (IIV) is due to pharmacokinetic or pharmacodynamic causes. However, if the response is dichotomous (i.e. movement versus no movement, survive versus succumb, etc.), then a quantal dose-response relationship can be investigated. Instead of relating intensity of effect to dose, quantal dose-response relationships can elucidate the percentage of a population that is affected.[93]

#### 2.4.4 Examples of Notable Pharmacodynamic Models

Two general types of pharmacodynamic models are direct effect models [94] and the indirect effect models [95]. Interestingly, the “early days” of pharmacokinetics and pharmacodynamic modeling in the context of these types of mathematical modeling only date back to the early 1960’s. A majority of the pharmacodynamic models in use today have been somehow derived from one of these two types of models.[96] The following subsections will describe the more developed forms of each model type - the Direct Effect Model and the Indirect Response Model - in some detail and will attempt to make the pharmacodynamic concepts a little more tangible.

##### 2.4.4.1 Direct Effect Models

###### 2.4.4.1.1 The Levy Equation

Direct effect models are derived under the assumption that drug effect is linearly related to the logarithm of dose.[94, 96] Equation 2-34 by Gerhard Levy in 1964 shows the linear relationship of effect  $E$  with the logarithm of dose  $R$ ,

$$E = m \times \log(R) + e \quad (\text{Eq. 2-34})$$

where  $m$  is the slope and  $e$  is the intercept term.[94] In a later work in 1966, Levy derived the following model:

$$E = E_0 - \frac{mk}{2.303}t \quad (\text{Eq. 2-35})$$

where  $m$  is the linear slope which characterizes the effect-log concentration relationship from Equation 2-34,  $E_0$  is the theoretical intercept, and  $k$  is the first-order rate constant for elimination of the drug.[97] Equation 2-35 was derived from Equation 2-34 and describes the relationship of single compartment drug pharmacokinetics and in vivo effects over time. Equation 2.35 was henceforth known as the Levy equation and was upheld by clinical data for drugs like the alkaloid tubocurarine that showed exponential decline following intramuscular dosing and linear decline in the resultant muscle relaxation. Later, the Levy equation led to the application of these linear and log-linear type model to in vivo data. These models were simple to calculate by linear regression and could provide slope values which translated to pharmacodynamic parameters. Unfortunately, the Levy equation fails in some cases. The Levy equation is deficient if the effect is not linear - less than 20% of the maximum effect  $E_{max}$  - or log-linear - between 20% and 80% of the  $E_{max}$ . Thus, the model cannot be extrapolated to capture the maximum effect  $E_{max}$ .[96]

#### 2.4.4.1.2 $E_{max}$ Model

These weaknesses led to the introduction of the Hill equation for the characterization of in vivo concentration-response relationships by John G. Wagner in 1968.[98] The Hill equation is based on receptor occupancy theory, and when concentration equilibrium conditions are assumed, the rate of change of the drug-receptor complex is represented by the following equation:

$$RC = \frac{R_T \times C_{action}}{K_D + C_{action}} \quad (\text{Eq. 2-36})$$

where  $R_T$  is the receptor density,  $K_D$  is the equilibrium dissociation constant, and  $C_{action}$  is the concentration at the site of action.[96] One assumption of receptor-occupancy theory is that the drug effect is directly proportional to the fraction of occupied receptors:

$$E = \gamma \times RC \quad (\text{Eq. 2-37})$$

where  $RC$  is the drug-receptor complex and  $\gamma$  is a proportionality constant. Under that assumption, combining Equation 2-36 and 2-37 can be rearranged to fit a form of the Hill equation:

$$E = \frac{E_{max} \times C_p}{EC_{50} + C_p} \quad (\text{Eq. 2-38})$$

where  $E_{max}$  is substituted for  $(\gamma \times R_T)$ , and  $EC_{50}$  is a sensitivity parameter that represents the drug concentration that causes 50% of maximum effect.

Equation 2-38 is commonly referred to as the  $E_{max}$  model and is one of the most frequently used direct response models in pharmacodynamics.[73] One

assumption of all forms of the  $E_{max}$  model is that maximum effect  $E_{max}$  and peak concentration  $C_{max}$  occur simultaneously. The premise of this assumption is that the plasma drug concentration and the relevant peripheral concentration reach rapid equilibrium after dosing. However, this overlap does not always occur.

There are a number of physiological reasons that drug effect would lag behind peak drug concentration. This disparity led to the development of models that capture the delay in terms of physiological mechanisms following peak concentration.[96] The first of these was the biophase model.

#### 2.4.4.1.3 Biophase Model

The term “biophase” was conceived in 1955 by Robert Furchgott to describe the drug site of action.[99, 96] Sheiner et al. then developed a novel modeling approach in

1979 which incorporated a hypothetical “effect” compartment, which was termed the biophase model. The biophase model is defined by the following equation:

$$\frac{dC_e}{dt} = k_{eo} \times C_p - k_{eo} \times C_e \quad (\text{Eq. 2-39})$$

where  $k_{eo}$  is a first-order distribution rate constant,  $C_e$  is the intensity of pharmacological effect, and  $C_p$  is the plasma concentration. The premise of the biophase model is that the delay in maximum drug effect and peak concentration is due to the time it takes for the drug in the plasma to be distributed to the target site or site of action. Adding the hypothetical compartment for the quantification of the actual effect at the drug site of action (i.e. the biophase) accounts for the delay by prolonging the time it takes for the effect to occur using the rate constant  $k_{eo}$ . The biophase model is illustrated in Figure 2-11.[96, 73] Many current, more mechanistic pharmacodynamic models today use effect compartments to resolve delays in treatment effect.[96, 100]

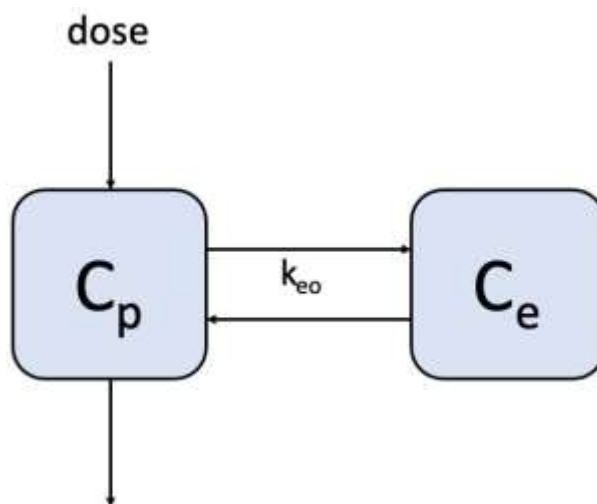


**Figure 2-11:** Simple schematic of the biophase model originally developed by Sheiner et al.[101], where  $C_p$  represents the concentration in plasma compartment,  $C_e$  represents the hypothetical effect compartment, and  $k_{eo}$  is the first order distribution rate constant between compartments

#### 2.4.4.1.4 Indirect Response Models

The concept of Indirect Response (IDR) models was first introduced by E.J. Ariens in 1964 with the suggestion that drugs may not interact directly with receptors at target sites to cause drug effects.[95] Instead, the drug may interact and affect the behaviour of endogenous compounds in the body. It could be the subsequent effect that those endogenous compounds have on the target site. In other words, the drug *indirectly* affects the site of action by *directly* affecting substances that act on the site of action.[96] Indirect Response models are also frequently used as another way to account for temporal lag between drug response and drug concentration.[73] There exists four formalized Indirect Response Models that were formalized by William Jusko's group in the early 1990's[102] and later found to be useful for characterizing many clinical pharmacodynamic effects.[103]

#### 2.4.4.1.5 IDR Model I

$$\frac{dR_{idr}}{dt} = k_{in} \left( 1 - \frac{I_{max} \times C_p}{IC_{50} + C_p} \right) - k_{out} \times R \quad (\text{Eq. 2-40})$$

#### 2.4.4.1.6 IDR Model II

$$\frac{dR_{idr}}{dt} = k_{in} - k_{out} \left( 1 - \frac{I_{max} \times C_p}{IC_{50} + C_p} \right) \times R \quad (\text{Eq. 2-41})$$

#### 2.4.4.1.7 IDR Model III

$$\frac{dR_{idr}}{dt} = k_{in} \left( 1 - \frac{S_{max} \times C_p}{SC_{50} + C_p} \right) - k_{out} \times R \quad (\text{Eq. 2-42})$$

#### 2.4.4.1.8 IDR Model IV

$$\frac{dR_{idr}}{dt} = k_{in} - k_{out} \left( 1 - \frac{S_{max} \times C_p}{SC_{50} + C_p} \right) \times R \quad (\text{Eq. 2-43})$$

where  $R_{idr}$  represents the response,  $I_{max}$  is the maximal effect of inhibition,  $IC_{50}$  is the concentration that triggers the half-maximal effect of inhibition,  $S_{max}$  is the maximal



effect of stimulation,  $SC_{50}$  is the concentration that triggers the half-maximal effect of stimulation. These four models apply to a wide range of clinical applications, but for the scope of this discussion, a few applications of IDR Model I will be briefly outlined.[73]

One notable application of IDR Model I as shown in Equation 2-40 was its use in modeling the pharmacokinetic-pharmacodynamic (PK/PD) relationship of warfarin. Warfarin inhibits the production of prothrombin, which is a plasma protein that is converted to the clotting factor thrombin during the coagulation process. By inhibiting prothrombin, a delayed anticoagulant effect is carried out in the blood.[104, 73] Another common drug for which the IDR Model I in Equation 2-40 is applied is ibuprofen. Ibuprofen inhibits prostaglandin  $E_2$ , which is known to temper immune response by regulating the expression of cytokines.[105] By controlling the expression of cytokines, ibuprofen reduces the inflammation which causes fever, and the measured pharmacodynamic response is fever. This is a clear example of how ibuprofen indirectly decreases fever, the pharmacodynamic response, by directly affecting cytokine expression.[106]

## 2.5 Summary of Pharmacokinetics and Pharmacodynamics

Previous sections have discussed how pharmacokinetics and pharmacodynamics have separately contributed to the understanding of a complete pharmacological profile of what the body does to the drug and what the drug does to the body, respectively.[69]

This section will discuss the combination of pharmacokinetics with response over time, which has more formally come to be known as pharmacokinetic / pharmacodynamic (PK/PD) modeling. PK/PD modeling unites a pharmacokinetic model with a pharmacodynamic model to capture the full relationship between drug administration and

response with time.[68] Figure 2-12 illustrates both the distinct differences and inter-dependence between PK and PD modeling.

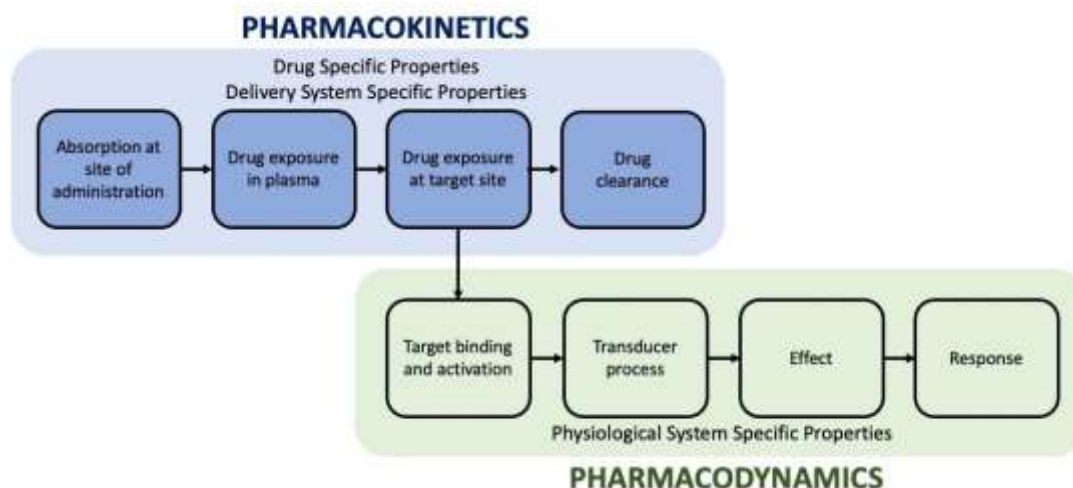


**Figure 2-12:** Schematic of the inter-relationship of pharmacokinetic and pharmacodynamic modeling (adapted from Zou et al.)[73]

One main distinction is that pharmacokinetics deals with the drug specific and delivery system specific parameters associated with the system, while pharmacodynamics deals with the physiological system specific parameters. Pharmacokinetic models tell the story from dose administration to target and out of the body. Pharmacodynamic models take it from delivery to the target and describes the drug effect and pharmacodynamic response.[73] There is no doubt that PK/PD modeling has tremendously aided in drug discovery, drug delivery, and general progress in understanding the effects of therapeutics on the body. However, there still exist some caveats that must be considered when applying a PK/PD model to a drug or clinical concern. There are many assumptions made in the development of PK/PD models that cannot be easily validated. These hard-to-validate assumptions are less of a concern for some of the simple examples noted earlier in this chapter, which have known mechanistic pathways. However, there are

more complex PK/PD relationships in advanced therapies that are in development today for which this challenge must be overcome. For instance, antibody-drug conjugates (ADCs) are complexes with a monoclonal antibody (mAb) and a linker loaded with a cytotoxic compound.[73] These types of drugs are of great interest as a novel approach to cancer therapies as new mode of delivering cytotoxic agents in a more targeted manner. One example of model of an ADC is a PK/PD model Brentuximab-Vedotin antibody-drug conjugate developed by Tsuchikama et al. in 2018. The assumption was made that the cell-killing effect in the tumor was directly related to the drug concentration.[107] However, without the ability to observe the distribution cascade directly, the validity of this assumption is in question.[73] As the field continues to advance alongside medical technology, 86 there may be more opportunity to validate these types of assumptions or better understand the mechanisms of action. It should also be noted that these assumptions made in PK/PD modeling are not random guesses, but instead are based on some pharmacological or physiological observation or knowledge. However, the limitations of the models must be noted so that future information can inform future models. Another obstacle in PK/PD modeling that is more relevant to the work to follow is the extrapolation from sub-clinical species (i.e. mice, rats, etc.) to humans. Fortunately, there are several current, reliable methods for minimizing error in scaling parameters across species. One more obvious method would be choosing an appropriate animal species for scaling to humans. It is known that dogs are the best preclinical species for assessing cardiac safety in humans.[73] Mini-pigs are considered the best preclinical species for dermal absorption in humans.[108] Additionally, using allometric scaling across multiple species from preclinical species to humans can be used to improve

predictions by minimizing error and increasing accuracy.[73] Simple allometry is a generally accepted method for small molecules that are renally excreted - which is the case for doxorubicin.[9] Some of these animal-to-human scaling relationships have already been developed and are more quickly accepted. The predictive power of PK/PD models informed by previous observations and carefully collected data is a valuable asset to pharmacology and the practice of medicine today. As mentioned previously, the advancement in new technologies can help improve the understanding of physicochemical properties of drugs and their delivery systems. Improved understanding will do nothing but bolster the predictive ability of future PK/PD models.[73]

## **2.6 Additional Considerations in PK/PD Modeling**

### **2.6.1 Disease Modeling**

Disease modeling is needed to understand whether therapeutic drug effects are curative, symptom mitigating, disease-modifying, or effective at all. Understanding how diseases behave and progress without medical intervention is vital to characterizing the effect of a drug in terms of treating the ailment. Disease modeling is sometimes referred to as natural history progression modeling. These types of models act as a control group to observe differences between treated and untreated group.[109] Disease modeling in humans can be precarious in terms of ethics. Clearly, it would be unethical and even cruel to withhold treatment from a human simply to study the natural progression of some disease.[110] In some cases, models are scaled from natural disease progression data gathered from sub-clinical species like mice, rats, pigs, etc. However, it is generally known that animal models do not scale perfectly to humans. Allometric scaling, a type of inter-species scaling, can be used to estimate model parameters extrapolated to

humans.[10] Additionally, data from disease models in animals can give insight into general disease behavior, which is sometimes used to build out probability models and simulations.[110] In addition to cancer, natural progression models are also widely used in long-term, progressive diseases with poor prognoses. These include neurodegenerative diseases like Muscular Sclerosis (MS)[111], Alzheimer’s Disease (AD)[112], and Duchenne Muscular Dystrophy (DMD)[113] for which there are scarce pharmacological interventions available.

#### 2.6.1.1 Modeling Tumor Dynamics

Many functional forms have been developed to characterize natural tumor growth in terms of ordinary differential equations. The most basic - linear, exponential, logistic, and Gompertz will be briefly explained below. Linear growth presumes that the natural growth of the tumor follows a constant zero-order growth rate as shown in the example curve in Figure 2-13A and the following equation:

$$\frac{dT}{dt} = k_g \quad (\text{Eq. 2-44})$$

where  $k_g$  is the tumor growth rate constant. Exponential growth assumes that the growth rate follows a first-order growth rate. That is, the growth rate is proportional to the tumor burden, as shown in Figure 2-13B and the following equation:

$$\frac{dT}{dt} = k_g \times T \quad (\text{Eq. 2-45})$$

where  $k_g$  is the tumor growth rate constant and  $T$  is the tumor burden.

The first two growth models, linear and exponential, assume that tumor growth has no upper limit. The tumor either grows at a constant rate or grows faster as the tumor volume becomes larger. However, the logistic and Gompertz growth models make a more

biologically realistic assumption that the tumor is limited by some carrying capacity or that the growth rate decreases over time.

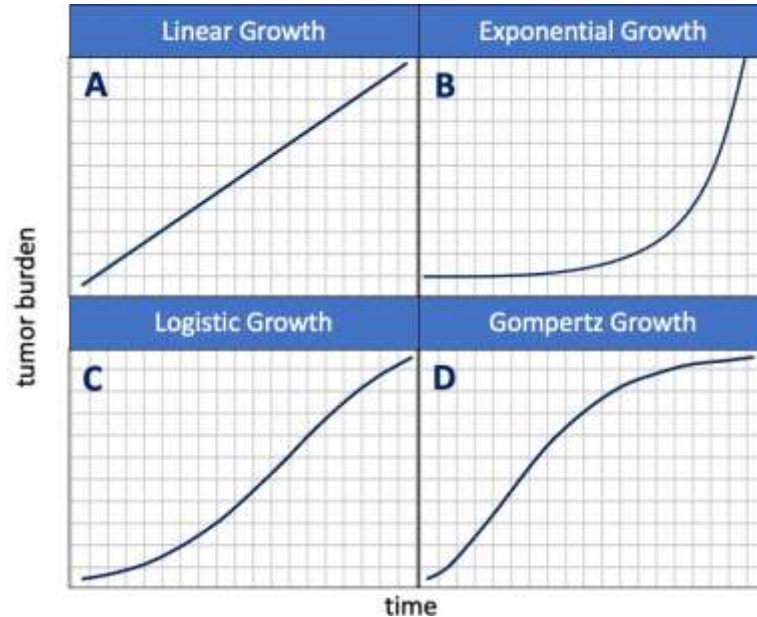


**Figure 2-13:** Examples of the general shapes of the four basic functional forms that natural tumor growth models take - linear (A), exponential (B), logistic (C) and Gompertz (D) (adapted from Yin et al.)[114]

Realistically, the tumor cannot grow to an infinite volume, as tumors are in some organ or tissue in the body that has a finite volume that can only yield to a certain extent. The logistic model assumes that the natural tumor growth is limited by a carrying capacity. In other words, the tumor has some limit ( $T_{max}$ ) to its total tumor burden, as shown in Figure 2-13C and the following equation:

$$\frac{dT}{dt} = k_g \times T \times \left(1 - \frac{T}{T_{max}}\right) \quad (\text{Eq. 2.46})$$

where  $k_g$  is the growth rate constant,  $T$  is the tumor burden, and  $T_{max}$  is the maximum tumor burden. As  $T$  increases, the growth rate is scaled by a smaller and smaller fraction

$(T/T_{max})$ . Once  $T$  is equal to  $T_{max}$ , the third term in Equation 2-46 goes to zero. The growth rate, then, goes to zero, which indicates no further growth can occur.

Similarly, the Gompertz model assumes that the tumor growth rate declines as it approaches its maximum tumor burden  $T_{max}$ . This is easy to see in the example curve in Figure 2-13D and in the following equation:

$$\frac{dT}{dt} = k_g \times T \times \ln \left( \frac{T_{max}}{T} \right) \quad (\text{Eq. 2.47})$$

where again,  $k_g$  is the tumor growth rate constant,  $T$  is the tumor burden, and  $T_{max}$  is the maximum tumor burden. From Equation 2-47, the growth rate is scaled by the natural logarithm of the proportion of  $T$  to  $T_{max}$ . As long as  $T_{max}$  is larger than  $T$ , the growth rate is positive. As  $T$  approaches the value of  $T_{max}$ , the growth rate becomes exponentially smaller until it reaches zero when  $T$  is exactly equal to  $T_{max}$ . [114]

#### 2.6.1.2 Disease Progression

Accurate disease modeling is vitally important for understanding clinical presentation, endpoints, and progression. Modeling disease progression in terms of clinical pharmacology joins the understanding of the disease model and the pharmacokinetic and pharmacodynamic profiles. Broadly, clinical pharmacology seeks to master the use of medicine to treat disease. Adding pharmacokinetic and pharmacodynamic modeling methods have allowed for more powerful, quantifiable characterization of time course of drug concentration and effect in both individuals and populations. [109] As mentioned previously in this section, these quantitative disease progression models help discern between symptom-mitigation and disease-modification in terms of drug action and effect. This depth of understanding is integral for regulatory decisions and therefore, patient care. [109] In the previous discussion about different

types of pharmacodynamic drug responses, it could be important to know if the response is related to the half-life or clearance of the drug.[68] Some drugs do not alter the course of disease progression but only gives temporary relief to some symptom of the greater illness. Disease progression models are much like pharmacokinetic or pharmacodynamic models as multiple observations can be made on the same patient. Instead of a plasma sample or white blood cell count, some metric of disease status is measured over time. Disease status over time can be combined with PK/PD modeling for a more holistic picture of the interrelation of disease and treatment.[109] This discussion of disease progression models in terms of clinical pharmacology leads into the clinical application of PK/PD modeling.

### **2.6.2 Clinical and Therapeutic Relevance**

All drugs are developed to treat some ailment. Likewise, all drugs have some adverse side effect. Some adverse effects are mild, as in the potential gastrointestinal discomfort following a dose of aspirin. Others have the potential to be much more dangerous, as in the case of doxorubicin and its notorious cardiotoxicity. However, any drug at the wrong dose can be deadly - for instance, a 200 - 300 milligram dose of aspirin could relieve a mild headache. A 10 gram dose could be fatal. [68] The greater objective for developing these PK/PD modeling methodologies is for the benefit it can have in the clinical setting. In much earlier years of medicine, the manner in which the correct dosing regimen was determined was through trial and error. While the eventual correct schedule can be determined under that method, many patients are at risk for suffering some level of unnecessary adverse effects. To compare, 0.125-0.25 mg of digoxin is given daily to treat congestive heart failure while morphine sulfate must be given in doses of 10-50 mg



up to 6 times a day to treat pain in terminal cancer patients. These treatment regimens were determined using this trial-and-error approach, which likely caused at the very least discomfort to the patients involved. Additionally, this approach adds almost nothing to the underlying understanding of effective dosing regimens for similar drugs.[68]

In the early 2000's PK and PD models have become a standard piece of regulatory applications for new drugs or new recommendations for current drugs.[115] As shown in Figure 2-14 which shows a flow chart of the drug discovery process from pre-clinical studies to post-marketing surveillance. At each stage of the process, some form of modeling is being done to guide the experimental design of the trials conducted along the way. Developing a PK/PD model is a step-wise process.

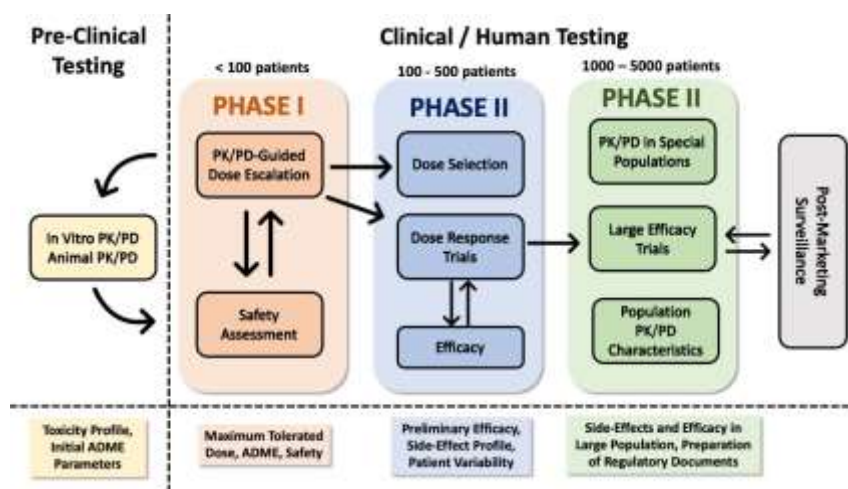


**Figure 2-14:** Simplified flow chart of the drug discovery process highlighting the contribution of PK and PD models at each phase of the process (adapted from Derendorf et al.[68])

First, the baseline natural disease model is developed. Next, the concentration versus time and the concentration versus effect data provide the basis for training a model to characterize the drug effect. The model's predictive power on a different dose or

treatment schedule can then be tested using a cross validation method (holdout, k-fold, etc.).[116] Once the model is considered sufficient, additional post-hoc studies can be done to glean relevant information. The addition of PK/PD methodologies have created a more rational framework for making decisions concerning drug administration. In addition to the fundamental concepts of 92 pharmacokinetics and pharmacodynamics that have been discussed at length in this chapter, a few basic concepts have added to this rational framework.

First, it was understood that the intensity of a drug effect tends to increase with increased exposure. This is intuitive. However, the intensity of the drug effect reaches a capacity at which the increase in effect no longer matches the increase in concentration. In other words, there is some maximum effect that a drug can produce. From that, it was accepted that while a very high exposure will cause a very large drug effect, some of the effects will be undesirable. This is because drugs act on more than just one part of the body, despite the drug effect being intended for just the site of action. Even if the type of response is the same, the maximum effect that can be reached may be quite different from even a similar drug. Taking analgesics for example, aspirin and morphine both provide pain relief. However, while even a maximum dose of aspirin could likely not relieve intense pain from severe trauma, morphine could. These ideas combined produced the concept of a therapeutic window. The paradox of the therapeutic window is that too low of an exposure leads to insufficient therapeutic response and too high of an exposure leads to unwanted side effects. The narrower the therapeutic window, the smaller the margin of safety. Continuing the digoxin and morphine sulfate example, we now know that both of the drugs have a narrow therapeutic window. Morphine is eliminated from

the body quickly. Instead of giving a large dose at one time, which could cause excessive respiratory depression and even death, a frequent dosing schedule of smaller doses allows for the maintenance of a concentration that manages pain. Digoxin is eliminated slowly, so a once-daily administration is adequate

## **CHAPTER 3**

### **PK/PD OF DOX AND DOXol**

Since doxorubicin (DOX) is used so broadly in cancer treatment, it is imperative that the understanding of its interaction with the body is continually improving. Better modeling techniques should aid in more precise dosing regimens and ultimately better outcomes for patients. While pharmacokinetic and pharmacodynamic models are often used in tandem, the majority of the models created for DOX are PK focused. However, since DOX is used in such a wide range of cancers, the range of pharmacodynamic models are too broad to discuss in detail. This section will cover current PK models of DOX, but will only give general general mention of pharmacodynamic details.

#### **3.1 Current Models of DOX and DOXol**

A variety of PK models have been developed to explain the problem of DOX dosing (Table 3-1 and Table 3-2), but there is a range in the appropriate number of compartments needed to accurately model DOX and its major metabolite, doxorubicinol (DOXol). Some models aim for a more simplistic approach and exclude the metabolite entirely. For example, Piscitelli et al. developed a simplified model, explaining the PK of DOX as either a two-compartment or a three-compartment based on select covariates like body surface area and age. This model lumped DOX and DOXol into one agent instead of trying to investigate the PK of each individually.[17]

**Table 3-1: Observed or Reported Half-Life Values for Sub-Clinical Species and Humans from Literature**

Observed half-life values					
Species	Dose	$t_{1/2}$	$t_{2/2}$	$t_{3/2}$	Source
Mouse	10mg/kg IV bolus	25.2min	10hr	N/A	[33]
Rat	6mg/kg slow IV bolus	5.3min	3hr	17.3hr	[45]
Rabbit	5mg/kg IV bolus	4.6min	1.92hr	N/A	[117]
Human	60mg/m <sup>2</sup>	4.8min	2.57hr	48.4hr	[35]
Human	N/A	5.2min	1.98hr	31.9hr	[118]
Human	20-100mg/m <sup>2</sup>	12min±8 min	3.3hr±2.2hr	29.6hr±13.5hr	[32]
Human	50mg IV bolus	10min±45sec	1.42hr±6 min	28.75hr±4.67 hr	[119]
Human	15mg/m <sup>2</sup> IV bolus	3.18min	35.53min	8.98hr	[120]
Human	30mg/m <sup>2</sup> IV bolus	3.38min	43.79min	26.46hr	[120]
Human	50mg/m <sup>2</sup> IV bolus	4.8min	1.37hr	20.42hr	[120]
Human	25mg/m <sup>2</sup> IV bolus	4.8min(3.6-6.6)	3.7hr(1.3-15.4)	31.5hr(21.0-67.3)	[121]
Human	75mg/m <sup>2</sup> IV bolus	4.8min(3.6-5.4)	2.4hr(0.5-4.5)	33.0hr(21.0-55.9)	[121]
Human	60mg/m <sup>2</sup> IV bolus	4.8min	2.57hr	48.4hr	[35]

**Table 3-2: Observed or Reported AUC Values for Sub-Clinical Species and Humans from Literature**

Observed AUC values				
Species	Dose	$AUC_{DOX}$ (ng×h/ml)	$AUC_{DOXol}$ (ng×h/ ml)	Source
Mouse	10mg/kg	1463	N/A	[33]
Mouse	5mg/kg	1818±45	N/A	[126]
Rat	5mg/kg	516±44	666.8±100.4	[127]
Rabbit	5mg/kg	1223.2±98.7	666.8±100.4	[128]
Rabbit	3mg/kg	407.64±119.57	244.584±152.186	[129]
Rabbit	3mg/kg	1216.67±116.67	N/A	[117]
Rabbit	3mg/kg	615±35	N/A	[117]
Human	50mg/m <sup>2</sup>	1426.5	N/A	[120]
Human	30mg/m <sup>2</sup>	951.34	N/A	[120]
Human	15mg/m <sup>2</sup>	519.5	N/A	[120]
Human	45-72mg/m <sup>2</sup>	1834±1007	2529.7±2699	[17]
Human	50-75mg/m <sup>2</sup>	2055±929	N/A	[130]
Human	60mg/m <sup>2</sup>	1973.9	1298.4	[35]
Human	50mg/m <sup>2</sup>	1660±680	N/A	[131]
Human	50mg/m <sup>2</sup>	1630±560	N/A	[131]

Another model by Kontny et al. incorporated a fourth compartment for DOXol in addition to a three-compartment model for DOX.[32]Perez-Blanco et al. further refined the model to a three-compartment model for DOX with two-compartments for DOXol.[31].

More compartments for drug plasma concentration does not necessarily equate to a better model. Most data collected for pharmacokinetic studies can be fit to several different models, but it is a matter of finding the best fit to describe the drug's action. Interestingly, the models of DOX that fit a two-compartment model have low initial doses, as shown in the Cusack rat model, the Brenner rabbit model, the Johansen rat model, and the third Erttmann human model in Table 3-3. Note that the third Erttmann model was given in 15 mg/m<sup>2</sup> doses every 10 hours, which is the lowest dose given in any of the cited models.[120] It is possible that a higher concentration must be reached in order for the third elimination phase to be apparent in data. This dose-dependence has been evidenced previously in literature.[122] In addition, the granularity of the model has a great deal to do with the quality and quantity of the samples and therefore the data entered into the model.[70] Although PK models like the aforementioned may have tolerably explained the drug's PK characteristics, none of them so far have ascertained the complex metabolic activity and toxicity of DOX.

A more extensive list of existing models of DOX in literature are listed in Table 3-3. There is a major effort in recent years to encapsulate DOX in liposomes and other nanoparticles in order to increase maximum residence time for better exposure or decrease the interaction of DOX with healthy cells outside of target site for less toxicity.[123, 124, 22, 28, 27, 125] However, the scope of this dissertation will be limited to un-encapsulated DOX, also referred to as "free doxorubicin". Because of the pivot toward encapsulating DOX in recent years, some of the PK models of DOX in the following section may seem aged. However, the models collected in this review are some of the most recent free DOX models in literature.

**Table 3-3: Summary of Existing Models of Un-Encapsulated or “Free” DOX in Sub-Clinical Species and in Humans, as Reported from Literature**

Existing Pharmacokinetic Models of DOX			
Species	Treatment	Compartments in Model	Source
Mouse	10mg/kg IV bolus	2 or 3	[33]
Rat	6mg/kg IV bolus	3	[45]
Rat	2mg/kg IV bolus	2	[127]
Rabbit	3mg/kg IV bolus	2	[129]
Rabbit	5mg/kg IV bolus	2	[117]
Pig	50mg/m <sup>2</sup> over 3 min IV	3	[132]
Human	40-60mg/m <sup>2</sup> IV bolus	3	[120]
Human	26.6-35mg/m <sup>2</sup> IV bolus	3	[120]
Human	60mg/m <sup>2</sup> over 40 hours IV	2	[120]
Human	70mg/m <sup>2</sup> IV bolus	3	[133]
Human	45-72mg/m <sup>2</sup> IV bolus	3	[17]
Human	20-110mg/m <sup>2</sup> IV bolus	3+1 for DOXol	[32]
Human	50mg/m <sup>2</sup> IV bolus[134]	3+2 for DOXol	[31]
Human	60mg/m <sup>2</sup> IV bolus	3	[35]
Human	50mg/m <sup>2</sup> IV bolus	3	[131]
Human Child	N/A	3+1 for DOXol	[118]
Human Child	10-75mg/m <sup>2</sup> IV bolus	3+1 for DOXol	[135]

### 3.2 Inter-Patient and Inter-Dose Variability

Another obstacle that makes DOX more complicated as a cancer therapy is its significant inter-individual variability on clearance, exposure as measured by area under the concentration-time curve (AUC), and volume of distribution.[17] The pharmacokinetic profiles of both DOX and DOXol are Inter-individual variability (IIV) is a term used to describe a drug that displays significant differences in bioavailability and toxicity among patients. Inter-patient variability is used clinically to understand the risk of over-dosing or under-dosing a patient based on factors like body mass index (BMI), certain gene expression profiles, or renal function. Additionally, inter-occasion variability (IOV) describes variability in parameters or behavior between doses on the same

individual. The three parameters that will be discussed in this portion of the chapter will be variation in DOX (i) clearance, (ii) volume of distribution, and (iii) exposure (AUC). These three parameters are certainly interrelated. The volume of distribution is directly proportional to clearance, scaled by the elimination constant  $K$  as described in Equation 2-3. This relationship is based on the idea that volume of distribution is the volume in which the drug is diluted.[68] DOX is eliminated linearly with first-order kinetics[31]. This means that the clearance is concentration dependent. A smaller volume of distribution for the same amount of drug results a higher concentration which effects clearance.[68] Further, the AUC and clearance are inversely proportional as shown in Equation 2-1. The lower the calculated AUC, the higher the clearance. The inverse is also true.[68] Practically, lower clearance means that the drug spends more time in the body and has a higher exposure (AUC). Variations in clearance are readily cited in the literature and may seem more heavily discussed in the following section, but it makes sense that high variability in clearance infers high variability in related parameters. Early conventional pharmacokinetic analyses reported from 2-fold to 5-fold inter-individual variability in DOX clearance in adult cancer patients with no noteworthy hepatic or renal impairment. This variability was present even after adjusting clearance values for body surface area (BSA).[46] Issues with IIV and IOV in DOX clearance still pose dangers in terms of cardiotoxicity and therapeutic effect.

Although this work is focused on free doxorubicin in adults, the extensive use in children with malignancies gives way to rich data on properties of DOX that are also of interest for adult populations. In a study of DOX in children, a significant difference was found in the clearance rates between boys and girls. Boys in this study had a considerably



higher mean clearance of 591 ml/min/m<sup>2</sup> compared to the girls whose mean clearance was 471 ml/min/m<sup>2</sup>.<sup>[19]</sup> An earlier study found that girls had a significantly higher concentration peak C<sub>max</sub> than boys in the same cohort.<sup>[32]</sup> Additional studies found that higher body fat percentage and an overweight body mass index correlated to lower clearance rates and higher C<sub>max</sub> values.<sup>[118, 44]</sup>

The same study also found a significant difference in clearance between groups of children under 2 years old (infants) and over 2 years old. Infants had a higher mean clearance rate of 538 ml/min/m<sup>2</sup> while children 2 and older had a mean clearance of only 446 ml/min/m<sup>2</sup> as shown in Table 3-4.<sup>[19]</sup> This finding is supported by other DOX studies in children. One study reported a significantly higher mean clearance in children younger than 10.5 years.<sup>[32]</sup> When studied in induction therapy for children acute lymphoblastic leukemia, the most common childhood malignancy, patients with lower clearance rates were statistically more likely to achieve complete remission.<sup>[19]</sup> This finding suggests that the residence time of DOX in the body is correlated to directly anticancer effect and therefore, patient outcome. The danger, however is that longer residence time could correlate with higher cardiotoxicity.

**Table 3-4: Observed or Reported Clearance Values for sub-Clinical Species and Humans from Literature**

Observed DOX Clearance			
Species	Dose	Clearance	Source
Mouse	10mg/kg IV	0.150 L/hr	[33]
Mouse	5mg/kg IV	4.5±0.1	[126]
Rat	2mg/kg IV	4.08 L/kg/hr	[127]
Rabbit	3mg/kg IV	7.74 ± L/kg/hr	[129]
Rabbit	5mg/kg IV	8.196±0.432 L/hr/kg	[117]
Rabbit	5mg/kg IV	4.24±0.462 L/hr/kg	[117]
Human	50mg/m <sup>2</sup> IV	32.0 L/hr	[131]
Human	20-110mg/m <sup>2</sup> IV	53.3 L/hr	[32]
Human	40-100mg/m <sup>2</sup> IV	63.6±22.7 L/h	[136]
Human	75mg/m <sup>2</sup> IV	44.1 (36.2 - 79.9) L/h	[121]
Human	25mg/m <sup>2</sup> IV	21.4(16.1-27.8) L/h	[121]
Human	40-75mg/m <sup>2</sup> IV	30.4 ± 6.3 L/hr/m <sup>2</sup>	[130]
Human	40-75mg/m <sup>2</sup> IV	49.6 ± 14.1 L/hr/m <sup>2</sup>	[130]
Human	40-75mg/m <sup>2</sup> IV	28.0 ± 9.5 L/hr/m <sup>2</sup>	[130]
Human	60mg/m <sup>2</sup> IV	56.8 L/hr (24 - 119)	[35]
Human Infant	75mg/m <sup>2</sup> IV	32.28 L/hr/m <sup>2</sup>	[19]
Human Child	75mg/m <sup>2</sup> IV	26.76 L/hr/m <sup>2</sup>	[19]

In Table 1-1 from the previous section, it is made evident that DOX is rarely used as a single agent. It has been observed to be more effective when given in combination therapy - most often with alkaloids like vincristine or vinblastine[137], the folate antagonist methotrexate[138], and the cytotoxic agent cyclophosphamide. [49, 17, 139] One study found that when given in combination with cyclophosphamide, DOX clearance was reduced by approximately 30%, which is consistent with the literature.[136] Prolonged clearance times has been shown to increase therapeutic effect in single-agent doxorubicin. It would be interesting to speculate whether the increased efficacy of DOX when in combination with other agents is due to some synergy between these other anticancer agents or the prolonged residence time due to reduced clearance. It is likely that in reality there is some combination of both scenarios.

Aside from the covariates like age, gender, body composition, and concomitant therapy that may effect the clearance of DOX, a wide range of studies in several species have reported a great deal of variation within relatively homogeneous groups. A comparison of several pharmacokinetic studies done by Kontny et al. reported a mean clearance value of 53.3 L/h for DOX with 17.7% inter-individual variability and inter-occasion variability of 21% in human cancer patients.[32] Another large study conducted by Rudek et al. found the mean clearance of DOX to be 63.6 L/hr with a standard deviation of 22.7 L/hr.[136] A comparative dose study in 16 adult female breast cancer patients was done by Twelves et al. to see how the pharmacokinetic parameters behaved at different doses (Table 3-5).

**Table 3-5:** *Observed or Reported Volumes of Distribution at Steady State of DOX for Sub-Clinical Species and Humans from Literature*

Volume of Distribution at Steady State of DOX		
Species	$V_{dist,ss}$	Source
Mouse	101.0 ± 3.8 L/kg	[126]
Mouse	2.009 L/kg	[33]
Rat	194 ± 19 L/kg	[127]
Rabbit	0.79 ± 0.11 L/kg	[117]
Rabbit	2.65 ± 0.50 L/kg	[117]
Rabbit	112.4 ± 0.77 L/kg	[129]
Human	20-30 L/kg	[32]
Human	681.6 ± 433 L/m <sup>2</sup>	[17]
Human	1081 L	[121]
Human	2198 L	[121]
Human	33.1 L/kg	[35]
Human	9.3 ± 0.97 L	[131]

For a dose of 25 mg/m<sup>2</sup>, the mean clearance was 21.4 L/hr with a range of 16.1 - 27.8 L/hr. For the 75 mg/m<sup>2</sup> dose, the clearance was 44.1 L/hr with a range of 36.2 to 79.9 L/hr.[121] Despite the small sample size, there is a noteworthy difference in the

clearance rates and the range of clearance rates observed. There is evidence in the literature that other pharmacokinetic parameters of DOX are dose-dependence, so this difference in clearance rates between dosing regimens is not surprising.[122] Another study in a randomly divided group of 26 sarcoma patients found significant difference between the three groups of patients. Two sets of data were used to train the model and a third set was used to test the model. The first training set had a mean clearance of  $30.4 \pm 6.3$  L/hr/m<sup>2</sup>, the second training set had a  $49.6 \pm 14.1$  L/hr/m<sup>2</sup>, and the test set had a mean clearance of  $28.0 \pm 9.5$  L/hr/m<sup>2</sup>. A statistically significant difference was found between the second training set and the other two sets, respectively.[130] These clearance values along with several other literature examples are listed in Table 3-4. Note that some clearance values are normalised by weight in kilograms or body surface area (BSA) while others are not. There is some debate as to whether normalising the dose of anticancer agents by the patient's BSA or weight, which is the standard of practice, actually decreases the inter-individual variability. Some patients still experience severe toxicity while others experience little to none at the same normalised BSA-based dose.[118] This discrepancy further drives the need for more individualized dosing regimens for drugs with narrow therapeutic windows.

### **3.3 PK Modeling Solutions to DOX Drawbacks**

Although the pharmacokinetic profile of DOX consistently exhibits significant inter-individual and inter-occasion variability, as of late, only one significant covariate, decreased dose in hepatically impaired patients, has been successful in improving dose adjustment.[11, 10] However, most chemotherapy drugs require dose adjustment for hepatic impairment since most anticancer agents, including DOX, are metabolized in the

liver.[140] This finding does not necessarily add to the knowledge of how to improve dosing in patients that are not hepatically impaired. As mentioned earlier, there has been some investigation into potential factors that affect key pharmacokinetic parameters such as body composition[118], age[32, 135], or even pH of urine.[117, 133] Despite these efforts, there are no universally accepted covariates that have modernized the guidance on dosing of DOX.

The literature does support that variations in infusion duration significantly impacts the exposure (AUC) and maximum concentration  $C_{max}$  in humans.[44] It is widely accepted that many DOX parameters are both dose-dependent and also schedule dependent.[136, 120] If there are no recommended dose adjustments for DOX based on typical covariates, optimizing the infusion duration and dose could be an avenue for improving therapeutic efficacy and reducing the cardiotoxic side effect. Several studies have cited that lower doses given frequently reduce incidence of cardiotoxic events in patients receiving DOX. Likewise, doses given over a long infusion duration tend to decrease incidence of cardiotoxic events.[124, 141, 142] Additionally, avoiding high initial DOX concentrations correlate with lower cumulative cardiotoxicity, regardless of lifetime dose.[120]

The focus of this work is to set up a framework for adjusting infusion rate and duration in order to simulate a number of scenarios to which the cardiotoxicity risk and therapeutic reward could be evaluated. As mentioned, the lower, more frequent dose or a lower dose over time has been observed to lower incidence of cardiotoxic events. Additionally, it has been shown that tumors are only in the  $G_0/G_1$  growth phase of their cell cycle for a short window of time. The therapeutic effect of the drug at the site of action

only acts on cancer cells in the growth phase. It is possible that some of the tumor killing effect is lessened when shorter infusions are given, regardless of magnitude of dose, since the drug effect has missed the window of time where the cell is vulnerable.[44] This work proposes evaluating exposure (AUC) and peak concentration ( $C_{max}$ ) at different doses - varying rate and duration - to provide a simulation framework for any clinical target.

The cardiotoxicity of DOX is largely attributed to the accumulation of its primary metabolite DOXol in the heart.[11] Getting any reasonable estimation of the amount of DOX that is metabolized and binds to heart tissue requires a more mechanistic or physiological model. Despite its cardiotoxicity and inter-patient clearance variability, the therapeutic value of DOX as a cancer drug has kept it a first-line chemotherapy agent for over four decades. The risk of potential toxicity seemingly outweighs the potential negative result of foregoing the drug.

Up to this point, the plasma drug concentration of DOX has been the central measurement of the models discussed in this work. PK/PD models typically use the plasma as the site of measurement and extrapolate or infer information about peripheral tissues based on the plasma drug concentration. Physiologically-based pharmacokinetic (PBPK) models incorporate more specific physiological parameters, additional compartments for specific tissues, and more mechanistic approaches to a full body model. This section will explore the use of PBPK models used for full body models that incorporate the drug's interaction within specific tissues. These models incorporate more than drug plasma clearance, including the absorption, deposition, metabolism and excretion (ADME) of the drug within the body's systems. PBPK models are promising for DOX and DOXol because

of its inclusion of tissues and organ systems, which will hopefully address its extensive deposition in tissues.

### **3.4 Investigating PBPK Models of DOX**

More physiological, and therefore mechanistic, modeling has come to the forefront in pharmaceutical discovery and development in recent decades.[143] Modeling systems dynamics has been used for decades to improve process control in industrial settings. Likewise, the idea of modeling physiological systems has been around since the early- to mid- 1900's. It has become markedly more popular in recent times due to its utility in drug discovery and development.[2] Modeling biological systems dynamics can help describe the body systems' response to perturbation — pharmaceutical or otherwise. Developments in computational capabilities and pharmaceutical insight has allowed for this discipline to better account for both drug and patient outcomes with more computationally burdensome models.[144] The computational burden for PBPK models is greater due to the increased dimensionality of the models, as well as the increased complexity of the equations and systems of equations needed to detail more mechanistic models.

Physiologically-based pharmacokinetic (PBPK) models are similar to more empirical, classic PK models in that they can produce important PK parameters like clearance and volume of distribution.[2] In addition, PBPK models include more in-detail physiological processes and parameters that are within the constraints of realistic physiological values.[143] Like classical PK modeling, these additional components are integrated into the model using theoretical compartments, each having their own general and intercompartmental clearance values based on its place in systemic function (Figure

3-1).[1] However, these compartments are less “theoretical” than in classical pharmacokinetic models and actually represent specific organs.[143] A more physiologically consistent model yields a mechanistic mathematical framework that can accommodate in-vitro in-vivo extrapolation (IVIVE) techniques for predicting drug specific parameters. They detail not only concentration-time data in plasma, but also in organs and tissue relevant to the specific drug and system in question. PBPK models are also quite useful for extrapolating an oral or intravenous dose from healthy volunteers to a diseased population, as long as applicable physiological properties of that target population are available.

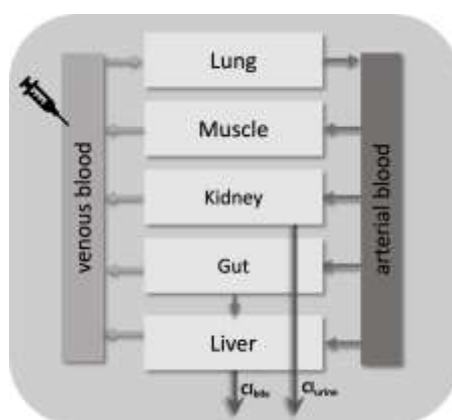


**Figure 3-1:** Example of a PBPK schematic, showing how each organ, represented as compartments, are connected by the circulatory system

The compartments are also connected by venous and arterial blood compartments which mimic or represent the actual circulatory system.[2] An optimized PBPK model is capable of quantitatively predicting and defining exposure in blood, organs, and tissue, which is vital for efficacy and toxicity analysis.[1] Exposure information for tissues, especially the heart, is key to understanding the full profile of DOX and its enigmatic cardiotoxic effect. However, in order to create a PBPK model, it is necessary to have a



reasonable understanding of the mechanism of the drug and its interaction with the system. A delicate balance must be struck between including important drug-system interactions without over-parameterizing the model.

In order to obtain that balance, the four most important components to understand are drug absorption, distribution, metabolism, and excretion (ADME). Absorption and distribution describes the passive/active transport or diffusion of the drug across membranes in the cells of various organs and tissues throughout the body. A general obstacle for this element of the model is predicting transport rates in each compartment. For small molecules like DOX, absorption and distribution are often concurrent. Metabolism for small molecules usually describes the enzymatic metabolism from the parent drug to its metabolites, whether by CYP or non-CYP enzymes. Finally, excretion explains the renal and biliary elimination.[1] Data for current PBPK models is a conglomerate of data from previous literature and experimental data from animal studies.

There is an abundance of data in previous literature for DOX because of its extensive use in cancer therapies. In vitro and in vivo studies have been done on both animals and humans over the past few decades. These studies have provided concentration values in plasma and tissues at a range of times post-infusion. This data was collected through timed blood draws or analysis of organs of sacrificed animals. Some of the earliest studies even give post-mortem organ concentrations collected from autopsy of human patients.[40] Despite the fact that a great deal of data is available for DOX, there is still much to overcome in constructing an acceptable PBPK model. As mentioned before, it is unclear the exact mechanism that governs the cytotoxic activity of

DOX.[32] There is also no definitive extent of metabolism[55], leaving these crucial values as unknowns to be speculated and estimated for the best possible model.

### **3.5 Middle Ground - Minimal PBPK Modeling Approach**

With current pharmacological knowledge of DOX, it seems nearly impossible to create an exhaustive PBPK model without having to estimate to the point of becoming arbitrary. Despite this, Dubbelboer et al. at Uppsala University in Sweden built a favorable model for DOX using previously collected data from two pre-clinical studies done in pigs. The Dubbelboer model was a semi-PBPK model, broadly meaning they did not incorporate every organ and system explicitly.[8] Another more common term for semi-PBPK models are minimal PBPK (mPBPK) models.[143] Instead, they focused on the most relevant interactions and processes and included the necessary tissues to reasonably encompass the drug's passage through applicable biological systems.[8] There has been a heightened interest recently in simplifying the structure of PBPK models for smoother applicability and increased transparency around what can be reasonably predicted.[143] The Dubbelboer model is such a model - using six tissue compartments, two blood compartments, and two excretion compartments as shown in Figure 3-2.

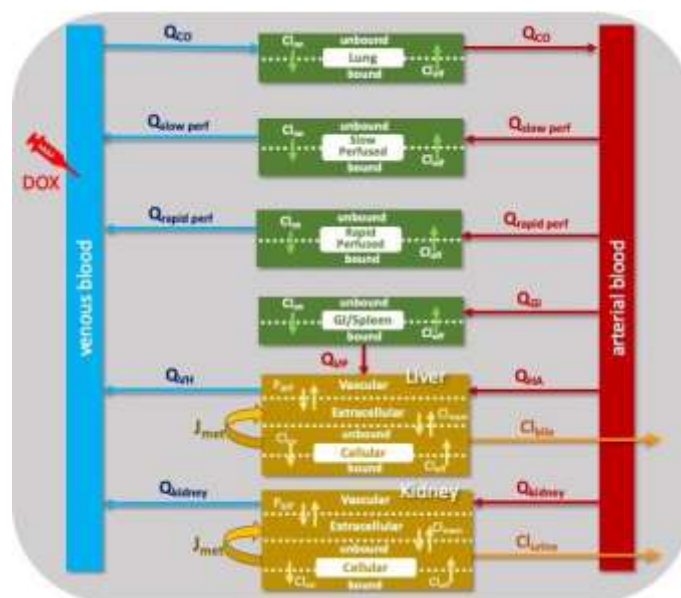


**Figure 3-2:** PBPK schematic of doxorubicin from the “binding specific” pig model created by Dubbelboer et al. 2017; arterial blood is denoted by the red arrows and boxes, venous blood by blue arrows and boxes, non-metabolizing tissues are in green, and metabolizing tissues are in gold

Arterial and venous blood made up the two blood compartments, and urine and bile made up the two excretion compartments. As there are far more than six tissue types in the body, the authors saw it fit to give autonomous compartments to the lung, liver, and kidney while lumping the GI tract, slow perfused tissue, and rapid perfused tissue into the remaining three compartments respectively. They based the tissue grouping on the physiological similarity of the tissue and its proposed interaction with DOX. These six compartments were then divided into two classes – metabolizing and non-metabolizing tissues.

From the animal studies and previous literature, they concluded that the metabolism of DOX to DOXol occurs primarily in tissue. They dealt with this in the model by isolating the two currently known locations of metabolism—the kidney and liver. With generic knowledge of passive diffusion and transport in hepatic and renal

cells, the metabolism from DOX to DOXol is incorporated into all metabolizing tissue compartments only as depicted in Figure 3-3.

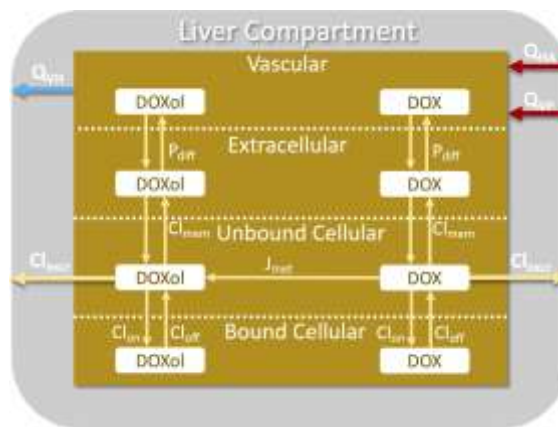


**Figure 3-3:** Liver compartment schematic describing movement, metabolism, and excretion of DOX and DOXol in metabolizing tissues

Concentration changes in each compartment and between compartments are described with ordinary differential equations as shown in Appendix A. However, in the Dubbelboer model, the heart compartment was left out of the specific compartments and presumably lumped into other tissue compartments. While this may seem surprising considering the established concern around cardiotoxicity, Dubbelboer's model was designed to investigate ways to model the intracellular binding of DOX rather than a full analysis of the effect of DOX and DOXol on pigs.[8] Additionally, previous work by Dubbelboer suggests that the interest in DOX in pigs was for the study of DOX as a primary agent for the treatment of hepatocellular carcinoma.[145]

This rationale was supported by conjectures from literature, mentioned in Section 1.3.1.[63, 64, 52, 66] Including a heart compartment as a metabolizing compartment like the liver and kidney gives a more realistic structure for capturing the cumulative effect of DOXol on the heart. The schematic of the heart compartment is shown in Figure 3-4.

Note that the structure is identical to that of the liver in Figure 3-3, except the heart does not have the excretion component. All other compartments remained unchanged, and due to the quite small percent of body weight that the heart makes up, its volume was subtracted from the slow perfused compartment to maintain the mass balance. Parameter values for each species can be found in Appendix G and will be discussed more in later sections.

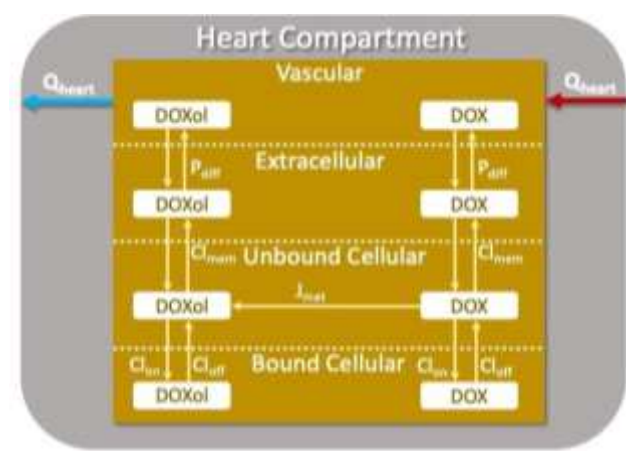


**Figure 3-4:** Heart compartment schematic describing movement and metabolism of DOX and DOXol in metabolizing tissues

In the updated model shown in Figure 3-5, not only was a heart compartment added, but the heart compartment is also a metabolizing compartment. It is true that higher concentrations of DOXol are found in the liver and the kidney than in the heart, gram for gram, in both animal species and in humans.[63, 64] However, aldo-keto reductases, the primary enzymes involved in the hydroxylation of DOX to DOXol, are present in all tissues.[52] The heart tissue is thought to be more vulnerable to the cytotoxic effect of DOXol than the liver and kidney since the latter two possess binding and inactivating compounds such as glutathione which curb the toxic effect.[65] As

such, the liver and the kidney are not typically sites of toxicity, while the heart profoundly is.

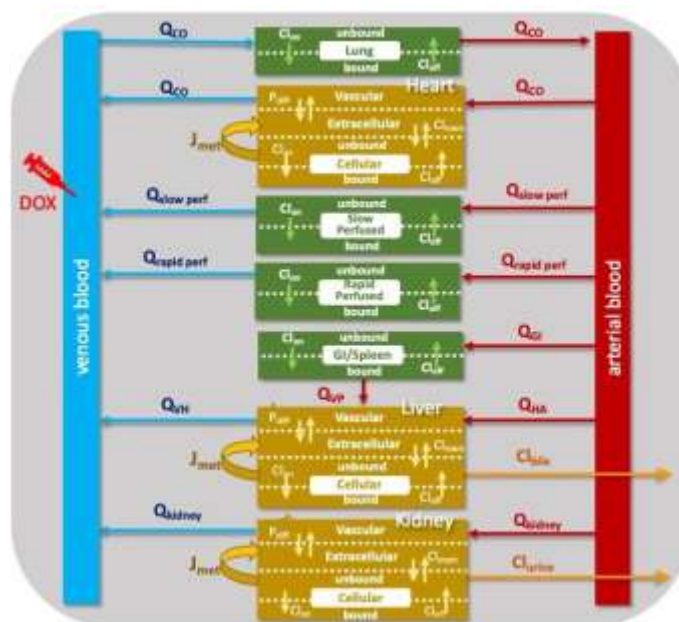


**Figure 3-5:** PBPK schematic of doxorubicin, adapted from the pig model created by Dubbelboer et al. 2017 to add a heart compartment as a metabolizing compartment; arterial blood is denoted by the red arrows and boxes, venous blood by blue arrows and boxes, non-metabolizing tissues are in green, and metabolizing tissues are in gold

There was no need to alter any of the other compartments in the original Dubbelboer model for two reasons. First, the model fit the data well without adding metabolism to any compartment, and it was not meaningful to add another compartment since the majority of the DOX-induced cardiotoxicity is related to the heart.[8] As mentioned earlier in this section, it is important to keep the number of equations and parameters to the fewest needed for ease of application and transparency.[143] The final model equations can be found in Appendix B. This approach appears to be the most practical in the case of DOX, as this model sufficiently describes the passage of DOX through the body. In general, necessary assumptions are made in order to reasonably

simplify the model while incorporating only the relevant details that affect the drug interaction. This prevents unneeded limitations on the system from cluttering the model and creating statistically insignificant variables for the sake of a more holistic model.

### 3.6 Conclusion

DOX is a crucial component in many cancer treatment protocols, and its continued use in patients is inevitable. However, as it stands, many patients are still under-dosed or over-dosed because dosing is often left to best estimates. A standard dose based on body weight or body surface area assumes that all patients will react in the same way to the drug. In reality, especially for drugs like 111 DOX, there is great disparity in the uptake, clearance, and metabolism among individuals. Optimizing individualized doses for patients based on identified characteristics will improve the overall therapeutic value of this already efficacious drug. Individualized dosing of DOX will also decrease the occurrence of cardiac damage in patients. The hope is to continue increasing the efficacy of treatment against their disease while minimizing cardiotoxic side effects.

The use of pharmacometrics will be key in the development of these individualized treatment protocols. Identifying key factors for variability and better understanding the clearance of DOX can someday be achieved through physiologically-based PK modeling. As shown, a semi-PBPK approach seems like the best method currently.

The semi-PBPK model proposed by Dubbelboer gave excellent insight on the plasma and respective tissue concentration without over-parameterizing. Since DOX considerably deposits in tissue, a physiological approach that incorporates tissue compartments along with blood compartments is ideal. However, biological and

physiological systems are complicated, intertwined systems that produce complex time courses. As shown in Chapter 2, even a drug with a relatively simple time course requires three coupled differential equations to capture the concentration-time profile of the plasma.[70, 36] Creating a whole-body model, even a minimal whole-body model, could require many more compartments and thus equations to adequately describe the system. As systems of equations get larger and more complex, it is more likely that an analytical or exact solution for that system is not possible. For these large systems of equations, numerical methods must be employed to solve the system. Some of the methods used to effectively solve the PBPK model of DOX described in this section will be discussed in Chapter 4.



## **CHAPTER 4**

### **NUMERICAL METHODS FOR PBPK MODELING**

Physiologically-based pharmacokinetic (PBPK) models are used to describe the concentration versus time profile of a drug or substance in a subject. While classic pharmacokinetic (PK) models only detail plasma concentration, a physiologically-based model, as its name suggests, uses physiological parameters to model the concentration in relevant organs and tissues. These organs, similar to a classic PK model, are generalized as compartments. Each compartment has a corresponding ordinary differential equation (ODE) with time as the independent variable that describes the rate of change of drug concentration in each compartment.

Unlike a classic PK model, a PBPK model requires more than a few compartments to describe the mass balance of the drug in the body. Thus, a very large system of ODEs is often associated with a PBPK model. However, the dimensionality of PBPK models can be computationally burdensome and inefficient. This is especially true in the programming language R, which is designed for statistical and data analysis, not necessarily for computation speed. It is generally known that ‘for’ loops and other conditional statements tend to be slow in the R language. R remains an extremely powerful open-source, free access tool across many fields. It remains one of the most flexible languages with a user-friendly interface R Studio, package building capabilities through Git, reporting features like RMarkdown, and app building capabilities through

RShiny. The R program is also extended by means of packages built and maintained by users themselves, which gives endless possibilities for the scope and expertise of its use. Despite its drawbacks, 112 113 the flexibility of the R language was the main rationale for using it for these models.[146]

## **4.1 Traditional Numerical Methods**

For large and complex systems of equations, numerical methods must be employed to solve the system. Some common numerical methods used to solve these systems include Euler's Method, Runge-Kutta Fourth Order method and Runge-Kutta Fehlberg Adaptive Step method. The following sections will cover these traditional methods since they were coded in R and applied to the PBPK model of interest.

For large and complex systems of equations, numerical methods must be employed to solve the system. Some common numerical methods used to solve these systems include Euler's Method, Runge-Kutta Fourth Order method and Runge-Kutta Fehlberg Adaptive Step method. The following sections will cover these traditional methods since they were coded in R and applied to the PBPK model of interest.:

### **4.1.1 Euler's Method**

Euler's Method is the most rudimentary technique for approximating the solution of initial value problems. The general concept of Euler's Method is to utilize multiple small line segments to approximate some actual curve  $y(t)$  versus  $t$ , assuming local linearity. Euler's Method is also called a tangent line approximation since each of these small line segments are tangent to the slope at that time point. Each step is based on the previous step's computed value.[147] Its simple construction is the basis for many other more complex approximation techniques. However, with its simplicity there are also

limitations, and due to these limitations, it is not always the appropriate method for real world problems. The goal of Euler's Method is to find the approximate solution to a well-posed initial value problem. Accordingly, the objective of Euler's Method is to solve the well-posed initial value problem,

$$\frac{dy}{dt} = f(t, y), a \leq t \leq b, y(a) = \alpha \quad (\text{Eq. 4-1})$$

Euler's Method does not give a continuous approximation of the solution  $y(t)$ . Instead, approximations of  $y$  are made at mesh points, which are values of  $t$  within the interval  $[a, b]$ . The approximations of  $y$  at other values of  $t$  within the interval can be derived through interpolation using the approximation generated at the mesh points. Because of this, a condition of Euler's Method is that mesh points are equally spaced throughout the interval. The uniform distance between mesh points is referred to as a step-size, denoted here as  $h$ , which is the value of  $t_{(i+1)} - t_i$ . This condition is ensured by choosing a positive integer value  $N$ , setting step-size  $h = (b - a)/N$ , then selecting the mesh points

$$t_i = a + ih, \quad (\text{Eq. 4-2})$$

for each  $i = 0, 1, 2, \dots, N$ .

Euler's Method can be derived from Taylor's Theorem, and that derivation can be found in Section 5.2 of Burden's Numerical Analysis.[5] The resulting equation for Euler's Method is

$$w_0 = \alpha, \quad (\text{Eq. 4-3})$$

$$w_{i+1} = w_i + hf(t_i, w_i) \quad (\text{Eq. 4-4})$$

for each  $i = 0, 1, \dots, N - 1$ .

This is called the difference equation associated with Euler's Method. With Euler's method, truncation and round-off error is not a major issue for systems with a short range of integration because relatively small time steps can be used without excessive computation time.[5]

Euler's Method was the first approximation technique tested on the system of ordinary differential equations related to the PBPK model. The benefit of trying Euler's Method first is that linearity of the system is not necessary, so long as the initial value problem is well-posed. Euler's Method is simple and easily to implement. However, as mentioned above, there are serious limitations to Euler's Method, which posed issues with the large, multifaceted ODE system needed to describe the PBPK model.

Euler's Method becomes unstable with a larger step size, so high accuracy and low relative error is only possible with very small time steps. For problems where the interval is reasonably small, one can use a small step size without suffering a long computing time. However, in the case of many pharmacokinetic models, the interest in the solution is the effect of the drug over some span of time. It was quickly apparent that the PBPK model here needed a much smaller time step than was reasonable to compute using Euler's method. The computational burden was high due to the small time step needed to capture the rapid change in concentration around each dose and the desired length of time to capture the clearance of the drug and metabolite from the system. These features of the PBPK model made Euler's Method computationally costly, with the rate-limiting step being the step size  $h$ . To make this method generalizable for PBPK models, a more efficient method was needed.

### 4.1.2 Runge-Kutta Methods

Methods like Euler's Method have the benefit of using the higher-order local truncation error, but have other drawbacks as mentioned in the previous section. Runge-Kutta Methods also have the benefit of higher-order local truncation error but forego the time-consuming process of calculating and evaluating the derivatives of the equation.

Runge-Kutta Fourth Order evaluates each equation four times per time step while Euler evaluates each equation only once per time step. To make Runge-Kutta Fourth Order more advantageous, a higher accuracy should be achieved at a step size four times larger than for Euler's Method. The formula for Runge-Kutta 116 Fourth Order contains a weighted average of  $f(t, y)$  at points within the interval  $t_n \leq t \leq t_{n+1}$  and is given by

$$\begin{aligned}
 w_0 &= \alpha, \\
 k_1 &= hf(t_i, w_i), \\
 k_2 &= hf\left(t_i + \frac{h}{2}, w_i + \frac{1}{2}k_1\right), \\
 k_3 &= hf\left(t_i + \frac{h}{2}, w_i + \frac{1}{2}k_2\right), \\
 k_4 &= hf(t_{i+1}, w_i + k_3), \\
 w_{i+1} &= w_i + \frac{1}{6}(k_1 + 2k_2 + 2k_3 + k_4),
 \end{aligned}$$

for each  $i = 0, 1, \dots, N - 1$ . This summation  $\frac{1}{6}(k_1 + 2k_2 + 2k_3 + k_4)$  is taken as an average slope. In the equations above,  $k_1$  is the slope at the left side of the interval,  $k_2$  is the slope at the midpoint using Euler's formula from  $t_n$  to  $t_n + \frac{h}{2}$ ,  $k_3$  is a second estimate of the slope at the midpoint, and  $k_4$  is the slope at the right side of the interval,  $t_n + h$ . As long as the solution has five continuous derivatives, Runge-Kutta Order Four has a local truncation error proportional to  $h^5$  for a finite time interval the global truncation error of

at most  $O(h^4)$ . Compared to Euler's method in the previous section, which has local truncation errors proportional to  $h$ ,  $h^2$ , and  $h^3$ , Runge-Kutta Order Four should be two to three orders of magnitude more accurate than Euler's method and other Taylor derived methods.[5]

The relative simplicity of the Runge-Kutta Order Four method and the improved accuracy was the rationale for applying it to our PBPK model. As mentioned before, for the same accuracy, the Runge-Kutta Order Four should be as accurate as Euler's Method with a step size four times as large. In practice, however, the step size still needed to be extremely small to capture the rapid change following the dose. With the increased complexity, the run times per iteration were actually much slower than with Euler's Method with only marginally better accuracy. It was apparent that there was a possibility that the ODE system was having issues with stiffness.

#### 4.1.2.1 Stiffness

A stiff differential equation is defined as an equation which becomes numerically unstable when solved using certain numerical methods, unless an extremely small time step is used. All approximation methods for initial value problems mentioned here, and in general, include error terms that are derivatives of higher order than the solution to the equation.[148] When the magnitude of the derivative increases but the magnitude of the solution does not, there is no predictable error bound that can be used to estimate the accuracy of the approximation. In these cases, the error can grow such that it dominates the calculation. An equation having this property is said to be a stiff equation.[7]

Our large system of equations evidently had some stiff and some non-stiff portions of only certain equations. In some cases, the volume that the concentration was

divided by was much smaller in one compartment and much larger in others. For example, when a concentration spread over a large volume, say the arterial blood, entered a smaller compartment like the cellular sub-compartment of the kidney, there would often be up to an order of magnitude of difference between the two volumes. As the drug entered the compartment, the concentration or amount would spike orders of magnitude as it was moved into a much smaller volume. This rapid change may happen at some time point in one equation, while the major change in the venous blood would occur mainly at the dosing intervals. In a complex system of 40 equations, these concentration spikes could happen at many different times. The primary issue, however, was the rapid change in concentration at each dose, which required a very small time step to capture the injection profile, followed by a period of very little change as the drug cleared the system. The very small time step needed over the first time interval was unnecessary for the remainder of the time interval, but without it, the injection profile was not well captured.

Of course, the human body is not divided into literal compartments, but the physiological challenge of representing the systems of the body must be discretized in some way. While these volume changes may not pose a problem in reality, these compartmental surrogates for human organs pose a mathematical challenge to overcome. The identification of the PBPK system as stiff led us to move on to more adaptive methods that were designed to better control the error bound.

#### **4.1.3 Adaptive-Step Runge-Kutta-Fehlberg**

To address the issue of stiffness in the PBPK system, adaptive-step methods were investigated. Adaptive methods incorporate error control, which adds an estimate of

truncation error without requiring the approximation of higher-order derivatives of the function.[7] In general, adaptive step methods will alter the step size as it moves through the time interval, based on the amount of change occurring in the sub-interval. The general idea is that given some tolerance  $\epsilon > 0$ , the fewest number of mesh points could be used to guarantee that the global error  $|y(t_i) - w_i|$  does not exceed the tolerance  $E$  anywhere in the solution. This concept of setting a tolerance to which the error cannot exceed is sometimes referred to as inequality in terms of error control.[5] While in general the global error cannot be determined directly, there is a close correlation between the local truncation error and the global error. To briefly summarize the idea, the general concept of adaptive step methods is to use the fewest data points while not exceeding a certain upper bound on error, which almost always requires that the step sizes be unequally spaced. When considering computation time, this optimization of number of mesh points is unnecessary for simple problems. In those cases, it may be possible to use a fairly large step size with adequate accuracy and a short computation time. However, in the case of stiff differential equations, the extremely small step size needed to control the error in some subintervals carries high computational burden when forced to apply a constant step size to the entire time interval.[148] As mentioned previously, in cases of pharmacokinetic models, one of the components of interest is the clearance of the drug, which can take anywhere from hours to days. For a stiff system in this context, the extremely small time step for an interval of many hours or days is not practical.

After already structuring the system for Runge-Kutta Method Order Four, the Runge-Kutta-Fehlberg Method was a logical adaptive step method to implement first.



The Runge-Kutta-Fehlberg method estimates the local error of a fourth-order Runge-Kutta method,

$$w_{i+1} = w_i + \frac{25}{216}k_1 + \frac{1408}{2565}k_3 + \frac{2197}{4104}k_4 - \frac{1}{5}k_5, \quad (\text{Eq. 4-5})$$

by using a Runge-Kutta method with local truncation error of order five

$$\tilde{w}_{i+1} = w_i + \frac{16}{135}k_1 + \frac{6656}{12825}k_3 + \frac{28561}{56430}k_4 - \frac{9}{50}k_5 + \frac{2}{55}k_6 \quad (\text{Eq. 4-6})$$

Where the coefficient equations are

$$k_1 = hf(t_i, w_i),$$

$$k_2 = hf\left(t_i + \frac{h}{4}, w_i + \frac{1}{4}k_1\right),$$

$$k_3 = hf\left(t_i + \frac{3h}{8}, w_i + \frac{3}{32}k_1 + \frac{9}{32}k_2\right),$$

$$k_4 = hf\left(t_i + \frac{12h}{13}, w_i + \frac{1932}{2197}k_1 - \frac{7200}{2197}k_2 + \frac{7296}{2197}k_3\right),$$

$$k_5 = hf\left(t_i + h, w_i + \frac{439}{216}k_1 - 8k_2 + \frac{3680}{513}k_3 - \frac{845}{4104}k_4\right),$$

$$k_6 = hf\left(t_i + \frac{h}{2}, w_i - \frac{8}{27}k_1 + 2k_2 - \frac{3544}{2565}k_3 + \frac{1859}{4104}k_4 - \frac{11}{40}k_5\right)$$

This Runge-Kutta method with the above coefficients define the Runge-Kutta Fehlberg method and require only six evaluations of the function. This particular 120 method has an advantage over more arbitrary Runge-Kutta methods combining fourth and fifth order. Such methods require at least four evaluations of the function for the fourth-order method and six evaluations for order five, bringing the total to a minimum of ten evaluations of the function per time step. This significantly decreases the computation time.

The difference in the two local truncation errors  $|w_{i+1} - \tilde{w}_{i+1}|$  is interchangeably denoted as  $R$  and compared to the tolerance  $\epsilon$  set by the user at the  $i^{\text{th}}$  step. This comparison essentially determines the action to be taken on the step size using an adjustment factor  $q$ . The value of  $q$  is used differently at each  $i^{\text{th}}$  step depending on whether or not  $R$  is greater than the defined tolerance  $\epsilon$ . That is to say, whether the error at that step is acceptable to the user.

If  $R > \epsilon$ , the initial choice of the step-size  $h$  at the  $i^{\text{th}}$  step is rejected and the calculation is repeated using a different step-size  $qh$ . If  $R \leq \epsilon$ , then the error is within the tolerance and the computed value at the  $i^{\text{th}}$  step is accepted. The step size is changed to  $qh$  for the  $(i + 1)^{\text{st}}$  step.

Repeating function evaluations is costly, so  $q$  is usually chosen conservatively to lessen the chance of  $R$  exceeding  $\epsilon$ . For example, for the Runge-Kutta-Fehlberg method with  $n = 4$ , is a common choice for calculation  $q$ . This convention was used when evaluating the PBPK model of interest.[7]

$$q = \left( \frac{\epsilon h}{2|w_{i+1} - \tilde{w}_{i+1}|} \right)^{\frac{1}{4}} \quad (\text{Eq. 4-7})$$

$$= 0.84 \left( \frac{\epsilon h}{|w_{i+1} - \tilde{w}_{i+1}|} \right)^{\frac{1}{4}} \quad (\text{Eq. 4-8})$$

$$= 0.84 \left( \frac{\epsilon}{R} \right)^{\frac{1}{n}}, \quad (\text{Eq. 4-9})$$

There are some optional additions to the algorithm that help eliminate large changes in step size from one step to the next. This is done to reduce time spent using small step sizes in regions with irregular derivatives of the function and avoid very large step sizes that could skip over sensitive regions. If the only concern is error control, only the step-size decrease procedure is needed and the step-size increase procedure could be

omitted from the algorithm.[5] In the case of our PBPK model, the computation time was a major inhibitor, so both procedures were implemented in the algorithm to save time.

When we executed the Runge-Kutta-Fehlberg Method, the accuracy improved considerably. However, despite efforts to save computation time, it was still extremely slow. The time step remained very small throughout the time interval, making it somewhat infeasible for the model fitting and parameter estimation necessary for the future purposes of our model. After much consideration and adjusting the model, it was best to move on to another method for solving the system.

#### **4.1.4 Summarizing Traditional Methods**

The first method used to solve the system was Euler's Method, since it is simple and its structure is common to many other more complicated methods. It is a great option for solving a system of linear equation as an initial value problem. However, the system was unstable except for very small time steps. Computation was unacceptably slow due to the length of the time interval needed for PBPK modeling. For better stability, the Runge-Kutta Order Four was implemented to solve the system. This method evaluates the function four times at each time point with the rationale that for the same accuracy as Euler's Method, a Runge-Kutta Order Four could use a step size four times larger. This feature was attractive. Unfortunately, very small time steps were still necessary to solve the system, and the complexity of the method actually slowed the computation down in R. It was at this point that we realized the system had an issue with stiffness, so an adaptive-step method – Runge-Kutta-Fehlberg Method – was applied. Using this method greatly improved the accuracy of the solution and handled the stiffness. However, the computation time was still too slow for practical purposes of model fitting.

## 4.2. Eigenvalue/Eigenvector Solution

The final method uses the eigenvalue/eigenvector solution to a system of linear ODEs.[149] At its core, R has a suite of operators for matrix calculations. Because of its design, matrix manipulation is computationally fast in R. Computation speed is critical for model fitting and parameter estimation, especially for large models, because of the need to calculate the solution many times. When using R, solving a system of equations as a matrix should compute faster than when written directly as a system of subsequent equations.[146]

In this method, the ODEs are represented as an  $n \times n$  rate coefficient matrix ( $A$ ) of blood flow rates divided by compartment volume and an  $n \times 1$  initial condition matrix ( $x$ ) define a system of homogeneous equations.[7, 149]

$$x'=Ax \quad (\text{Eq. 4-10})$$

In the homogeneous case, some of the injection profile is lost. The model only captures the flow of drug through the body and its clearance, as if at  $t_0$ , the full injection amount exists in the venous blood compartment. The model realistically could only capture bolus type infusions or quasi-instantaneous injections. This can be remedied by the addition of a rate vector  $g(t)$ , but this also makes the system non-homogeneous.

For a non-homogeneous system, the additional vector is added as shown below. This column vector  $g(t)$  represents injection rate as a function of time. This system not only allows for the infusion profile to be captured but also allows for more realistic scenarios.

$$x'=Ax +g(t) \quad (\text{Eq. 4-11})$$

Very large systems of ODEs are often difficult to solve analytically, so in order to show our method is accurate for large systems, we will walk through a smaller example from Elementary Differential Equations by Boyce et al.[7] This simple example will be written and solved in R and compared to the analytical solution to verify the accuracy of the method choice and the code. The example will take the place of the formula for the method, since it is a much clearer illustration than the direct definition.

#### 4.2.1 Simple Homogeneous Example

Consider the simple homogeneous case,

$$x' = \begin{pmatrix} -2 & 1 \\ 1 & -2 \end{pmatrix} x = Ax. \quad (\text{Eq. 4-12})$$

The coefficient matrix A is real and symmetric, and we assume that  $\mathbf{x} = \xi e^{rt}$ , we obtain the algebraic system,

$$\begin{pmatrix} -2-r & 1 \\ 1 & -2-r \end{pmatrix} \begin{pmatrix} \xi_1 \\ \xi_2 \end{pmatrix} = \begin{pmatrix} 0 \\ 0 \end{pmatrix}. \quad (\text{Eq. 4-13})$$

The Eigenvalues satisfy

$$(-2-r)(-2-r) - 1 = r^2 + 4r + 3 = (r+3)(r+1) = 0 \quad (\text{Eq. 4-14})$$

so  $r_1 = -3$  and  $r_2 = -1$ . For  $r = -3$ , Equation 4.13 becomes

$$\begin{pmatrix} 1 & 1 \\ 1 & 1 \end{pmatrix} \begin{pmatrix} \xi_1 \\ \xi_2 \end{pmatrix} = \begin{pmatrix} 0 \\ 0 \end{pmatrix}. \quad (\text{Eq. 4-15})$$

Hence,  $\xi_2 = \xi_1$  and the corresponding eigenvector  $\xi^{(1)}$  corresponding to the eigenvalue,  $r_1 = -3$  can be taken as

$$\xi^{(1)} = \begin{pmatrix} 1 \\ 1 \end{pmatrix} \quad (\text{Eq. 4-16})$$

Similarly, for  $r = -1$ , Equation 4-13 becomes

$$\begin{pmatrix} -1 & 1 \\ 1 & -1 \end{pmatrix} \begin{pmatrix} \xi_1 \\ \xi_2 \end{pmatrix} = \begin{pmatrix} 0 \\ 0 \end{pmatrix}. \quad (\text{Eq. 4-17})$$

Hence,  $\xi_1 = \xi_2$  and the corresponding eigenvector  $\xi^{(2)}$  corresponding to the eigenvalue  $r_2 = -1$  can be taken as

$$\xi^{(2)} = \begin{pmatrix} 1 \\ -1 \end{pmatrix} \quad (\text{Eq. 4-18})$$

Thus, a fundamental set of solutions for the system in Equation 4.12 is

$$x^{(1)}(t) = \begin{pmatrix} 1 \\ 1 \end{pmatrix} e^{-t}, x^{(2)}(t) = \begin{pmatrix} 1 \\ -1 \end{pmatrix} e^{-3t}. \quad (\text{Eq. 4-19})$$

and the general solution is

$$x = c_1 x^{(1)}(t) + c_2 x^{(2)}(t) = c_1 \begin{pmatrix} 1 \\ 1 \end{pmatrix} e^{-t} + c_2 \begin{pmatrix} 1 \\ -1 \end{pmatrix} e^{-3t}. \quad (\text{Eq. 4-20})$$

The general solution of the homogeneous case is key to obtaining the particular solution for the non-homogeneous case. The fundamental matrix  $\Psi(t)$  is the starting point for nearly all methods of solving non-homogeneous systems.  $\Psi(t)$  obtained from the general solution by the following method.[7]

#### 4.2.2 Simple Non-Homogeneous Example

Suppose that that  $\mathbf{x}^{(1)}, \dots, \mathbf{x}^{(n)}$  form a fundamental set of solutions as in Equation 4.19 for the equation

$$\mathbf{x}' = \mathbf{P}(t)\mathbf{x} \quad (\text{Eq. 4-21})$$

on some interval  $\alpha < t < \beta$ . Then the matrix

$$\Psi(t) = \begin{pmatrix} x_1^{(1)}(t) & \cdots & x_1^{(n)}(t) \\ \vdots & \ddots & \vdots \\ x_n^{(1)}(t) & \cdots & x_n^{(n)}(t) \end{pmatrix} \quad (\text{Eq. 4-22})$$

whose columns are the vectors  $\mathbf{x}^{(1)}, \dots, \mathbf{x}^{(n)}$  is said to be a fundamental matrix for the system. So, for the example above, the fundamental matrix is

$$\Psi(t) = \begin{pmatrix} e^{-t} & e^{-3t} \\ e^{-t} & -e^{-3t} \end{pmatrix} \quad (\text{Eq. 4-23})$$

which is useful for solving the non-homogeneous system,

$$x' = \begin{pmatrix} -2 & 1 \\ 1 & -2 \end{pmatrix} x + \begin{pmatrix} 2e^{-t} \\ 3t \end{pmatrix} = Ax + g(t). \quad (\text{Eq. 4-24})$$

We use Variation of Parameters to solve this system. The solution  $\mathbf{x}$  of this system is given as  $\mathbf{x} = \Psi(t)\mathbf{u}(t)$ , where  $\mathbf{u}(t)$  satisfies  $\Psi(t)\mathbf{u}(t) = \mathbf{g}(t)$ , or

$$\begin{pmatrix} e^{-t} & e^{-3t} \\ e^{-t} & -e^{-3t} \end{pmatrix} \begin{pmatrix} u_1' \\ u_2' \end{pmatrix} = \begin{pmatrix} 2e^{-t} \\ 3t \end{pmatrix} \quad (\text{Eq. 4-25})$$

By left-multiplying the fundamental matrix on both sides, the  $\mathbf{u}(t)$  vector can be obtained. This approach is used in the consequent code, but for now, the following equations are obtained by row reduction.

$$u_1' = e^{2t} - \frac{3}{2}te^{3t}, u_2' = 1 + \frac{3}{2}te^t. \quad (\text{Eq. 4-26})$$

Hence,

$$\mathbf{x} = \Psi(t)\mathbf{u}(t) \quad (\text{Eq. 4-27})$$

$$= c_1 \begin{pmatrix} 1 \\ 1 \end{pmatrix} e^{-t} + c_2 \begin{pmatrix} 1 \\ -1 \end{pmatrix} e^{-3t} + \begin{pmatrix} 1 \\ 1 \end{pmatrix} te^{-t} + \frac{1}{2} \begin{pmatrix} 1 \\ -1 \end{pmatrix} e^{-t} + \begin{pmatrix} 1 \\ 2 \end{pmatrix} t - \frac{1}{3} \begin{pmatrix} 4 \\ 5 \end{pmatrix}. \quad (\text{Eq. 4-28})$$

To determine the integration constants, the system should be solved at some time point in the interval. For the remaining points in the solution, the integration constants  $c_1$  and  $c_2$  do not change. For instance, when  $x_0 = 0$ ,  $t = 0$ , constants  $c_1$ ,  $c_2$  are  $-\frac{2}{3}$  and  $\frac{3}{2}$ , respectively. [7] Those constants will remain true as long as the initial conditions and equations do not change.

Once these integration constants are determined, this process provides a solution to the system at any specified time. Its major limitation being it only produces a solution for the last time point, which should be a reasonably small time interval in order to capture the change in  $y$  adequately. However, we are able to use that solution as the initial condition for the next iteration of the function.

### 4.2.3 Numerical Integration: Series of Eigenvalue/Eigenvector Solutions of Initial Value Problems

This small non-homogeneous system is solved in preparation for the ultimate goal of solving a large system of equations. This larger physiological system will be solved over a fairly long time interval since the clearance of the drug from the body, a behavior of interest, can be many hours or days long depending on the half-life of the drug. Because this large time interval is much greater than a suitable interval for a single iteration of our Eigenvalue/Eigenvector solution described in the previous section. Instead, the solution to a sufficiently small time interval will become the new initial condition for the next iteration of the method. These exact solutions are then to be integrated over using a numerical integration method. Numerical integration is needed since in some cases, there is no explicit or easy obtainable anti-derivative to be calculated for the equations of the system. [150]

Numerical integration is based on a summation technique called numerical quadrature, which simply means using a sum  $\sum_{i=0}^n a_i f(x_i)$  to approximate  $\int_a^b f(x) dx$ . The method requires choosing a set of distinct points on the interval  $[a, b]$ . From the chosen points, numerical quadrature calls for integrating over a Lagrange interpolating polynomial. Common methods that use Lagrange interpolating polynomials with equally spaced points include the Trapezoidal Rule and Simpson's Rule. These types of methods are in the family of Newton-Cotes formulas. More detail and derivations for these techniques in Section 4.3 of Burden's Numerical Analysis.[5] Using a Taylor Series expansion and the Weighted Mean Value Theorem for Integrals gives Simpson's 1/3 Rule:



$$\int_{x_0}^{x_2} f(x)dx = \frac{h}{3} [f(x_0) + 4f(x_1) + f(x_2)] - \frac{h^5}{90} f^{(4)}(\xi(x)). \quad (\text{Eq. 4-29})$$

Notice in Equation 4.29 that the error term in Simpson's Rule involves the fourth derivative of  $f$ , meaning it gives an exact result when applied to a polynomial of degree three or less. In contrast, the error term of the Trapezoidal rule ( can only give an exact result for a polynomial of degree one. When choosing a numerical integration technique, Simpson's Rule was preferable simply due to its improved accuracy. Aside from the higher-order derivative in the error term, the midpoint calculation included in Simpson's Rule gives the approximation more balance. Returning to the problem, the integration from  $x_0$  and  $x_2$  using Simpson's Rule described in Equation 4.29 are replaced by some  $u'(t)$  from Variation of Parameters (recall Equation 4.26). We obtain the values for each time point  $\tau$  by solving  $u'(t)$  at an odd number of time points.[5] This integral effectively replaces the integral portion of the equation since  $u'(t)$  is obtained by multiplying the inverted fundamental matrix by the 'g vector' at the given time interval.[7]

$$x(t) = \Phi(t)x^0 + \Phi(t) \int_{t_0}^t \Phi^{-1}(s)g(s)ds, \quad (\text{Eq. 4-30})$$

Once  $x(t)$  is calculated, it becomes the new initial condition for the next iteration; thus becoming a series of initial value problems. The schematic of the general process is shown in Figure 4-1 and the model code is available in Appendix E.

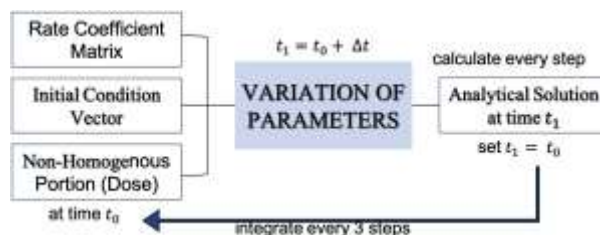


**Figure 4-1:** A schematic of the general process of the matrix-based numerical method

Figure 4-2 shows that the accuracy for larger step sizes is comparable to smaller ones. The previous examples show that the concept of utilizing an eigenvalue / eigenvector solution with numerical integration is a valid technique for solving large systems of ordinary differential equations. However, one of the primary issues with the physiological system of interest is stiffness.

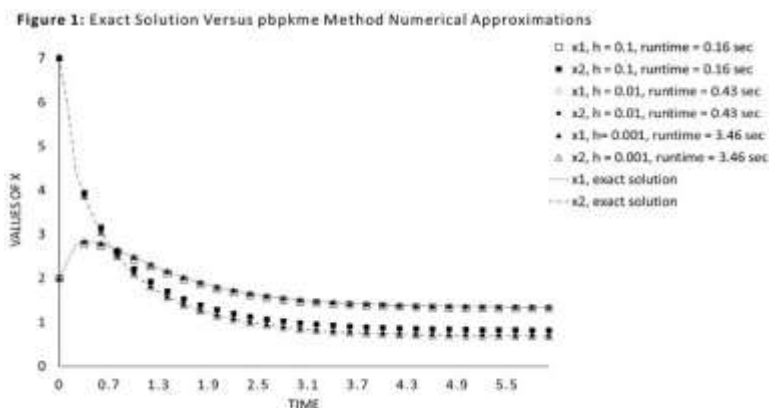


**Figure 4-2:** Solutions to 2 x 2 example, solved with three different step-sizes and compared to the exact solution at each time point. The accuracy compared to the step-size here demonstrates the negligible loss of accuracy for larger step sizes using this method

For stiff systems, there are even more appropriate numerical integration techniques that can be implemented to improve efficiency. Similar to the Adaptive-Step Runge-Kutta-Fehlberg method discussed in Section 4.1.3, numerical integration methods can be extended to adaptive numerical quadrature methods. Recalling that, in general, adaptive step methods seek to use the fewest data points while not exceeding a certain upper bound on error. This goal is rarely achieved with equally spaced points. Instead, adaptive step methods adjust the step size with each iteration, depending on the amount of change occurring in that particular 130 time interval. The primary issue with stiffness is the need to maintain a very small step size in order for the system to be stable.[7, 148]

A small time step size over long time periods cause concern with computational efficacy. For the purposes of this work in solving the 44 compartment PBPK model, using the matrix framework allowed for even models with time intervals spanning up to 96 hours at step sizes of 0.05 to solve within minutes. The issue of stiffness, while still present in this model system, did not hinder the computation speed enough to justify the additional effort and complexity. Therefore, a more complex adaptive method would not add a necessary improvement in this case. Were this method to become necessary for a particularly stiff physiological system, the following approach would be appropriate for varying the step size.

#### *4.2.3.1 Adaptive Numerical Integration*

If a more efficient option had become necessary, this matrix method could be further generalized by equipping the method to solve both stiff and non-stiff systems. For large systems with significant changes in some time intervals and not in others, the issue of stiffness could be remedied by implementing an adaptive numerical integration technique to increase computation efficiency. Since the structure of Simpson's Rule was already present for the matrix method, it would be intuitive to choose the adaptive step method corresponding to Simpson's Rule - Adaptive Composite Simpson's Rule. First, we must briefly explain the structure of Composite Simpson's Rule in order to move on to the adaptive version. The primary difference in Simpson's Rule and Composite Simpson's Rule is how the step-size  $h$  is calculated. While Simpson's Rule calculates  $h$  as  $(b - a)/2$ , Composite Simpson's Rule uses  $h = (b - a)/n$  for any positive even integer  $n$ . This gives the flexibility of subdividing the interval  $[a, b]$  into  $n$  even sub-intervals instead of 2 in regular Simpson's Rule's. In general, Newton-Cotes methods like

Simpson's Rule, Trapezoidal rule, and the like, are less suitable for long integration intervals than piece-wise methods. Composite Simpson's Rule is one such method that uses a lower-order Simpson's Rule. To maintain accuracy over a large interval, a high-degree formula would be required since higher-degree polynomials tend to oscillate. Coefficients for high-order formulas are difficult to obtain, so using a lower-order Newton-Cotes formula like Simpson's Rule for a piece-wise approach is beneficial. The lower order derivative The lower order derivative in the error term is compensated for by the ability to make the step-size  $h$  considerably smaller for intervals with considerably more change. This method is outlined in Section 4.4 of Burden's Numerical Analysis, specifically in Algorithm 4.1. Composite Simpson's Rule is the most frequently used quadrature algorithm for general purposes.[5]

Then, with the added advantage of choosing an even integer value for  $n$ , Adaptive Composite Simpson's Rule uses Algorithm 4.3 in Section 4.6 of Burden's Numerical Analysis to continue to divide sub-intervals into increasingly more sub-intervals for areas where there is great change until the error is below some tolerance. In Algorithm 4.3, the error is determined using the difference between the approximation of Simpson's Rule and the approximation for the summation of the approximations for the halved sub-intervals. In other words, if the total interval  $a$  to  $b$  is bisected by  $c$ , then the Algorithm calculates from  $a$  to midpoint  $c$  with a midpoint between. The same process is done for the sub-interval  $c$  to  $b$ . The sum of the approximations of those two halves are compared against the original Simpson's Rule approximation to see if error falls within a tolerance. If it does, the approximation is accepted, and the integration progresses to the next time-step. If it does not, each half sub-interval is halved again, and the process described above

is carried out on each of the two new halves.[5] For very tricky systems, this algorithm could be a great solution, and it may be interesting to consider for future work.

### 4.3 Comparison of Methods

Unlike the traditional numerical methods, this matrix method is not susceptible to issues with stiffness since the analytical solution for each time interval is calculated and then numerically integrated using Adaptive Composite Simpson's rule. It allows the modeler to use an adaptive time step, maintaining fewer mesh points for the same accuracy. Thus, any linear or approximately linear system can be described using this method in a more efficient way than traditional adaptive-step methods. This textbook example solved analytically and using this matrix-based numerical approach served as an initial validation for the R code. As mentioned in earlier sections, the overall process for solving any system of linear ordinary differential equations is broken down into a few matrices that go into one simple function and output a matrix of concentrations from the initial time to the final time at increments of two times the step size (Figure 4-3). The increments are twice the step size due to the numerical integration in Composite Simpson rule. The function in R contains all the matrix manipulation shown in the sections for Variation Parameters along with the implementation of Simpson's 1/3 Rule for the integration over time.

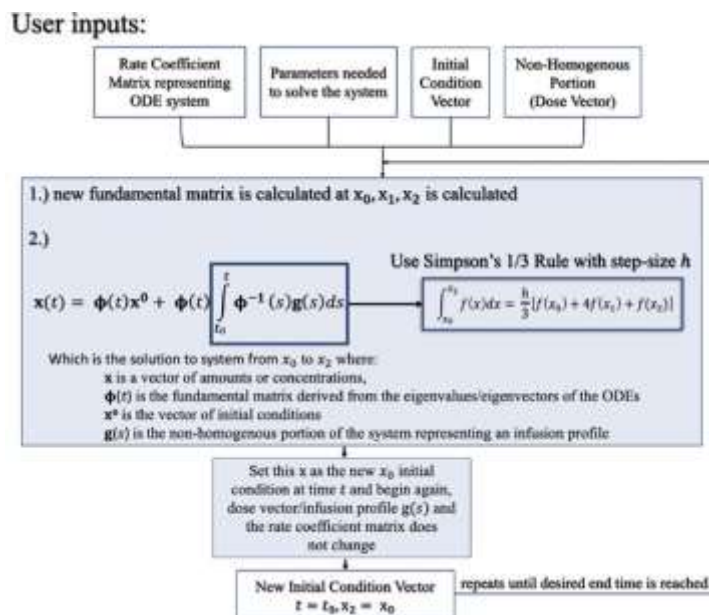


**Figure 4-3:** A more detailed flow of the inputs and outputs of the matrix-based numerical method

## 4.4 Compartmental Model Examples

### 4.4.1 Three-Compartment PK Model Example

Once the functions for calculating the solutions were trustworthy, we were wary of making a jump from a 2 x 2 matrix example to a 40 x 40 complex physiological system without an intermediate step. From the literature, a simple three-compartment pharmacokinetic model of Remifentanil was chosen.[151] This model was described by three coupled first-order ordinary differential equations that were clearly published in the paper with all necessary parameters and plots, making it ideal for reproduction for validation. The equations shown below describe the model in Figure 4-4.

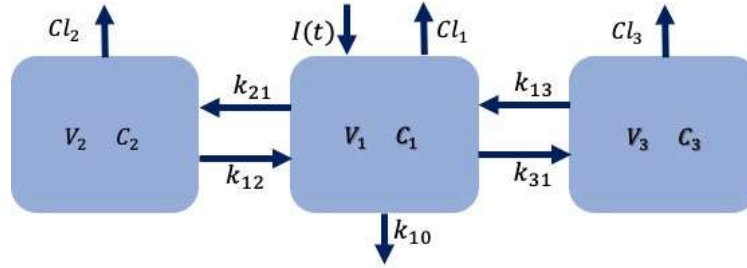


**Figure 4-4:** A traditional representation of a three-compartment pharmacokinetic model described by Cascone et al

Central Compartment

$$V_1 \frac{dC_p}{dt} = -CL_1 C_1 + k_{21} V_2 C_2 + k_{31} C_3 V_3 - [(k_{12} + k_{13} + k_{10}) C_1] V_1 + I(t)$$

Highly Perfused Compartment

$$V_2 \frac{dC_2}{dt} = k_{12} C_1 V_1 - k_{21} C_2 V_2 - C_{12} C_2$$

Scarcely Perfused Compartment

$$V_3 \frac{dC_3}{dt} = k_{13} C_1 V_1 - k_{31} C_3 V_3 - C_{13} C_3$$

Instead of representing the system in the traditional equation format, the same equations can be represented in matrix format as shown below, where the matrix  $\mathbf{A}$  represents the rate coefficients and parameters,  $x$  represents the initial conditions, or in this case, the initial concentrations,  $\mathbf{g}(t)$  is the dose vector, and  $x'$  is the solution to the system at a given time.[7]

$$\begin{pmatrix} -\left(\frac{Cl_1}{V_1} + k_{12} + k_{13} + k_{10}\right) & k_{21}V_2/V_1 & k_{31}V_3/V_1 \\ k_{12}V_1/V_2 & -\left(\frac{Cl_2}{V_2} + k_{21}\right) & 0 \\ k_{13}V_1/V_3 & 0 & -\left(\frac{Cl_3}{V_3} + k_{31}\right) \end{pmatrix} \begin{pmatrix} C_1 \\ C_2 \\ C_3 \end{pmatrix} + \begin{pmatrix} I(t) \\ 0 \\ 0 \end{pmatrix} = \begin{pmatrix} dC_1/dt \\ dC_2/dt \\ dC_3/dt \end{pmatrix} \quad (\text{Eq. 4-31})$$

Instead of attempting to solve directly for the analytical solution over the two-hour span of observations, a plot from the paper digitized paper and compared it to the solution generated by our matrix method. The observations overlaid on our model predictions using the author's parameters are shown in Figure 4-5. As you can see, the model fit is good, and the curve is comparable to the curve generated by the original authors. [151] The source R code for this model example is available in Appendix C.

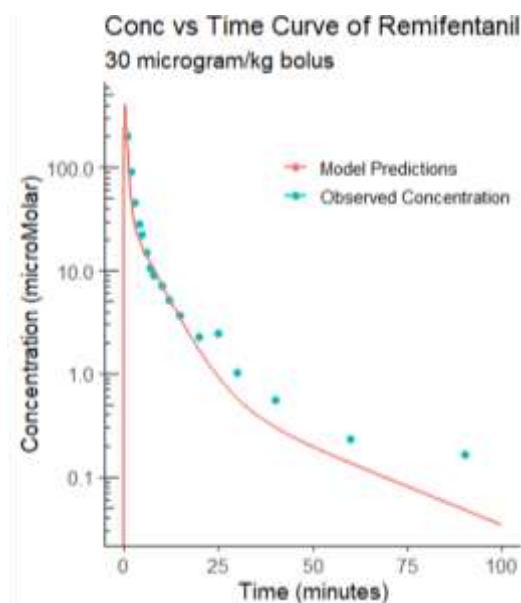


**Figure 4-5:** Plot of observed versus model predicted values for the human Remfentanyl model, illustrating that the pbpkme method works at least as well as traditional numerical methods on classic compartmental pharmacokinetic models



#### 4.4.2 Physiologically-Based Pharmacokinetic (PBPK) Example

The solutions from the three-compartment model were validation enough to move forward to this forty compartment PBPK model of doxorubicin (DOX) from literature, which is the model of interest. There were too many equations to reasonably list them all for the purpose of this paper, but the full equations can be found in the online Supplementary Material from the original paper.[8] The general schematic of the PBPK model (Figure 4-6) is complex in itself, including both bound and unbound drug for five non-metabolizing compartments, two blood compartments, two metabolizing compartments with three sub-compartments each, for both the parent drug, doxorubicin, and the metabolite, doxorubicinol.

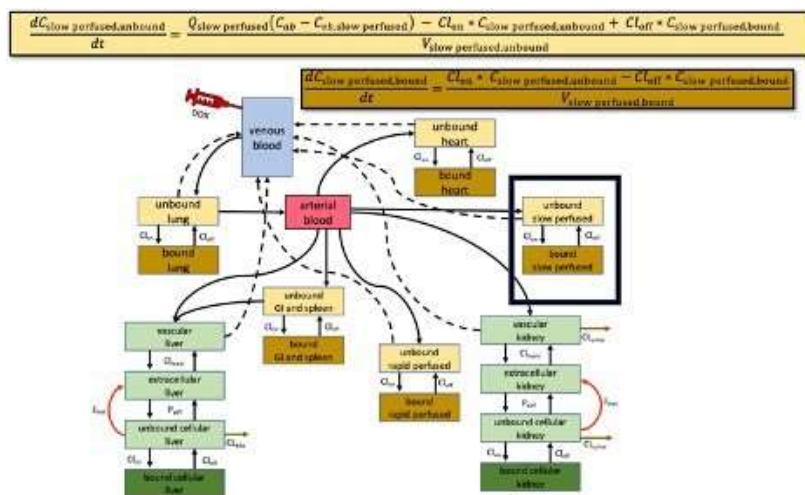


**Figure 4-6:** Plot of observed versus model predicted values for the human Remfentamil model, illustrating that the pbpkme method works at least as well as traditional numerical methods on classic compartmental pharmacokinetic models

The metabolism from DOX to DOXol in this model is described by Michaelis-Menten kinetics[83], and for DOX, the substrate concentration is negligibly smaller than the Michaelis constant.[17, 66, 128] This means the reaction rate and concentration are

directly proportionate to each other, the reaction remains first-order linear. The two equations highlighted in Figure 4-6 show that these types of models, while described by first-order ordinary differential equations, have considerable complexity in addition to dimensionality.

It should be little surprise that a system like this would run into issues of stiffness and computational efficiency. Just like in the previous three-compartment model, we represent the differential equations in matrix format. The detail in a model this large complex would make the actual matrix unreadable here, but the structure is shown above. The matrix components,  $\mathbf{A}$ ,  $\mathbf{x}$ ,  $\mathbf{g}(t)$ , and  $\mathbf{xt}$  retain the same meaning as in the three-compartment model.[7, 151] This matrix structure is universal no matter how many ordinary differential equations are in the system, which makes it generalizable. With the variety and complexity of mathematical models needed throughout the field of pharmaceutical sciences, this structure is ideal for application in pharmacometrics.

$$\begin{pmatrix} -(Q_1/V_1) & \cdots & (Q_n/V_1) \\ \vdots & \ddots & \vdots \\ -(Q_1/V_n) & \cdots & (Q_n/V_n) \end{pmatrix} \begin{pmatrix} C_{10} \\ \vdots \\ C_{n0} \end{pmatrix} = \begin{pmatrix} dC_{10}/dt \\ \vdots \\ dC_{n0}/dt \end{pmatrix} \quad (\text{Eq. 4-32})$$

No exact solution can be computed for this model, so another visual predictive check was implemented for validation. A plot from the original paper[8] was digitized and compared to the solution generated by the matrix-based method, and the results are shown in Figure 4-7. The red dashed line is from literature, and the matrix solution is in blue – you can see they overlay almost exactly, which was an excellent validation that this method works.

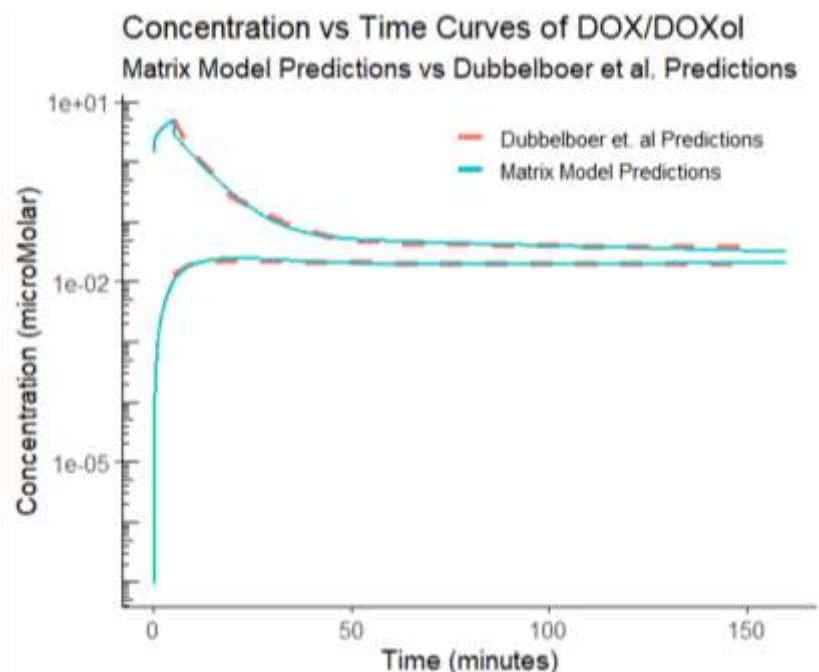


**Figure 4-7:** Predictions from the model solved with the matrix-based numerical method overlaid on the predictions generated by the digitized predictions from Dubbelboer et al.

#### 4.5 Conclusion

Linear systems of ordinary differential equations have limitless application in all fields of study and in countless real-world problems. Combining two established methods – Variation of Parameters[7] and Simpson’s 1/3 Rule[5] – gives an elegant framework for solving any linear system of ordinary differential equations, but especially those dealing with stiffness and long computation time. In those cases, this matrix-based numerical method is likely to perform better than many traditional methods when solved in R. Stiff, high-dimensional ODE systems are unsurprisingly common in PK and PBPK models, since they are characterizing a physiological system. One limitation to this method is that, as briefly mentioned in Section 2.2.1, there is an assumption of linearity. The systems of equations for most PBPK models can be assumed to be linear or can be linearized. This assumption can generally be made since there is physiological reality tied to the bounds

on the parameters. These bounds are generally of such small magnitude that in practice, concentration values never reach a point that the behavior cannot be captured with linear or first-order kinetics.[36, 68, 152] Most often, non-linearity occurs when, at some time point, a critical concentration is reached where the binding or metabolism kinetics causes non-linear clearance.[153] If a non-linear system of differential equations is necessary to describe the system, several approaches have been applied successfully to these PBPK models. Some of these approaches include Runge-Kutta methods and inductive methods of generating approximations for these non-linear systems using iterative linearization as described by Duffull.[152] PK and PBPK modeling are becoming standard of practice for many regulatory agencies, and because of that, most major players in the pharmaceutical industry prefer to use PK and PBPK modeling at some point in their pipeline.[154]

## **CHAPTER 5**

### **INTER-SPECIES SCALING**

In the previous sections, a whole-body minimal PBPK model of DOX was developed by modifying a previous porcine model from literature.[8] The purpose of the PBPK model was to estimate the behavior of DOXol in the heart in order give better insight into dose adjustments for DOX due to its limiting cardiotoxicity. Next, a matrix-based method was developed for efficiently solving large, complex systems of differential equations that describe the PBPK model.[6, 5] While the ability to achieve insight into DOXol concentration in the heart of a mouse, a rat, or even a pig is useful for gaining a deeper understanding of DOX, it is less useful clinically. Since the availability of data of DOXol in the heart is virtually non-existent in humans, it becomes necessary to accurately scale the parameters in the model from the sub-clinical species that *do* have the heart DOXol concentrations. In the case of the data collected for this dissertation, the only DOXol concentration versus time data in the heart available was in a mouse model. Thankfully, extrapolation across species of common pre-clinical animals is a central process in pharmaceutical research and development.[155]

#### **5.1 Allometry Concepts**

One of the most common ways of this inter-species extrapolation is through allometry. Allometry is broadly defined as the study of size and its consequences. The

term first originated in engineering and was coined by Huxley and Tessier in 1936 to describe properties that change proportionally with size.[156] Just a few years later, Benedict demonstrated that basal metabolic rate (BMR) did not scale linearly with body weight by plotting total heat production against body weight. Kleiber defined the metabolic rate for mammals by the allometric equation:

$$P_{met} = 70 \times M^{3/4} \quad (\text{Eq. 5-1})$$

which is still widely used today.[156] The concept of allometric scaling was originally based on the power-log relationship that exists between the body weight and drug clearance in mammals. The general form of this power function is:

$$Y = aW^b \quad (\text{Eq. 5-2})$$

where  $Y$  is the new parameter or parameter of interest,  $a$  is the coefficient,  $W$  is the body weight of the subject, and  $b$  is the exponent of the allometric equation. The parameters  $a$  and  $b$  are fitted empirically where the exponent  $b$  is the slope of the regression line when plotted on a log-log scale.[157]

Allometric scaling methods have been modified and updated for the past several decades and have become a fast and convenient way to either interpolate or extrapolate pharmacokinetic parameters between species.[156] It is one of the most commonly used methods for scaling clearance from sub-clinical species to humans.[158] However, studies have indicated that drug clearance cannot, in every case, be reliably predicted by just Equation 5-2.[157]. Some improvements have been made over the years to bolster the predictive ability of allometric scaling. Adjustments for brain weight (BRW), maximum life-span potential (MLP), unbound fraction in plasma, liver blood flow (LBF) methods, and corrections for metabolic clearance.[159, 160, 161, 162, 163] As is true with most

applied mathematical methods, different allometric scaling methods have advantages and disadvantages, and in some cases, more sophisticated inter-species scaling methods are necessary.[156] The main benefit to single-species allometry is its cost effectiveness.[9] For the model described throughout this work, simple allometry was used to scale parameters between species.

## 5.2 Inter-Species Scaling of Doxorubicin

The most common pharmacokinetic parameters extrapolated using allometry are clearance, volume-of-distribution, and elimination half-life.[164] In DOX, these three parameters have been identified as having high inter-patient variability as well as inter-occasion variability. The inter-species scaling of pharmacokinetic parameters like clearance is generally well-predicted using simple allometry for both macro-molecule drugs and small-molecule drugs that are excreted renally. Small molecules that are hepatically eliminated, however, tend to have higher prediction error using simple allometry, even with multiple species. The prediction error is generally linked to hepatically eliminated, small-molecule drugs that have low hepatic extraction ratio (Eh).[9] The hepatic extraction ratio is a drug-specific parameter that is a combination of several other drug-specific physiological PK parameters - fraction of unbound drug in blood, hepatic intrinsic clearance of unbound drug, and hepatic blood flow.[165] Fortunately, prediction error has been shown to be reduced by correcting the simple allometric equation by Maximum Life-Span Potential (MLP) or brain weight (BRW).[9] The MLP and BRW for mouse, rabbit, dog, pig, and human are listed in Table 5-1.

**Table 5-1:** *Calculated Maximum-Lifespan Potential and Brain Weight - Values Commonly Used as Correction Factors for Inter-Species Scaling of Hepatically Eliminated Drugs like DOX in Several Laboratory Animals and to Humans (Source [161, 166, 167, 168, 169])*

Correction Factors for Allometric Scaling		
Species	Calculated MLP (years)	Brain Weight (% body weight)
Mouse	2.67	1.65
Rat	4.70	0.72
Rabbit	8.00	0.39
Dog	19.70	0.78
Pig	11.40	0.50
Human	93.40	2.00

For small-molecule drugs like DOX, even single species allometry with a fixed allometric exponent can be useful. Finding a single best value for the allometric exponent is difficult, but in general, allometric exponent values of between 0.65 and 0.70 give acceptable predictions for common PK parameters across species and to humans.[9]

### 5.2.1 Determination of Model Parameters

For the inter-species scaling performed in this work, physiological parameters for mouse, rat, rabbit, dog, pig, and human were obtained from literature. The data was collected by digitizing plots using the Quintessa Graph Grabber software.[170] Sampling times were recorded from literature, when available, and the data series' pulled from the graphs were pulled at those time points with reasonable accuracy. Some of the graphs were from very old studies and had poor image quality. Some graphs for DOX and DOXol have very long observation times that were measured in hours due to the long half-lives of DOX and DOXol (recall Table 3-1).[31, 32] In these cases especially, it was difficult to distinguish between a 5 and 15 minute time point on a graph. It is understood that some additional variation was introduced with human error. However, for all the digitized data, the shape and magnitude were congruous with that of the original data



presentation. Any units for dose or concentration measurements were standardized to  $\mu\text{M}$  for consistency. For weight-adjusted dosing by body weight in kilograms, the reported mean weight of the subjects was used. If no mean weight in kilograms was reported, accepted average values were used.[171] Similarly, in larger mammals and in human, body surface area (BSA) is a common way to adjust dosing by size.[118] If BSA was used in dose calculations, the BSA was estimated using mass in kilograms with conversion factors from Nair et al.[171] Dose volumes, if not given explicitly in the paper or supplementary information, were taken from recommended industry dosing guidelines for laboratory animals.[172]

Since the original model from which our matrix model was adapted was a pig model [8], the pig parameters were the initial values used. As such, several specific parameters that were incorporated into the model were not readily available in literature. One reason for this is that the Dubbelboer pig model was designed as a minimal PBPK model, as noted in Section 3.5. A notable advantage in the Dubbelboer model is its simplified approach to association/dissociation constants -  $Cl_{on}$  and  $Cl_{off}$  - as opposed to the traditional approach of assigning compartment specific partition coefficients (generally denoted as  $K_{p,u,tissue}$ ). The benefit of this approach is that it helps keep a rather complex model from becoming over parameterized. The Dubbelboer model also included several binding parameters which are similar but nuanced. The  $F_{up,DOX}$  and  $F_{up,DOXol}$  represents the formal fraction of the tissue compartments that were unbound. The movement between the bound and unbound compartments were dictated by the  $Cl_{on}$  and  $Cl_{off}$  parameters. The intracellular binding site, designated as *bind site*, represents the volume the tissue compartment that was available for binding. It is a surrogate for the

arbitrary volume for the nucleus of the tissue's cells, DNA, and cardiolipin. This fraction represents all intracellular binding sites for DOX and DOXol. The value for *bind site* was set to 0.2, to represent the extensive binding of DOX to intracellular structures within tissues. In other words, effectively 20% of the tissue volume is available for binding in most compartments. The only exception being the kidney, liver, and heart, in which the cellular sub-compartment is the only portion that contains intracellular binding sites. This effect was accomplished by multiplying the volume fraction (Tables 5.2 and 5.3) by *bind site* for the bound tissue compartment and  $(1 - \textit{bind site})$  for the unbound tissue compartment.

**Table 5-2:** *Fraction of Body Weight of Each Sub-Compartment Within the Kidney and the Liver Originally Determined in the Dubbelboer Pig Model and Used Throughout All Species in this Inter-Species Scaling (Source [8])*

Sub-Compartment Breakdown of Volume in Liver and Kidney	
Kidney - Vascular	0.05
Kidney - Extracellular	0.159
Kidney - Cellular	0.791
Liver - Vascular	0.055
Liver - Extracellular	0.159
Liver - Cellular	0.786

**Table 5-3:** Fraction of Total Body Weight for Each Respective Compartment for Each Species used in Inter-Species Scaling of DOX. The Pig Parameters in Both Tables were Adapted from Dubbelboer.[145] Mouse, Rat, Dog, and Human Parameters were Adapted from the International Life Sciences Institute Resource.[173] The parameters for the Rabbit were Adapted from a Meta-Analyses Done by Davies.[174]

Physiological Parameters for Various Sub-Clinical Species						
	Mouse	Rat	Rabbit	Dog	Pig	Human
Volume (Fraction of Total Body Weight)						
Blood	0.049	0.075	0.082	0.082	0.0553	0.079
Lung	0.007	0.006	0.0085	0.008	0.0109	0.025
Heart	0.005	0.025	0.003	0.008	0.005	0.005
Kidney	0.017	0.008	0.0075	0.005	0.0055	0.004
GI/Spleen	0.099	0.071	0.0604	0.08	0.0861	0.031
Liver	0.055	0.035	0.0499	0.033	0.0316	0.026
Slow Perfused	0.726	0.718	0.674	0.779	0.7154	0.794
Rapid Perfused	0.042	0.064	0.115	0.008	0.0952	0.053

However, it posed a challenge for finding equitable parameters in the literature that represented these universal association and dissociation constants. Additionally, intra-organ clearance parameters that represented passive diffusion ( $P_{diff}$ ) and membrane clearance ( $Cl_{mem}$ ) were universal for all compartments, which is less common in PBPK modeling. Even more so, the original Dubbelboer model did not include a heart compartment, which was vital to the research question of this work. In order to maintain the mass balance of *drug in* to *drug out*, original values of the physiological parameters in the Dubbelboer had to be adjusted.

A wealth of parameter data for a range of species was found in a meta-analysis of the literature by the International Life Sciences Institute. This resource was used to properly adjust the volume fractions to a physiologically relevant balance that included the heart.[173] The exact breakdown of the sub-compartments of the liver and kidney and the combination of tissues given specific compartments versus lumped into slow or rapid perfused tissue were unique to the Dubbelboer model. In order to create physiological

parameter sets analogous to the structure of the Dubbelboer model, values from literature were used to determine realistic values for each of the compartments included in the model.[173] The final physiological parameters in the model are listed in Table 5-2, Table 5-3, and Table 5-4.

**Table 5-4:** *Fraction of Total Cardiac Output for Each Respective Compartment for Each Species used in Inter-Species Scaling of DOX. The Pig Parameters in Both Tables were Adapted from Dubbelboer.[145] Mouse, Rat, Dog, and Human Parameters were Adapted from the International Life Sciences Institute Resource.[173] The Parameters for the Rabbit were Adapted from a Meta-Analyses Done by Davies.[174]*

Physiological Parameters for Various Sub-Clinical Species						
	Mouse	Rat	Rabbit	Dog	Pig	Human
Blood Flow (Fraction of Cardiac Output)						
Portal Vein	0.14	0.153	0.264	0.46	0.21	0.18
Hepatic Artery	0.02	0.021	0.0698	0.251	0.05	0.047
Lung	1	1	1	1	1	1
Heart	0.066	0.049	0.0302	0.046	0.04	0.04
Kidney	0.091	0.141	0.151	0.173	0.114	0.175
GI/Spleen	0.14	0.153	0.226	0.046	0.21	0.18
Liver	0.161	0.141	0.334	0.297	0.114	0.175
Slow Perfused	0.217	0.528	0.292	0.277	0.05	0.342
Rapid Perfused	0.033	0.023	0.0604	0.022	0.536	0.13

The pig parameters in all three tables were adapted from Dubbelboer.[145] Mouse, rat, dog, and human parameters were adapted from the International Life Sciences Institute resource.[173] The parameters for the rabbit were adapted from a meta-analyses done by Davies.[174] In Section 3.5, the structure of the sub-compartments of the metabolizing compartments were illustrated in Figure 3-3 for organs with both metabolism and excretion - liver and kidney- and Figure 3-4 for metabolism only - the heart. Note that since the heart compartment was not included in the original model, equivalent tissue parameter breakdowns for the sub-compartment of the heart as a metabolizing compartment were not available.[8] The kidney values for the fraction of

the compartment that is vascular, extracellular, and cellular were used for the heart compartment. The rationale for this was that the kidney and heart were closer in total body volume (Table 5-3) and fraction of cardiac output (Table 5-4). Additionally, in Section 1.3.1, it was discussed higher DOX and DOXol concentrations per gram than the heart but were not major sites of toxicity. A reason cited for this paradox is that the liver and kidney contain a greater number of inactivating and binding enzymes that reduce the toxic effect and eliminate the parent drug. As mentioned, DOX is hepatically eliminated so one possibility is that the concentration of inactivating and eliminating enzymes is higher in the liver. The heart tissue does not contain the as high of a concentration per gram of those enzymes that a true metabolizing and excreting organ would. Thus, the liver may be a less suitable analog for the heart than the kidney, which is known to be responsible for less metabolism of DOX. Additionally, Table 1-2 from a human autopsy study done in humans showed that the concentration per gram of DOX and DOXol in the heart was more similar to the kidney.[40]

As shown in Table 1-2, the liver and kidney both have higher concentrations per gram than the heart. Higher DOX and DOXol concentrations in the liver and kidney are also observed in animal species.[63, 64] However, the liver and kidney are not major sites of toxicity for patients receiving DOX, which leads to conjecture other factors differentiating DOX and DOXol behavior in tissues. One such conjecture is that liver and kidney tissues are rich in binding and inactivating substances due to their excretory and metabolic functionalities, which prevent DOX and DOXol from causing cellular damage in those tissues.[40] For example, reduced DOX toxicity is observed in the presence of glutathione - a common antioxidant found in the liver.[65]



**Table 5-6:** The First Section Contains Parameter Values with Variability in Percent Coefficient of Variation Reported by Dubbelboer Et Al. [8] if no %CV Is Reported, then the Parameter was Assumed or Taken from Literature by The Authors. The Second Section Contains Parameters that were Estimated for the New Model, Based on the Dubbelboer Model, Containing the Heart Compartment. These Parameters Remained Constant Across All the Data Sets Used in Scaling

<i>Parameters in the Final Model</i>		
<i>Parameters Directly from Dubbelboer et al.</i>		
<i>Parameter</i>	<i>Value (%CV )</i>	<i>Units</i>
<i>Pdiff,DOX</i>	15	<i>L/min</i>
<i>Pdiff,DOXol</i>	15	<i>L/min</i>
<i>Clmem,DOXol</i>	0.00357 (52)	<i>L/min</i>
<i>Clon,DOXol</i>	0.109 (38)	<i>L/min</i>
<i>Cloff,DOX</i>	0.000115 (11)	<i>L/min</i>
<i>Clexcr,ki,DOX</i>	0.215 (24)	<i>L/min</i>
<i>Clexcr,ki,DOXol</i>	0.0154 (42)	<i>L/min</i>
<i>Clexcr,li,DOX</i>	0.213 (450)	<i>L/min</i>
<i>Clexcr,li,DOXol</i>	0.178 (65)	<i>L/min</i>
<i>SFkidney</i>	14.7 (17)	-
<i>SFheart</i>	3.39 (240)	-
<i>SFliver</i>	1.21 (22)	-
<i>CbCp<sub>DOX</sub></i>	1.3	-
<i>CbCp<sub>DOXol</sub></i>	1.3	-
<i>GFR</i>	2.4	<i>ml/min/kg</i>
<i>Vmax,liver</i>	337	<i>pmol/(mg protein ×min)</i>
<i>Km,liver</i>	163	<i>μM</i>
<i>Vmax,kidney</i>	127	<i>pmol/(mg protein ×min)</i>
<i>Km,kidney</i>	134	<i>μM</i>
<i>Parameters Fitted to Final Model</i>		
<i>Clmem,DOX</i>	0.9	<i>L/min</i>
<i>Clon,DOX</i>	0.3465	<i>L/min</i>
<i>Cloff,DOXol</i>	0.00000284	<i>L/min</i>
<i>Vmax,heart</i>	85	<i>pmol/(mg protein ×min)</i>
<i>Km,heart</i>	15	<i>μM</i>
<i>Fup,DOX</i>	0.00007	-
<i>Fup,DOXol</i>	0.00007	-
<i>bind site</i>	0.2	-

### 5.2.2 Extrapolation to Humans

Rather than starting from scratch, allometric equations for DOX existing in literature were collected and were tested on the observations from literature. Many of the

papers suggested scaling parameters from a rodent model (i.e. rat or mouse) since that is generally the earliest in vivo data that is collected in a pharmacokinetic study.[36, 9, 156] Additionally, the mouse was chosen as the standard for scaling purposes since it is one of the few data sets that clearly included the metabolite DOXol concentration in the heart compartment.

The van der Vijgh data set became the basis for all subsequent scaling since it had both venous blood and heart observations for both DOX and DOXol.[12] The venous blood DOX concentration and the heart DOXol concentration were the two concentration-time courses of interest due to the desire to maximize therapeutic effect (venous blood, DOX) and minimize cardiotoxicity (heart, DOXol).

A sensitivity analysis was carried out on the van der Vijgh data set by varying the original parameter values by  $\pm 5\%$ ,  $\pm 10\%$ , and  $\pm 20\%$  and measuring the percent change in the objective function. The objective function was a least squares regression measurement between the observed values of concentration and the model predictions.[175] These results of this sensitivity analysis are shown in Table 5-5. The percent change in the objective function value for each respective percent change in the parameter value was ranked from most change to least change. There is a clear order of magnitude difference in percent change between the third and fourth parameters in Table 5-5. Thus, the first parameter -  $B : P$ - was considered to be sensitive and the others were fixed. The Blood:Plasma Partition Coefficient ( $B : P$ ) is a measurement of a drug concentration between whole blood and plasma. Plasma measurements are typically the favored method of measurement in pharmacokinetic studies, which can be misleading if the drug has a particularly high affinity for binding to red blood cells (RBC) in whole



blood.[176] It is determined experimentally using an RBC partitioning assay where whole blood is centrifuged and the concentration of the compound is measured in the separated fluids - plasma and red blood cells.[177] Understanding a drug's interaction with red blood cells is important for whole body PBPK models. Drugs with a high binding affinity to red blood cells could cause a concentration sink in the whole blood that is not captured in plasma concentration measurements.[176] DOX has been shown to heavily interact and bind with red blood cells and even negatively affect their function and integrity.[178] It is not wholly surprising, then, that this Blood:Plasma Partition Coefficient ( $B : P$ ) was a sensitive parameter in the model. The fraction of DOX bound to red blood cells directly affects the remaining DOX available in the plasma. The concentration of DOX in plasma is then divided again into bound and unbound fractions ( $F_{up,DOX}$  and  $F_{up,DOXol}$ ). Recall that only *unbound* drug in the plasma is bioavailable.

The remaining fixed parameters are listed in Table 5-6. The top section of Table 5-6 contains parameter values with variability in percent coefficient of variation reported by Dubbelboer et al.[8] If no %CV is reported, then the parameter was assumed or taken from literature by the authors. The bottom section contains parameters that were estimated for the new model, based on the Dubbelboer model, containing the heart compartment. The parameters listed in this table remained constant across all the data sets used in scaling. A flow chart of the process of developing the model structure and parameters are shown in Figure 5-1.

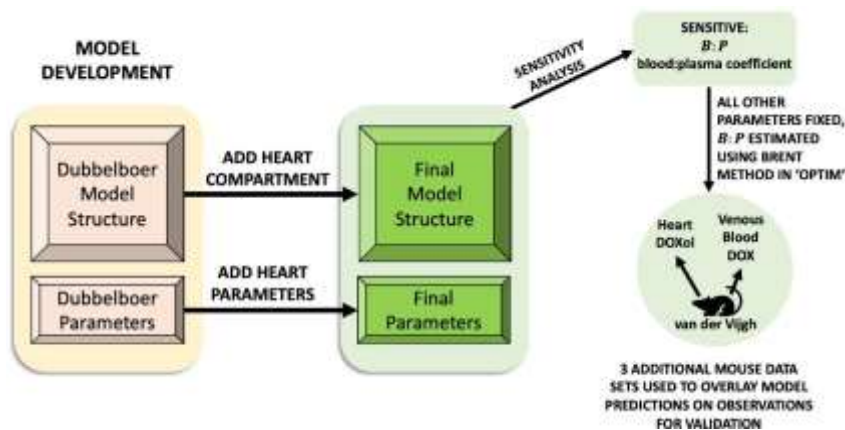


**Figure 5-1:** Flow chart of the process of developing the model structure and parameters, starting with Dubbelboer Model[8] and progressing to the mouse model that was used for inter-species scaling.[12]

The other parameter that was varied between species was cardiac output (CO). There are a range of values that have been observed in different laboratory animals and in humans.[179] Cardiac output was one of the most influential physiological parameters that affected the fit of the various models. The cardiac output (CO) is measured as the stroke volume times the heart rate in beats per minute. It is difficult to measure cardiac output since stroke volume is defined as the volume pumped out of the left ventricle during each systolic contraction.[180] Because of the need for invasive measurement in a living animal, there is some disagreement around the best way to measure cardiac output in lab animals.[180, 181, 179, 182] One study done by Cabrales et al. found that for animals less than 100 grams, cardiac output scales linearly at  $197 \text{ (ml/min)/kg} \pm 18.8$ . [183] For 20 gram mice, that translates to  $39.4 \text{ ml/min} \pm 3.76 \text{ ml/min}$  which is consistent with the model fits for the mouse models.[12, 33, 126]) Other factors could also contribute to variation in cardiac output. Since heart beats per minute directly affects cardiac output, anesthetized animals, resting animals, and active animals of identical species and size could have two disjoint ranges of cardiac output measurements.[173] For

instance, Beznack tested cardiac output of 180 gram - 240 gram laboratory rats in various states of activity, which wildly varied their cardiac output reporting values as low as  $31 \pm 5$  ml/min and as high as  $178 \pm 11$  ml/min [184]. An early study by Howell found that the mean cardiac output for dogs was 236 ml/min with a wide range (91 ml/min - 509 ml/min).[185]

Despite the known variability in cardiac output, Figure 5-2 shows a general upward trend in cardiac output with respect to body weight. First, the most sensitive parameter  $B : P$  was estimated on heart DOXol and venous blood DOX concentration observations in mice from van der Vijgh et al. using the 'optim' package in RStudio. A built-in Brent method within 'optim' was used to fit the parameter by asking the function to minimize the least squares objective function.[12, 146, 186] The most important agreement between observations and predictions from the van der Vijgh data set is the DOXol concentration in the heart compartment, which is shown in Figure 5-3.

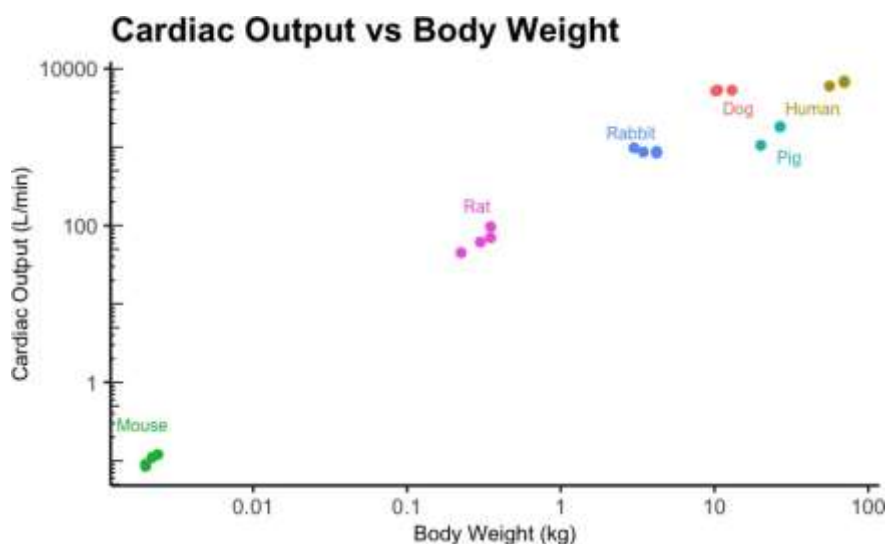


**Figure 5-2:** Plot of cardiac output by body weight in kilograms of each study used for the allometric inter-species scaling

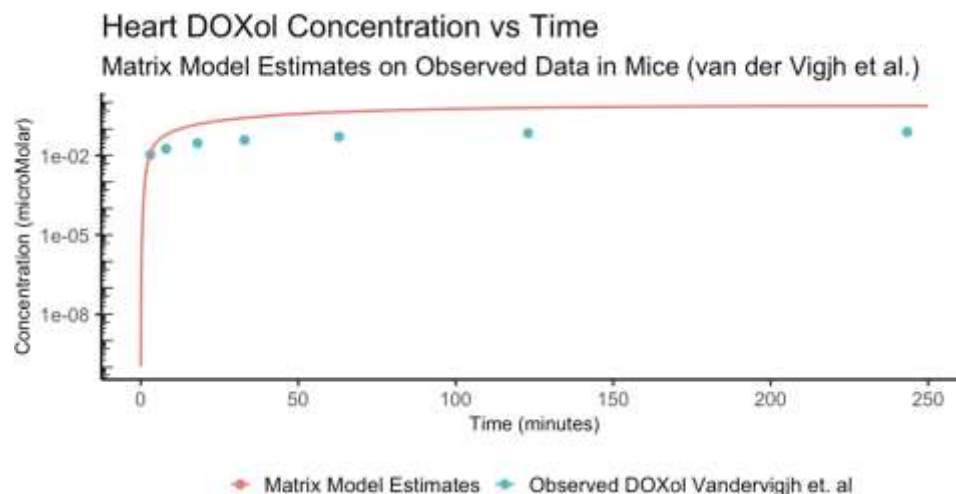


**Figure 5-3:** Heart DOXol concentration observations from van der Vijgh mouse data set with model predictions overlaid[12]

Observations for three additional mouse data sets were then used to overlay model predictions on the observed data to validate the model.[187, 188, 127] The results of these predictions are shown in Figure 5-4, demonstrating that the model could reasonably predict DOX concentration in mice.

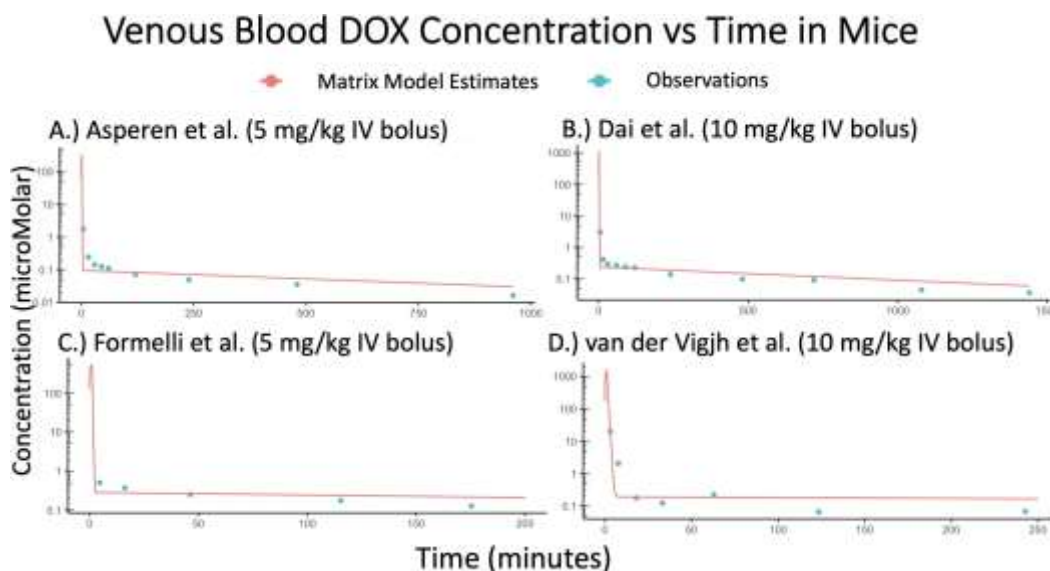


**Figure 5-4:** Venous blood DOX concentration observations from four mouse data sets - A.) Asperen et al.[126], B.) Dai et al.[189], C.) Formelli et al.[33], and D.) van der Vijgh et al.[12] - with model predictions overlaid

Next, the blood:plasma coefficient  $B : P$  value was estimated for one data set from each species using each allometric equation to see how the model performed in scaling from mouse to the other species. Rahman, Johansen, Oosterbaan, Dubbelboer, and Krarup were chosen as representative data sets for rats, rabbits, dogs, pigs, and humans, respectively. The following equation was the first to be tested on these data:

$$PAR_{new} = PAR_{mouse} \times \left( \frac{BW_{new}}{BW_{mouse}} \right)^{0.67} \quad (\text{Eq. 5-3})$$

where  $PAR_{new}$  is the scaled parameter for the larger species,  $PAR_{mouse}$  is the mouse parameter,  $BW_{new}$  is the body weight for the larger species,  $BW_{mouse}$  is the mouse body weight and the 0.67 is the allometric exponent that was utilized for scaling DOX from mouse to man in a study by Lee et al. This study who a similar meta-analysis to examine how specifically DOX PK parameters scaled from a mouse to a human using simple allometry.[64] Allometric exponents between 0.6 to 0.7 are typically acceptable for scaling small-molecule drugs across species.[9]

The equation worked well for mouse to rabbit and reasonably well for mouse to rat, but it did not scale well for mouse to pig, dog, human.[12, 133, 132, 190, 192] This issue was not entirely surprising though, since it is known that adjustments for BRW or MLP reduce prediction error in scaling with small-molecules that are hepatically eliminated.[9] It was also known that DOX is one of these hepatically eliminated small-molecule drugs that has been characterized as having low, medium, and high hepatic extraction ratio (ranging from 0.14 to 0.79) by different studies.[11] Due to this range and the fact that prediction error is linked to low hepatic extraction ratio, the adjustments suggested in Huh et al. were implemented in order to improve the overall fit of the models as they were scaled. This study found that there was benefit in implementing the

correction factor of Maximum Life-Span Potential or Brain Weight for the low hepatic extraction ratio drugs.[9] An exception can be made if the allometric exponent is  $< 0.71$ . While the allometric exponent estimated in the study by Lee et al. was below that threshold at 0.67, the decision was made to move forward with adding a correction factor. The general rule is if the allometric exponent is between 0.71 and 1, MLP is the appropriate correction factor. If the allometric exponent is  $> 1$ , BRW is the appropriate correction factor. Since Equation 5.3 did fit some of the species well, its general form was maintained with just the correction factor added. The following equation resulted:

$$\text{PAR}_{\text{new}} \times \text{MLP}_{\text{new}} = \text{PAR}_{\text{mouse}} \times \left( \frac{BW_{\text{new}}}{BW_{\text{mouse}}} \right)^{0.67} \quad (\text{Eq. 5-4})$$

where MLP is specific to the new species used in scaling as listed in Table 5-1. This correction factor remedied the poor fits in the pig, dog, and human species and improved the fit in rats. The plots of the observed and predicted concentration over time for each species are shown in Figures 5.5 - 5.9. Additional data sets for each species, having different mean body weights  $BW$ , dose regimens, and experiment conditions, to test how this equation performed. The final parameter values for  $CO$ ,  $BW$ , and the scaling factors for each of the individual data sets are in Table 5-7 for sub-clinical species and Table 5-8 in humans. The plots of the concentration versus time predictions over the observed data for each respective data set fit by the allometric scaling are listed in Appendix F.

An important clarification about this allometric equation is that all other species parameters are scaled from the mouse parameters. In other words, the scaling does not proceed from mouse to rat, then rat to rabbit, and so on. Instead, the mouse scales to the rat or to the rabbit or to the human. This approach is cost effective in practice since mouse studies are generally much less expensive than those in larger animals.

### Venous Blood DOX Concentrations with Time Representative Rat Fits

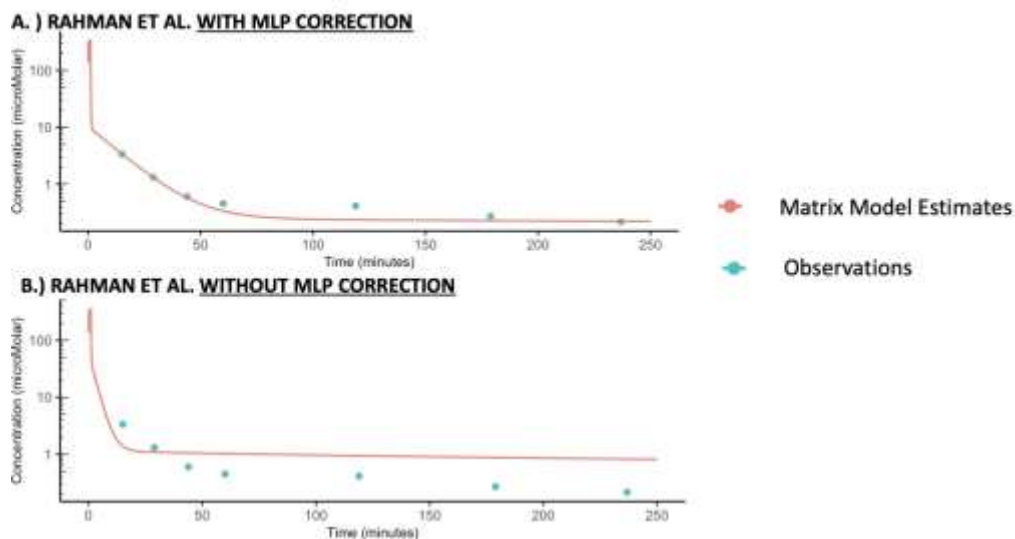


**Figure 5-5:** Observed and predicted venous blood DOX concentration in rats after applying allometric scaling - A.) *with* MLP Correction Factor and B.) *without* MLP Correction Factor to the parameter  $B : P$  (Data source: Rahman et al.[45])

### Venous Blood DOX Concentrations with Time Representative Rabbit Fits

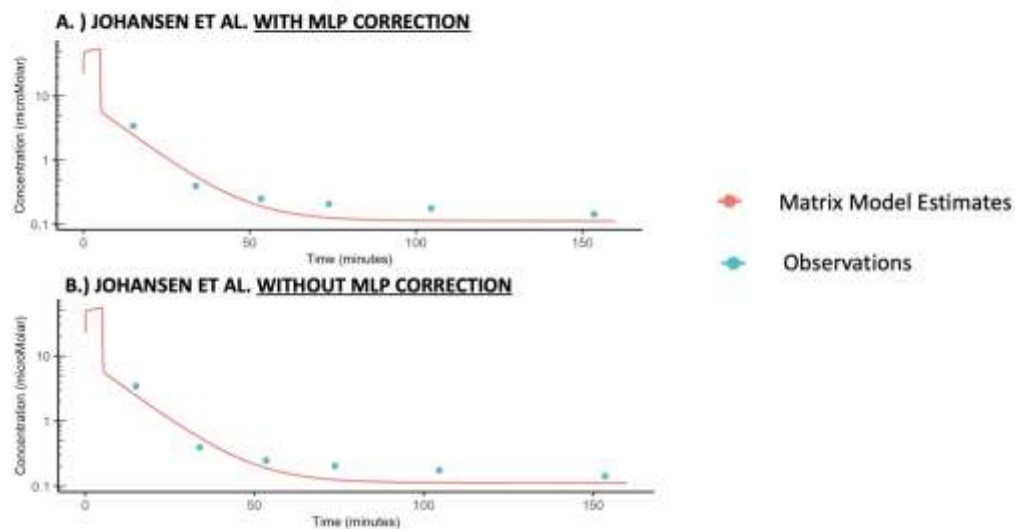


**Figure 5-6:** Observed and predicted venous blood DOX concentration in rabbits after applying allometric scaling - A.) *with* MLP Correction Factor and B.) *without* MLP Correction Factor to the parameter  $B : P$  (Data source: Johansen et al.[117])

## Venous Blood DOX Concentrations with Time Representative Dog Fits

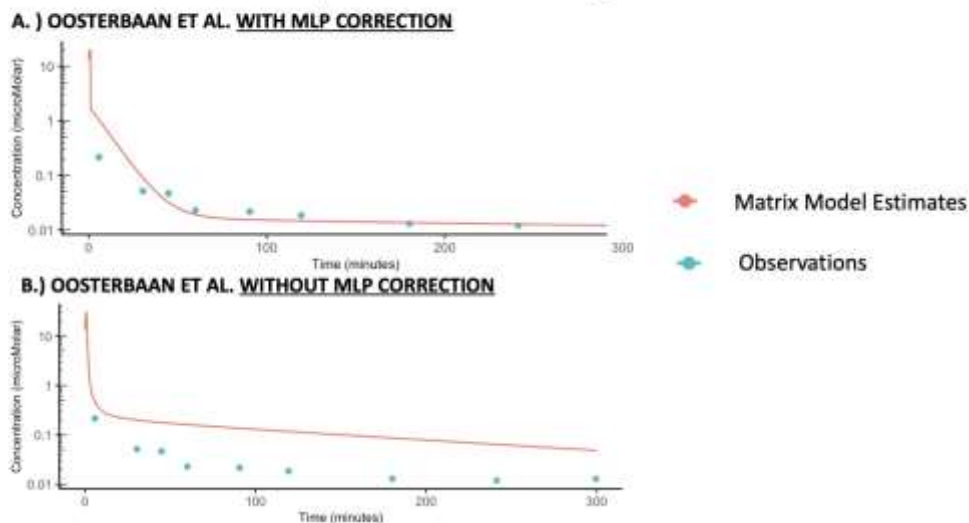


**Figure 5-7:** Observed and predicted venous blood DOX concentration in dogs after applying allometric scaling - A.) *with* MLP Correction Factor and B.) *without* MLP Correction Factor to the parameter  $B : P$  (Data source: Oosterbaan et al.[192])

## Venous Blood DOX Concentrations with Time Representative Pig Fits

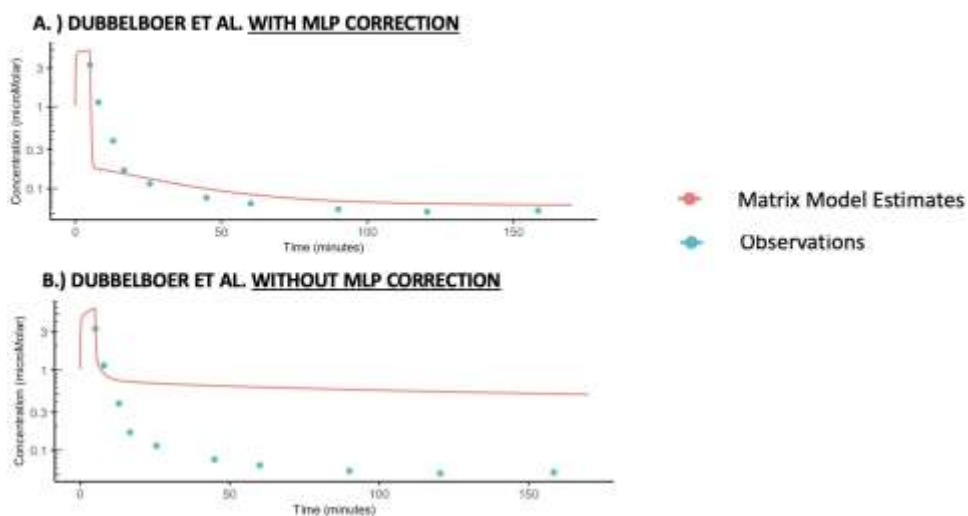


**Figure 5-8:** Observed and predicted venous blood DOX concentration in pigs after applying allometric scaling - A.) *with* MLP Correction Factor and B.) *without* MLP Correction Factor to the parameter  $B : P$  (Data source: Dubbelboer et al.[8])



## Venous Blood DOX Concentrations with Time Representative Humans Fits

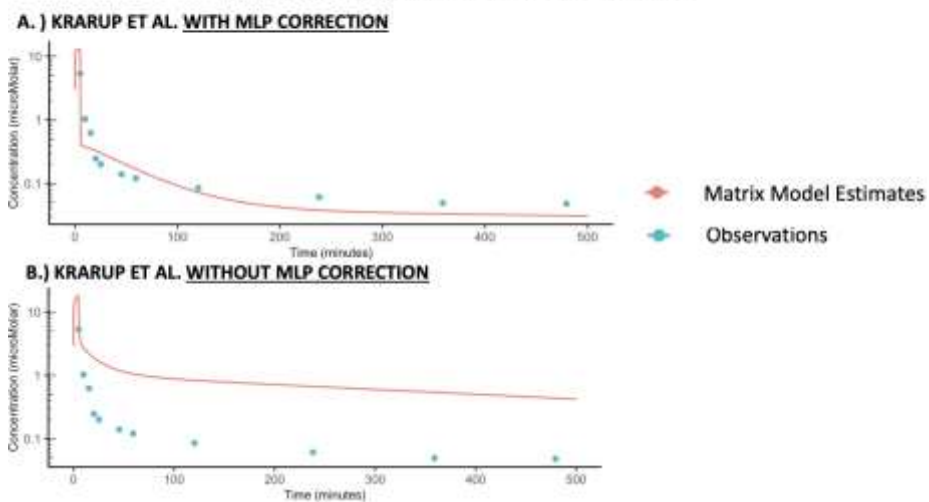


**Figure 5-9:** Observed and predicted venous blood DOX concentration in humans after applying allometric scaling - A.) *with* MLP Correction Factor and B.) *without* MLP Correction Factor to the parameter  $B : P$  (Data source: Krarup et al.[45])

**Table 5-7: Final Parameter Values for CO, BW , and the Scaling Factors for Each of the Individual Data Sets**

<b>Mouse</b>				
	van der Vijgh[12]	Formelli[33]	Dai[189]	Asperen[126]
BP	1.5	1.5	1.5	1.5
CO (L/min/kg)	30	50	40	50
BW (kg)	0.002	0.002	0.0035	0.0022
dose	10 mg/kg	5 mg/kg	10 mg/kg	5 mg/kg
duration (min)	1	1	1	1
<b>Rat</b>				
	Colombo[187]	Rahman[45]	Cusack[127]	Yesair[188]
BP	7.56	10.16	10.16	9.16
CO (L/min/kg)	260	200	290	205
BW (kg)	0.225	0.35	0.35	0.3
$\frac{BW_{rat}^{0.67}}{BW_{mouse}}$	23.674	31.829	31.829	28.707
MLP (years)	4.7	4.7	4.7	4.7
dose	5 mg/kg	6 mg/kg	2 mg/kg	10 mg/kg
duration (min)	1	1	1	1
<b>Rabbit</b>				
	Johansen[117]	Bachur[190]	Cusack[191]	Brenner[12]
BP	28.36	31.67	31.67	25.18
CO (L/min/kg)	250.14	200	200	325
BW (kg)	3.45	4.2	4.2	3
$\frac{BW_{rabbit}^{0.67}}{BW_{mouse}}$	147.451	168.224	168.224	134.3
MLP (years)	8	8	8	8
dose	5 mg/kg	5 mg/kg	5 mg/kg	3 mg/kg
duration (min)	5	1	1	5
<b>Dog</b>				
	Oosterbaan[192]	Oosterbaan[192]	Baldwin[193]	
BP	23.31	22.86	27.31	
CO (L/min/kg)	509	509	410	
BW (kg) ( BWdog )0.67	10.5	10.2	13	
BWmouse	310.818	304.840	358.634	
MLP (years)	19.7	19.7	19.7	
dose	1.5 mg/kg	1.27 mg/kg	1.5 mg/kg	
duration (min)	1	1	1	
<b>Pig</b>				
	August[194]	Dubbelboer[8]	Dubbelboer[8]	
B : P	62.89	76.42	76.42	
CO (L/min/kg)	55.14	68.14	85.14	
BW (kg) ( BWpig )0.67	20	26.7	26.7	
BWmouse	478	580.8	580.8	
MLP (years)	8	8	8	
dose	1 mg/kg	0.6 mg/kg	0.63 mg/kg	
duration (min)	90	5.05	50	

**Table 5-8: Final Model Parameters for 5 Human Data Sets in which Equation 5-4 was used to Scale B:P by Body Weight**

Estimated or Assumed Parameters in Humans Determined with Inter-Species Scaling					
Source	[133]	[34]	[34]	[120]	[80]
<i>BP</i>	15.32	17.79	17.79	17.79	17.79
<i>CO</i> (L/min/kg)	107.14	97.1	97.1	97.1	107.14
<i>BW</i> (kg)	56	70	70	70	70
$\frac{BW_{human}^{0.67}}{BW_{mouse}}$	954.104	1107.964	1107.964	1107.964	1107.964
<i>MLP</i> (years)	93.4	93.4	93.4	93.4	93.4
dose	70 mg/m <sup>2</sup>	36 mg/m <sup>2</sup>	30 mg/m <sup>2</sup>	15 mg/m <sup>2</sup>	75 mg/m <sup>2</sup>
duration (min)	1	5760	1	1	15

Additionally, since regulatory agencies require testing to be conducted in a rodent and non-rodent species before proceeding to humans, having insight into moving *from* rodent *to* non-rodent studies is both cost- and time-efficient. In terms of the Blood:Plasma Coefficient *B : P*, an interesting trend was observed when looking at the Log-Log plots of the *B : P* values versus the body weight *BW* of the animals (Figure 5-10).

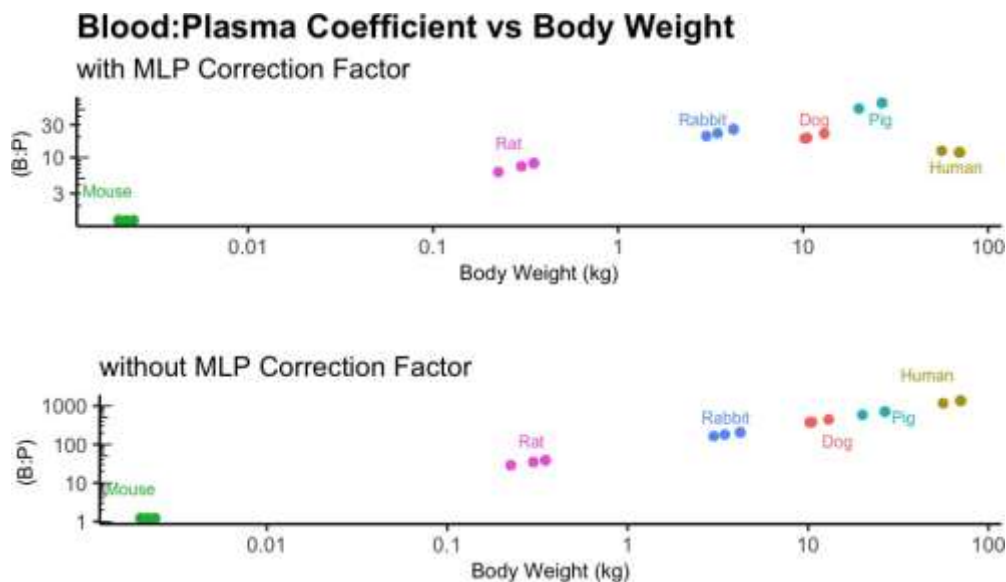


**Figure 5-10:** Plot of Blood:Plasma Partition Coefficient for each study used in the allometric interspecies scaling - the top plot shows the trend in the parameter with the Maximum Life-Span Potential (MLP) Correction Factor while the bottom plot shows the trend in the parameter without the correction factor.

Without the Maximum Life-Span (*MLP*) correction factor (bottom plot in Figure 5-10), there is a neat positive correlation of  $B : P$  based on body size, which is to be expected with allometric scaling. However, when the *MLP* correction factor is added, the  $B : P$  values for the human are much lower. This deviates from pure allometry in that the parameter scales not only on body weight, but also in longevity. The idea that *MLP* is an appropriate corrector for hepatically cleared small-molecule drugs originates from the inverse correlation between longevity and hepatic cytochrome P450 (CYP450) drug oxidation rates.[161, 9] In other words, the longer the lifespan of a particular species, the lower the hepatic oxidation of CYP450.[195] CPR receives an electron from NADPH and distributes it to CYP450, which then becomes capable of metabolizing drugs.[196] This detail is particularly interesting for DOX since, while DOXol is metabolized by aldo-keto- and carbonyl- reductases, both aglycone metabolite formations involve the

CYP450 enzyme.[4] The aglycone metabolites, doxorubicin deoxyglycone and doxorubicin semiquinone radical, are both notably less cardiotoxic than DOXol.[52] The extent to which the more cardiotoxic metabolite, DOXol, metabolizes versus its aglycone counterparts could be affected by this correlation of species longevity and CYP450 oxidation rates in the liver. While this is an interesting conjecture, it is beyond the scope of this work. Whether  $B : P$  is the actual parameter that affects the predictive ability of this model to scale from mouse to rat, rabbit, dog, pig, and human is beyond the scope of the available data and interest for this work. Overall,  $B : P$  affects the availability of DOX in plasma and by proxy, *free* DOX in plasma available for metabolism, cell-killing, clearance, and binding.[68] Whether the effect is direct or indirect, the adjustment of the  $B : P$  parameter has a major effect on the behavior of the DOX and DOXol predictions with this model across species.

The corresponding R code for the physiological parameters shown in Table 5-3, Table 5-4, Table 5-2 for each species are available in Appendix G. The equations for the final model are available in Appendix B and the corresponding R code in Appendix D.

## CHAPTER 6

### CONCLUSIONS

#### 6.1 Future Work

##### 6.1.1 Therapeutic Drug Monitoring for DOX

###### 6.1.1.1 Therapeutic Index

In earlier chapters, a minimal physiology-based pharmacokinetic model was constructed that could accurately predict the concentration of DOX and DOXol over time. Physiologic and pharmacokinetic parameters were established that could predict specifically the venous blood concentration of DOX and heart concentration of DOXol using an allometric scaling equation. PBPK models have been recognized as a promising tool for characterization of tissue-level parameters for better understanding of individualized pharmacologic response. As previously mentioned, PBPK models are more likely to be over-parameterized and therefore, less reliable for predictions. More work is needed in bolstering and validation of the use of PBPK models for drugs with high inter-patient and inter-occasion variability and narrow therapeutic windows for drugs with organ-specific toxicities.[197]

The concept of a therapeutic window was introduced in Chapter 2. A related term that quantifies the width of this “window” is the therapeutic index (TI). The therapeutic index is defined as the range of doses at which a drug is considered effective without adverse side effects. In animals, this is measured by the lethal dose of the drug for 50% of

the population divided by the minimum effective concentration for 50% of the population as shown in Eq. 6-1.

$$TI = \frac{LC_{50}}{EC_{50}} \quad (\text{Eq. 6-1})$$

where  $LC_{50}$  and  $EC_{50}$  is the lethal dose and minimum effective concentration for 50% of the population, respectively. Equation 6.1 is a very straightforward definition of therapeutic index, but assessing the therapeutic index in humans requires a larger margin of safety and is more difficult to define.[197]

In humans, the therapeutic index is the range of doses that were effective in clinical trials for the median of the participants without unacceptable adverse effects. For most drugs, this range is wide enough that the maximum plasma concentration  $C_{max}$  and area under the plasma concentration-time curve ( $AUC$ ) fall well above the minimum therapeutic concentration and well below the toxic concentration. In other words, the therapeutic index is wide enough that for most people at recommended prescribed doses, these drugs show clinical efficacy with a healthy margin of safety.[198] The difficulty in determining the therapeutic index in humans, especially in anticancer drugs, is there is not a well-defined number that works universally.[44]

#### 6.1.1.2 Therapeutic Drug Monitoring for DOX and DOXol

As mentioned in Chapter 1, despite the known narrow therapeutic index and high inter-patient and inter-occasion variability of DOX, there are almost no covariates that significantly inform dose adjustments.[11, 64] Dose adjustments for body mass index [118], age [32, 135], acidity of urine [117, 133], and hepatic impairment [140] have all been investigated thoroughly. The only truly significant factor that improves the dose of DOX is adjustment for hepatic impairment, which is essentially standard practice for

antineoplastic agents.[140]. This discrepancy further drives the need for more individualized dosing regimens for drugs with narrow therapeutic windows.[11, 64]

However, the exposure ( $AUC$ ) and the maximum concentration  $C_{max}$  in humans are significantly impacted by the rate and duration of DOX infusions.[44] The dose- and schedule- dependence of the pharmacokinetic parameters of DOX has been widely observed.[136, 120] Clinically, the side effects of doxorubicin (nausea, vomiting, cardiotoxicity) have been shown to decrease as the maximum venous blood concentration  $C_{max}$  in venous blood.[44, 141]. The amount of drug in venous blood is directly correlated to the amount of drug distributed to the various tissues, i.e. the heart, since the venous blood is the compartment in which the dose is administered.[8] Recall that the total dose that goes to the venous blood is transported through the lung to be oxygenated and into the arterial blood. The total dose then moves from the arterial blood into the to the extent of the flow rate and volume for the vascular compartment of the heart. This proportionality leads to the idea that a similar reduction in side effects could likewise be linked to the  $C_{max}$  in the heart. In a study comparing a homogeneous group of breast cancer patients receiving DOX either in the conventional IV bolus or a continuous 48 or 96 hour infusion,  $\approx 47\%$  of the patients in the IV bolus group developed severe morphological changes in cardiac tissue as opposed to only  $\approx 9\%$  of the patients receiving continuous extended doses.[141] A study done in rabbits showed a 15-fold reduction in  $C_{max}$  from an IV bolus injection to a 69 minute IV infusion.[44]

It has been observed that the values of  $AUC$  and  $C_{max}$  are proportional to the total amount of drug administered in an intravenous bolus under the assumption of linear kinetics. A similar, more comprehensive study was conducted by Eksborg where the  $C_{max}$



and  $AUC$  were calculated from patients receiving I.V. infusions of DOX ranging from 20 to 60 mg/m<sup>2</sup> with varying infusion times ranging from 3 minutes to 16 hours. The results from this study showed that increasing the infusion duration from 45 minutes to 16 hours showed a relatively unchanged therapeutic exposure (plasma  $AUC$ ), but a 25-fold decrease in normalized maximum plasma concentration  $C_{max}$  at 4 hours and a greater than 65-fold decrease at 16 hours. It has been reported that clinically, side effects were considered tolerable when  $C_{max}$  is below 60 ng/ml. This constraint means that a 30 mg/m<sup>2</sup> dose should no shorter than 16 hours in order to avoid unacceptable adverse effects, by their calculations.[44] This type of dose adjustment based on peak concentration could be especially useful if a peak heart DOXol concentration, extrapolated from a plasma concentration sample using the PBPK model, could be determined in a similar way.

Referring again to Table 1-1, most doses are given clinically in fractionated, repeated lower doses, which likely allow for clearance of the drug before the subsequent dose.[199] However, there may be reason to believe that fractionated dosing has a detrimental effect on the therapeutic drug effect on tumor cells. This same recovery time that allows DOX to clear the system may also give tumor cells time to recover between doses.[142] Additionally, the faster the drug clears, the lower the residence time. Since tumors are cell-cycle dependent, lower residence time decreases the chance that the drug will reach the tumor cells during their most vulnerable growth phase.[44] As mentioned in Chapter 2, the breadth of cancer types that DOX treats makes the relation of pharmacodynamic response and dosing schedule too broad of a topic to include in the scope of this work. It would certainly be a compelling next step to find an optimum balance between tumor killing effect and cardiotoxicity. The extent to which this study

will contribute to that balance is by developing a framework that can predict concentration in specific tissues for dose monitoring. In general, there is compelling evidence in literature that any dose given over a longer time and fractionated doses given more frequently can reduce the incidence of cardiotoxicity.[141, 142]

A similar approach is taken in this work, except instead of the maximum plasma concentration, the maximum heart concentration of the metabolite DOXol is extrapolated from the PBPK model for the assessment of toxicity. PBPK models lend themselves as a useful tool for modeling metabolism kinetics and concentration in a specific tissue or organ. The total drug exposure or therapeutic effect, as measured by area under the concentration-versus-time curve (AUC), was maximized using the PBPK model and 'optimize' function in R.[200, 146, 8]. This optimization function was a better choice than other multi-dimensional optimization packages like those used in fitting the PBPK model parameters ('optim'), since only one parameter was being maximized for the function.[186] The 'optimization' function takes an interval of possible values to search, the choice of minimization or maximization of the function, the function to be optimized. The method used by this function utilizes a combination of the golden search method and successive parabolic interpolation and is designed for continuous functions and one-dimensional optimization.[200] The golden search method is similar to bisection methods and searches within the interval for the extrema within the interval. This is particularly useful for optimizations like this study which have physiological bounds within these values must lie. The algorithm can be relatively slow, but it is robust.[201] The ranges in which the rate or total dose were tested were  $9 \text{ mg/m}^2$  -  $75 \text{ mg/m}^2$  based on the extremes of the ranges which DOX is currently given in humans (Table 1-1).[199]. This equated to

a range of 32  $\mu\text{M}$  to 350  $\mu\text{M}$ . A range of 30  $\mu\text{M}$  to 500  $\mu\text{M}$  was implemented as the upper and lower bounds for possible rates in order to give the optimization more room to explore higher doses that are still within physiological possibility. Since the rate or total dose was the parameter being estimated, the optimization was run in intervals of 1, 5, 30, 60, 120, 360, 720, 1440, 2160, 2880, and 4320. These are based on clinical dosing duration values for DOX in adult humans.[34, 121, 133, 80] A penalty on the objective function was added for the maximum concentration of DOXol in the heart exceeding  $10^{-3}$  based on the observed values of DOXol in the mouse heart reported by van der Vijgh.[12] The values for the physiological and pharmacokinetic parameters in the PBPK model used for these minimizations are those listed in Table 5-6.

The optimization routine for the PBPK model predictions was run for each infusion duration listed in Table 6-1 with the goal of maximizing the exposure for that length of infusion without exceeding  $10^{-3}$ . Figure 6-1 shows a schematic of the iterative process of the therapeutic dose monitoring approach. Figure 6-2 shows both AUC and dose given (infusion rate) versus the infusion duration given the maximum concentration of DOXol in the heart stayed below  $10^{-3}$ . The red vertical line indicates the infusion rate/dose and infusion duration where the AUC is maximized while still maintaining  $C_{max,heart,DOXol}$  of below  $10^{-3}$ . Interestingly, these results show that there is a diminishing return for increasing the dose for a greater than 2 hour infusion. To maximize therapeutic efficacy only to the extent that some  $C_{max,heart,DOXol}$  is not exceeded, a 2 hour infusion duration at a total dose of 69.3  $\mu\text{M}$ . The plots of this infusion rate and duration combination are shown in Figures 6.3 and 6.4. The significant binding of DOXol in the heart is seen in Figure 6-4, since the peak concentration occurs  $\approx 45$  hours following the

end of the infusion. Only then does it begin to clear from the heart tissue, whereas in the venous blood, the concentration is more than an order of magnitude lower at the same time point of 2728.25 minutes.

**Table 6-1:** *AUC and  $C_{max}$  for the Predictions Generated by the PBPK Model*

Infusion Time (min)	Total Dose	$AUC_{vb}$	$C_{max,heart,DOXol}$ ( $\mu\text{M}$ )
1	55.0	73.62	0.00099
5	66.0	75.71	0.00099
30	68.5	75.80	0.00099
60	69.0	76.01	0.00099
120	69.3	76.07	0.00099
720	69.35	74.71	0.00099
1440	69.4	73.13	0.00099
2160	69.5	71.53	0.00099
2880	70.15	70.38	0.00099
4320	71.0	67.08	0.00099

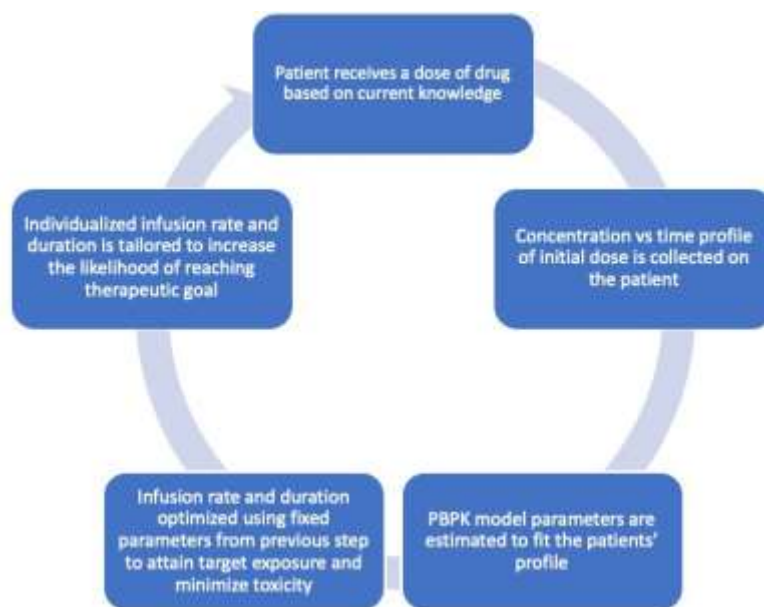


**Figure 6-1:** Schematic of the iterative process of the therapeutic dose monitoring approach outlined in this work for individualizing DOX therapy

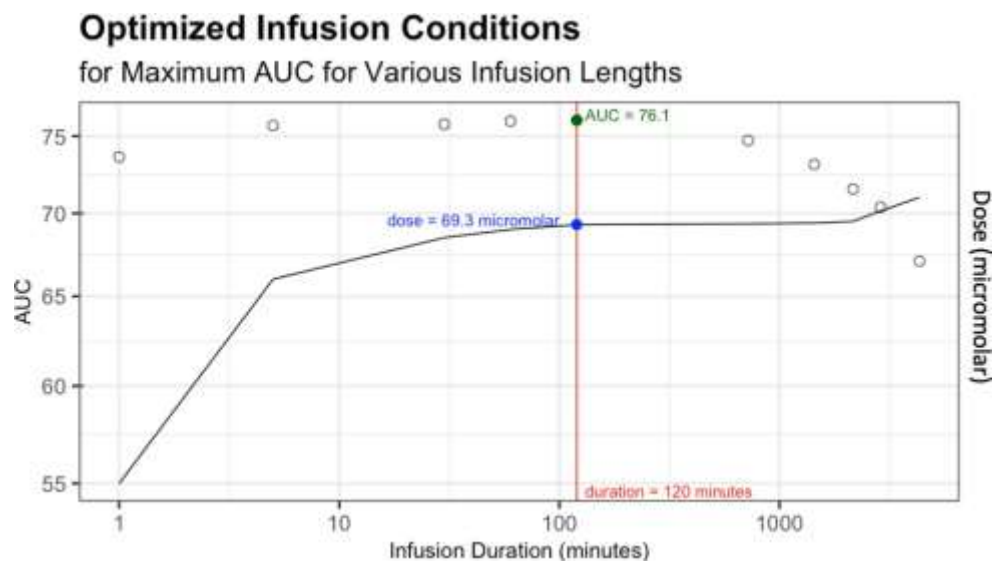


**Figure 6-2:** Plot of venous blood *AUC* values versus infusion duration at the maximum dose that does not exceed  $C_{max,heart,DOXol}$  of  $10^{-3}$  -the open circles represent the *AUC* values, the closed dark green circle indicates the point at which the *AUC* is highest; the solid line represents the infusion rate or maximum total dose for the corresponding infusion duration, with the blue closed circle indicating the dose at which the *AUC* is highest; the vertical line highlights the optimal infusion duration at which *AUC* is maximized while still remaining below  $C_{max,heart,DOXol}$

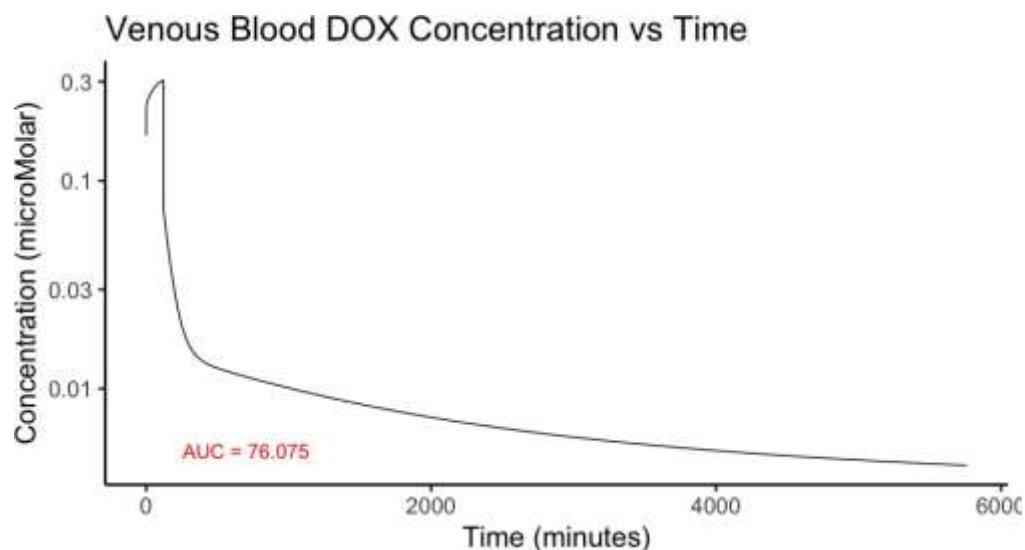


**Figure 6-3:** DOX venous blood concentration versus time plot in humans using the infusion parameters (infusion rate -  $69.3 \mu\text{M}$  over 120 minutes) from the optimization shown in Table 6-1 and Figure 6-2 - *AUC* for the infusion simulated out to 96 hours

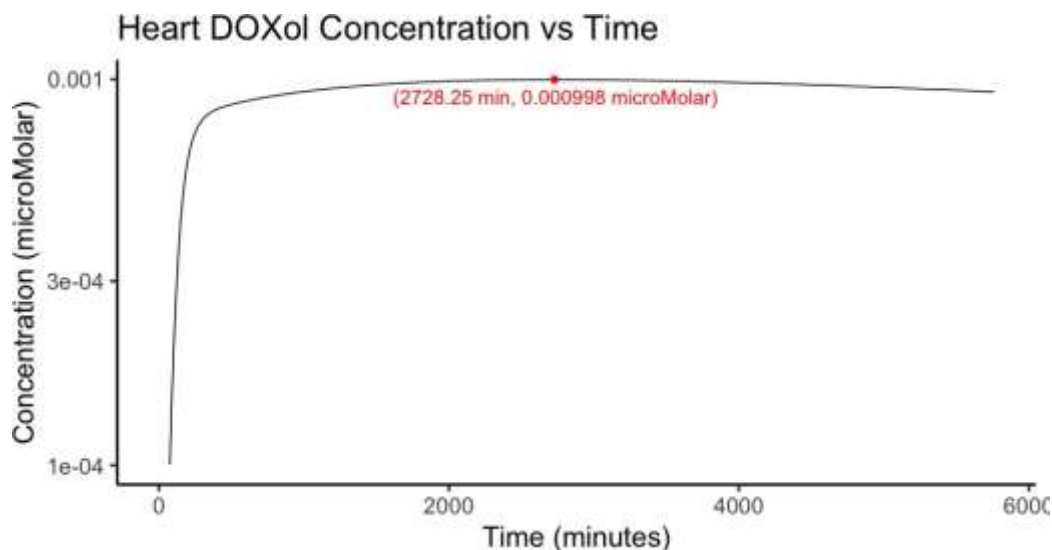


**Figure 6-4:** DOXol heart concentration versus time plot in humans using the infusion parameters (infusion rate -  $69.3 \mu\text{M}$  over 120 minutes) from the optimization shown in Table 6-1 and Figure 6-2 -  $C_{max,heart,DOXol}$  is reached at 2827.25 minutes but does not exceed the threshold of  $10^{-3}$  for the infusion simulated out to 96 hours

#### 6.1.1.3 Use of PBPK Predictions for Therapeutic Dose Monitoring of DOX

Similar to the study done by Eksborg where the  $C_{max}$  and  $AUC$  in plasma were compared for different infusion durations, a framework such as this could allow for deeper insight into the relationship between infusion parameters and exposure and toxicity profiles for DOX. It would be interesting to eventually develop a valid PBPK model such that a clinical threshold for adverse effects of DOX could be established for  $C_{max,heart,DOXol}$  as it has been for  $C_{max,vb}$ . [202] If achieved, a therapeutic drug monitoring process could be used to predict the infusion duration necessary to maintain a  $C_{max,heart,DOXol}$  below that clinical threshold to significantly reduce the incidence of cardiotoxicity from a more direct measure. Not only could this predictive framework be useful for dose improvement based on organ-specific toxicities, but also for toxicity related to metabolites since PBPK models are well-suited for modeling more complex mechanistic metabolite activity. [2] The utility of a predictive model such as the one

demonstrated here could be extremely useful in any number of narrow therapeutic index drugs.

The general process of how the predictive PBPK model could be used for individualized therapeutic drug monitoring is illustrated in Figure 6.1. First, an initial dose would be given to the patient in accordance with the standard dose calculations for the respective disease. Plasma samples would be collected at various time points. From that data, the pharmacokinetic parameters would be estimated for that particular patient. The infusion rate and duration could then be optimized by fixing the parameters from the previous step using PBPK model predictions to obtain the desired target exposure that does not exceed the maximum DOXol concentration in the heart. The next dose would follow the updated infusion parameters. The knowledge gained from the predictions of a PBPK model like the one in this study could be used to help individualize DOX dosing regimens in the future.

### **6.1.2 Pharmacodynamic Studies**

It has been observed that frequent, fractionated doses tend to decrease DOX-induced cardiotoxicity. Additionally, there is evidence that since a certain  $C_{max}$  threshold is correlated clinically to adverse effects, prolonged infusions may also decrease cardiotoxicity for roughly the same exposure ( $AUC$ ).<sup>[44]</sup> Some studies claim that therapeutic efficacy may even be increased for 10 - 96 hour intravenous infusions compared to the same dose over a shorter period.<sup>[203]</sup> One reason for this could be that tumor cells are only in the growth phase, the time when they are most vulnerable to drug effect, for a short period of time. The circadian pacemaker in the hypothalamus of the brain guides the daily flux of activity in peripheral organs and is best recognized as the

“circadian rhythm” that regulates sleep. The circadian rhythm is also known to control the time Cancer tissues show tissue-specific daily variation in DNA synthesis activity and are more susceptible to drug effect during different times of the day. Therefore, even the time of day could effect the potency of a drug on a target tissue depending on the current phase of the cell cycle. [204] Therefore, there is a possibility that the shorter, intermittent infusions like those used clinically could be missing the tumor growth phase “window” in some instances.[44] Since longer infusions also decrease cardiotoxicity, it may be interesting to see if an optimum exists among infusion rate, infusion duration, exposure, maximum dose, and therapeutic efficacy.

Future work could include adding a pharmacodynamic component which would add the concentration-effect piece to the current concentration-time profiles described here. Having an understanding of how infusion rate and duration affects cardiotoxicity is useful, but if the therapeutic purpose of the drug is compromised, then the potential morbidity of the disease being treated quickly outweighs the potential morbidity of cardiotoxic adverse effects.

### **6.1.3 Application to Other Drugs**

As mentioned before, the utility of this approach is not exclusive to DOX, but could be extended to any drug with a narrow therapeutic index with a tissue-specific toxicity. While this may seem like a limited scope, the drugs that fall into this category are some of the most widely used for their respective indications. For instance, methotrexate is a competitive inhibitor of dihydrofolate reductase, which is a key enzyme for synthesizing nucleic acid.[197] It is used in some of the most common forms of cancer - for example, acute lymphoblastic leukemia (ALL), lung cancer, brain tumors,



and carcinomas. Toxicities include leukopenia, thrombocytopenia, and acute kidney injury (AKI).[197, 205] Timed blood draws are needed in order to monitor the renal clearance of methotrexate, but it may be useful to gain more insight into the methotrexate concentration in the kidney for more individually tailored dosing. Similarly, aminoglycoside antibiotics like Streptomycin are used to treat systemic, life-threatening infections. However, severe nephrotoxicity can occur in patients due to the high inter-patient variability in clearance. Perhaps a more interesting application could be the anti-manic agent lithium. Therapeutic drug monitoring is vital for lithium for both efficacy and to prevent brain lithium toxicity. While the blood concentration of lithium has been known to be approximately analogous to brain concentration, a PBPK model-informed prediction of brain concentration may improve the understanding of the drug and drugs similar.[197]

## 6.2 Conclusion

Pharmacometrics is a discipline that quantifies what the body does to the drug - pharmacokinetics - and what the drug does to the body - pharmacodynamics.[67, 69] Pharmacokinetics (PK) is described as the science of characterizing the time course of drug concentration through four processes - absorption, distribution, metabolism, and excretion. These processes are often referred to as ADME processes.[130, 68] Pharmacokinetic models generally represent different locations in the body as compartments, which are represented by mathematical equations. Although they are representative of physiological spaces in the body, they do not hold any true physiological reality and may not correspond directly to any real tissue or fluid compartment. Classic PK models are generally broken into a central compartment with a

few peripheral compartments that allow the system to empirically mimic the complex time course that a drug actually takes when binding, metabolizing, and clearing the body. Physiology-based pharmacokinetic (PBPK) modeling are more heavily based on the physiology of the system and tend to have compartments and inter-compartmental clearance rates that are more representative of specific tissues and physiological processes.[1, 2] Some important considerations in the development of PBPK models include both passive and active diffusion rates across cell membranes, metabolic pathways, extent of binding to blood components and proteins, and excretion or clearance parameters which are crucial to building a more mechanistic model.[143, 2]

Doxorubicin (DOX) is the drug of interest for this particular work. DOX is an anthracycline antibiotic drug that is administered in a wide range of cancer types due to its potent cytotoxicity. However, with its robust cell-killing properties comes a high incidence of debilitating cardiotoxicity which can lead to cardiomyopathy and congestive heart failure linked to accumulated dose.[3, 40] Cumulative doses of 400 mg/m<sup>2</sup> to 550 mg/m<sup>2</sup> have shown increased incidence of these cardiac adverse events and will sometimes lead to discontinuation of therapy.[141] Since its development in the late 1960's, many pharmacokinetic models have been developed to better characterize DOX and have described its clearance as either a two- or a three- compartment model in sub-clinical species such as mice, rats, and pigs as well as in humans.[12, 45, 8, 121] It has been observed experimentally across species that lower doses tend to exhibit bi-phasic clearance (two-compartment model) while moderate to high doses tend to exhibit tri-phasic clearance behavior (three-compartment model).[44, 121] The extenuating issue with DOX is that its cardiotoxicity is related to accumulation of its primary metabolite,

doxorubicinol (DOXol) in the heart.[40, 12] Since classic compartmental pharmacokinetic models are not tissue-specific enough to characterize and simulate the DOXol concentration in the heart, PBPK models of DOX have been developed for better understanding of the binding of the drug in tissues.[8, 64] A PBPK model of DOX was constructed by adapting an existing pig model from the literature to include a heart compartment in order to characterize the DOXol concentration in the heart.[8] Since cardiotoxicity is known to be related to the accumulation of DOXol in the heart, it was also designated as a metabolizing compartment.[4]

While classic PK models are generally represented by a few ordinary differential equations (ODEs), PBPK models can have many ordinary differential equations with a larger number of parameters to describe the physiological processes involved in the model.[2] For large systems of ODEs, numerical methods are needed to solve the system.[147, 5] Each numerical method for solving ODE systems come with benefits and drawbacks, but the general strategy is to begin with the simplest method possible and add complexity as needed.[5] Euler's Method was the first method used to solve the system, but it proved to require too small of a time step for the needed efficiency.[147] The fourth-order Runge-Kutta method was the next method used since it has a higher accuracy and is typically more stable, but it still required a very small time step to capture the concentration-time profile of DOX. Additionally, it was discovered that the system had issues with stiffness, so an adaptive Runge-Kutta method was implemented next. The Runge-Kutta Fehlberg method is a numerical method which varies the length of the time step according to the amount of change occurring in the time interval, which decreases the computation time while maintaining the accuracy needed.[5] Unfortunately, the added

complexity of the equations in this method was still computationally slow when executed in R.[146] Since matrices tend to be more palatable in R, the system of equation was converted into matrix format, which consisted of (i) a rate coefficient matrix describing the rate of change in drug concentration in each compartment relative to each concentration ( $A$  matrix), (ii) an initial conditions matrix representing the amount of drug in each compartment at the beginning of the respective time interval ( $x$  vector), and (iii) the dose vector representing the dose that will be administered in each respective tissue/compartment ( $g$  vector). Variation of Parameters was used to solve the matrix system,

$$\mathbf{Ax} + \mathbf{g}(t) = \mathbf{x}'$$

at three equidistant time points ( $t_0$ ,  $t_1$ , and  $t_2$ ). Those three time points were then numerically integrated over using Composite Simpson's Rule. That solution  $\mathbf{x}^t$  then becomes the new initial condition for  $\mathbf{x}$  for the next iteration of what becomes a series of initial value problems. [7, 5]

This method was able to solve the PBPK model, represented by a system of a total of 44 first-order ordinary differential equations, reasonably quickly. Physiological parameters such as volume and blood flow fractions were obtained from literature for mice, rats, rabbits, pigs, and humans. [8, 174, 173] First, the parameters were estimated for a mouse data set that contained concentration versus time data for both the venous blood and the heart for both DOX and DOXol.[12] These parameters were then fixed and scaled to predict rat, rabbit dog, pig, and human data sets using an allometric scaling equation on the blood:plasma partition coefficient  $B : P$  .[8, 9, 10] The allometric equation was derived from a previous inter-species scaling study for DOX which took the

approach of scaling from mice other rodents, non-rodents, or humans.[64] This equation successfully scaled using  $B : P$  for rat and human data sets, but failed to adequately predict in rabbits, dogs, or pigs. Another study suggested the addition of the correction factor of Maximum Life-Span potential for hepatically-eliminated small-molecule drugs with low hepatic extraction ratios ( $E_h$ ). DOX has been described as such a drug. [9] The addition of this correction factor allowed for the mouse parameter set to adequately predict the DOX concentration in venous blood ( $C_{vb,DOX}$ ) and the DOXol concentration in the heart ( $C_{heart,DOXol}$ ). The ultimate goal was to scale from mouse to humans for therapeutic drug monitoring. Additional validation for the equation came from the fact that the allometric equation also fit for rats, rabbits, dogs, and pigs.

Despite numerous studies and pharmacokinetic models of DOX, there are almost no covariates that consistently improve the dose of DOX, with the exception of dose reduction for hepatic impairment.[11, 140] However, dosing schedule – infusion rate and duration- have been shown to affect both drug efficacy and incidence of cardiotoxicity.[11] A study done in data from cancer patients receiving DOX at different infusion durations showed that increasing the infusion length did not greatly affect exposure ( $AUC$ ) but did significantly decrease the maximum concentration ( $C_{max}$ ). Clinically, values of  $C_{max}$  above a certain threshold have been correlated to adverse effects. This study suggested extending the infusion length for the necessary dose in order to avoid exceeding that  $C_{max}$  value since there was no noticeable loss in therapeutic exposure.[202]

A framework similar to the one in this study such as could allow for deeper insight into the relationship between infusion parameters and exposure and toxicity

profiles for DOX. However, in this case, the criterion for decreasing incidence of cardiotoxicity was maintaining a sub-toxic  $C_{max,heart,DOXol}$  in the heart while maximizing exposure, represented by area under the concentration-time-curve ( $AUC$ ). The PBPK model was optimized at 10 time points between 1 minute and 72 hours (4320 minutes). The 'optimize' function in R was given an interval of  $30\mu\text{M}$  to  $500\mu\text{M}$  to search, which is approximately the range which DOX is given clinically.[146, 200, 199] The goal of the optimization was to maximize the value of ( $AUC$ ) without the  $C_{max,heart,DOXol}$  value of  $10^{-3}$  Using these predictions, by way of a penalty on the objective function value.

Especially since many other covariates have failed to improve dosing schedules for DOX, understanding the relationship of infusion rate and duration on exposure and toxicity of DOX is invaluable. The potential for reduction of cardiotoxicity without compromising the therapeutic exposure of DOX could inform future studies and improve outcomes for the many patients who are treated with DOX for various cancer types.[11, 202] During a patient's first dose of DOX with standard dosing parameters, plasma samples could be collected and a concentration-time profile for the individual patient could be created. The PBPK model predictions could provide  $AUC$  and  $C_{max,heart,DOXol}$  data, and an assessment could be made whether or not the infusion rate and duration are appropriate for maximum therapeutic effect without elevating the risk for cardiotoxic adverse effects. If necessary, the infusion parameters could then be adjusted for that patient's next dose. Clinical thresholds for  $C_{max,vb}$  have been established for incidence of adverse effects, and in future work, perhaps a similar threshold for cardiotoxicity could also be established using tissue-specific measures. As the use of PBPK models in drug

discovery and drug delivery increase, it is not unreasonable to think that this approach to therapeutic drug monitoring is feasible in the near future.[143] The knowledge gained from the predictions of a PBPK model like the one in this study could be used to help individualize DOX dosing regimens in the future.

**APPENDIX A**  
**EQUATIONS FROM DUBBELBOER MODEL**



## A.1 Blood and Lung Compartments

**Equation 1:** Concentration in arterial blood:

$$V_{ab} \times \frac{dC_{ab}}{dt} = Q_{co}(C_{vb,lu} - C_{ab})$$

**Equation 2:** Concentration in venous blood:

$$V_{vb} \times \frac{dC_{vb}}{dt} = \Sigma(Q_{co} \times C_{vb,lu}) - Q_{co} \times C_{vb} + R_{in}$$

**Equation 3:** Concentration in lung:

$$(V_{lu} - V_{lu,b}) \times \frac{dC_{vb,lu,u}}{dt} = Q_{co}(C_{vb} - C_{vb,lu}) - Cl_{on} \times C_{lu,u} + Cl_{off} \times C_{lu,b}$$

## A.2 Binding and Partitioning Equations

**Equation 4:** Partitioning from blood to all non-eliminating tissues:

$$C_{vb,t} = \frac{C_t \times B : P \times f_{u,p}}{K_{p,t}}$$

**Equation 5:** Concentration of bound drug in the liver, kidney, lung, slow perfused, rapid perfused compartments, and GI/spleen (eliminating and non-eliminating

tissues):

$$V_{t,b} \times \frac{dC_{t,b}}{dt} = Cl_{on} * C_{t,u} - Cl_{off} \times C_{t,b}$$

### A.3 Non-Eliminating/Non-Metabolizing Compartments

**Equation 6:** Concentration in GI/spleen and slow and rapid perfused tissues (non-eliminating tissues):

$$(V_t - V_{t,b}) \times \frac{dC_{t,u}}{dt} = Q_t(C_{ab} - C_{vb,t}) - Cl_{on} \times C_{t,u} + Cl_{off} \times C_{t,b}$$

### A.4 Metabolizing and Eliminating Compartments

**Equation 7:** Concentration in the vascular subcompartment of the liver:

$$V_{va,li} \times \frac{dC_{va,li}}{dt} = Q_{vp} \times C_{vb,gu} + Q_{ha} \times C_{ab} - (Q_{vp} + Q_{ha}) \times C_{va,li} - P_{diff} \times \left( \frac{C_{va,li} \times f_{u,p}}{CbCp} - C_{ex,li} \times f_{u,p} \right)$$

**Equation 8:** Concentration in the extracellular subcompartment of the liver:

$$V_{ex,li} \times \frac{dC_{ex,li}}{dt} = P_{diff} \times \left( \frac{C_{va,li} \times f_{u,p}}{CbCp} \right) - C_{ex,li} \times f_{u,p} - Cl_{mem} \times f_{u,p} - C_{cel,li,u} \times f_{u,cel,li}$$

**Equation 9:** Concentration of unbound drug in the cellular subcompartment of the liver:

$$(V_{cel,li} - V_{cel,li,b}) \times \frac{dC_{cel,li,u}}{dt} = Cl_{mem} \times (C_{ex,li} \times f_{u,p} - C_{cel,li,u}) -$$

$$Cl_{excr,li} \times C_{cel,li,u} - Cl_{on} \times C_{cel,li,u} + Cl_{off} \times C_{cel,li,b} \pm J_{met,li} \text{ (from Equation 10)}$$

**Equation 10:** Metabolism of DOX to DOXol in the liver - negative in the DOX equation to represent metabolism and positive in the DOXol equation to represent formation:

$$J_{met,li} = \frac{V_{max,li} \times C_{cel,li,u} \times f_{u,cel,li}}{K_{m,li} + C_{cel,li,u} \times f_{u,cel,li}} \times SF_{met,li}$$

**Equation 11:** Amount of drug excreted into bile:

$$\frac{dA_{bile}}{dt} = Cl_{excr,li} \times C_{cel,li,u} \times f_{u,cel,li}$$

**Equation 12:** Concentration in the vascular subcompartment of the kidney:

$$V_{va,ki} \times \frac{dC_{va,ki}}{dt} = Q_{ki} \times (C_{ab} - C_{vb,ki}) - P_{diff} \times (C_{va,ki} \times f_{u,p} - C_{ex,ki} \times$$

**Equation 13:** Concentration in the extracellular compartment of the kidney:

$$V_{ex,ki} \times \frac{dC_{ex,ki}}{dt} = P_{diff} \times (C_{va,ki} \times f_{u,p} - C_{ex,ki} \times f_{u,p}) -$$

$$Cl_{mem} \times (C_{ex,ki} \times f_{u,p} - C_{cel,ki} \times f_{u,cel,ki})$$

**Equation 14:** Concentration of unbound drug in the cellular subcompartment of the kidney:

$$(V_{cel,ki} - V_{cel,ki,b}) \frac{dC_{cel,ki,u}}{dt} = Cl_{mem} \times (C_{ex,ki} \times f_{u,p} - C_{cel,ki,u}) - Cl_{excr,ki} \times C_{cel,ki,u} -$$

$$Cl_{on} \times C_{cel,ki,u} + Cl_{off} \times C_{cel,ki,b} \pm J_{met,ki} \text{ (from Equation 15)}$$

**Equation 15:** Metabolism of DOX to DOXol in the kidney - negative in the DOX equation to represent metabolism and positive in the DOXol equation to represent formation:

$$J_{met,ki} = \frac{V_{max,ki} \times C_{cel,ki,u} \times f_{u,cel,ki}}{K_{m,ki} + C_{cel,ki,u} \times f_{u,cel,ki}} \times SF_{met,ki}$$

**Equation 16:** Amount of drug excreted into urine:

$$\frac{dA_{urine}}{dt} = GFR \times BW \times C_{va,ki} \times f_{u,p} + Cl_{excr,ki} \times C_{cel,ki,u} \times f_{u,cel,ki}$$

**APPENDIX B**  
**FINAL MODEL EQUATIONS**

## APPENDIX B: FINAL MODEL EQUATIONS

### B.1 Blood and Lung Compartments

#### Equation 1: Concentration in Venous Blood

$$\begin{aligned}
 V_{vb} \times \frac{dC_{vb}}{dt} = & \Sigma(Q_{tissue} \times \frac{V_{tissue,bound}}{V_{tissue}} \times BP \times F_{unbound}) \times C_{tissue,bound} \\
 & + \Sigma(Q_{tissue} \times \frac{V_{tissue,unbound}}{V_{tissue}} \times BP \times F_{unbound}) \times C_{tissue,unbound} + Q_{vH} \times C_{va,liver} \\
 & + Q_{heart} \times C_{va,heart} + Q_{kidney} \times C_{va,kidney} - Q_{CO} \times C_{vb}
 \end{aligned}$$

where tissue refers to all non-metabolizing compartments

#### Equation 2: Concentration in Arterial Blood

$$\begin{aligned}
 V_{ab} \times \frac{dC_{ab}}{dt} = & Q_{CO} \times BP \times (\frac{V_{lung,bound}}{V_{lung}} \times F_{unbound} \times C_{lung,bound} + \\
 & Q_{CO} \times BP \times (\frac{V_{lung,unbound}}{V_{lung}} \times F_{unbound} \times C_{lung,unbound}) - Q_{CO} \times C_{ab}
 \end{aligned}$$

#### Equation 3: Concentration in Bound Fraction of Lung

$$V_{lung,bound} \times \frac{dC_{lung,bound}}{dt} = Cl_{on} \times C_{lung,unbound} - Cl_{off} \times C_{lung,bound}$$

#### Equation 4: Concentration in Unbound Fraction of Lung

$$V_{lung,unbound} \times \frac{dC_{lung,unbound}}{dt} = Q_{CO} \times C_{vb} + Cl_{off} \times C_{lung,bound}$$

$$-Q_{CO} \times BP \times \left( \frac{V_{lung,unbound}}{V_{lung}} \right) \times F_{unbound}$$

## B.2 Non-Metabolizing Tissue Compartments

**Equation 5: Concentration in Bound Fraction of GI/Spleen**

$$V_{GI/spleen,bound} \times \frac{dC_{GI/spleen,bound}}{dt} = Cl_{on} \times C_{GI/spleen,unbound} - Cl_{off} \times C_{GI/spleen,bound}$$

**Equation 6: Concentration in Unbound Fraction of GI/Spleen**

$$V_{GI/spleen,unbound} \times \frac{dC_{GI/spleen,unbound}}{dt} = Q_{GI/spleen} \times C_{ab} + Cl_{off} \times C_{GI/spleen,bound} -$$

$$Q_{GI/spleen} \times BP \times \frac{V_{GI/spleen,bound}}{V_{GI/spleen}} \times C_{GI/spleen,bound} -$$

$$Q_{GI/spleen} \times BP \times \frac{V_{GI/spleen,unbound}}{V_{GI/spleen}} \times C_{GI/spleen,unbound} - Cl_{on} \times C_{GI/spleen,unbound}$$

**Equation 7: Concentration in Bound Fraction of Slow Perfused Tissues**

$$V_{sp,bound} \times \frac{dC_{sp,bound}}{dt} = Cl_{on} \times C_{sp,unbound} - Cl_{off} \times C_{sp,bound}$$

**Equation 8: Concentration in Unbound Fraction of Slow Perfused Tissues**

$$V_{sp,unbound} \times \frac{dC_{sp,unbound}}{dt} = Q_{sp} \times C_{ab} + Cl_{off} \times C_{sp,bound} -$$

$$Q_{sp} \times BP \times \frac{V_{sp,bound}}{V_{sp}} \times C_{sp,bound} -$$

$$Q_{sp} \times BP \times \frac{V_{sp,unbound}}{V_{sp}} \times C_{sp,unbound} - Cl_{on} \times C_{sp,unbound}$$

**Equation 9: Concentration in Bound Fraction of Rapid Perfused Tissues**

$$V_{rp,bound} \times \frac{dC_{rp,bound}}{dt} = Cl_{on} \times C_{rp,unbound} - Cl_{off} \times C_{rp,bound}$$

**Equation 10: Concentration in Unbound Fraction of Rapid Perfused Tissues**

$$V_{rp,unbound} \times \frac{dC_{rp,unbound}}{dt} = Q_{rp} \times C_{ab} + Cl_{off} \times C_{rp,bound} -$$

$$Q_{rp} \times BP \times \frac{V_{rp,bound}}{V_{sp}} \times C_{rp,bound} -$$

$$Q_{rp} \times BP \times \frac{V_{rp,unbound}}{V_{rp}} \times C_{rp,unbound} - Cl_{on} \times C_{rp,unbound}$$

## B.3 Metabolizing Tissue Compartments

### B.3.1 Non-Excreting Compartments

**Equation 11: Concentration in Vascular Sub-Compartment of the Heart**

$$V_{va,heart} \times \frac{dC_{va,heart}}{dt} = Q_{heart} \times C_{ab} + P_{diff} \times C_{extra,heart} \times F_{unbound} -$$

$$Q_{heart} \times C_{va,heart} - P_{diff} \times C_{va,heart}$$

**Equation 12: Concentration in Extracellular Sub-Compartment of the Heart**

$$V_{extra,heart} \times \frac{dC_{extra,heart}}{dt} = P_{diff} \times F_{unbound} \times C_{va,heart} +$$

$$Cl_{mem} \times F_{unbound} \times C_{cel,unbound,heart} - P_{diff} \times C_{extra,heart} - Cl_{mem} \times C_{extra,heart}$$

**Equation 13: Concentration in Bound Cellular Sub-Compartment of the Heart**

$$V_{cel,bound,heart} \times \frac{dC_{cel,bound,heart}}{dt} = Cl_{on} \times C_{cel,unbound,heart} - Cl_{off} \times C_{cel,bound,heart}$$

Equation 14 includes the Michaelis-Menten metabolism term (first term) that is negative in the DOX equation and positive in the DOXol equation, signifying DOX to DOXol metabolism. Equation 14: Concentration in



### Unbound Cellular Sub-Compartment of the Heart

$$V_{cel,unbound,heart} \times \frac{dC_{cel,unbound,heart}}{dt} = \left( \frac{V_{max,heart}}{K_m,heart} \right) \times S F_{heart} \times F_{unbound} \times C_{cel,unbound,heart} +$$

$$Cl_{mem} \times F_{unbound} \times C_{extra,heart} + Cl_{off} \times C_{cel,bound,heart} - Cl_{mem} \times C_{cel,unbound,heart} -$$

$$Cl_{on} \times C_{cel,bound,heart} - Cl_{excr,heart} \times F_{unbound} \times C_{cel,bound,heart}$$

### B.3.2 Excreting Compartments

#### Equation 15: Concentration in Vascular Sub-Compartment of the Kidney

$$V_{va,kidney} \times \frac{dC_{va,kidney}}{dt} = Q_{kidney} \times C_{ab} + P_{diff} \times C_{extra,kidney} \times F_{unbound} -$$

$$Q_{kidney} \times C_{va,kidney} - P_{diff} \times C_{va,kidney}$$

#### Equation 16: Concentration in Extracellular Sub-Compartment of the Kidney

$$V_{extra,kidney} \times \frac{dC_{extra,kidney}}{dt} = P_{diff} \times F_{unbound} \times C_{va,kidney} +$$

$$Cl_{mem} \times F_{unbound} \times C_{cel,unbound,kidney} - P_{diff} \times C_{extra,kidney} - Cl_{mem} \times C_{extra,kidney}$$

#### Equation 17: Concentration in Bound Cellular Sub-Compartment of the Kidney

$$V_{cel,bound,kidney} \times \frac{dC_{cel,bound,kidney}}{dt} = Cl_{on} \times C_{cel,unbound,kidney} - Cl_{off} \times C_{cel,bound,kidney}$$

Equation 18 includes the Michaelis-Menten metabolism term (first term) that is negative in the DOX equation and positive in the DOXol equation, signifying DOX to DOXol metabolism.

#### Equation 18: Concentration in Unbound Cellular Sub-Compartment

of the Kidney

$$V_{cel,unbound,kidney} \times \frac{dC_{cel,unbound,kidney}}{dt} = \left( \frac{V_{max,kidney}}{K_m,kidney} \right) \times S F_{kidney} \times F_{unbound} \times C_{cel,unbound,kidney} +$$

$$Cl_{mem} \times F_{unbound} \times C_{extra,kidney} + Cl_{off} \times C_{cel,bound,kidney} - Cl_{mem} \times C_{cel,unbound,kidney} -$$

$$Cl_{on} \times C_{cel,bound,kidney} - Cl_{excr,kidney} \times F_{unbound} \times C_{cel,bound,kidney}$$

**Equation 19: Concentration in Vascular Sub-Compartment of the Liver**

$$V_{va,liver} \times \frac{dC_{va,liver}}{dt} = Q_{VP} \times BP \times \frac{V_{GI/spleen,bound}}{V_{GI/spleen}} \times C_{GI/spleen,bound} \times F_{unbound} +$$

$$Q_{VP} \times BP \times \frac{V_{GI/spleen,unbound}}{V_{GI/spleen}} \times C_{GI/spleen,unbound} \times F_{unbound} +$$

$$Q_{HA} \times C_{ab} - Q_{VH} \times C_{va,liver} - P_{diff} \times \frac{F_{unbound}}{CbCp}$$

**Equation 20: Concentration in Extracellular Sub-Compartment of the Liver**

$$V_{extra,liver} \times \frac{dC_{extra,liver}}{dt} = P_{diff} \times F_{unbound} \times C_{va,liver} +$$

$$Cl_{mem} \times F_{unbound} \times C_{cel,unbound,liver} - P_{diff} \times C_{extra,liver} - Cl_{mem} \times C_{extra,liver}$$

**Equation 21: Concentration in Bound Cellular Sub-Compartment of the Liver**

$$V_{cel,bound,liver} \times \frac{dC_{cel,bound,liver}}{dt} = Cl_{on} \times C_{cel,unbound,liver} - Cl_{off} \times C_{cel,bound,liver}$$

Equation 22 includes the Michaelis-Menten metabolism term (first term) that is negative in the DOX equation and positive in the DOXol equation, signifying DOX to DOXol metabolism.

**Equation 22: Concentration in Unbound Cellular Sub-Compartment**

of the Liver

$$\begin{aligned}
 V_{cel,unbound,liver} \times \frac{dC_{cel,unbound,liver}}{dt} = & \left( \frac{V_{max,liver}}{K_m,liver} \right) \times S F_{liver} \times F_{unbound} \times C_{cel,unbound,liver} + \\
 Cl_{mem} \times F_{unbound} \times C_{extra,liver} + Cl_{off} \times C_{cel,bound,liver} - Cl_{mem} \times C_{cel,unbound,liver} - \\
 Cl_{on} \times C_{cel,bound,liver} - Cl_{excr,liver} \times F_{unbound} \times C_{cel,bound,liver}
 \end{aligned}$$

## **APPENDIX C**

### **THREE COMPARTMENT MODEL EXAMPLE CODE**

## APPENDIX C: THREE COMPARTMENT MODEL EXAMPLE CODE

```
rm(list=ls())

## run this chunk once to install package needed to download 'pbpkme'
## from Github
## skip if you've already done this
install.packages("devtools")
library(devtools)
install_github("hillaryhusband/pbpkme")
#####
library("pbpkme")
library(pracma)
library(readxl)
library(lattice)
library(ggplot2)
library(tidyverse)
library(ggthemes)

dt = 0.01
tfinal = 60

### Parameters and model based on Remifentanyl model by Cascone et al.:
```

```
## Cascone S, Lamberti G, Titomanlio G, Piazza D.
## Pharmacokinetics of Remifentanyl:
## a three-compartmental modeling approach.
## Translational Medicine. 2013;7(4):18{22

#parameters

k10 <- 0.172 # min-1
k12 <- 0.373 # min-1
k13 <- 0.0367 # min-1
k21 <- 0.103 # min-1
k31 <- 0.0124 # min-1

V1 <- 7.88 #mL
V2 <- 23.9 #mL
V3 <- 13.8 #mL

CL1 <- 2.08 # mL/min
CL2 <- 0.828 # mL/min
CL3 <- 0.0784 # mL/min

body_weight <- 79 # kg (mean value)

p_matrix = matrix(0, nrow=3, ncol=3)
p_matrix[1,1] = -((CL1/V1) + k12 + k13 + k10)
p_matrix[1,2] = (k21 * V2) / V1
p_matrix[1,3] = (k31 * V3) / V1
p_matrix[2,1] = (k12 * V1) / V2
p_matrix[2,2] = -((CL2/V2) + k21)
p_matrix[3,1] = (k13 * V1) / V3
```

```

p_matrix[3,3] = -((CL3/V3) + k31)

params <- c(k10 = 0.172, k12 = 0.373, k13 = 0.0367, k21 = 0.103,
k31 = 0.0124, V1 = 7.88, V2 = 23.9, V3 = 13.8, CL1 = 2.08,
CL2 = 0.828, CL3 = 0.0784)

# drug injection
# R_in = 5 * body_weight

# C1 = 0
# C2 = 0
# C3 = 0

init_cond_matrix = matrix(0, nrow = 3, ncol = 1)

init_cond_matrix[1,1] = 0 #C1
init_cond_matrix[2,1] = 0 #C2
init_cond_matrix[3,1] = 0 #C3

#dC1_dt = (((-CL1*C1 + k21*V2*C2 + k31*V3*C3 -
#           (k12+k13+k10)*C1)*V1) + R_in) / V1
#dC2_dt = (k12 *C1*V1 - k21*C2*V2 - CL2*C2) / V2
#dC3_dt = (k13*C1*V1 - k31*C3*V3 - CL3*C3) / V3

p_matrix = matrix(0, nrow=3, ncol=3)
p_matrix[1,1] = -((CL1/V1) + k12 + k13 + k10)
p_matrix[1,2] = (k21 * V2) / V1

```

```
p_matrix[1,3] = (k31 * V3) / V1
p_matrix[2,1] = (k12 * V1) / V2
p_matrix[2,2] = -((CL2/V2) + k21)
p_matrix[3,1] = (k13 * V1) / V3
p_matrix[3,3] = -((CL3/V3) + k31)

begin <- 0
end <- 0.5
dose_number <- 1
dose_amt <- 30

modell <- pbpkme(minute = tfinal, h = dt, rate_coeff = p_matrix,
  init_condition = init_cond_matrix,
  pars = params, number_of_doses = dose_number,
  dose = dose_amt, start_time = begin, stop_time = end)

## create continuous time vector and pull out compartments from final matrix
time <- seq(from=0, to = tfinal, by = dt)
conc1 <- modell[1,]
conc2 <- modell[2,]
conc3 <- modell[3,]

## merge time vector and concentrations for plotting in ggplot
C1 <- data.frame(time, conc1)
C2 <- data.frame(time, conc2)
C3 <- data.frame(time, conc3)
```



```
plot1 <- ggplot(data = C1, aes(x = time, y = conc1))+ geom_line() +  
  theme_base() +  
  xlab("Time (minutes)") +  
  ylab("Concentration (microMolar)") +  
  ggtitle("Concentration vs Time", subtitle = "Compartment 1") +  
  scale_y_log10()  
plot2 <- ggplot(data = C1, aes(x = time, y = conc2))+ geom_line() +  
  theme_base() +  
  xlab("Time (minutes)") +  
  ylab("Concentration (microMolar)") +  
  ggtitle("Concentration vs Time", subtitle = "Compartment 2") +  
  scale_y_log10()  
plot3 <- ggplot(data = C1, aes(x = time, y = conc3))+ geom_line() +  
  theme_base() +  
  xlab("Time (minutes)") +  
  ylab("Concentration (microMolar)") +  
  ggtitle("Concentration vs Time", subtitle = "Compartment 3") +  
  scale_y_log10()
```

**APPENDIX D**  
**FINAL MODEL CODE IN R**

## APPENDIX D: FINAL MODEL CODE IN R

```

### Coefficient Matrix for ODE system ###
rate_coeff = matrix(0, nrow=matrix_size, ncol=matrix_size)
# venous blood DOX/DOXol
rate_coeff[1,1] = - Q_CO/V_vb
rate_coeff[1,13] = Q_slow_perfused*BP*F_up_DOX*
                    (V_slow_perfused_b_DOX/V_slow_perfused)
                    / V_vb
rate_coeff[1,15] = Q_slow_perfused*BP*F_up_DOX*
                    ((V_slow_perfused - V_slow_perfused_b_DOX)
                    / V_slow_perfused)
                    / V_vb
rate_coeff[1,17] = Q_rapid_perfused*BP*F_up_DOX*
                    (V_rapid_perfused_b_DOX/V_rapid_perfused)
                    / V_vb
rate_coeff[1,19] = Q_rapid_perfused*BP*F_up_DOX*
                    ((V_rapid_perfused - V_rapid_perfused_b_DOX)
                    / V_rapid_perfused)
                    / V_vb
rate_coeff[1,25] = Q_VH/ V_vb
rate_coeff[1,33] = Q_ki/V_vb
rate_coeff[1,23] = Q_heart/V_vb
rate_coeff[2,2] = - Q_CO/V_vb
rate_coeff[2,14] = Q_slow_perfused*BP*F_up_DOXol*

```

```

(V_slow_perfused_b_DOXol/V_slow_perfused)
/ V_vb
rate_coeff[2,16] = Q_slow_perfused*BP*F_up_DOXol*
((V_slow_perfused - V_slow_perfused_b_DOXol)
/ V_slow_perfused)
/ V_vb
rate_coeff[2,18] = Q_rapid_perfused*BP*F_up_DOXol*
(V_rapid_perfused_b_DOXol/V_rapid_perfused)
/ V_vb
rate_coeff[2,20] = Q_rapid_perfused*BP*F_up_DOXol*
((V_rapid_perfused - V_rapid_perfused_b_DOXol)
/V_rapid_perfused) / V_vb
rate_coeff[2,26] = Q_VH / V_vb
rate_coeff[2,34] = Q_ki/V_vb
rate_coeff[2,22] = Q_heart / V_vb

# bound lung DOX/DOXol
rate_coeff[3,5] = Cl_on_DOX / V_lu_b_DOX
rate_coeff[3,3] = - Cl_off_DOX / V_lu_b_DOX
rate_coeff[4,6] = Cl_on_DOXol / V_lu_b_DOXol
rate_coeff[4,4] = - Cl_off_DOXol / V_lu_b_DOXol

# unbound lung DOX/DOXol
rate_coeff[5,1] = Q_CO/(V_lu - V_lu_b_DOX)
rate_coeff[5,3] = (Cl_off_DOX - (Q_CO*BP*F_up_DOX*
(V_lu_b_DOX/V_lu)))/(V_lu - V_lu_b_DOX)
rate_coeff[5,5] = - (Cl_on_DOX + (Q_CO*BP*F_up_DOX*
((V_lu - V_lu_b_DOX)/V_lu)))
/ (V_lu - V_lu_b_DOX)

```

```

rate_coeff[6,2] = Q_CO/(V_lu - V_lu_b_DOXol)
rate_coeff[6,4] = (Cl_off_DOXol - (Q_CO*BP*F_up_DOXol*
                    (V_lu_b_DOXol/V_lu)))/(V_lu - V_lu_b_DOXol)
rate_coeff[6,6] = - (Cl_on_DOXol + (Q_CO*BP*F_up_DOXol*
                    ((V_lu - V_lu_b_DOXol)/V_lu)))
                    / (V_lu - V_lu_b_DOXol)
rate_coeff[7,3] = (Q_CO*BP*F_up_DOX*(V_lu_b_DOX/V_lu))/ V_ab
rate_coeff[7,5] = (Q_CO*BP*F_up_DOX*
                    ((V_lu - V_lu_b_DOX)/V_lu))/ V_ab
rate_coeff[7,7] = - Q_CO / V_ab
rate_coeff[8,4] = (Q_CO*BP*F_up_DOXol*(V_lu_b_DOXol/V_lu))/ V_ab
rate_coeff[8,6] = (Q_CO*BP*F_up_DOXol*((V_lu - V_lu_b_DOXol)/V_lu))
                    / V_ab
rate_coeff[8,8] = - Q_CO / V_ab

```

```

## non-metabolising tissue

```

```

# bound GI spleen DOX/DOXol

```

```

rate_coeff[9,11] = Cl_on_DOX / V_GI_spleen_b_DOX
rate_coeff[9,9] = - Cl_off_DOX / V_GI_spleen_b_DOX
rate_coeff[10,12] = Cl_on_DOXol / V_GI_spleen_b_DOXol
rate_coeff[10,10] = - Cl_off_DOXol / V_GI_spleen_b_DOXol

```

```

# unbound GI spleen DOX/DOXol

```

```

rate_coeff[11,7] = Q_GI_spleen/(V_GI_spleen - V_GI_spleen_b_DOX)
rate_coeff[11,9] = (Cl_off_DOX - (Q_GI_spleen*BP*F_up_DOX*
                    (V_GI_spleen_b_DOX/V_GI_spleen))) /
                    (V_GI_spleen - V_GI_spleen_b_DOX)
rate_coeff[11,11] = - (Q_GI_spleen*BP*F_up_DOX * ((V_GI_spleen -

```

```

        V_GI_spleen_b_DOX) / V_GI_spleen) + Cl_on_DOX) /
        (V_GI_spleen - V_GI_spleen_b_DOX)
rate_coeff[12,8] = Q_GI_spleen / (V_GI_spleen - V_GI_spleen_b_DOXol)
rate_coeff[12,10] = (Cl_off_DOXol - (Q_GI_spleen*BP*F_up_DOXol*
        (V_GI_spleen_b_DOXol/V_GI_spleen))) /
        (V_GI_spleen - V_GI_spleen_b_DOXol)
rate_coeff[12,12] = - (Q_GI_spleen*BP*F_up_DOXol*
        ((V_GI_spleen - V_GI_spleen_b_DOXol)
        / V_GI_spleen) + Cl_on_DOXol) /
        (V_GI_spleen - V_GI_spleen_b_DOXol)

# bound slow perfused DOX/DOXol
rate_coeff[13,15] = Cl_on_DOX / V_slow_perfused_b_DOX
rate_coeff[13,13] = - Cl_off_DOX / V_slow_perfused_b_DOX
rate_coeff[14,16] = Cl_on_DOXol / V_slow_perfused_b_DOXol
rate_coeff[14,14] = - Cl_off_DOXol / V_slow_perfused_b_DOXol

# unbound slow perfused DOX/DOXol
rate_coeff[15,7] = Q_slow_perfused / (V_slow_perfused -
        V_slow_perfused_b_DOX)
rate_coeff[15,13] = (Cl_off_DOX - (Q_slow_perfused*BP*F_up_DOX*
        (V_slow_perfused_b_DOX/V_slow_perfused))) /
        (V_slow_perfused - V_slow_perfused_b_DOX)
rate_coeff[15,15] = - (Q_slow_perfused*BP*F_up_DOX*((V_slow_perfused -
        V_slow_perfused_b_DOX) / V_slow_perfused)
        + Cl_on_DOX) / (V_slow_perfused -
        V_slow_perfused_b_DOX)
rate_coeff[16,8] = Q_slow_perfused / (V_slow_perfused -
        V_slow_perfused_b_DOXol)

```

```

rate_coeff[16,14] = (Cl_off_DOXol - (Q_slow_perfused*BP*F_up_DOXol*
                                (V_slow_perfused_b_DOXol/V_slow_perfused))) /
                                (V_slow_perfused - V_slow_perfused_b_DOXol)
rate_coeff[16,16] = - (Q_slow_perfused*BP*F_up_DOXol*((V_slow_perfused -
                                V_slow_perfused_b_DOXol) / V_slow_perfused) +
                                Cl_on_DOXol) / (V_slow_perfused -
                                V_slow_perfused_b_DOXol)

```

```
# bound rapid perfused DOX/DOXol
```

```

rate_coeff[17,19] = Cl_on_DOX / V_rapid_perfused_b_DOX
rate_coeff[17,17] = - Cl_off_DOX / V_rapid_perfused_b_DOX
rate_coeff[18,20] = Cl_on_DOXol / V_rapid_perfused_b_DOXol
rate_coeff[18,18] = - Cl_off_DOXol / V_rapid_perfused_b_DOXol

```

```
# unbound rapid perfused DOX/DOXol
```

```

rate_coeff[19,7] = Q_rapid_perfused/(V_rapid_perfused -
                                V_rapid_perfused_b_DOX)
rate_coeff[19,17] = (Cl_off_DOX - (Q_rapid_perfused*BP*F_up_DOX*
                                (V_rapid_perfused_b_DOX/V_rapid_perfused))) /
                                (V_rapid_perfused - V_rapid_perfused_b_DOX)
rate_coeff[19,19] = - (Q_rapid_perfused*BP*F_up_DOX*((V_rapid_perfused -
                                V_rapid_perfused_b_DOX)/V_rapid_perfused)
                                + Cl_on_DOX)/(V_rapid_perfused
                                - V_rapid_perfused_b_DOX)
rate_coeff[20,8] = Q_rapid_perfused/(V_rapid_perfused
                                - V_rapid_perfused_b_DOXol)
rate_coeff[20,18] = (Cl_off_DOXol - (Q_rapid_perfused*BP*F_up_DOXol *
                                (V_rapid_perfused_b_DOXol/V_rapid_perfused))) /
                                (V_rapid_perfused - V_rapid_perfused_b_DOXol)

```

```

rate_coeff[20,20] = - (Q_rapid_perfused*BP*F_up_DOXol*((V_rapid_perfused -
                    V_rapid_perfused_b_DOXol)/V_rapid_perfused) +
                    Cl_on_DOXol) / (V_rapid_perfused -
                    V_rapid_perfused_b_DOXol)

## heart ##

# vascular heart DOX/DOXol
rate_coeff[21,7] = Q_heart/V_va_heart
rate_coeff[21,23] = (P_diff_DOX*F_up_DOX)/V_va_heart
rate_coeff[22,8] = Q_heart/V_va_heart
rate_coeff[22,22] = -(Q_heart + P_diff_DOX*F_up_DOXol) / V_va_heart
rate_coeff[22,24] = P_diff_DOXol*F_up_DOXol/V_va_heart

# extracellular heart DOX/DOXol
rate_coeff[23,21] = (P_diff_DOX*F_up_DOX)/V_extra_heart
rate_coeff[23,23] = - (P_diff_DOX*F_up_DOX + Cl_mem_DOX*F_up_DOX)
                    / V_extra_heart
rate_coeff[23,43] = (Cl_mem_DOX*F_up_DOX) / V_extra_heart
rate_coeff[24,22] = (P_diff_DOXol*F_up_DOXol)/V_extra_heart
rate_coeff[24,24] = -(P_diff_DOXol*F_up_DOXol + Cl_mem_DOXol*F_up_DOXol)
                    / V_extra_heart
rate_coeff[24,44] = (Cl_mem_DOXol*F_up_DOXol) / V_extra_heart

# cellular heart bound DOX/DOXol
rate_coeff[41,43] = Cl_on_DOX / V_cel_b_heart
rate_coeff[41,41] = - Cl_off_DOX / V_cel_b_heart
rate_coeff[42,44] = Cl_on_DOXol / V_cel_b_heart
rate_coeff[42,42] = - Cl_off_DOXol / V_cel_b_heart

# cellular heart unbound DOX/DOXol
rate_coeff[43,23] = Cl_mem_DOX*F_up_DOX/ (V_cel_heart - V_cel_b_heart)
rate_coeff[43,41] = Cl_off_DOX / (V_cel_heart - V_cel_b_heart)

```



```

rate_coeff[43,43] = -(Cl_mem_DOX*F_up_DOX+Cl_on_DOX +
                    ((V_max_heart/K_m_heart)*
                     SF_heart*F_up_DOX)) / (V_cel_heart-V_cel_b_heart)
rate_coeff[44,43] = ((V_max_heart / K_m_heart) * SF_heart * F_up_DOX) /
                    (V_cel_heart - V_cel_b_heart)
rate_coeff[44,24] = (Cl_mem_DOXol*F_up_DOXol)/(V_cel_heart
                                                - V_cel_b_heart)
rate_coeff[44,42] = Cl_off_DOXol / (V_cel_heart - V_cel_b_heart)
rate_coeff[44,44] = - (Cl_mem_DOXol*F_up_DOXol + Cl_on_DOXol) /
                    (V_cel_heart - V_cel_b_heart)

## liver ##
# vascular liver
# DOX
rate_coeff[25,9] = (Q_VP*BP*F_up_DOX*(V_GI_spleen_b_DOX /
                    V_GI_spleen)) / V_va_liver
rate_coeff[25,11] = (Q_VP*BP*F_up_DOX*((V_GI_spleen -
                    V_GI_spleen_b_DOX) / V_GI_spleen)) / V_va_liver
rate_coeff[25,7] = Q_HA/V_va_liver
rate_coeff[25,25] = -(Q_VH + P_diff_DOX*(F_up_DOX/CbCp_DOX))
                    / V_va_liver
rate_coeff[25,27] = P_diff_DOX*F_up_DOX/V_va_liver
# DOXol
rate_coeff[26,10] = (Q_VP*BP*F_up_DOXol * (V_GI_spleen_b_DOXol
                    / V_GI_spleen)) / V_va_liver
rate_coeff[26,12] = (Q_VP*BP*F_up_DOXol*((V_GI_spleen -
                    V_GI_spleen_b_DOXol) / V_GI_spleen))/V_va_liver
rate_coeff[26,8] = Q_HA/V_va_liver
rate_coeff[26,26] = -(Q_VH + P_diff_DOX*(F_up_DOXol/CbCp_DOXol))

```

```

                                / V_va_liver
rate_coeff[26,28] = P_diff_DOXol*F_up_DOXol/V_va_liver
# extracellular liver
# DOX
rate_coeff[27,25] = (P_diff_DOX*(F_up_DOX/CbCp_DOX))
                                / V_extra_liver
rate_coeff[27,27] = - (P_diff_DOX*F_up_DOX + Cl_mem_DOX*F_up_DOX)
                                / V_extra_liver
rate_coeff[27,31] = Cl_mem_DOX*F_up_DOX / V_extra_liver
# DOXol
rate_coeff[28,26] = (P_diff_DOXol*(F_up_DOXol/CbCp_DOXol))
                                / V_extra_liver
rate_coeff[28,28] = - (P_diff_DOXol*F_up_DOXol +
                                Cl_mem_DOXol*F_up_DOXol) / V_extra_liver
rate_coeff[28,32] = Cl_mem_DOXol*F_up_DOXol / V_extra_liver

# cellular liver, bound
# DOX
rate_coeff[29,31] = Cl_on_DOX / V_cel_b_liver
rate_coeff[29,29] = - Cl_off_DOX / V_cel_b_liver
# DOXol
rate_coeff[30,32] = Cl_on_DOXol / V_cel_b_liver
rate_coeff[30,30] = - Cl_off_DOXol / V_cel_b_liver

# cellular liver, unbound
# DOX
rate_coeff[31,27] = Cl_mem_DOX*F_up_DOX/ (V_cel_liver - V_cel_b_liver)
rate_coeff[31,29] = Cl_off_DOX / (V_cel_liver - V_cel_b_liver)
rate_coeff[31,31] = - (Cl_mem_DOX*F_up_DOX_liver +

```

```

Cl_excr_li_DOX*F_up_DOX_liver +
Cl_on_DOX + ((V_max_liver / K_m_liver) *
SF_liver * F_up_DOX)) / (V_cel_liver - V_cel_b_liver)

# DOXol
rate_coeff[32,28] = Cl_mem_DOXol*F_up_DOXol
                    / (V_cel_liver - V_cel_b_liver)
rate_coeff[32,30] = Cl_off_DOXol / (V_cel_liver - V_cel_b_liver)
rate_coeff[32,31] = ((V_max_liver / K_m_liver)*SF_liver*F_up_DOX) /
                    (V_cel_liver - V_cel_b_liver)
rate_coeff[32,32] = - (Cl_mem_DOXol*F_up_DOXol_liver + Cl_excr_li_DOXol*
                    F_up_DOXol_liver + Cl_on_DOXol)
                    / (V_cel_liver - V_cel_b_liver)

## kidney
# vascular kidney
rate_coeff[33,7] = Q_ki/V_va_kidney
rate_coeff[33,33] = - (Q_ki + P_diff_DOX * F_up_DOX +
                    (GFR * body_weight * F_up_DOX))
                    / V_va_kidney
rate_coeff[33,35] = P_diff_DOX*F_up_DOX/V_va_kidney
rate_coeff[34,8] = Q_ki/V_va_kidney
rate_coeff[34,34] = - (Q_ki + P_diff_DOXol * F_up_DOXol +
                    (GFR * body_weight * F_up_DOXol)) / V_va_kidney
rate_coeff[34,36] = P_diff_DOXol*F_up_DOXol/V_va_kidney

# extracellular kidney
rate_coeff[35,33] = (P_diff_DOX*F_up_DOX)/V_extra_kidney
rate_coeff[35,35] = - (P_diff_DOX * F_up_DOX + Cl_mem_DOX * F_up_DOX)
                    / V_extra_kidney DOX
rate_coeff[35,39] = Cl_mem_DOX * F_up_DOX_kidney / V_extra_kidney

```



```
# concentration matrix
conc = matrix(0, nrow = matrix_size, ncol = 1)

# venous blood DOX/DOXol
conc[1,1] = C_vb_DOX_temp
conc[2,1] = C_vb_DOXol_temp

# bound lung DOX/DOXol
conc[3,1] = C_lu_b_DOX_temp
conc[4,1] = C_lu_b_DOXol_temp

# unbound lung DOX/DOXol
conc[5,1] = C_lu_u_DOX_temp
conc[6,1] = C_lu_u_DOXol_temp

# arterial blood DOX/DOXol
conc[7,1] = C_ab_DOX_temp
conc[8,1] = C_ab_DOXol_temp

# bound GI/spleen DOX/DOXol
conc[9,1] = C_GI_spleen_b_DOX_temp
conc[10,1] = C_GI_spleen_b_DOXol_temp

# unbound GI/spleen DOX/DOXol
conc[11,1] = C_GI_spleen_u_DOX_temp
conc[12,1] = C_GI_spleen_u_DOXol_temp

# bound slow perfused DOX/DOXol
conc[13,1] = C_slow_perfused_b_DOX_temp
conc[14,1] = C_slow_perfused_b_DOXol_temp
```

```
# unbound slow perfused DOX/DOXol
conc[15,1] = C_slow_perfused_u_DOX_temp
conc[16,1] = C_slow_perfused_u_DOXol_temp

# bound rapid perfused DOX/DOXol
conc[17,1] = C_rapid_perfused_b_DOX_temp
conc[18,1] = C_rapid_perfused_b_DOXol_temp

# unbound rapid perfused DOX/DOXol
conc[19,1] = C_rapid_perfused_u_DOX_temp
conc[20,1] = C_rapid_perfused_u_DOXol_temp

# vascular heart DOX/DOXol
conc[21,1] = C_va_heart_DOX_temp
conc[22,1] = C_va_heart_DOXol_temp

# extracellular heart DOX/DOXol
conc[23,1] = C_extra_heart_DOX_temp
conc[24,1] = C_extra_heart_DOXol_temp

# cellular heart DOX/DOXol bound
conc[41,1] = C_cel_heart_b_DOX_temp
conc[42,1] = C_cel_heart_b_DOXol_temp

# cellular heart DOX/DOXol unbound
conc[43,1] = C_cel_heart_u_DOX_temp
conc[44,1] = C_cel_heart_u_DOXol_temp
```

```
# vascular heart DOX/DOXol
conc[25,1] = C_va_liver_DOX_temp
conc[26,1] = C_va_liver_DOXol_temp

# extracellular liver DOX/DOXol
conc[27,1] = C_extra_liver_DOX_temp
conc[28,1] = C_extra_liver_DOXol_temp

# cellular liver DOX/DOXol bound
conc[29,1] = C_cel_liver_b_DOX_temp
conc[30,1] = C_cel_liver_b_DOXol_temp

# cellular liver DOX/DOXol unbound
conc[31,1] = C_cel_liver_u_DOX_temp
conc[32,1] = C_cel_liver_u_DOXol_temp

# vascular kidney DOX/DOXol
conc[33,1] = C_va_kidney_DOX_temp
conc[34,1] = C_va_kidney_DOXol_temp

# extra kidney DOX/DOXol
conc[35,1] = C_extra_kidney_DOX_temp
conc[36,1] = C_extra_kidney_DOXol_temp

# cellular kidney DOX/DOXol bound
conc[37,1] = C_cel_kidney_b_DOX_temp
conc[38,1] = C_cel_kidney_b_DOXol_temp

# cellular kidney DOX/DOXol unbound
```

```
conc[39,1] = C_cel_kidney_u_DOX_temp
```

```
conc[40,1] = C_cel_kidney_u_DOXol_temp
```



**APPENDIX E**  
**MATRIX ODE SOLVER CODE**

## APPENDIX E: MATRIX ODE SOLVER CODE

```

# initialize matrices
x_matrix_save <- vector()
u_matrix <- matrix(0, nrow = matrix_size, ncol = 1)
g_vector <- matrix(0, nrow = matrix_size, ncol = 1)
fund_matrix <- matrix(0, nrow = matrix_size, ncol = matrix_size)

for (t_index in seq(from = 1, to = t_index_max, by = 1)) {

  # eigenvalue/eigenvector solution

  # eigenvalues and eigenvectors of coefficient matrix
  eigen_matrix <- eigen(rate_coeff)

  # print eigenvalues and eigenvectors
  eigen_matrix$values
  eigen_matrix$vectors

  # separate real and imaginary parts of eigenvectors
  a_real_eigenvec <- Re(eigen_matrix$vectors)
  b_imag_eigenvec <- Im(eigen_matrix$vectors)

  # print real and complex eigenvectors
  a_real_eigenvec

```

```

b_imag_eigenvec

# separate real and imaginary parts of eigenvalues
lambda <- Re(eigen_matrix$values)
mu <- Im(eigen_matrix$values)

# print real and complex eigenvalues
lambda
mu

## solver function starts here
g_vector[1,1] <- injection_rate[t_index]

t= 0
## calculate fundamental matrix and inverse of
## fundamental matrix for 0, h, 2*h
while (t <= h*2) {
  i <- 1
  while (i <= matrix_size){
    j <- 1
    while (j <= matrix_size) {
      if (mu[j] == 0) {
        fund_matrix[i,j] <- exp(lambda[j]*t)*(a_real_eigenvec[i,j]
          * cos(mu[j]*t))
        j <- j + 1
      }
      else {
        fund_matrix[i,j] <- exp(lambda[j]*t) * (a_real_eigenvec[i,j]
          * cos(mu[j]*t) - b_imag_eigenvec[i,j] * sin(mu[j]*t))
      }
    }
    i <- i + 1
  }
  t <- t + h
}

```

```

        j <- j + 1
        fund_matrix[i,j] <- exp(lambda[j]*t) * (a_real_eigenvec[i,j]
            * sin(mu[j]*t) + b_imag_eigenvec[i,j] * cos(mu[j]*t))
        j <- j + 1
    }
}
i = i + 1
}

inv_fund_matrix = solve(fund_matrix, tol = tol_value)
if (t == 0) {
    int_constants = inv_fund_matrix %*% conc
    u_prime_matrix0 = inv_fund_matrix %*% g_vector
} else if (t == h) {
    u_prime_matrix1 = inv_fund_matrix %*% g_vector
} else if (t == 2* h) {
    u_prime_matrix2 = inv_fund_matrix %*% g_vector
}

t = t + h

}

## Simpson's 1/3 Rule for 0 to 2*h
sim_soln <- (h/3) * (u_prime_matrix0 +
                    (4 * u_prime_matrix1) + u_prime_matrix2)
sim_soln <- matrix(sim_soln)

## u_matrix should be term by term u_prime_matrix

```

```
## integrated w.r.t. t and bounds 0 to time point
x_matrix = fund_matrix %*% int_constants + fund_matrix %*% sim_soln
x_matrix_save <- cbind(x_matrix_save, x_matrix)

## x_matrix solution becomes initial condition for next tau
conc = x_matrix
}
return(x_matrix_save)
```

**APPENDIX F**  
**MODEL FITS BY SPECIES**

## APPENDIX F: MODEL FITS BY SPECIES

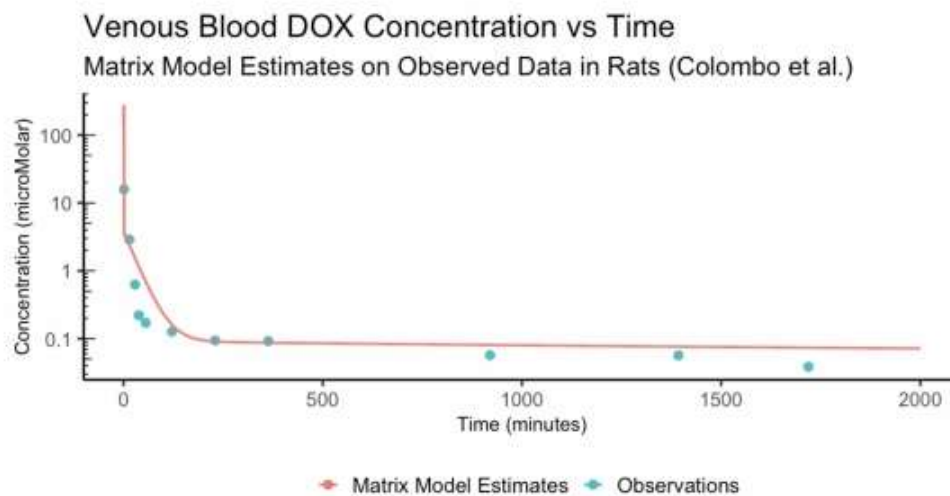


Figure F.1: Plot of venous blood concentration versus time of DOX in rats - 5 mg/kg IV bolus in  $\approx 225$  g rats (Source [187])

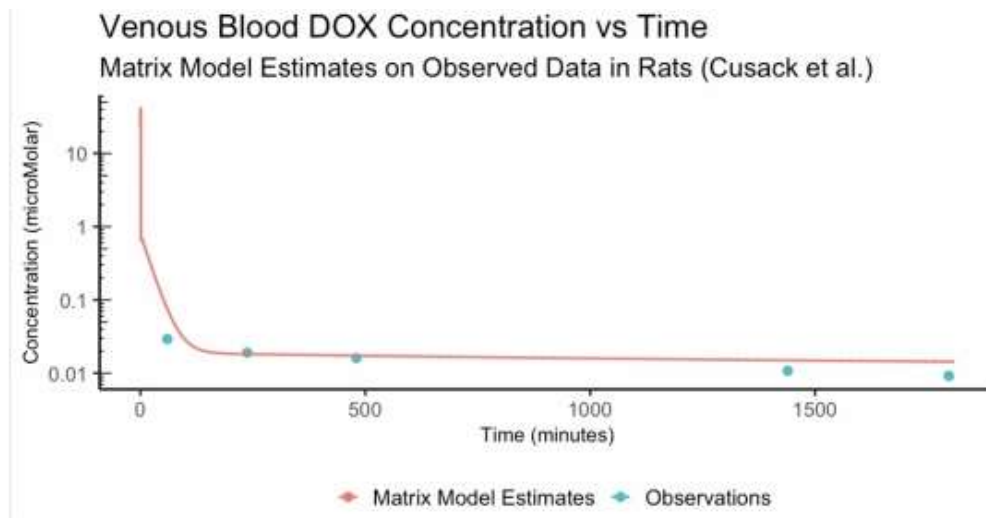


Figure F.2: Plot of venous blood concentration versus time of DOX in rats - 2 mg/kg IV bolus in  $\approx 350$  g rats (Source [127])

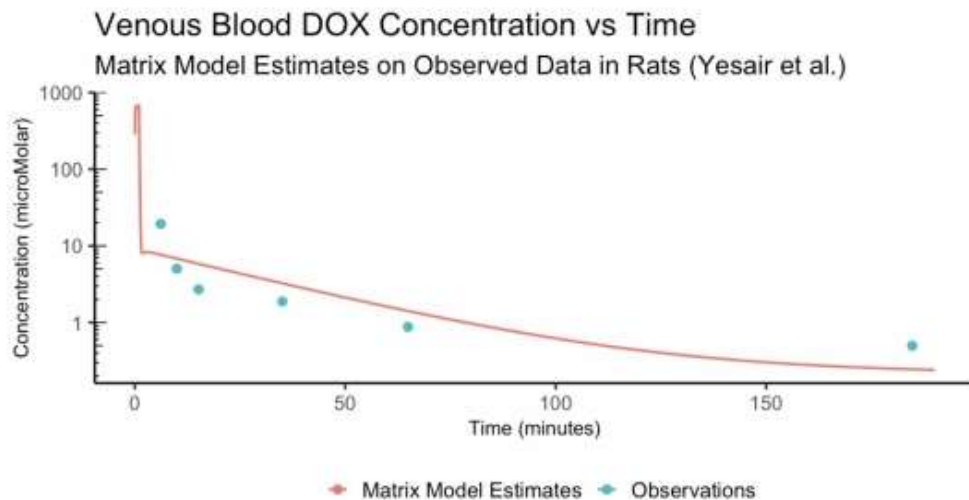


Figure F.3: Plot of venous blood concentration versus time of DOX in rats - 10 mg/kg IV bolus in  $\approx 300$  g rats (Source [188])



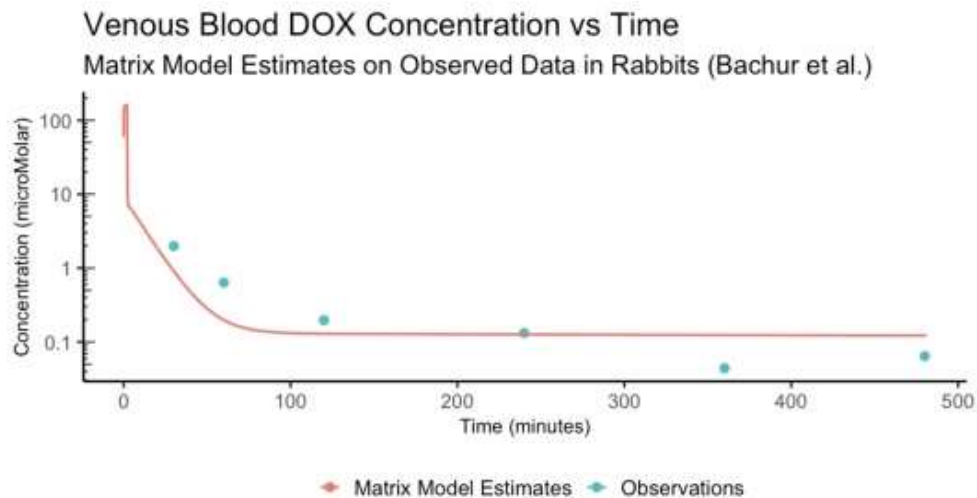


Figure F.4: Plot of venous blood concentration versus time of DOX in rabbits - 5 mg/kg IV bolus in a 4.2 kg rabbit (Source [190])

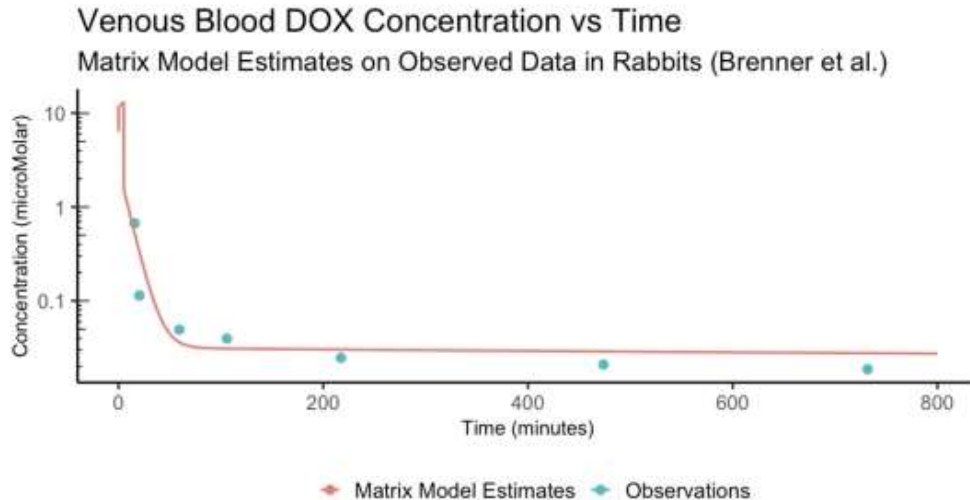


Figure F.5: Plot of venous blood concentration versus time of DOX in rabbits - 3 mg/kg IV over 5 minutes in a 3 kg rabbit (Source [129])

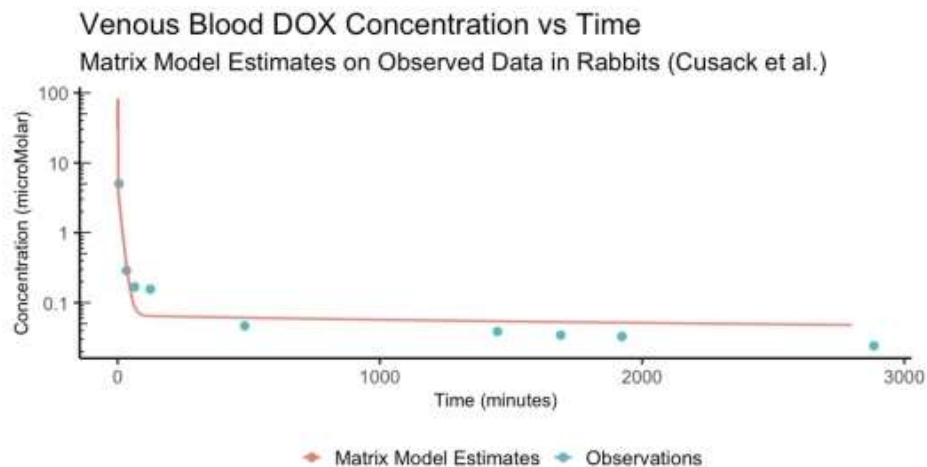


Figure F.6: Plot of venous blood concentration versus time of DOX in rabbits - 5 mg/kg IV bolus in a 4.2 kg rabbit (Source [191])

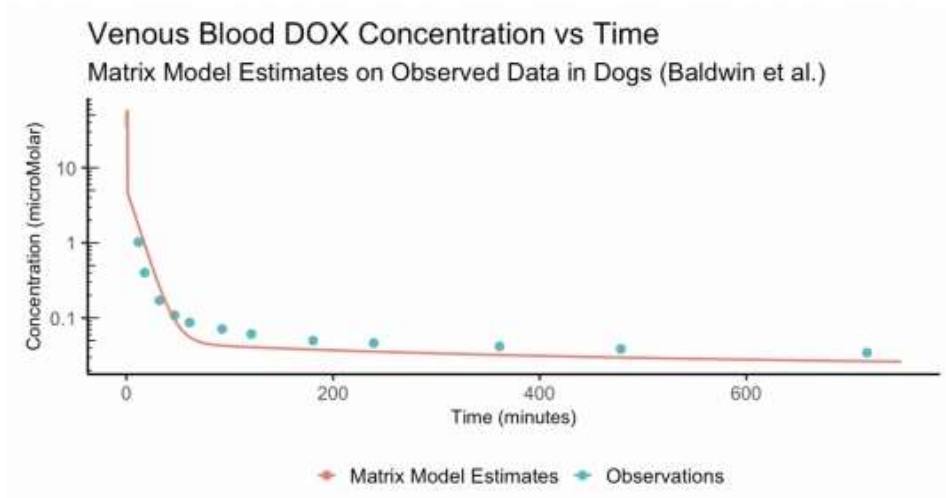


Figure F.7: Plot of venous blood concentration versus time of DOX in dogs - 1.5 mg/kg IV bolus in  $\approx 13$  kg dogs (Source [193])

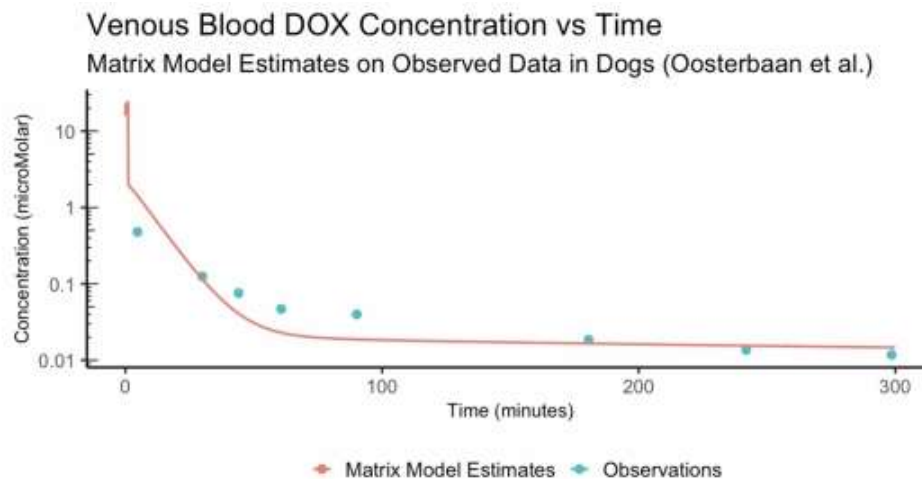


Figure F.8: Plot of venous blood concentration versus time of DOX in dogs - 1.5 mg/kg IV bolus in a 10.2 kg dog (Source [192])

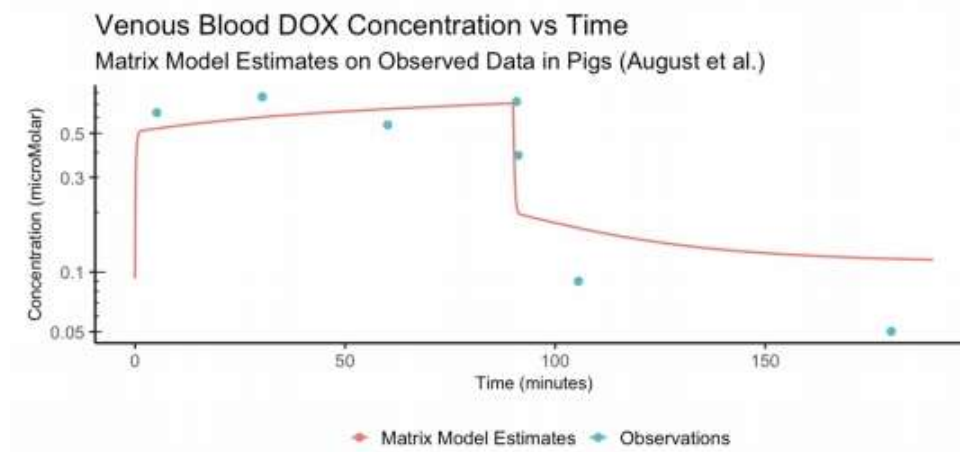


Figure F.9: Plot of venous blood concentration versus time of DOX in pigs - 1 mg/kg IV over 90 minutes in  $\approx 20$  kg pigs (Source [194])

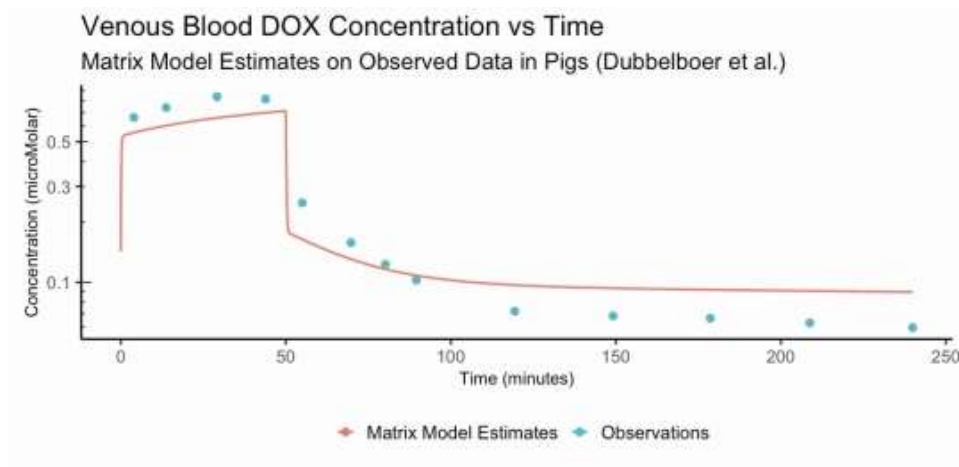


Figure F.10: Plot of venous blood concentration versus time of DOX in pigs - 85.7  $\mu\text{M}$  IV over 50 minutes in  $\approx 26.7$  kg pigs (Source [8])

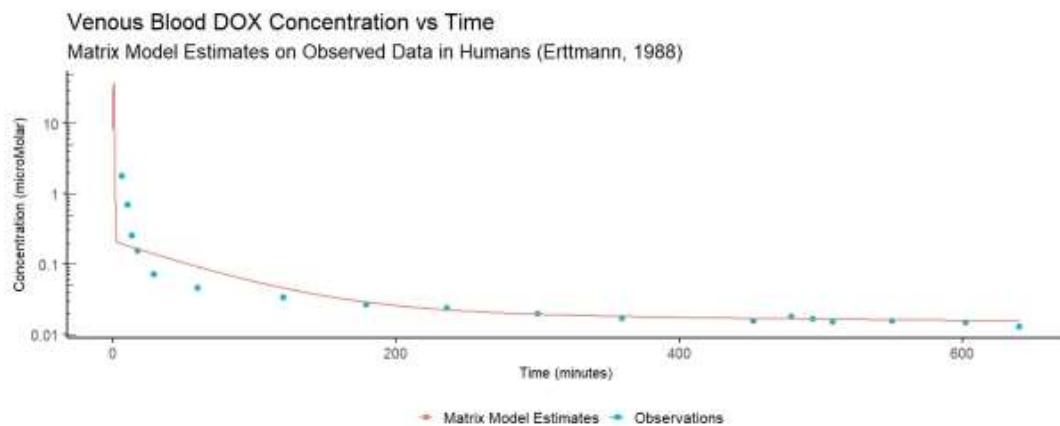


Figure F.11: Plot of venous blood concentration versus time of DOX in humans - 15  $\text{mg}/\text{m}^2$  IV bolus in a  $\approx 70$  kg human (Source [120])

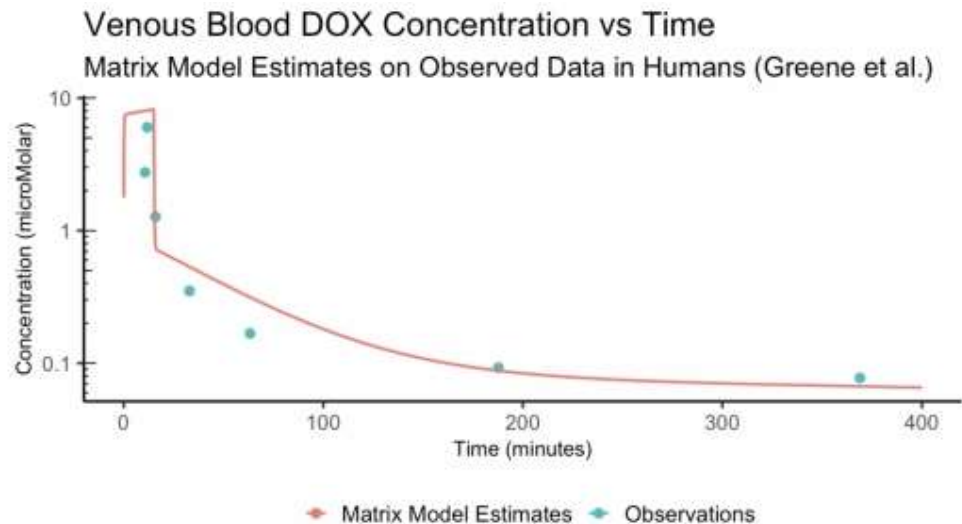


Figure F.12: Plot of venous blood concentration versus time of DOX in humans -  $75 \text{ mg/m}^2$  IV over 15 minutes in a  $\approx 70 \text{ kg}$  human (Source [80])

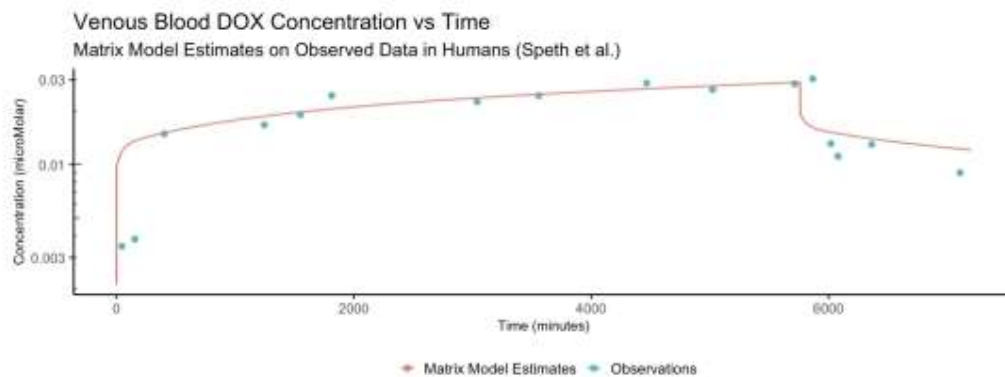


Figure F.13: Plot of venous blood concentration versus time of DOX in humans -  $30 \text{ mg/m}^2$  IV bolus in a  $\approx 70 \text{ kg}$  human (Source [34])

**APPENDIX G**  
**CODE SETUP FOR PBPK PARAMETERS**

## APPENDIX G: CODE SETUP FOR PBPK PARAMETERS

### G.1 Mouse Physiological Parameters

```
# compartment volumes #MOUSE  
V_ab <- 0.5*0.049*body_weight  
V_vb <- 0.5*0.049*body_weight  
V_lu <- 0.007*body_weight  
V_lu_b_DOX <- 0.007*body_weight*bind_site  
V_lu_b_DOXol <- 0.007*body_weight*bind_site  
V_GI_spleen <- 0.099*body_weight  
V_GI_spleen_b_DOX <- 0.099*body_weight*bind_site  
V_GI_spleen_b_DOXol <- 0.099*body_weight*bind_site  
V_slow_perfused <- 0.706*body_weight  
V_slow_perfused_b_DOX <- 0.706*body_weight*bind_site  
V_slow_perfused_b_DOXol <- 0.706*body_weight*bind_site  
V_rapid_perfused <- 0.042*body_weight  
V_rapid_perfused_b_DOX <- 0.042*body_weight*bind_site  
V_rapid_perfused_b_DOXol <- 0.042*body_weight*bind_site  
V_liver <- 0.055*body_weight  
V_va_liver <- 0.055*0.055*body_weight  
V_extra_liver <- 0.055*0.159*body_weight  
V_cel_liver <- 0.055*0.786*body_weight
```

```
V_cel_b_liver <- 0.055*0.786*body_weight*bind_site
V_kidney <- 0.017*body_weight
V_va_kidney <- 0.017*0.05*body_weight
V_extra_kidney <- 0.017*0.159*body_weight
V_cel_kidney <- 0.017*0.791*body_weight
V_cel_b_kidney <- 0.017*0.791*body_weight*bind_site
V_heart <- 0.025*body_weight
V_va_heart <-0.025*0.055*body_weight
V_extra_heart <-0.025*0.159*body_weight
V_cel_heart <- 0.025*0.786*body_weight
V_cel_b_heart <- 0.025*0.786*body_weight*bind_site

# volume fractions
x_liver = 0.16
x_portal_vein = 0.14
x_hepatic_artery = 0.02
x_GI_spleen = 0.14
x_kidney = 0.091
x_rapid_perfused = 0.033
x_slow_perfused = 0.127
x_heart = 0.156

# flow rates
Q_CO = CO * body_weight / 1000
## blood flow of cardiac output (L/min)
## divided by 1000 to get from mL/min to L/min
Q_lung = Q_CO
Q_heart = x_heart * Q_CO
Q_slow_perfused = x_slow_perfused * Q_CO
```



```

Q_rapid_perfused = x_rapid_perfused * Q_CO
Q_GI_spleen = x_GI_spleen * Q_CO
Q_ki = x_kidney * Q_CO
Q_HA = x_hepatic_artery * Q_CO
Q_VP = x_portal_vein * Q_CO
Q_liver = x_liver * Q_CO
Q_VH = Q_VP + Q_HA

```

## G.2 Rat Physiological Parameters

```

# compartment volumes #RAT
V_ab <- 0.5*0.075*body_weight
V_vb <- 0.5*0.075*body_weight
V_lu <- 0.006*body_weight
V_lu_b_DOX <- 0.006*body_weight*bind_site
V_lu_b_DOXol <- 0.006*body_weight*bind_site
V_GI_spleen <- 0.071*body_weight
V_GI_spleen_b_DOX <- 0.071*body_weight*bind_site
V_GI_spleen_b_DOXol <- 0.071*body_weight*bind_site
V_slow_perfused <- 0.718*body_weight
V_slow_perfused_b_DOX <- 0.718*body_weight*bind_site
V_slow_perfused_b_DOXol <- 0.718*body_weight*bind_site
V_rapid_perfused <- 0.064*body_weight
V_rapid_perfused_b_DOX <- 0.064*body_weight*bind_site
V_rapid_perfused_b_DOXol <- 0.064*body_weight*bind_site
V_liver <- 0.035*body_weight
V_va_liver <- 0.035*0.055*body_weight
V_extra_liver <- 0.035*0.159*body_weight
V_cel_liver <- 0.035*0.786*body_weight

```

```
V_cel_b_liver <- 0.035*0.786*body_weight*bind_site
V_kidney <- 0.008*body_weight
V_va_kidney <- 0.008*0.05*body_weight
V_extra_kidney <- 0.008*0.159*body_weight
V_cel_kidney <- 0.008*0.791*body_weight
V_cel_b_kidney <- 0.008*0.791*body_weight*bind_site
V_heart <- 0.025*body_weight
V_va_heart <- 0.025*0.055*body_weight
V_extra_heart <- 0.025*0.159*body_weight
V_cel_heart <- 0.025*0.786*body_weight
V_cel_b_heart <- 0.025*0.786*body_weight*bind_site

# volume fractions
x_liver = 0.183
x_portal_vein = 0.153
x_hepatic_artery = 0.021
x_GI_spleen = 0.153
x_kidney = 0.141
x_rapid_perfused = 0.023
x_slow_perfused = 0.438
x_heart = 0.139

# flow rates
Q_CO = CO * body_weight / 1000
## blood flow of cardiac output (L/min)
## divided by 1000 to get from mL/min to L/min
Q_lung = Q_CO
Q_heart = x_heart * Q_CO
Q_slow_perfused = x_slow_perfused * Q_CO
```

```

Q_rapid_perfused = x_rapid_perfused * Q_CO
Q_GI_spleen = x_GI_spleen * Q_CO
Q_ki = x_kidney * Q_CO
Q_HA = x_hepatic_artery * Q_CO
Q_VP = x_portal_vein * Q_CO
Q_liver = x_liver * Q_CO
Q_VH = Q_VP + Q_HA

```

```
\section{Rabbit Physiological Parameters}
```

```

# compartment volumes #RABBIT
V_ab <- 0.5*0.082*body_weight
V_vb <- 0.5*0.082*body_weight
V_lu <- 0.0085*body_weight
V_lu_b_DOX <- 0.0085*body_weight*bind_site
V_lu_b_DOXol <- 0.0085*body_weight*bind_site
V_GI_spleen <- 0.0604*body_weight
V_GI_spleen_b_DOX <- 0.0604*body_weight*bind_site
V_GI_spleen_b_DOXol <- 0.0604*body_weight*bind_site
V_slow_perfused <- (0.674-offsetV)*body_weight
V_slow_perfused_b_DOX <- (0.674-offsetV)*body_weight*bind_site
V_slow_perfused_b_DOXol <- (0.674-offsetV)*body_weight*bind_site
V_rapid_perfused <- 0.06*body_weight
V_rapid_perfused_b_DOX <- 0.06*body_weight*bind_site
V_rapid_perfused_b_DOXol <- 0.06*body_weight*bind_site
V_liver <- 0.0499*body_weight
V_va_liver <- 0.0499*0.055*body_weight
V_extra_liver <- 0.0499*0.159*body_weight
V_cel_liver <- 0.0499*0.786*body_weight
V_cel_b_liver <- 0.0499*0.786*body_weight*bind_site

```

```
V_kidney <- 0.0075*body_weight
V_va_kidney <- 0.0075*0.05*body_weight
V_extra_kidney <- 0.0075*0.159*body_weight
V_cel_kidney <- 0.0075*0.791*body_weight
V_cel_b_kidney <- 0.0075*0.791*body_weight*bind_site
V_va_heart <- 0.003*0.055*body_weight
V_extra_heart <- 0.003*0.159*body_weight
V_cel_heart <- 0.003*0.786*body_weight
V_cel_b_heart <- 0.003*0.786*body_weight*bind_site

# volume fractions
x_liver = 0.334
x_portal_vein = 0.264
x_hepatic_artery = 0.0698
x_GI_spleen = 0.017
x_kidney = 0.151
x_rapid_perfused = 0.0604
x_slow_perfused = 0.292
x_heart = 0.0302

# flow rates
Q_CO = CO * body_weight / 1000
## blood flow of cardiac output (L/min)
## divided by 1000 to get from mL/min to L/min

Q_lung = Q_CO
Q_heart = x_heart * Q_CO
Q_slow_perfused = x_slow_perfused * Q_CO
```

```

Q_rapid_perfused = x_rapid_perfused * Q_CO
Q_GI_spleen = x_GI_spleen * Q_CO
Q_ki = x_kidney * Q_CO
Q_HA = x_hepatic_artery * Q_CO
Q_VP = x_portal_vein * Q_CO
Q_liver = x_liver * Q_CO
Q_VH = Q_VP + Q_HA

```

### G.3 Dog Physiological Parameters

```

# compartment volumes #DOG
V_ab <- 0.5*0.08*body_weight
V_vb <- 0.5*0.08*body_weight
V_lu <- 0.008*body_weight
V_lu_b_DOX <- 0.008*body_weight*bind_site
V_lu_b_DOXol <- 0.008*body_weight*bind_site
V_GI_spleen <- 0.08*body_weight
V_GI_spleen_b_DOX <- 0.08*body_weight*bind_site
V_GI_spleen_b_DOXol <- 0.08*body_weight*bind_site
V_slow_perfused <- 0.779*body_weight
V_slow_perfused_b_DOX <- 0.779*body_weight*bind_site
V_slow_perfused_b_DOXol <- 0.779*body_weight*bind_site
V_rapid_perfused <- 0.008*body_weight
V_rapid_perfused_b_DOX <- 0.008*body_weight*bind_site
V_rapid_perfused_b_DOXol <- 0.008*body_weight*bind_site
V_liver <- 0.0304*body_weight
V_va_liver <- 0.0304*0.055*body_weight
V_extra_liver <- 0.0304*0.159*body_weight
V_cel_liver <- 0.0304*0.786*body_weight

```

```
V_cel_b_liver <- 0.0304*0.786*body_weight*bind_site
V_kidney <- 0.005*body_weight
V_va_kidney <- 0.005*0.05*body_weight
V_extra_kidney <- 0.005*0.159*body_weight
V_cel_kidney <- 0.005*0.791*body_weight
V_cel_b_kidney <- 0.005*0.791*body_weight*bind_site
V_va_heart <- 0.003*0.055*body_weight
V_extra_heart <- 0.003*0.159*body_weight
V_cel_heart <- 0.003*0.786*body_weight
V_cel_b_heart <- 0.003*0.786*body_weight*bind_site

# volume fractions
x_liver = 0.297
x_portal_vein = 0.046
x_hepatic_artery = 0.251
x_GI_spleen = 0.046
x_kidney = 0.173
x_rapid_perfused = 0.022
x_slow_perfused = 0.227
x_heart = 0.046

# flow rates
Q_CO = CO * body_weight / 1000

## blood flow of cardiac output (L/min)
## divided by 1000 to get from mL/min to L/min

Q_lung = Q_CO
Q_heart = x_heart * Q_CO
Q_slow_perfused = x_slow_perfused * Q_CO
Q_rapid_perfused = x_rapid_perfused * Q_CO
```

```

Q_GI_spleen = x_GI_spleen * Q_CO
Q_ki = x_kidney * Q_CO
Q_HA = x_hepatic_artery * Q_CO
Q_VP = x_portal_vein * Q_CO
Q_liver = x_liver * Q_CO
Q_VH = Q_VP + Q_HA

```

## G.4 Pig Physiological Parameters

```

# compartment volumes #PIG
V_ab <- 0.5*0.0553*body_weight
V_vb <- 0.5*0.0553*body_weight
V_lu <- 0.0109*body_weight
V_lu_b_DOX <- 0.0109*body_weight*bind_site
V_lu_b_DOXol <- 0.0109*body_weight*bind_site
V_GI_spleen <- 0.0851*body_weight
V_GI_spleen_b_DOX <- 0.0851*body_weight*bind_site
V_GI_spleen_b_DOXol <- 0.0851*body_weight*bind_site
V_slow_perfused <- (0.7124-offsetV)*body_weight
V_slow_perfused_b_DOX <- (0.7124-offsetV)*body_weight*bind_site
V_slow_perfused_b_DOXol <- (0.7124-offsetV)*body_weight*bind_site
V_rapid_perfused <- 0.0942*body_weight
V_rapid_perfused_b_DOX <- 0.0942*body_weight*bind_site
V_rapid_perfused_b_DOXol <- 0.0942*body_weight*bind_site
V_liver <- 0.0316*body_weight
V_va_liver <- 0.0316*0.055*body_weight
V_extra_liver <- 0.0316*0.159*body_weight
V_cel_liver <- 0.0316*0.786*body_weight
V_cel_b_liver <- 0.0316*0.786*body_weight*bind_site

```

```
V_kidney <- 0.0055*body_weight
V_va_kidney <- 0.0055*0.05*body_weight
V_extra_kidney <- 0.0055*0.159*body_weight
V_cel_kidney <- 0.0055*0.791*body_weight
V_cel_b_kidney <- 0.0055*0.791*body_weight*bind_site
V_heart <- 0.005*body_weight
V_va_heart <- 0.005*0.055*body_weight
V_extra_heart <- 0.005*0.159*body_weight
V_cel_heart <- 0.005*0.786*body_weight
V_cel_b_heart <- 0.005*0.786*body_weight*bind_site

# volume fractions
x_liver = 0.26
x_portal_vein = 0.21
x_hepatic_artery = 0.05
x_GI_spleen = 0.21
x_kidney = 0.114
x_rapid_perfused = 0.536
x_slow_perfused = 0.09 - 0.04
x_heart = 0.04

# flow rates
Q_CO = CO * body_weight / 1000
## blood flow of cardiac output (L/min)

Q_lung = Q_CO
Q_heart = x_heart * Q_CO
Q_slow_perfused = x_slow_perfused * Q_CO
Q_rapid_perfused = x_rapid_perfused * Q_CO
Q_GI_spleen = x_GI_spleen * Q_CO
```



```

Q_ki = x_kidney * Q_CO
Q_HA = x_hepatic_artery * Q_CO
Q_VP = x_portal_vein * Q_CO
Q_liver = x_liver * Q_CO
Q_VH = Q_VP + Q_HA

```

## G.5 Human Physiological Parameters

```

# compartment volumes #HUMAN
V_ab <- 0.5*0.079*body_weight
V_vb <- 0.5*0.079*body_weight
V_lu <- 0.008*body_weight
V_lu_b_DOX <- 0.008*body_weight*bind_site
V_lu_b_DOXol <- 0.008*body_weight*bind_site
V_GI_spleen <- 0.031*body_weight
V_GI_spleen_b_DOX <- 0.031*body_weight*bind_site
V_GI_spleen_b_DOXol <- 0.031*body_weight*bind_site
V_slow_perfused <- 0.794*body_weight
V_slow_perfused_b_DOX <- 0.794*body_weight*bind_site
V_slow_perfused_b_DOXol <- 0.794*body_weight*bind_site
V_rapid_perfused <- 0.053*body_weight
V_rapid_perfused_b_DOX <- 0.053*body_weight*bind_site
V_rapid_perfused_b_DOXol <- 0.053*body_weight*bind_site
V_liver <- 0.026*body_weight
V_va_liver <- 0.026*0.055*body_weight
V_extra_liver <- 0.026*0.159*body_weight
V_cel_liver <- 0.026*0.786*body_weight
V_cel_b_liver <- 0.026*0.786*body_weight*bind_site
V_kidney <- 0.004*body_weight

```

```
V_va_kidney <- 0.004*0.05*body_weight
V_extra_kidney <- 0.004*0.159*body_weight
V_cel_kidney <- 0.004*0.791*body_weight
V_cel_b_kidney <- 0.004*0.791*body_weight*bind_site
V_heart <- 0.005*body_weight
V_va_heart <- 0.005*0.055*body_weight
V_extra_heart <- 0.005*0.159*body_weight
V_cel_heart <- 0.005*0.786*body_weight
V_cel_b_heart <- 0.005*0.786*body_weight*bind_site

# volume fractions
x_liver = 0.227
x_portal_vein = 0.18
x_hepatic_artery = 0.047
x_GI_spleen = 0.18
x_kidney = 0.175
x_rapid_perfused = 0.13
x_slow_perfused = 0.342
x_heart = 0.04
Q_CO = CO * body_weight / 1000
## blood flow of cardiac output (L/min)
## divided by 1000 to get from mL/min to L/min

Q_lung = Q_CO
Q_heart = x_heart * Q_CO
Q_slow_perfused = x_slow_perfused * Q_CO
Q_rapid_perfused = x_rapid_perfused * Q_CO
Q_GI_spleen = x_GI_spleen * Q_CO
Q_ki = x_kidney * Q_CO
```

$$Q_{HA} = x_{\text{hepatic\_artery}} * Q_{CO}$$

$$Q_{VP} = x_{\text{portal\_vein}} * Q_{CO}$$

$$Q_{liver} = x_{liver} * Q_{CO}$$

$$Q_{VH} = Q_{VP} + Q_{HA}$$

**APPENDIX H**  
**THERAPEUTIC OPTIMIZATION CODE**

## APPENDIX H: THERAPEUTIC OPTIMIZATION CODE

```
tdm_fun <- function(rate) {  
  
  pbpk_me(rate, duration, minute, h)  
  
  vbconcDOX <- x_matrix_save[1,]  
  vbconcDOX <- as.data.frame(vbconcDOX)  
  vbconcDOX <- na.omit(vbconcDOX)  
  
  heartconcDOXol1 <- 0.053*x_matrix_save[24,]  
  heartconcDOXol2 <- 0.159*x_matrix_save[22,]  
  heartconcDOXol3 <- 0.786*bind_site*x_matrix_save[44,]  
  heartconcDOXol4 <- 0.786*(1-bind_site)*x_matrix_save[42,]  
  heartconcDOXol <- vector()  
  for (c in 1:(ncol(x_matrix_save))) {  
    heartconcDOXol[c] = heartconcDOXol1[c] +  
    heartconcDOXol2[c] +  
    heartconcDOXol3[c] +  
    heartconcDOXol4[c]  
  }  
  heartconcDOXol <- as.data.frame(heartconcDOXol)  
  heartconcDOXol <- na.omit(heartconcDOXol)
```

```
C_max_heart <- max(heartconcDOXol)
C_max_heart
AUC <- matrix(0)
for (i in 1:(nrow(vbconcDOX))) {
  AUC[i] <- (vbconcDOX[i,1] + vbconcDOX[i+1,1]) * (h/2)
  i = i + 1
}

AUC <- sum(AUC, na.rm = TRUE)
AUC

if (C_max_heart > 0.0001 ){
  AUC = AUC - 1000000
}
return(AUC)
}

results <- optimize(f = tdm_fun, interval = c(30,500), maximum = TRUE)
```

**APPENDIX I**  
**ADDITIONAL ABBREVIATIONS**

## APPENDIX I: ADDITIONAL ABBREVIATIONS

### List of Acronyms

**mPBPK** minimal physiologically-based pharmacokinetic

$A_1$  amount of drug at administration site

$A_2$  amount of drug in the body

$A$  amount of drug in the body at equilibrium

**ADME** four main processes in pharmacokinetics - absorption, distribution, metabolism, excretion

**AKI** acute kidney injury

**AKR** aldo-keto reductase

**ALL** acute lymphoid leukemia

**AML** acute myeloid leukemia

**AMPK** adenosine monophosphate-activated protein kinase

**ATP** adenosine triphosphate

**AUC** area under the concentration-time curve - a measure of drug exposure

**BBB** blood brain barrier

**BMI** body mass index



**BMR** basal metabolic rate

**BRW** brain weight

**BSA** body surface area

$C_{action}$  drug concentration at the site of action

$C_{max}$  maximum drug concentration

$C_{ss}$  concentration at steady state

$C_{TW}$  concentration in aqueous volume outside the plasma

$C_{u,t}$  unbound drug concentration in tissues

$C_{wb}$  concentration of drug in whole blood

$C_p$  concentration in the central compartment - usually the plasma

$C_u$  concentration of unbound drug

$C$  drug concentration

**CBR** carbonyl reductase

**CHF** congestive heart failure

$CL$  clearance

**CNS** central nervous system

**CPC** cardiac progenitor cell

**CPR** cytochrome P-450 reductase

**CYP450** cytochrome P450

**DDM** doxorubicin deoxyglycone metabolite

**DNA** deoxyribonucleic acid

**DOX** Doxorubicin

**DOXol** Doxorubicinol

**DSR** doxorubicin semi-quinone radical

$E_{max}$  maximum drug effect

$E_0$  theoretical intercept for drug effect

$E$  drug effect

$EC_{50}$  sensitivity parameter representing the drug concentration that causes 50% of maximum drug effect

**Eh** hepatic extraction ratios

$F_{u,TW}$  fraction of unbound drug concentration in aqueous volume outside the plasma

$F_{u,t}$  fraction of unbound drug concentration in tissue

$F/F_u$  fraction unbound or bioavailability of a drug

$I_{max}$  the maximal effect of inhibition in Indirect Response Model

$IC_{50}$  concentration of an inhibitor where 50% response is observed

**IDR** Indirect Response

**IIV** inter-individual variability

**IOV** inter-occasion variability

**IVIG** intravenous immunoglobulin

**IVIVE** in-vitro in-vivo extrapolation

$k_a$  absorption rate

$K_D$  equilibrium dissociation constant in the  $E_{max}$  Model

$k_g$  tumor growth rate constant

$K_m$  Michaelis constant - theoretical maximum rate of a capacity-limited reaction  
(here, metabolism)

$K_p$  tissue-to-plasma partition coefficient

$k$  elimination constant, inversely proportional to half-life

**LAR** lifetime attributable risk

**LBF** liver blood flow

$LC_{50}$  lethal dose for 50% of the population

$m$  slope of effect-log concentration relation in Levy equation

**MAPK** mitogen-activated protein kinases

$MLP$  maximum life-span potential

**MRT** mean residence time

**MTD** maximum tolerated dose

**NAD** nicotinamide adenine dinucleotide

**NADH** nicotinamide adenine dinucleotide + hydrogen

**NADPH** nicotinamide adenine dinucleotide phosphate

**NDUFS** NADH dehydrogenase

**NOS** nitric oxide synthase

**NQO1** NADPH quinone oxireductases

**ODE** ordinary differential equation

$P$  permeability

**PBPK** physiologically-based pharmacokinetics

**PD** pharmacodynamic

**PK** pharmacokinetic

**PK/PD** pharmacokinetic-pharmacodynamic as used to describe models with concentration time and concentration effect components

$R_{idr}$  response measure in Indirect Response Model

$R_{in}$  infusion rate

$R_0$  zero-order drug input

$R_T$  receptor density

$R$  dose parameter in Levy equation

**RBC** red blood cell

$RC$  receptor complex

**RNA** ribonucleic acid

**ROS** reactive oxygen species

$S_{max}$  the maximal effect of stimulation in Indirect Response Model

**SA** surface area

$SC_{50}$  the drug which causes the half maximal effect of stimulation

$T_{max}$  maximum tumor burden

$T$  tumor burden

**TBW** total body water

**TDM** therapeutic drug monitoring

**TI** therapeutic index

$V_{dist}$  volume of distribution

$V_{max}$  theoretical maximum rate of a capacity-limited reaction (here metabolism)

$V_{TW}$  aqueous volume outside the plasma where drug is distributed

$V_p$  plasma volume

$V_t$  tissue volume

**XDH** xanthine dehydrogenase

## I.1 Definitions/Abbreviations Used in Dubbelboer Model

$K_m$  Michaelis-Menten constant of DOX-to-DOXol metabolism ( $\mu\text{M}$ )

$K_p$  Partition coefficient tissue:plasma (-)

$P_{diff}$  Passive diffusion between vascular space and extracellular space in liver and kidney (L/min)

$Q$  Blood flow (L/min)

$R_{in}$  Constant infusion rate for DOX administration ( $\mu\text{mol}/\text{min}$ )

$SF$  Scaling factor

$V$  Volume (L)

$V_{max}$  Maximum DOX-to-DOXol metabolic rate ( $\mu\text{mol}/\text{min}$ )

### I.1.1 Subscripts

**vb(,t)** venous blood (leaving tissue compartment)

**vp** vena porta

**ab** arterial blood

**b** bound to e.g. DNA or cardiolipins

**cel** cellular compartment

**co** cardiac output

**ex** extracellular compartment

**excr** excretion

**GFR** Glomerular filtration rate

**gu** gastrointestinal tract and spleen

**ha** hepatic artery

**ki** kidney

**li** liver

**lu** lung

**met** metabolism

**off** from bound to unbound

**on** from unbound to bound

**p** plasma

**t** tissue compartment

**u** unbound

**va** vascular compartment in kidney

## I.2 Definitions/Abbreviations Used in Final Model

*BP* blood:plasma ratio

*CbCp* bile:plasma partition coefficient

**cel** cellular sub-compartment in metabolizing tissues

*Cl<sub>excr</sub>* clearance by excretion to bile or urine

*Cl<sub>mem</sub>* membrane clearance between extracellular and cellular space

*Cl<sub>off</sub>* dissociation coefficient

*Cl<sub>on</sub>* association coefficient

*CO* cardiac output

**extra** extracellular sub-compartment in metabolizing tissues

*F<sub>unbound</sub>* fraction unbound

**GI** gastrointestinal tract

**HA** hepatic artery

*K<sub>m</sub>* Michealis-Menten constant of DOX to DOXol metabolism

*P<sub>diff</sub>* passive diffusion between vascular and extracellular space

*Q* flow rate

*V* volume of distribution

**va** vascular sub-compartment in metabolizing tissues

**vb** venous blood

**VH** hepatic vein

$V_{max}$  maximum metabolic rate of DOX to DOXol metabolism

**VP** portal vein



## REFERENCES

- [1] Katherine Tyner et al. “Physiologically Based Pharmacokinetic (PBPK) Modeling of Pharmaceutical Nanoparticles”. In: *AAPS Journal* (2016). doi: 10.1208/s12248-016-0010-3.
- [2] H. M. Jones and K. Rowland-Yeo. “Basic concepts in physiologically based pharmacokinetic modeling in drug discovery and development”. In: *CPT: Pharmacometrics and Systems Pharmacology* 2.8 (Aug. 2013). issn: 21638306. doi: 10.1038/psp.2013.41.
- [3] Edward A. Lefrak et al. “A clinicopathologic analysis of adriamycin cardiotoxicity”. In: *Cancer* 32.2 (1973), pp. 302–314. issn: 10970142. doi: 10.1002/1097-0142(197308)32:2<302::AID-CNCR2820320205>3.0.CO;2-2.
- [4] M Del Tacca et al. “Might Adriamycinol Contribute To Adriamycin-Ind Cardiotoxicity ?” In: *Pharmacological Research Communications* 17.11 (1985), pp. 1073–1084.
- [5] Richard L. Burden, J. Douglas Faires, and Annette M. Burden. *Numerical Analysis*. 10th ed. Boston, MA: Cengage, 2016. isbn: 978-1305253667.
- [6] S. B. Duffull. A Philosophical Framework for Integrating Systems Pharmacology Models into Pharmacometrics. Dec. 2016. doi: 10.1002/psp4.12148.
- [7] William E. Boyce and Richard C. DiPrima. *Elementary Differential Equations and Boundary Value Problems*. 10th. Hoboken, NJ: Wiley, 2012. isbn: 978-0-470-45831-0.
- [8] Ilse R. Dubbelboer et al. “A Model-Based Approach To Assessing the Importance of Intracellular Binding Sites in Doxorubicin Disposition”. In: *Molecular Pharmaceutics* 14 (2017), pp. 686–698. issn: 15438392. doi: 10.1021/acs.molpharmaceut.6b00974.
- [9] Yeamin Huh, David E. Smith, and Meihau Rose Feng. “Interspecies scaling and prediction of human clearance: Comparison of small- and macro-moleculedrugs”. In: *Xenobiotica* 41.11 (Nov. 2011), pp. 972–987. issn: 00498254. doi: 10.3109/00498254.2011.598582.

- [10] Jong Bong Lee et al. “Interspecies prediction of pharmacokinetics and tissue distribution of doxorubicin by physiologically-based pharmacokinetic modeling”. In: *Biopharmaceutics and Drug Disposition* 41.4-5 (Apr. 2020), pp. 192–205. issn: 1099081X. doi: 10.1002/bdd.2229.
- [11] Leandro Francisco Pippa et al. “Total, renal and hepatic clearances of doxorubicin and formation clearance of doxorubicinol in patients with breast cancer: Estimation of doxorubicin hepatic extraction ratio”. In: *Journal of Pharmaceutical and Biomedical Analysis* 185 (June 2020). issn: 07317085. doi: 10.1016/j.jpba.2020.113231.
- [12] Wim J.F. van der Vijgh, Paul A. Maessen, and Herbert M. Pinedo. “Comparative metabolism and pharmacokinetics of doxorubicin and 4-epidoxorubicin in plasma, heart and tumor of tumor-bearing mice”. In: *Cancer Chemotherapy and Pharmacology* 26.1 (1990), pp. 9–12. issn: 14320843. doi: 10.1007/BF02940286.
- [13] Food and Drug Administration. *Highlights of Prescribing Information - Doxorubicin Hydrochloride*. url: [https://www.accessdata.fda.gov/drugsatfda\\_docs/label/2013/050467s0731bl.pdf](https://www.accessdata.fda.gov/drugsatfda_docs/label/2013/050467s0731bl.pdf).
- [14] Tomáš Šimunek et al. “Anthracycline-induced cardiotoxicity: Overview of studies examining the roles of oxidative stress and free cellular iron. Tech. rep. 2 Giorgio Minotti et al. *Anthracyclines: Molecular advances and pharmacologic developments in antitumor activity and cardiotoxicity*. June 2004. doi: 10.1124/pr.56.2.6.009.
- [15] Giorgio Minotti et al. *Anthracyclines: Molecular advances and pharmacologic developments in antitumor activity and cardiotoxicity*. June 2004. doi: 10.1124/pr.56.2.6.
- [16] R Minow, R Benjamin, and Jeffrey A. Gottlieb. “Adriamycin (NSC-123127) Cardiomyopathy - An Overview with Determination of Risk Factors”. In: *Cancer Chemotherapy Reports* 6 (1975), pp. 195–201.
- [17] Stephen Piscitelli et al. “Pharmacokinetics and pharmacodynamics of doxorubicin in patients with small cell lung cancer”. In: *Clinical Pharmacology & Therapeutics* 53.5 (1993), pp. 555–561.
- [18] Swantje Voller et al. “Towards a Model-Based Dose Recommendation for Doxorubicin in Children”. In: *Clinical Pharmacokinetics* 56 (2017), pp. 215–223. issn: 11791926. doi: 10.1007/s40262-016-0451-y.

- [19] Josefine Palle et al. “Doxorubicin pharmacokinetics is correlated to the effect of induction therapy in children with acute myeloid leukemia nnerholm a on behalf of the Nordic Society for Pediatric Hematology and Oncology”. In: *Anti-Cancer Drugs* 17.17 (2006).
- [20] B. M. Frost et al. “Pharmacokinetics of doxorubicin in children with acute lymphoblastic leukemia: Multi-institutional collaborative study”. In: *Medical and Pediatric Oncology* 38 (2002), pp. 329–337. issn: 00981532. doi: 10.1002/mpo.10052.
- [21] Bharat Pateliya, Vinod Burade, and Sunita Goswami. “Combining naringenin and metformin with doxorubicin enhances anticancer activity against triple-negative breast cancer in vitro and in vivo”. In: *European Journal of Pharmacology* 891 (Jan. 2021). issn: 00142999. doi: 10.1016/j.ejphar.2020.173725
- [22] Debra Wu et al. “Gemcitabine and doxorubicin in immunostimulatory monophosphoryl lipid A liposomes for treating breast cancer”. In: *Bioengineering and Translational Medicine* 6.1 (Jan. 2021). issn: 23806761. doi: 10.1002/btm2.10188.
- [23] Anusha Pusuluri et al. “Role of synergy and immunostimulation in design of chemotherapy combinations: An analysis of doxorubicin and camptothecin”. In: *Bioengineering & Translational Medicine* 4.2 (May 2019). issn: 2380-6761. doi: 10.1002/btm2.10129.
- [24] Najmeh Alizadeh et al. “Preparation of an injectable doxorubicin surface modified cellulose nanofiber gel and evaluation of its anti-tumor and anti-metastasis activity in melanoma”. In: *Biotechnology Progress* 34.2 (Mar. 2018). issn: 87567938. doi: 10.1002/btpr.2598.
- [25] Xi Su et al. “Lenvatinib promotes the antitumor effect of doxorubicin in anaplastic thyroid cancer”. In: *OncoTargets and Therapy* 13 (2020), pp. 11183–11192. issn: 11786930. doi: 10.2147/OTT.S278349.
- [26] Katy Mercer et al. “ACCEPT - combining acalabrutinib with rituximab, cyclophosphamide, doxorubicin, vincristine and prednisolone (R-CHOP) for Diffuse Large B-cell Lymphoma (DLBCL): Study protocol for a Phase Ib/II open-label non-randomised clinical trial”. In: *F1000Research* 9 (2020). issn: 1759796X. doi: 10.12688/f1000research.22318.1.
- [27] Manjarika De et al. “Combining doxorubicin with stearylamine-bearing liposomes elicits Th1 cytokine responses and cures metastasis in a mouse model”. In: *Cancer Immunology, Immunotherapy* 69.9 (Sept. 2020), pp. 1725–1735. issn: 14320851. doi: 10.1007/s00262-020-02578-9.

- [28] Chuchu Lin et al. “Self-assembled nanomedicine combining a berberine derivative and doxorubicin for enhanced antitumor and antimetastatic efficacy via mitochondrial pathways”. In: *Nanoscale* 13.13 (2021). issn: 2040-3364. doi: 10.1039/D1NR00032B.
- [29] Ji-Eon Kim et al. “The limited intestinal absorption via paracellular pathway is responsible for the low oral bioavailability of doxorubicin”. In: *Xenobiotica* 43.7 (July 2013). issn: 0049-8254. doi: 10.3109/00498254.2012.751140
- [30] Rachel J. Ryu et al. “Pharmacokinetics of doxorubicin in pregnant women”. In: *Cancer Chemotherapy and Pharmacology* 73.4 (2014), pp. 789–797. issn: 14320843. doi: 10.1007/s00280-014-2406-z.
- [31] Jonas Perez-Blanco et al. “Population pharmacokinetics of doxorubicin and doxorubicinol in patients diagnosed with non-Hodgkin’s lymphoma”. In: *British Journal of Clinical Pharmacology* 82 (2016), pp. 1517–1527.
- [32] Nina Kontny et al. “Population pharmacokinetics of doxorubicin: establishment of a NONMEM model for adults and children older than 3 years”. In: *Cancer Chemotherapy Pharmacology* 71 (2013), pp. 749–763.
- [33] Franca Formelli, Roberto Carsana, and Carmen Pollini. “Comparative pharmacokinetics and metabolism of doxorubicin and 4-demethoxy-4’-O-methyl-doxorubicin in tumor-bearing mice\*”. In: *Cancer Chemother Pharmacol* 16 (1986), pp. 15–21.
- [34] Paj Speth QGCM van Hoese and C Haanen. Clinical Pharmacokinetics of Doxorubicin. *Tech. rep.*
- [35] Carlo M Camaggi et al. Cancer Chemotherapy and Pharmacology Epirubicin and doxorubicin comparative metabolism and pharmacokinetics: A cross-over study. *Tech. rep.* 1988, pp. 221–228.
- [36] Milo Gibaldi and Donald Perrier. *Pharmacokinetics*. Ed. by James Swarbrick. Second. Vol. 15. New York, New York: Marcel Dekker, Inc, 1982.
- [37] H. Hochster et al. “Pharmacokinetics of the Cardioprotector ADR-529 (ICRF-187) in Escalating Doses Combined With Fixed-Dose Doxorubicin”. In: *JNCI Journal of the National Cancer Institute* 84.22 (Nov. 1992). issn: 0027-8874. doi: 10.1093/jnci/84.22.1725.
- [38] Sheila Annie Peters. *Physiologically-Based Pharmacokinetic (PBPK) Modeling and Simulations: Principles, Methods, and Applications in the Pharmaceutical Industry*. 2012. isbn: 9780470484067. doi: 10.1002/9781118140291

- [39] Dawn N Waterhouse et al. A Comparison of Liposomal Formulations of Doxorubicin with Drug Administered in Free Form Changing Toxicity Profiles. *Tech. rep.*
- [40] D. J. Stewart et al. “Concentrations of doxorubicin and its metabolites in human autopsy heart and other tissues”. In: *Anticancer Research* 13 (1993), pp. 1945–1952. issn: 02507005
- [41] Christopher R“a”af et al. “Introduction of a method to calculate cumulative age- And gender-specific lifetime attributable risk (LAR) of cancer in populations after a large-scale nuclear power plant accident”. In: *PLoS ONE* 15.2 (Feb. 2020). issn: 19326203. doi: 10.1371/journal.pone.0228549
- [42] Sandra M. Swain, Fredrick S. Whaley, and Michael S. Ewer. “Congestive heart failure in patients treated with doxorubicin: A retrospective analysis of three trials”. In: *Cancer* 97.11 (June 2003), pp. 2869–2879. issn: 0008543X. doi: 10.1002/cncr.11407.
- [43] D Von Hoff et al. “Risk Factors for Doxorubicin-Induced Congestive Heart Failure”. In: *Annals of Internal Medicine* 91 (1979), pp. 710–717.
- [44] S Eksborg et al. European Journal of Clinical Pharmacology Pharmacokinetic Study of IV Infusions of Adriamycin. *Tech. rep.* 1985, pp. 205–212.
- [45] Aquilur Rahman et al. “Comparative Pharmacokinetics of Free Doxorubicin and Doxorubicin Entrapped in Cardioliipin Liposomes”. In: *Cancer Research* 46 (1986), pp. 2295–2299.
- [46] Benedetta C. Sallustio and Alan V. Boddy. *Is there scope for better individualisation of anthracycline cancer chemotherapy?* Feb. 2021. doi: 10 . 1111 / bcp . 14628.
- [47] Wayne J. Aston et al. “A systematic investigation of the maximum tolerated dose of cytotoxic chemotherapy with and without supportive care in mice”. In: *BMC Cancer* 17.1 (Oct. 2017). issn: 14712407. doi: 10.1186/s12885- 017-3677-7
- [48] Jasbir Saini. “Reversibility of Severe Left Ventricular Dysfunction Due to Doxorubicin Cardiotoxicity”. In: *Annals of Internal Medicine* 106.6 (June 1987). issn: 0003-4819. doi: 10.7326/0003-4819-106-6-814.
- [49] ConnectiveRX. *Doxorubicin hydrochloride - Drug Summary*. url: <https://www.pdr.net/drug-summary/Adriamycin-doxorubicin-hydrochloride1379.740>.
- [50] Andrea Bacigalupo et al. “Defining the Intensity of Conditioning Regimens: Working Definitions”. In: *Biology of Blood and Marrow Transplantation* 15.12 (Dec. 2009), pp. 1628–1633. issn: 10838791. doi: 10.1016/j.bbmt. 2009.07.004

- [51] Ivan Pasic et al. “Subcutaneous immunoglobulin in allogeneic hematopoietic cell transplant patients: A prospective study of feasibility, safety, and healthcare resource use”. In: *Hematology/ Oncology and Stem Cell Therapy* (2021). issn: 16583876. doi: 10.1016/j.hemonc.2021.01.001.
- [52] Derek W Edwardson et al. “Current Drug Metabolism Current Drug Metabolism The international journal for timely in-depth reviews on Drug Metabolism The international journal for timely in-depth reviews on Drug Metabolism Role of Drug Metabolism in the Cytotoxicity and Clinical Efficacy of Anthracyclines”. In: *Current Drug Metabolism* 16 (2015), pp. 412–426. issn: 1875-5453.
- [53] Yves Pommier et al. *DNA topoisomerases and their poisoning by anticancer and antibacterial drugs*. 2010. doi: 10.1016/j.chembiol.2010.04.012.
- [54] Fan Yang, Christopher J. Kemp, and Steven Henikoff. “Doxorubicin enhances nucleosome turnover around promoters”. In: *Current Biology* 23.9 (May 2013), pp. 782–787. issn: 09609822. doi: 10.1016/j.cub.2013.03.043.
- [55] National Institute of Health. HSDB: *Doxorubicin*. 1989. url: <https://toxnet.nlm.nih.gov/cgi-bin/sis/search2/r?dbs+hsdb:@term+@rn+@rel+23214-92-8>
- [56] Hilal Taymaz-Nikerel et al. “Doxorubicin induces an extensive transcriptional and metabolic rewiring in yeast cells”. In: *Scientific Reports* 8.1 (Dec. 2018). issn: 20452322. doi: 10.1038/s41598-018-31939-9.
- [57] Tadaatsu Goto and James C Wang. Cloning of yeast TOPI, the gene encoding DNA topoisomerase I, and construction of mutants defective in both DNA topoisomerase I and DNA topoisomerase II (*Saccharomyces cerevisiae*/DNA topoisomerase mutants). *Tech. rep.* 1985, pp. 7178–7182.
- [58] Jessica M. Scott et al. “Modulation of anthracycline-induced cardiotoxicity by aerobic exercise in breast cancer: Current evidence and underlying mechanisms”. In: *Circulation* 124.5 (Aug. 2011), pp. 642–650. issn: 00097322. doi: 10.1161/CIRCULATIONAHA.111.021774.
- [59] Pierre May and Evelyne May. Twenty years of p53 research: structural and functional aspects of the p53 protein. *Tech. rep.* 1999. url: <http://www.stocktonpress.co.uk/onc>.
- [60] Seon-Young Kim et al. “Doxorubicin-induced reactive oxygen species generation and intracellular Ca<sup>2+</sup> increase are reciprocally modulated in rat cardiomyocytes”. In: *Experimental and Molecular Medicine* 38.5 (2006), pp. 535–545. url: <https://www.nature.com/articles/emm200663>.

- [61] Herbert Loveless et al. Comparative Mammalian Metabolism of Adriamycin and Daunorubicin. *Tech. rep.* 1978.
- [62] David J. Stewart et al. "Human tissue distribution of platinum after cis-diamminedichloroplatinum". In: *Cancer Chemotherapy and Pharmacology* 10.1 (Dec. 1982). issn: 0344-5704. doi: 10.1007/BF00257239.
- [63] John H. Peters et al. "Tissue distribution of doxorubicin and doxorubicinol in rats receiving multiple doses of doxorubicin". In: *Cancer Chemotherapy and Pharmacology* 7 (1981), pp. 65–69. issn: 14320843. doi: 10.1007/BF00258216
- [64] Yeu-Tsu N. (Margaret) Lee, Kenneth K. Chan, and Phillip A. Harris. "Tissue disposition of doxorubicin in experimental animals". In: *Medical and Pediatric Oncology* 10.3 (1982). issn: 00981532. doi: 10.1002/mpo.2950100306.
- [65] A Russo and J B Mitchell. "Potentiation and protection of doxorubicin cytotoxicity by cellular glutathione modulation". In: *Cancer Treatment Reports* 69.11 (Nov. 1985), pp. 1293–1296.
- [66] Richard D Olson et al. "Doxorubicin cardiotoxicity may be caused by its metabolite, doxorubicinol (adriamycin/anthracycline/cardiomyopathy/ion pumps)". In: *Medical Sciences* 85 (1988), pp. 3585–3589.
- [67] Mirjam N. Trame et al. "Perspective on the State of Pharmacometrics and Systems Pharmacology Integration". In: *CPT: Pharmacometrics and Systems Pharmacology* 7.10 (Oct. 2018), pp. 617–620. issn: 21638306. doi: 10.1002/psp4.12313.
- [68] Hartmut Derendorf and Stephan Schmidt. *Rowland and Tozer's Clinical Pharmacokinetics and Pharmacodynamics*. Ed. by Matt Hauber and Amy Millholen. 5th. Philadelphia, PA: Wolters Kluwer, 2020.
- [69] Nicholas H.G. Holford and Lewis B. Sheiner. "Kinetics of pharmacologic response". In: *Pharmacology & Therapeutics* 16.2 (Jan. 1982). issn: 01637258. doi: 10.1016/0163-7258(82)90051-1.
- [70] Mark J. Ratain and Jr William K. Plunkett. "Principles of Pharmacokinetics". In: *NCBI* (2003). url: <https://www.ncbi.nlm.nih.gov/books/NBK12815/>.
- [71] Richard Felder, Ronald Rousseau, and Lisa Bullard. *Elementary Principles of Chemical Processes*. Ed. by Ashley Patterson, Don Fowley, and Kelsey Randomski. 4th ed. Wiley, Aug. 2020.
- [72] Leslie Z Benet and Parnian Zia-amirhosseini. "Basic Principles of Pharmacokinetics\*". In: *Toxicologic Pathology* 23 (1995), pp. 115–123.

- [73] Huixi Zou et al. *Application of Pharmacokinetic-Pharmacodynamic Modeling in Drug Delivery: Development and Challenges*. July 2020. doi: 10.3389/fphar.2020.00997.
- [74] Michael N Sawka, Samuel N Cheuvront, and Robert Carter. “Human Water Needs”. In: (2005), pp. 30–39. doi: 10.1301/nr.2005.jun.S30.
- [75] John T. Hansen and Bruce M. Koeppen. *Netter’s Atlas of Human Physiology (Netter’s Basic Science)*. Ed. by W.B. Saunders. 1st ed. Philadelphia, PA, 2002, pp. 1–223. isbn: 1-929007-01-9.
- [76] John E. Hall. *Guyton and Hall Textbook of Medical Physiology*. Ed. by Rebecca Grulicow and Laura Stingelin. 12th ed. Philadelphia, PA: Saunders Elsevier, 2011. isbn: 978-1-4160-4574-8.
- [77] N Joan Abbott. “Inflammatory Mediators and Modulation of Blood-Brain Barrier Permeability”. In: *Cellular and Molecular Neurobiology* 20.2 (2000), pp. 131–147.
- [78] L. Palanikumar et al. “pH-responsive high stability polymeric nanoparticles for targeted delivery of anticancer therapeutics”. In: *Communications Biology* 3.1 (Dec. 2020). issn: 23993642. doi: 10.1038/s42003-020-0817-4.
- [79] Jiunn Huei Lin et al. In Vitro and In Vivo Evaluation of the Tissue-to-Blood Partition Coefficient for Physiological Pharmacokinetic Models. *Tech. rep.* 6. 1982.
- [80] Raymond F Greene et al. “Plasma Pharmacokinetics of Adriamycin and Adriamycinol: Implications for the Design of in Vitro Experiments and Treatment Protocols”. In: *Cancer Research* 43 (1983), pp. 3417–3421.
- [81] Jennifer Le. *Drug Metabolism*. Kenliworth, New Jersey, Oct. 2020. url: <https://www.merckmanuals.com/professional/clinical-pharmacology/pharmacokinetics/drug-metabolism#>
- [82] Mitesh Patel, Kunal S. Taskar, and Maciej J. Zamek-Gliszczynski. “Importance of Hepatic Transporters in Clinical Disposition of Drugs and Their Metabolites”. In: *Journal of Clinical Pharmacology* (2016), S23–S39. issn: 15524604. doi: 10.1002/jcph.671.
- [83] Boseung Choi, Grzegorz A. Rempala, and Jae Kyoung Kim. “Beyond the Michaelis-Menten equation: Accurate and efficient estimation of enzyme kinetic parameters”. In: *Scientific Reports* 7.1 (Dec. 2017). issn: 20452322. doi: 10.1038/s41598-017-17072-z.



- [84] Jennifer Le. Drug Excretion. Sept. 2020. url: <https://www.merckmanuals.com/professional/clinical-pharmacology/pharmacokinetics/drugexcretion#>.
- [85] Martin R. Pollak et al. "The glomerulus: The sphere of influence". In: *Clinical Journal of the American Society of Nephrology* 9.8 (2014), pp. 1461–1469. issn: 1555905X. doi: 10.2215/CJN.09400913.
- [86] Georg Hempel. "Dose and therapy individualization in cancer chemotherapy". In: *Handbook of Analytical Separations*. Vol. 7. Elsevier B.V., Jan. 2020, pp. 291–319. doi: 10.1016/B978-0-444-64066-6.00013-7.
- [87] Nicholas H.G. Holford. "Clinical Pharmacokinetics and Pharmacodynamics of Warfarin". In: *Clinical Pharmacokinetics* 11.6 (1986). issn: 0312-5963. doi: 10.2165/00003088-198611060-00005.
- [88] Marissa N. Lassere et al. Is blood pressure reduction a valid surrogate endpoint for stroke prevention? An analysis incorporating a systematic review of randomised controlled trials, a by-trial weighted errors-in-variables regression, the surrogate threshold effect (STE) and the biomarker-surrogacy (BioSurrogate) Evaluation Schema (BSES). 2012. doi: 10.1186/1471-2288-12-27.
- [89] Se Eun Park, Cheol-Young Park, and Gary Sweeney. "Biomarkers of insulin sensitivity and insulin resistance: Past, present and future". In: *Critical Reviews in Clinical Laboratory Sciences* 52.4 (July 2015). issn: 1040-8363. doi: 10.3109/10408363.2015.1023429
- [90] Amira Syahira et al. "Cortisol on Circadian Rhythm and Its Effect on Cardiovascular System". In: *J. Environ. Res. Public Health* 17 (2021). doi: 10.3390/ijerph17240000.
- [91] M.T Epstein, J.M Hockaday, and T.D.R Hockaday. "Migraine and Reproductive Hormones Throughout the Menstrual Cycle". In: *The Lancet* 305.7906 (Mar. 1975). issn: 01406736. doi: 10.1016/S0140-6736(75)91558-5.
- [92] Luana Colloca. Preface: The Fascinating Mechanisms and Implications of the Placebo Effect. Jan. 2018. doi: 10.1016/S0074-7742(18)30027-8.
- [93] Colin A Shanks et al. A Pharmacokinetic-Pharmacodynamic Model for Quantal Responses with Thiopental. *Tech. rep.* 3. 1993.
- [94] Gerhard Levy. "Relationship Between Elimination Rate of Drugs and Rate of Decline of Their Pharmacologic Effects". In: *Journal of Pharmaceutical Sciences* 53.3 (Mar. 1964). issn: 00223549. doi: 10.1002/jps.2600530325.
- [95] E J Ariens. *Molecular Pharmacology*. Ed. by EJ Ariens. 1st. Vol. 3. New York, New York: Academic Press, 1964.

- [96] Donald E. Mager, Elzbieta Wyska, and William J. Jusko. “Diversity of Mechanism-Based Pharmacodynamic Models”. In: *Drug Metabolism and Disposition* 31.5 (May 2003). issn: 0090-9556. doi: 10.1124/dmd.31.5. 510.
- [97] Gerhard Levy. “Kinetics of pharmacologic effects”. In: *Clinical Pharmacology & Therapeutics* 7.3 (May 1966). issn: 00099236. doi: 10.1002/cpt196673362.
- [98] J.G. Wagner. “Kinetics of pharmacologic response I. Proposed relationships between response and drug concentration in the intact animal and man”. In: *Journal of Theoretical Biology* 20.2 (Aug. 1968). issn: 00225193. doi: 10.1016/0022-5193(68)90188-4.
- [99] Robert F Furchgott. “The Pharmacology of Vascular Smooth Muscle”. In: *Pharmacology Review* 7.2 (1955), pp. 183–265.
- [100] Tim Cardilin et al. “Model-Based Evaluation of Radiation and Radiosensitizing Agents in Oncology”. In: *CPT: Pharmacometrics and Systems Pharmacology* 7.1 (Jan. 2018), pp. 51–58. issn: 21638306. doi: 10.1002/psp4.12268.
- [101] Lewis B Sheiner et al. Simultaneous modeling of pharmacokinetics and pharmacodynamics: Application to d-tubocurarine. *Tech. rep.* 1979.
- [102] Natalie L Dayneka, Varun Garg, and William J Jusko. Comparison of Four Basic Models of Indirect Pharmacodynamic Responses. *Tech. rep.* 1993.
- [103] William J Jusko and Hui C Ko. “Physiologic indirect response models characterize diverse types of pharmacodynamic effects”. In: *Clinical Pharmacology and Therapeutics* 56.4 (Oct. 1994). issn: 0009-9236. doi: 10.1038/clpt.1994.155.
- [104] R. Nagashima, R. A. O’Reilly, and G. Levy. “Kinetics of pharmacologic effects in man: The anticoagulant action of warfarin”. In: *Clinical Pharmacology & Therapeutics* 10.1 (Jan. 1969). issn: 00099236. doi: 10.1002/cpt196910122.
- [105] Willem J. Sander, Hester Gertruida O’Neill, and Carolina H. Pohl. Prostaglandin E2 as a modulator of viral infections. Feb. 2017. doi: 10.3389/fphys.2017.00089.
- [106] Amarnath Sharma, William J Jusko, and Hochstetter Hall. Characteristics of indirect pharmacodynamic models and applications to clinical drug responses Indirect pharmacodynamic response model A fundamental physiologic model for drugs that produce. *Tech. rep.* 1998, pp. 229–239.
- [107] Kyoji Tsuchikama and Zhiqiang An. Antibody-drug conjugates: recent advances in conjugation and linker chemistries. Jan. 2018. doi: 10.1007/s13238-016-0323-0.

- [108] Huadong Tang and Michael Mayersohn. Porcine prediction of pharmacokinetic parameters in people: A pig in a poke? Nov. 2018. doi: 10.1124/dmd.118.083311.
- [109] Nick Holford. “Clinical pharmacology = disease progression + drug action”. In: *British Journal of Clinical Pharmacology* 79.1 (2015), pp. 18–27. issn: 13652125. doi: 10.1111/bcp.12170.
- [110] Sylvia K Plevritis et al. “A natural history model of stage progression applied to breast cancer”. In: *Statistics in Medicine* 26 (Apr. 2007), pp. 581–595.
- [111] M. J. Hohol, E. J. Orav, and H. L. Weiner. “Disease Steps in multiple sclerosis: A simple approach to evaluate disease progression”. In: *Neurology* 45.2 (Feb. 1995). issn: 0028-3878. doi: 10.1212/WNL.45.2.251.
- [112] C. Holmes et al. “Systemic inflammation and disease progression in Alzheimer disease”. In: *Neurology* 73.10 (Sept. 2009). issn: 0028-3878. doi: 10.1212/WNL.0b013e3181b6bb95.
- [113] Lora Hamuro et al. “Developing a natural history progression model for Duchenne muscular dystrophy using the six-minute walk test”. In: *CPT: Pharmacometrics and Systems Pharmacology* 6.9 (Sept. 2017), pp. 596–603. issn: 21638306. doi: 10.1002/psp4.12220.
- [114] Anyue Yin et al. A Review of Mathematical Models for Tumor Dynamics and Treatment Resistance Evolution of Solid Tumors. Oct. 2019. doi: 10.1002/psp4.12450.
- [115] Food and Drug Administration (FDA). Guidance for Industry Exposure-Response Relationships-Study Design, Data Analysis, and Regulatory Applications. *Tech. rep.* Apr. 2003. url: <http://www.fda.gov/cder/guidance/index.htm> or <http://www.fda.gov/cber/guidelines.htm>.
- [116] R. Bro et al. “Cross-validation of component models: A critical look at current methods”. In: *Analytical and Bioanalytical Chemistry* 390.5 (Mar. 2008), pp. 1241–1251. issn: 16182642. doi: 10.1007/s00216-007-1790-1.
- [117] Peter B. Johansen et al. “Pharmacokinetics of doxorubicin and its metabolite doxorubicinol in rabbits with induced acid and alkaline urine”. In: *Cancer Chemotherapy and Pharmacology* 13.1 (June 1984), pp. 5–8. issn: 03445704. doi: 10.1007/BF00401437.
- [118] Patrick A. Thompson et al. “Impact of body composition on pharmacokinetics of doxorubicin in children: A Glaser Pediatric Research Network study”. In: *Cancer Chemotherapy and Pharmacology* 64 (2009), pp. 243–251. issn: 03445704. doi: 10.1007/s00280-008-0854-z.

- [119] F Leca et al. “New data on the pharmacokinetics of adriamycin and its major metabolite, adriamycinol”. In: *European Journal of Drug Metabolism and Pharmacokinetics* 16.2 (1991), pp. 107–111.
- [120] R Erttmann et al. Pharmacokinetics of doxorubicin in man: dose and schedule dependence\*. *Tech. rep.* 1988, pp. 509–513.
- [121] C J Twelves et al. Comparative pharmacokinetics of doxorubicin given by three different schedules with equal dose intensity in patients with breast cancer. *Tech. rep.* 1991, pp. 302–307.
- [122] RC Boston and DR Phillips. “Evidence of possible dose-dependent doxorubicin plasma kinetics in man”. In: *Cancer Treatment Reports* 67.1 (Jan. 1983), pp. 63–69.
- [123] Fredrik Kullenberg et al. “In Vitro Cell Toxicity and Intracellular Uptake of Doxorubicin Exposed as a Solution or Liposomes: Implications for Treatment of Hepatocellular Carcinoma”. In: *Cells* 10.7 (July 2021), p. 1717. doi: 10.3390/cells10071717.
- [124] David S Alberts and Dava J Garcia. Safety Aspects of Pegylated Liposomal Doxorubicin in Patients with Cancer. *Tech. rep.* 1997, pp. 30–35.
- [125] Y Matsumura et al. “Phase I clinical trial and pharmacokinetic evaluation of NK911, a micelle-encapsulated doxorubicin”. In: *British Journal of Cancer* 91.10 (2004), pp. 1775–1781. issn: 0007-0920. doi: 10 . 1038 / sj . bjc 6602204. url: <http://www.nature.com/doifinder/10.1038/sj.bjc.6602204>.
- [126] J Asperen et al. “Increased accumulation of doxorubicin and doxorubicinol in cardiac tissue of mice lacking mdr1a P-glycoprotein”. In: *British Journal of Cancer* 79.1 (1999), pp. 108–113.
- [127] Barry J. Cusack et al. “Effect of dexrazoxane on doxorubicin pharmacokinetics in young and old rats”. In: *Cancer Chemotherapy and Pharmacology* 51.2 (Feb. 2003), pp. 139–146. issn: 03445704. doi: 10 . 1007 / s00280 - 002 - 0544-1.
- [128] Barry J Cusack et al. Cancer Chemotherapy and Pharmacology Effect of phenytoin on the pharmacokinetics of doxorubicin and doxorubicinol in the rabbit. *Tech. rep.* 1988, pp. 294–298.
- [129] Dean E Brenner, Jerry C Collins, and Kenneth R Hande. Cancer Chemotherapy and Pharmacology The effects of cimetidine upon the plasma pharmacokinetics of doxorubicin in rabbits\*. *Tech. rep.* 1986, pp. 219–222.
- [130] Mark J Ratain, Jacques Robert, and Wim J F Van Der Vijgh. Limited Sampling Models for Doxorubicin Pharmacokinetics. *Tech. rep.* 1991.

- [131] Gilles Freyer et al. "Population pharmacokinetics of doxorubicin, etoposide and ifosfamide in small cell lung cancer patients: results of a multicentre study". In: *British Journal of Clinical Pharmacology* 50 (2000), pp. 315–324.
- [132] M. Anderson et al. "Pharmacokinetics and central haemodynamic effects of doxorubicin and 4'epi-doxorubicin in the pig". In: *Acta Oncologica* 28.5 (1989), pp. 709–714. issn: 0284186X. doi: 10.3109/02841868909092298.
- [133] A. Krarup-Hansen et al. "Pharmacokinetics of doxorubicin in man with induced acid or alkaline urine". In: *Acta Oncologica* 27.1 (1988), pp. 25–30. issn: 0284186X. doi: 10.3109/02841868809090314.
- [134] David Cunningham et al. "Rituximab plus cyclophosphamide, doxorubicin, vincristine, and prednisolone in patients with newly diagnosed diffuse large B-cell non-Hodgkin lymphoma: A phase 3 comparison of dose intensification with 14-day versus 21-day cycles". In: *The Lancet* 381.9880 (2013), pp. 1817–1826. issn: 1474547X. doi: 10.1016/S0140-6736(13)60313-X.
- [135] Swantje Völler et al. "Age-Dependent Pharmacokinetics of Doxorubicin in Children with Cancer". In: *Clinical Pharmacokinetics* 54.11 (Nov. 2015), pp. 1139–1149. issn: 11791926. doi: 10.1007/s40262-015-0272-4.
- [136] M. A. Rudek et al. "Factors affecting pharmacokinetic variability following doxorubicin and docetaxel-based therapy". In: *European Journal of Cancer* 40 (2004), pp. 1170–1178. issn: 09598049. doi: 10.1016/j.ejca.2003.12.026.
- [137] Mary Ann Jordan, Richard H Hirnes, and Leslie Wilson<sup>3</sup>. Comparison of the Effects of Vinblastine, Vincristine, Vindesine, and Vinepidine on Microtubule Dynamics and Cell Proliferation in Vitro. *Tech. rep.* 1985, pp. 2741–2747.
- [138] Laurent Genestier et al. "Mechanisms of action of methotrexate". In: *Immunopharmacology* 47.2-3 (May 2000). issn: 01623109. doi: 10.1016/S0162-3109(00)00189-2.
- [139] Charles M Bagley, Frieda W Bostick, and Vincent T Devita. Clinical Pharmacology of Cyclophosphamide. *Tech. rep.* 1973.
- [140] Sidra Khalid et al. "Dosage Adjustments for Chemotherapy and Targeted Therapies in Colorectal and Pancreatic Cancer Patients with Hepatic Impairment". In: *Cureus* (June 2018). issn: 2168-8184. doi: 10.7759/cureus.2798.
- [141] Sewa S. Legha. "Reduction of Doxorubicin Cardiotoxicity by Prolonged Continuous Intravenous Infusion". In: *Annals of Internal Medicine* 96.2 (Feb. 1982). issn: 0003-4819. doi: 10.7326/0003-4819-96-2-133.

- [142] Anna Cabanes et al. Comparative Study of the Antitumor Activity of Free Doxorubicin and Polyethylene Glycol-coated Liposomal Doxorubicin in a Mouse Lymphoma Model. *Tech. rep.* 1998, pp. 499–505.
- [143] Peter Bloomingdale et al. “Minimal brain PBPK model to support the preclinical and clinical development of antibody therapeutics for CNS diseases”. In: *Journal of Pharmacokinetics and Pharmacodynamics* (Aug. 2021). issn: 1567-567X. doi: 10.1007/s10928-021-09776-7. url: <https://link.springer.com/10.1007/s10928-021-09776-7>.
- [144] K. Gadkar et al. “A six-stage workflow for robust application of systems pharmacology”. In: *CPT: Pharmacometrics and Systems Pharmacology* 5 (2016), pp. 235–249. issn: 21638306. doi: 10.1002/psp4.12071.
- [145] Ilse R. Dubbelboer et al. “The effects of lipiodol and cyclosporin A on the hepatobiliary disposition of doxorubicin in pigs”. In: *Molecular Pharmaceutics* 11.4 (2014), pp. 1301–1313. issn: 15438392. doi: 10.1021/mp4007612.
- [146] R Core Team. *R : A language and environment for statistical computing*. Vienna, Austria, 2019.
- [147] B N Biswas et al. A Discussion On Euler Method: A Review. *Tech. rep.* 2. 2013, pp. 2090–792. url: <http://ejmaa.6te.net/>.
- [148] Desmond J Higham and Lloyd N Trefethen. “Stiffness of ODEs”. In: *BIT* 33 (1993), pp. 285–303.
- [149] Gareth. Hegarty et al. Solving systems of ordinary differential equations that arise in PKPD. Part 1, First order (time-varying) linear systems. *Tech. rep.* 2012, p. 21.
- [150] D. Bakhurst. *On lying and deceiving*. 1992. doi: 10.1136/jme.18.2.63.
- [151] Sara Cascone et al. “Pharmacokinetics of Remifentanyl: a three-compartmental modeling approach”. In: *Translational Medicine* 7.4 (2013), pp. 18–22.
- [152] Stephen B Duffull. “An Inductive Approximation to the Solution of Systems of Nonlinear Ordinary Differential Equations in Pharmacokinetics-Pharmacodynamics”. In: *Journal of Theoretical and Computational Science* 02.01 (2014). doi: 10.4172/jtco.1000119.
- [153] Andrew M. Stein and Lambertus A. Peletier. “Predicting the Onset of Nonlinear Pharmacokinetics”. In: *CPT: Pharmacometrics and Systems Pharmacology* 7.10 (Oct. 2018), pp. 670–677. issn: 21638306. doi: 10.1002/psp4.12316.

- [154] Venkatesh A. Bhattaram et al. “Impact of pharmacometrics on drug approval and labeling decisions: A survey of 42 new drug applications”. In: *The AAPS Journal* 7.3 (Sept. 2005). issn: 1550-7416. doi: 10.1208/aapsj070351.
- [155] Christoph Thiel et al. “A systematic evaluation of the use of physiologically based pharmacokinetic modeling for cross-species extrapolation”. In: *Journal of Pharmaceutical Sciences* 104.1 (2015), pp. 191–206. issn: 15206017. doi: 10.1002/jps.24214. url: <http://dx.doi.org/10.1002/jps.24214>.
- [156] Qingbiao Huang and Jim E. Riviere. *The application of allometric scaling principles to predict pharmacokinetic parameters across species*. 2014. doi: 10.1517/17425255.2014.934671.
- [157] Whitney P. Caron et al. “Allometric scaling of pegylated liposomal anticancer drugs”. In: *Journal of Pharmacokinetics and Pharmacodynamics* 38.5 (Oct. 2011), pp. 653–669. issn: 1567567X. doi: 10.1007/s10928-011-9213-5.
- [158] Huadong Tang et al. “Interspecies prediction of human drug clearance based on scaling data from one or two animal species”. In: *Drug Metabolism and Disposition* 35.10 (Oct. 2007), pp. 1886–1893. issn: 00909556. doi: 10.1124/dmd.107.016188.
- [159] Thierry Lave et al. “Interspecies scaling of bosentan, a new endothelin receptor antagonist and integration of in vitro data into allometric scaling”. In: *Pharmaceutical Research* 13.1 (1996). issn: 07248741. doi: 10.1023/A:1016037519116.
- [160] Meihua Rose Feng et al. “Allometric pharmacokinetic scaling: towards the prediction of human oral pharmacokinetics.” In: *Pharmaceutical Research* 17.4 (2000). issn: 07248741. doi: 10.1023/A:1007520818956.
- [161] Harold Boxenbaum. “Interspecies scaling, allometry, physiological time, and the ground plan of pharmacokinetics”. In: *Journal of Pharmacokinetics and Biopharmaceutics* 10.2 (Apr. 1982). issn: 0090-466X. doi: 10.1007/BF01062336.
- [162] I. Mahmood and J. D. Balian. “Interspecies scaling: predicting clearance of drugs in humans. Three different approaches”. In: *Xenobiotica* 26.9 (Jan. 1996). issn: 0049-8254. doi: 10.3109/00498259609052491.
- [163] Rakesh Nagilla and Keith W. Ward. “A comprehensive analysis of the role of correction factors in the allometric predictivity of clearance from rat, dog, and monkey to humans”. In: *Journal of Pharmaceutical Sciences* 93.10 (Oct. 2004). issn: 00223549. doi: 10.1002/jps.20169.

- [164] I Mahmood. “Application of allometric principles for the prediction of pharmacokinetics in human and veterinary drug development”. In: *Advanced Drug Delivery Reviews* 59.11 (Sept. 2007). issn: 0169409X. doi: 10.1016/j.addr.2007.05.015.
- [165] F. Salem et al. “Considering Age Variation When Coining Drugs as High versus Low Hepatic Extraction Ratio”. In: *Drug Metabolism and Disposition* 44.7 (June 2016). issn: 1521-009X. doi: 10.1124/dmd.115.067595.
- [166] XD Liu. Prediction of drug clearance in humans from laboratory animals based on body surface area. *Tech. rep.* 4. 2001, pp. 249–256.
- [167] Suein Choi et al. “Quantitative prediction of human pharmacokinetics and pharmacodynamics of ckd519, a potent inhibitor of cholesteryl ester transfer protein (Cetp)”. In: *Pharmaceutics* 11.7 (July 2019). issn: 19994923. doi: 10.3390/pharmaceutics11070336. 262
- [168] Scott Obach et al. “The Prediction of Human Pharmacokinetic Parameters from Preclinical and In Vitro Metabolism Data”. In: *The Journal Of Pharmacology And Experimental Therapeutics* 283.1 (1997), pp. 46–58.
- [169] Els Van Peer et al. “Organ data from the developing Göttingen minipig: first steps towards a juvenile PBPK model”. In: *Journal of Pharmacokinetics and Pharmacodynamics* 43.2 (Apr. 2016), pp. 179–190. issn: 15738744. doi: 10.1007/s10928-015-9463-8.
- [170] Steven Benbow. *Graph Grabber*. Feb. 2020. url: <http://www.quintessa.org/graph-grabber>.
- [171] AnroopB Nair and Shery Jacob. “A simple practice guide for dose conversion between animals and human”. In: *Journal of Basic and Clinical Pharmacy* 7.2 (2016), p. 27. issn: 0976-0105. doi: 10.4103/0976-0105.177703.
- [172] IQ 3R Leadership Group. Recommended Dose Volumes for Common Laboratory Animals. *Tech. rep.*
- [173] International Life Science Institute (ILSI) Risk Science Institute (RSI). Physiological parameter values for PBPK models. *Tech. rep.* 1994, pp. 1–142. url: <https://nepis.epa.gov/Exe/ZyNET.exe/9100K030.txt?ZyActionD=ZyDocument&Client=EPA&Index=1991%20Thru%201994&Docs=&Query=&Time=&EndTime=&SearchMethod=1&TocRestrict=n&Toc=&TocEntry=&QField=&QFieldYear=&QFieldMonth=&QFieldDay=&UseQField=&IntQFieldOp=0&ExtQFieldOp=>.
- [174] Brian Davies and Tim Morris. “Physiological Parameters in Laboratory Animals and Humans”. In: *Pharmaceutical Research* 10.7 (1993), pp. 1093–1095.



- [175] Lehana Thabane et al. *A tutorial on sensitivity analyses in clinical trials: The what, why, when and how*. 2013. doi: 10.1186/1471-2288-13-92.
- [176] Michał Romański et al. “In Vivo Red Blood Cells/Plasma Partition Coefficient of Treosulfan and Its Active Monoepoxide in Rats”. In: *European Journal of Drug Metabolism and Pharmacokinetics* 43.5 (Oct. 2018), pp. 565–571. issn: 21070180. doi: 10.1007/s13318-018-0469-7.
- [177] P. V. Deshmukh, P. C. Badgular, and M. M. Gatne. “In-vitro red blood cell partitioning of doxycycline”. In: *Indian Journal of Pharmacology* 41.4 (Oct. 2009), pp. 173–175. issn: 02537613. doi: 10.4103/0253-7613.56073.
- [178] F Misiti et al. Doxorubicin metabolites and erythrocyte energy metabolism. *Tech. rep.* 12. 2003, pp. 1643–1651.
- [179] Rob A Phillips et al. “Cardiac Output Measurement in Animals Using the Non-Invasive USCOM Device”. In: *Journal of Veterinary Emergency and Critical Care*. 2006. url: <https://www.researchgate.net/publication/270105609>.
- [180] Lester A. Critchley, Anna Lee, and Anthony M.-H. Ho. “A Critical Review of the Ability of Continuous Cardiac Output Monitors to Measure Trends in Cardiac Output”. In: *Anesthesia & Analgesia* 111.5 (2010), pp. 1180–1192.
- [181] K A Shoshenko. Cardiac Output and Its Interorgan Distribution in Mammals at Rest. *Tech. rep.* 4. 2004, pp. 285–289.
- [182] Neerav Patel et al. “Measuring Cardiac Output in a Swine Model”. In: *Journal of Visualized Experiments* 171 (May 2021). issn: 1940-087X. doi: 10.3791/62333.
- [183] Pedro Cabrales et al. “Measurement of the cardiac output in small animals by thermodilution”. In: *Microvascular Research* 66.2 (Sept. 2003). issn: 00262862. doi: 10.1016/S0026-2862(03)00044-X.
- [184] Makgaret Beznak. Cardiac Output in Rats During the Development of Cardiac Hypertrophy. *Tech. rep.* url: <http://ahajournals.org>.
- [185] Charles D. Howell, Steven M. Horvath, and Enid Allbaugh Farrand. “Evaluation of variability in the cardiac output of dogs”. In: *American Journal of Physiology-Legacy Content* 196.1 (Dec. 1958). issn: 0002-9513. doi: 10.1152/ajplegacy.1958.196.1.193.
- [186] R Documentation and R Core Team. *optim: General Purpose Optimization*. doi: 10.2307/3214721.
- [187] T Colombo et al. “Doxorubicin toxicity and pharmacokinetics in old and young rats”. In: *Experimental Gerontology* 24.2 (1989), pp. 151–179.

- [188] D.W. Yesair et al. "Pharmacokinetics and Metabolism of Adriamycin and Daunomycin". In: *International Symposium on Adriamycin*. 1971, pp. 117–123.
- [189] Chun Ling Dai et al. "Tetrandrine achieved plasma concentrations capable of reversing MDR in vitro and had no apparent effect on doxorubicin pharmacokinetics in mice". In: *Cancer Chemotherapy and Pharmacology* 60.5 (Oct. 2007), pp. 741–750. issn: 03445704. doi: 10 . 1007 / s00280 - 007-0420-0.
- [190] N.R. Bachur, R.C. Hildebrand, and R.S. Jaenke. "Adriamycin and Daunorubicin Disposition in the Rabbit". In: *Journal of Pharmacology and Experimental Therapeutics* 191.2 (1974), pp. 331–340.
- [191] Barry J Cusack et al. Effect of a low-protein diet on doxorubicin pharmacokinetics in the rabbit\*. *Tech. rep.* 1992, pp. 145–148.
- [192] Marijn Oosterbaan et al. "Pharmacokinetics of Anthracyclines in Dogs: Evidence for Structure-Related Body Distribution and Reduction to their Hydroxy Metabolites". In: *Pharmaceutical Research* 1 (1984), pp. 33–38. url: <https://link.springer.com/article/10.1023/A:1016378609450>.
- [193] John R. Baldwin et al. "Influence of the cardioprotective agent dexrazoxane on doxorubicin pharmacokinetics in the dog". In: *Cancer Chemotherapy and Pharmacology* 30 (2004), pp. 433–438.
- [194] D A August et al. An evaluation of hepatic extraction and clearance of doxorubicin. *Tech. rep.* 1986, pp. 65–71.
- [195] Kari T Kivisto, Heyo K Kroemer, and Michel Eichelbaum. "The role of human cytochrome P450 enzymes in the metabolism of anticancer agents: implications for drug interactions". In: *Br J Clin Pharmacol* 40 (1995), pp. 523–530.
- [196] Mikuru Iijima et al. "Coupling of Redox and Structural States in Cytochrome P450 Reductase Studied by Molecular Dynamics Simulation". In: *Scientific Reports* 9.1 (Dec. 2019). issn: 20452322. doi: 10 . 1038 / s41598 - 019 - 45690-2.
- [197] Amitava Dasgupta. *Therapeutic Drug Monitoring*. Ed. by Amitava Dasgupta. 1st ed. Academic Press, 2012.
- [198] Juan Tamargo, Jean Yves Le Heuzey, and Phillipe Mabo. "Narrow therapeutic index drugs: A clinical pharmacological consideration to flecainide". In: *European Journal of Clinical Pharmacology* 71.5 (May 2015), pp. 549–567. issn: 14321041. doi: 10.1007/s00228-015-1832-0.
- [199] Doxorubicin Pathway (Cardiomyocyte Cell), *Pharmacodynamics Overview* — PharmGKB. url: <https://www.pharmgkb.org/pathway/PA165292164>.

- [200] R Core Team. optimize function - *RDocumentation*. url: <https://www.rdocumentation.org/packages/stats/versions/3.6.2/topics/optimize>.
- [201] J. Kiefer. “Sequential minimax search for a maximum”. In: *Proceedings of the American Mathematical Society* 4.3 (Mar. 1953). issn: 0002-9939. doi: 10.1090/S0002-9939-1953-0055639-3.
- [202] Staffan Eksborg, Hans Ehrsson, and Britta Ekqvist. and Protein Binding of Anthraquinone Glycosides, with Special Reference to Adriamycin. *Tech. rep.* 1982, pp. 7–10.
- [203] R. S. Benjamin et al. “Adriamycin Cardiac Toxicity — An Assessment of Approaches to Cardiac Monitoring and Cardioprotection”. In: *Organ Directed Toxicities of Anticancer Drugs*. Ed. by Hacker M.P., Lazo J.S., and Tritton T.R. Vol. 53. Boston, MA: Springer US, 1988. doi: 10.1007/978-1-4613-2023-4{\\\_}5.
- [204] Samuel Bernard et al. “Tumor growth rate determines the timing of optimal chronomodulated treatment schedules”. In: *PLoS Computational Biology* 6.3 (Mar. 2010). issn: 1553734X. doi: 10.1371/journal.pcbi.1000712.
- [205] Scott C. Howard et al. “Preventing and Managing Toxicities of High-Dose Methotrexate”. In: *The Oncologist* 21.12 (Dec. 2016), pp. 1471–1482. issn: 1083-7159. doi: 10.1634/theoncologist.2015-0164